NEW INTRACELLULAR MECHANISMS INVOLVED IN ALZHEIMER'S DISEASE AND FRONTOTEMPORAL DEMENTIA

Eva Borger

A Thesis Submitted for the Degree of PhD
at the
University of St Andrews

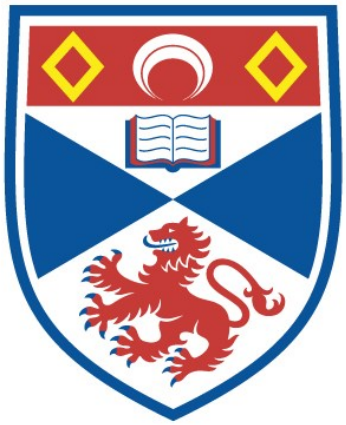

2012

New intracellular mechanisms involved in Alzheimer's disease and frontotemporal dementia

Eva Borger

Dipl. hum. biol

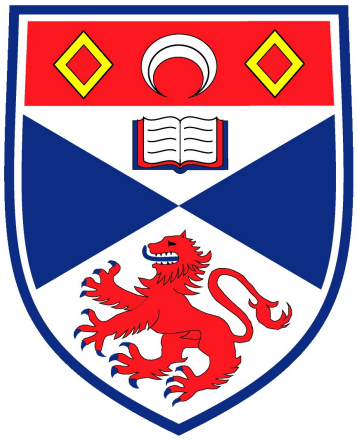

This thesis is submitted in partial fulfilment for the degree of

Doctor of Philosophy at the

University of St Andrews

June 2012

Abstract

Dementia causes an increasing social and economic burden worldwide, demanding action regarding its diagnosis, treatment and everyday management. Recent years have seen many advances in neurodegeneration research, but the search for new truly disease modifying therapies for Alzheimer's disease (AD) and frontotemporal dementia (FTD) has so far not been successful. This is mainly due to a lack of understanding of the precise intracellular events that lead up to neuronal dysfunction in early and in late stages of the disease.

This thesis describes the approaches taken to extend the current knowledge about the intracellular effects of neuronal amyloid-β and the signalling pathways causing neuronal death or disturbed synaptic function in dementia. Endophilin-1 (Ep-1), amyloid-binding alcohol dehydrogenase (ABAD), peroxiredoxin-2 (Prx-2) and the EF-hand domain family, member D2 (EFHD2) have been found to be elevated in the human brain with dementia and in mouse models for frontotemporal lobar degeneration (FTLD) or AD. The expression of these proteins as well as the expression of c-Jun N-terminal kinase (JNK), c-Jun and APP were analysed by western blotting and real-time PCR in human brains affected by AD or FTLD as well as in mouse models for AD. This provided a new insight into the regulation of these proteins in relation to each other in the aging brain and uncovered a new potential link between elevated levels of EFHD2, Prx-2 and APP in FTLD.

By studying the effects of the overexpression of Ep-1 in neurons, this research has led to a better understanding of its role in JNK-activation. It furthermore verified a protective role for Prx-2 against neurotoxicity and pointed towards a new function for Prx-2 in the regulation of JNK-signalling. The analysis of the

effect of increased levels of EFhD2 uncovered for the first time its involvement in the PI3K-signalling cascade in neuronal cells.

The current work has therefore contributed to the knowledge about the cellular processes that are affected by Ep-1, Prx-2 and EFhD2 in different types of dementia and will greatly benefit future research into their actions in the neuronal network.

Declaration

I, Eva Borger, hereby certify that this thesis, which is approximately 50,000 words in length, has been written by me, that it is the record of work carried out by me and that it has not been submitted in any previous application for a higher degree.

I was admitted as a research student in October 2008 and as a candidate for the degree of Ph.D. in September 2009; the higher study for which this is a record was carried out in the University of St Andrews between 2008 and 2012.

Date:June 6, 2012 Signature of Candidate:.....

I hereby certify that the candidate has fulfilled the conditions of the Resolution and Regulations appropriate for the degree of PhD in the University of St Andrews and that the candidate is qualified to submit this thesis in application for that degree.

Date:June 6, 2012 Signature of Supervisor:.....

Copyright Declaration

In submitting this thesis to the University of St Andrews I understand that I am giving permission for it to be made available for use in accordance with the regulations of the University Library for the time being in force, subject to any copyright vested in the work not being affected thereby. I also understand that the title and abstract will be published, and that a copy of the work may be made and supplied to any bona fide library or research worker, that my thesis will be electronically accessible for personal or research use, and that the library has the right to migrate my thesis into new electronic forms as required to ensure continued access to the thesis. I have obtained any third-party copyright permissions that may be required in order to allow such access and migration.

The following is an agreed request by candidate and supervisor regarding the electronic publication of this thesis:

Embargo on both of printed copy and electronic copy for the same fixed period of

two years on the following grounds: publication would be commercially damaging to the researcher and to the supervisor and the University; publication would preclude future publication.

Date: June 6, 2012 Signature of Candidate:.....

Signature of Supervisor:.....

Acknowledgements

It goes without saying that the undertaking of a Ph.D. would not have been possible without the help and support from others, who I would like to acknowledge at this point.

I would first like to thank Prof. Frank Gunn-Moore for giving me the opportunity to work on a fascinating topic in a great environment, for giving me the freedom to follow up ideas and for his kind words, great discussions, feedback and patience.

I am grateful for all the practical help I got in and around the lab in St Andrews without which I could not have produced this work. Thanks to Dr. Gayle Doherty, wiz with primary neuronal cultures, one of the most crucial things to learn for this project. Dr. Paul Reynolds introduced me to the lentiviral technique which helped us to take this project down new avenues. Thanks also to all the technical and administrative staff in the Schools of Biology and Medicine and the SMAU for being the good spirits around our labs and offices.
Dr. Gareth Miles and Dr. Sheila Unkles provided helpful and unbiased advice during our Ph.D. progress meetings which is highly appreciated.
I am glad Prof. David Mann (Manchester Brain Bank, University of Manchester) got interested in our work and has been extremely helpful with providing the human tissue and with giving advice on all the formalities around this.

Not only hands-on knowledge and practical assistance but also lots of friendship for which I am deeply grateful, came from Petra Popvics, Dr. Katherine Feeney

and Dr. Elaine Campbell. The same gratitude goes out to all the past and present members of the Gunn-Moore group. I spent many a weekend in the lab and office with Dr. Lotte Angus, who I thank for great discussions white board drawings and trips to curry restaurants. Thanks Zoe Allen, for being PA, social rep and a great help for keeping the lab running! Thanks Laura Aitken (keep going, you are next!), Susana Moleirinho and Andrew Lunel and everybody in Physics for great discussions, kind words and patience. Thanks Dr. Kirsty Muirhead for being my personal editor!
Going abroad would probably not have happened without the encouragement from my friends and colleagues in Marburg. Thank you Andrea, Jens and Reiner and Conny for your help and friendship.

Thank you Neil for your love, company and support during the busiest time of this project called Ph.D. I should be more on the sane side (for a while ;-)) from now on!

But in the end, most importantly, I would not be here or anywhere else without the endless love and support from my family throughout the years. Difficult times come and go and they have always been there. Thank you.

Science is wonderfully equipped to answer the question "How?" but it gets terribly confused when you ask the question "Why?" Erwin Chargaff

CONTENTS

LIST OF FIGURES

LIST OF TABLES

ABBREVIATIONS

ABAD	Amyloid-binding alcohol dehydrogenase
Aβ	Amyloid-β peptide
AD	Alzheimer's disease
ADDL	Amyloid derived diffusible ligands
ApoE	Apolipoprotein E
Amp	Ampicillin
AMPA	2-amino-3-(5-methyl-3-oxo-1,2-oxazol-4-yl)propanoic acid
APP	Amyloid precursor protein
BDNF	Brain derived neurotrophic factor
bp	Base pair
BSA	Bovine serum albumin
cDNA	Complementary DNA
C-terminus	Carboxy-terminus
CoA	Coenzyme-A
CSF	Cerebrospinal fluid
CypD	Cyclophilin D
DAPI	4',6-diamidino-2-phenylindole
DEPC	Diethyl pyrocarbonate
DMEM	Dulbecco's modied Eagle's medium
DMSO	Dimethyl sulfoxide
DNA	Deoxyribonucleic acid
dNTP	Deoxynucleotide triphosphate
DTT	Dithiothreitol
E. Coli	*Escherichia coli*
EDTA	Ethylenediaminetetraacetic acid
EGTA	Ethyleneglycol-bis-(β-aminoethyl)-N,N'-tetraacetic acid
EFHD2	EF-Hand domain containing protein D 2 (also: Swiprosin-1)

Ep-1	Endophilin A1
FACS	Fluorescence activated cell scan
FAD	Familial Alzheimer's disease
FCS	Foetal calf serum
5-FdU	5-fluorodeoxyuridine
FTD	Frontotemporal dementia
FTLD	Frontotemporal lobar degeneration
g	Gravitational constant
GFP	Green fluorescent protein
GLK	Germinal center like kinase
HEK-293	Human embryonic kidney cell line
HEPES	4-(2-hydroxyethyl)-1-piperazineethanesulfonic acid
HFIP	1,1,1,3,3,3-hexafluoroisopropanol
HRP	Horseradish peroxidase
IPTG	Isopropyl β-D-1-thiogalactopyranoside
JNK	c-Jun-N-terminal kinase
KAN	Kanamycin
kb	kilobase
LB	Luria-Bertani broth
LTP	Long-term potentiation
mAPP	mutant amyloid precursor protein
MAPK	Mitogen activated protein kinase
MCI	Mild cognitive impairment
MEK	MAP/ERK kinase (also: MAP2K)
MEM	Minimum essential medium
mRNA	messenger RNA
MeOH	Methanol
MQ	Milli-Q purified water
MTT	3-(4,5-Dimethylthiazol-2-yl)-2,5-diphenyltetrazolium bromide
MW	Molecular weight
NADH	Nicotinamide adenine dinucleotide hydrate
NGF	Nerve growth factor
NMDA	N-methyl-D-aspartate
NFTs	Neurofirbillary tangles
N-terminus	Amino-terminus
PI3K	Phosphatidylinositol 3 kinase
PBS	Phosphate buffered saline
PCR	Polymerase chain reaction
PFA	Paraformaldehyde
pH	Potential for hydrogen ion concentration

PHF	Paired helical filament
PI	Propidium iodide
PMSF	Phenylmethylsulfonyl fluoride
Prx-2	Peroxiredoxin-2
PSEN-1 (or 2)	Presenilin-1 (or 2)
PSB	Protein sample buffer
qPCR	Quantitative real time PCR
RFP	Red fluorescent protein
RNA	Ribonucleic acid
ROS	Reactive oxygen species
rpm	revolutions per miniute
SD	Standard deviation
SEM	Standard error of the mean
SDS	Sodium dodecyl sulfate
SDS PAGE	Sodium dodecyl sulfate polyacrylamide gel electrophoresis
siRNA	Small interference RNA
SK-N-SH	human neuroblastoma cell line
SR-2	Serum replacement-2
SOC	Super optimal catabolite repression broth
TBE	Tris-borate-EDTA
TBS	Tris buffered saline
TBS-T	Tris buffered saline with 0.1% Tween-20
Tris	Tris(hydroxymethyl)aminomethane
Triton-X100	Octylphenolpoly(ethyleneglycolether)
Tween 20	Polyoxyethylenesorbitan monolaurate
UV	Ultra violet
X-gal	5-bromo-4-chloro-3-indolyl-galactopyranoside

CHAPTER 1

INTRODUCTION

1.1 Alzheimer's disease and dementia

Dementia is the widespread impairment of higher cognitive functions beyond the decline that would normally be expected during aging. It predominantly affects elderly people over the age of 65 but can also occur in the younger population, where it is referred to as early-onset or presenile dementia. Apart from memory loss and partly because of it, dementia also includes symptoms such as confusion and disorientation, mood changes and difficulties with communication and problem solving. The continuing decline of these brain functions in progressive types of dementia eventually leads to the patients' complete social dependence.

Alzheimer's disease (AD) is the most common cause of dementia, underlying about 60% of all cases, followed by vascular disease (30%), dementia with Lewy bodies and frontotemporal dementia, which is the most prevalent form in early-onset dementia (Luengo-Fernandez, 2010). AD is named after the German neuropathologist Alois Alzheimer, who first presented its pathology in connection with early-onset dementia at a conference in 1906 (Alzheimer, 1906) and then published the results in 1907 (Alzheimer, 1907). Despite the long time since its discovery, the mechanism underlying this complex and multi-faceted disease is still obscure and without a cure at hand, available treatments for AD focus on the management of the symptoms of cognitive loss or emotional and behavioural challenges.

It is estimated that around 35.6 million people, close to 0.5% of the population, are suffering from dementia worldwide, causing an immense social and economic burden, which amounted to $604 billion in 2010 (Abbott, 2011). A report on dementia in the UK in the same year found that that about 820,000 people

suffered from dementia, costing £23 billion per year, which is more than the costs caused by cancer and heart disease combined (Luengo-Fernandez, 2010). These figures, together with the social impact of this debilitating condition, illustrate the importance of finding ways to diagnose and treat dementia and especially Alzheimer's disease.

1.1.1 Symptoms and diagnosis of Alzheimer's disease

Patients suffering from Alzheimer's disease typically present with some or all signs of dementia and in the case of AD, this state is often preceded by a phase of mild cognitive impairment (MCI) with less pronounced symptoms. Guidelines for the clinical diagnosis of MCI and AD are provided by the National Institute of Neurological and Communicative Disorders and Stroke and the Alzheimers Disease and Related Disorders Association (NINCDS/ADRDA). Cognitive impairment is usually assessed on the basis of the patient's history and by mental status examination or more detailed neuropsychological testing. MCI is defined if at least two of the following cognitive domains are impaired: episodic memory (acquisition and recollection of new information), reasoning and handling of complex tasks (understanding of safety risks, managing finances, planning), visiospatial abilities (recognition of faces, finding or orienting objects), language functions (speech, spelling and writing) and personality traits (McKhann et al., 2011). If the symptoms appear gradually and are clearly worsening, a diagnosis of probable AD is achieved and the patient's status can be further defined as either an amnestic (mainly involvement of episodic memory together with other deficits) or a non-amnestic type (mainly involving either language, visiospatial abilities or

executive functions together with other deficits) (McKhann et al., 2011).

In addition to these neuropsychological criteria, biomarkers are sometimes used to corroborate the initial diagnosis of probable AD. Accepted biomarkers include the detection of significant amyloid deposition in the brain by positron emission tomography (PET) using Pittsburgh compound B (PiB) (see Figure 1.1, top), which is accompanied by a decrease in soluble 42 amino acid long amyloid peptide (Aβ42) detectable in the cerebrospinal fluid (CSF). In addition, the detection of markers for neurodegeneration can be used, which include elevated levels of total and phosphorylated tau protein in the CSF, reduced glucose uptake by the brain tissue measured by fluorodeoxyglucose positron emission tomography (FDG-PET) (see Figure 1.1, bottom) as well as atrophy of the brain in the temporal lobe and medial parietal cortex, which can be seen by magnetic resonance imaging (MRI) (McKhann et al., 2011).

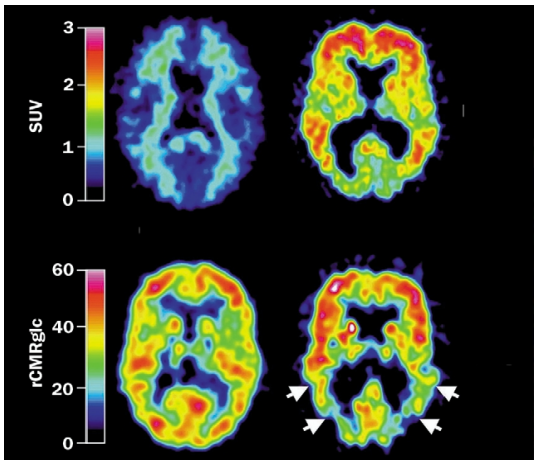

Figure 1.1: Diagnosis of AD by FDG-PET and detection of PiB. PET images from a 67-year old healthy individual (left) and a 79-year old AD patient (right). Top: Pittsburgh compound B (PiB) retention shown by yellow and red colours is high in the frontal and temporal lobes of the AD patient. Bottom: ^{18}F-FDG-labelling indicating a marked reduction of glucose metabolism in the AD brain. Reproduced with permission from Elsevier Ltd (Nordberg, 2004)

Despite these clinical and biochemical tests, the definitive diagnosis of AD can only be made *post mortem* by histological examination of the brain tissue. As mentioned above, brains from Alzheimer patients typically show brain atrophy caused by loss of neurons and synapses, which affects the cortex (temporal and parietal lobes) as well as subcortical structures such as the hippocampus and entorhinal cortex, the amygdala and the basal forebrain at different stages of the disease (Zakzanis et al., 2003) (see Figure 1.3). It is in these brain regions where the histological hallmarks of AD, senile plaques and neurofibrillary tangles (NFTs), can be detected and are used to confirm the diagnosis. Senile plaques (Figure 1.2a) are extracellular depositions in the brain parenchyma which mainly contain the amyloid-β (Aβ) peptide, derived from the amyloid precursor protein (APP) by enzymatic cleavage (see section 1.2.1). Their morphology is variable and can be focal, diffuse or stellate in appearance after immunohistochemical staining of the amyloid peptide. Focal deposits are also readily detected by amyloid staining techniques using congo-red or thioflavin S or T (Duyckaerts et al., 2009), which exploit the tendency of these aromatic dyes to bind to beta-sheet rich proteinaceous material.

In contrast, neurofibrillary tangles (Figure 1.2b) are intracellular accumulations of the hyperphosphorylated microtubule binding protein tau in axons and dendrites of neurons (Kosik et al., 1986). Accordingly, the neurofibrillary pathology typically progresses along anatomical tracts within the brain and its extent corresponds to the stage of disease and atrophy of the brain (Duyckaerts et al., 2009). Tau pathology however, unlike amyloid pathology, is not genetically linked to AD (Crawford et al., 1999) and is not specific for AD as it can also be observed in other neurodegenerative diseases such as progressive supranuclear palsy

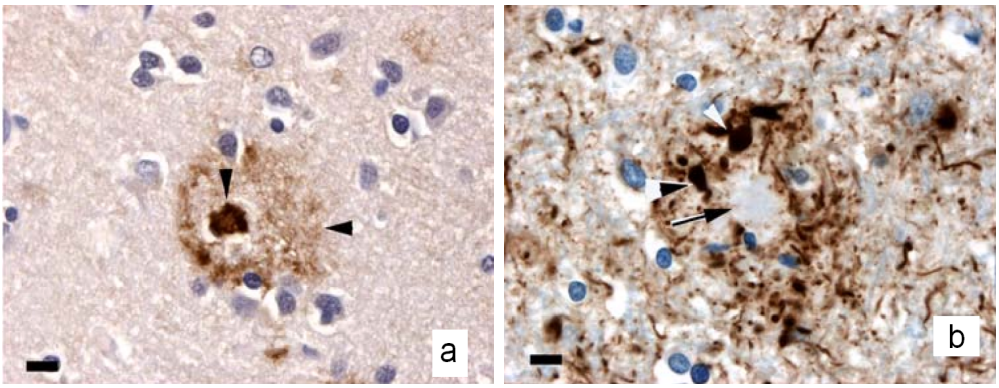

Figure 1.2: Histological hallmarks of AD. (a) A senile plaque visualised after staining with anti-Aβ antibody with a focal deposit (arrowhead) surrounded by a halo and corona (arrow) of lighter staining. (b) Neuritic crown of the plaque stained with AT8 anti-phosphorylated tau antibody. Tau-labelled tangle bearing processes (arrowhead), surrounding the plaque core (arrow). Scale bar = 10 μm. Reproduced with permission from Springer (Duyckaerts et al., 2009).

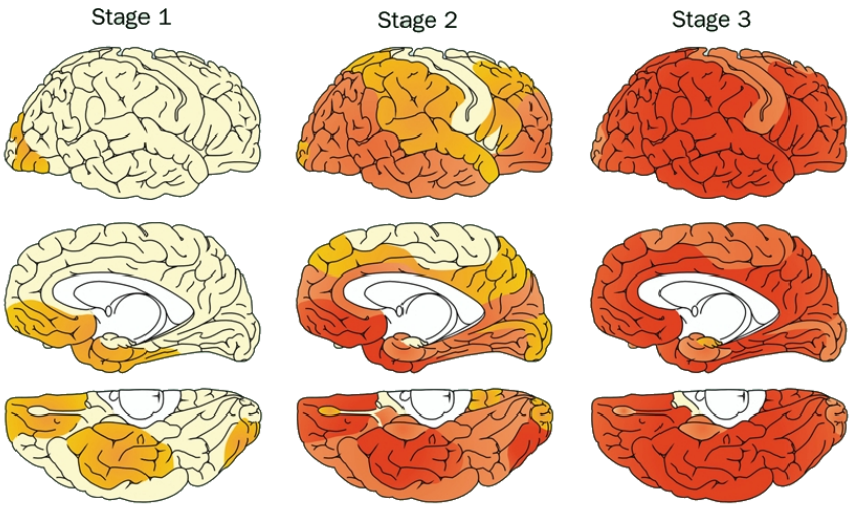

Figure 1.3: Staging of AD according to Braak et al. (Braak H, 1993). There are 3 stages distinguished from the analysis of the presence of amyloid in various brain regions. Reproduced with permission from Elsevier (Nordberg, 2004).

(PSP), corticobasal degeneration, Pick's disease and frontotemporal dementia with Parkinsonism linked to chromosome 17 (FTDP-17) (Goetz, 2001; LaFerla and Oddo, 2005). Some researchers therefore regard the formation of neurofibrillary tangles as an event downstream of amyloid pathology in the development of AD.

1.1.2 Causes and risk factors

Alzheimer's disease results from the dysfunction and death of neurons but underlying triggers for these events are still obscure. A subset of less than 1% of patients are diagnosed with a genetically linked form referred to as familial AD (FAD) and often suffer from dementia at a younger age (<65 years). These patients have dominant mutations in the genes encoding the amyloid precursor protein (APP) on chromosome 21 (Goate, 1991; Tanzi et al., 1988a), presenilin-1 (PSEN1) on chromosome 14 (Sherrington et al., 1995) or presenilin-2 (PSEN2) on chromosome 1 (Rogaev et al., 1995) (a comprehensive database of these mutations can be found at http://www.molgen.ua.ac.be/ADMutations), which mostly lead to an increased amount of Aβ peptide being produced and it is thought that processes affecting APP and Aβ also increase the risk for sporadic AD, as defined in the amyloid hypothesis (Hardy and Selkoe, 2002). Another group of patients who usually develop AD comparably early in life (between the age of 35 and 45) are patients with Down syndrome, who have a triplication of chromosome 21 (Lott and Head, 2005). However, the majority of cases are counted among the sporadic late-onset form of AD, which is currently thought to be caused by a complex set of genetic predisposition together with environmental and life-style

factors (Lambert and Amouyel, 2011). Accordingly, a large number of studies have established a link between medical conditions like head injury, hypertension, stroke, obesity, diabetes and hypercholesterinemia and an increased risk of AD (reviewed in Mayeux (2003); Hoelscher (2011)), however, the exact mechanisms in AD are still elusive. For both FAD and sporadic AD, the strongest non-genetic risk factor is age, which is signified by its incidence increasing dramatically after the age of 65 (Hebert et al., 1995).

Genetic risk factors for the development of late-onset AD have also been identified. The strongest and best characterised one is a variant of the gene coding for apolipoprotein E, APOE $\epsilon 4$, which has been found to be 2.5 times more abundant in late-onset AD patients than in the normal population (Saunders et al., 1993). The gene product ApoE is a protein associated with lipoprotein particles in the blood such as chylomicron remnants and very low, intermediate and low density lipoproteins (VLDL/IDL/LDL). It targets these particles to special sites within the body, especially in the brain and is essential for the delivery of triglycerides, cholesterol and lipid soluble molecules to these locations. The ApoE $\epsilon 4$ variant however is less efficient at this compared to the more common ApoE $\epsilon 3$ version and therefore interferes with cerebral glucose metabolism, cholesterol synthesis, signal transduction and APP processing in the brain (Lane and Farlow, 2005). Single nucleotide polymorphisms (SNPs) of the SORL1 gene, which cause reduced expression of the SORL1 gene product in neurons have also been linked to sporadic AD (Rogaeva et al., 2007). This gene encodes the membrane protein sortilin-1, which is involved in the sorting of other membrane proteins to endocytic recycling vesicles and had previously been linked to the regulation of APP processing (Andersen et al., 2005). Furthermore, reduced expression levels

of sortilin-1 have been found in affected brain regions of AD patients (Zhao et al., 2007) and have been linked to the development of AD pathology in mouse models for the disease (Dodson et al., 2008). Genome wide association studies (GWAS) have recently identified more genetic risk factors. SNPs in the genes encoding clusterin (also known as ApoJ), Phosphatidylinositol binding clathrin assembly protein (PICALM) (Harold et al., 2009) and complement receptor 1 (CR1) (Lambert et al., 2009) have been associated with a small but significantly increased risk of developing AD. Each of these proteins has been reported to play a role in the transport and clearance of amyloid-β in the brain; clusterin by acting similarly to ApoE and assisting clearance through the blood–brain barrier; CR-1, a complement cell surface receptor, by mediating uptake of amyloid-β by immune cells; and PICALM through its function in endocytosis, which could influence Aβ production or its clearance through the endothelium of blood vessels (Lambert and Amouyel, 2011; Olgiati, 2011). Other genes that have been linked to the incidence of late-onset AD mostly affect proteins involved in cellular metabolism and the production of free radicals. Such genes encode e.g. the transporter of the outer mitochondria membrane (TOM40) (Bekris et al., 2009), nitric oxide synthase 3 (NOS3) (Dahiyat et al., 1999) and the insulin degrading enzyme (IDE) (Bjork et al., 2007). Mitochondrial import processes involving the TOM40 protein are of crucial importance for their function in cellular metabolism and are therefore also central to neuronal function as described in sections 1.4.1 and 1.4.2.2. Furthermore, variations in the TOM40 gene might also be relevant for the intracellular amyloid-pathology observed in AD as outlined in Section 1.4.2.2. IDE is an intra- and extracellular metalloprotease belonging to the pitrilysin family of peptidases, which is able to degrade Aβ (Falkevall et al., 2006). Inside cells, IDE is located in

the cytosol and mitochondria, where it has been found to be responsible for the degradation of cleaved mitochondrial targeting sequences (Leissring et al., 2004). In addition to the genetic variations observed in AD patients (Bjork et al., 2007), another study investigating late-onset AD cases linked to chromosome 10 (harbouring the IDE gene) found reduced systemic activity of IDE in these cases compared to controls while its protein expression levels were not affected (Kim et al., 2007), indicating that genuine malfunction of IDE might contribute to an icreased risk for developing AD. Its relevance for AD pathology has been furhter supported by the finding that IDE and Aβ can interact *in vitro* in a way that results in a very stable complex resistant to denaturing conditions and such complexes could also be extracted from rat and human AD-affected brains (Llovera et al., 2008), suggesting a failure of Aβ-degradation in these cases. Of interest, S-nitrosylation of essential cysteine residues has been reported to compromise its enzyme activity (Cordes et al., 2009). This sort of post-translational modification, described as nitrosative stress when it occurs in excess, has emerged as an important factor in neurodegenerative processes in AD (Uehara et al., 2006; Cho et al., 2009) and therefore variations in the gene encoding nitric oxide synthase might play a role in the increased levels of nitrosative stress observed (Dahiyat et al., 1999). Additionally, IDE protein levels are positively regulated by the PI3-kinase/Akt signalling pathway, which is defective in the AD brain (Zhao et al., 2004; Ryder et al., 2004) (see also Section 1.2.3.2). It is therefore conceivable that oxidative and nitrosative stress brought about by Aβ itself or other age related processes together with genetic risk factors, can affect IDE and contribute to a build-up of Aβ inside the cytosol and mitochondria.

A summary of the current understanding of the interplay between causes and

risk factors in AD is given in Figure 1.4.

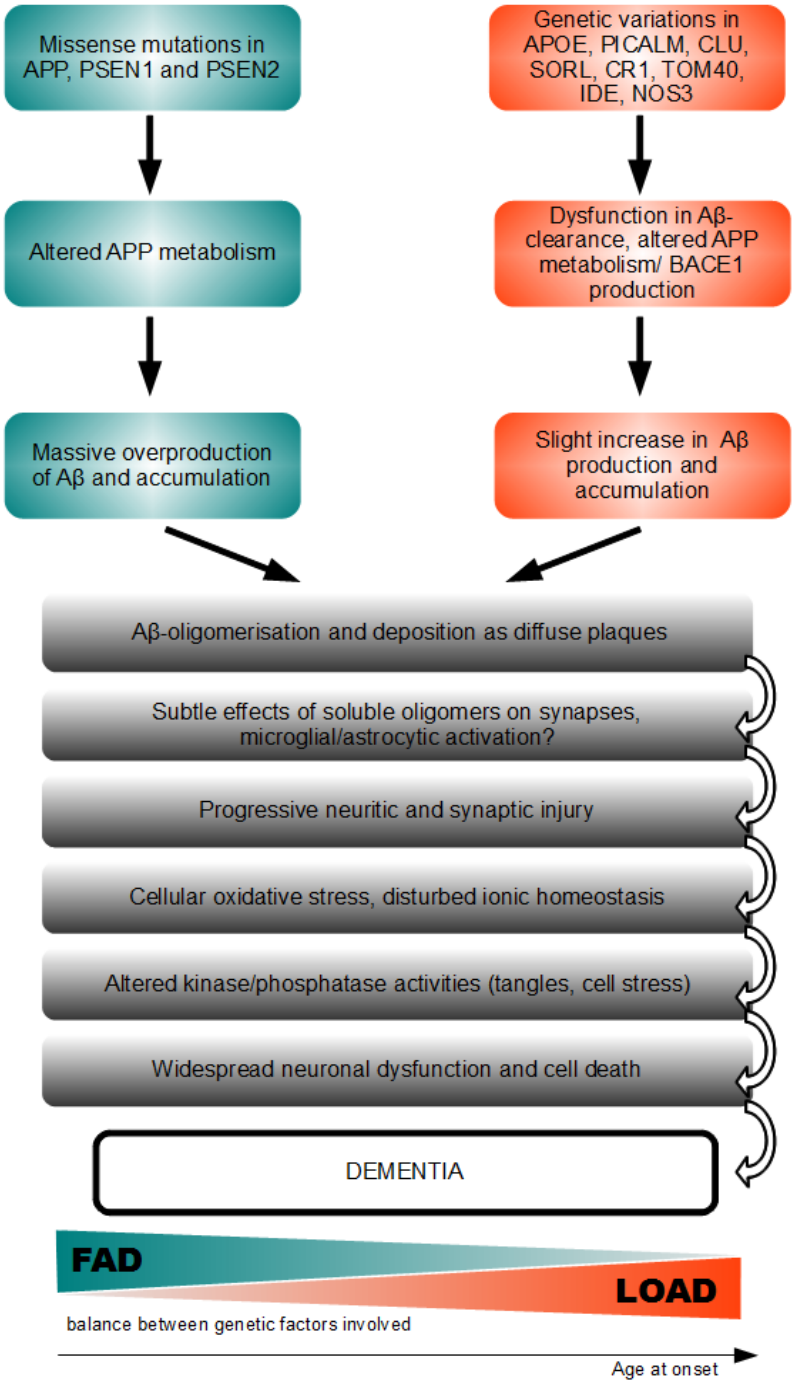

Figure 1.4: Causes and risk factors and the amyloid hypothesis in AD.

Figure 1.4: Causes and risk factors and the amyloid hypothesis in AD (continued). The sequence of events leading to dementia according to the amyloid hypothesis defined by Hardy and Selkoe (Hardy and Selkoe, 2002) and its involvement with risk factors for famial AD (FAD) and late-onset AD (LOAD). Modified with permission from Nature publishing group (Citron, 2004; Lambert and Amouyel, 2011).

1.1.3 Treatment of AD

A cure for AD does not currently exist and so the available treatment options are confined to the management of symptoms and do not halt the progression of the disease (Hogan et al., 2008; Herrmann and Gauthier, 2008). It is therefore generally recommended to approach treatment of symptoms as well as potential risk factors (hypertension, lack of physical and cognitive exercise, hypercholesterinemia) by pharmacological and non-pharmacological means (NCCMH, 2006-2011). Neuropsychological symptoms of dementia like depression, agitation and psychosis can also be treated pharmacologically in order to assist the disease management, although non-pharmacological approaches are recommended here first because of the treatment-associated risks for stroke and death (Herrmann and Gauthier, 2008).

One class of available medicines specifically targeting AD focuses on correcting imbalances between neurotransmitters in the brain which are caused by the death of neurons (Figure 1.5). For mild to moderate AD these are the acetylcholinesterase inhibitors Aricept, Exelon and Reminyl, which are designed to inhibit the breakdown of acetylcholine and therefore increase the concentration of available neurotransmitter and maintain synaptic transmission essential for cognitive function (Hogan et al., 2008) (Figure 1.5(a)).

In cases of severe AD, these can be combined with the other class of medicine,

which is the NMDA-receptor (NMDA-R) antagonist Memantine. NMDA-R overstimulation is a feature of AD can be result of the built-up of glutamate in the synaptic cleft due to its imparied recycling by the exitatory amino acid transporter into glia cells (Chen et al., 2011) or be caused by the binding of Aβ peptides (see Section 1.2.1) to the NMDA-receptor itself, causing its activation (Pellistri et al., 2008). In agreement with a failure of the glutamaterigic system in the brain is also that mRNA and protein levels of the vesicular glutamate transporter 1 (VGLUT1), which is responsible for the loading of glutamate into pre-synaptic vesicles in the cerebral cortex and hippocampus, are significantly decreased in the *post mortem* prefrontal (Kashani et al., 2008; Chen et al., 2011) and parietal/occipital (Kirvell et al., 2010) cortices of AD patients. This correlates not only with disease duration and severity but also with a reduction of the synaptic vesicle marker synaptophysin (Chen and Yan, 2010; Kashani et al., 2008), indicating that loss of VGLUT1 expressing synapses as a whole may be the underlying cause of this reduction. Memantine is designed to protect glutamatergic synapses by reversibly blocking NMDA-receptors in a similar way to its natural inhibitor Mg^{2+} (Herrmann and Gauthier, 2008) (Figure 1.5(b)).

It is important to note however, that neither of these drugs are able to stop the underlying pathological mechanisms and that their efficacy therefore decreases with disease progression.

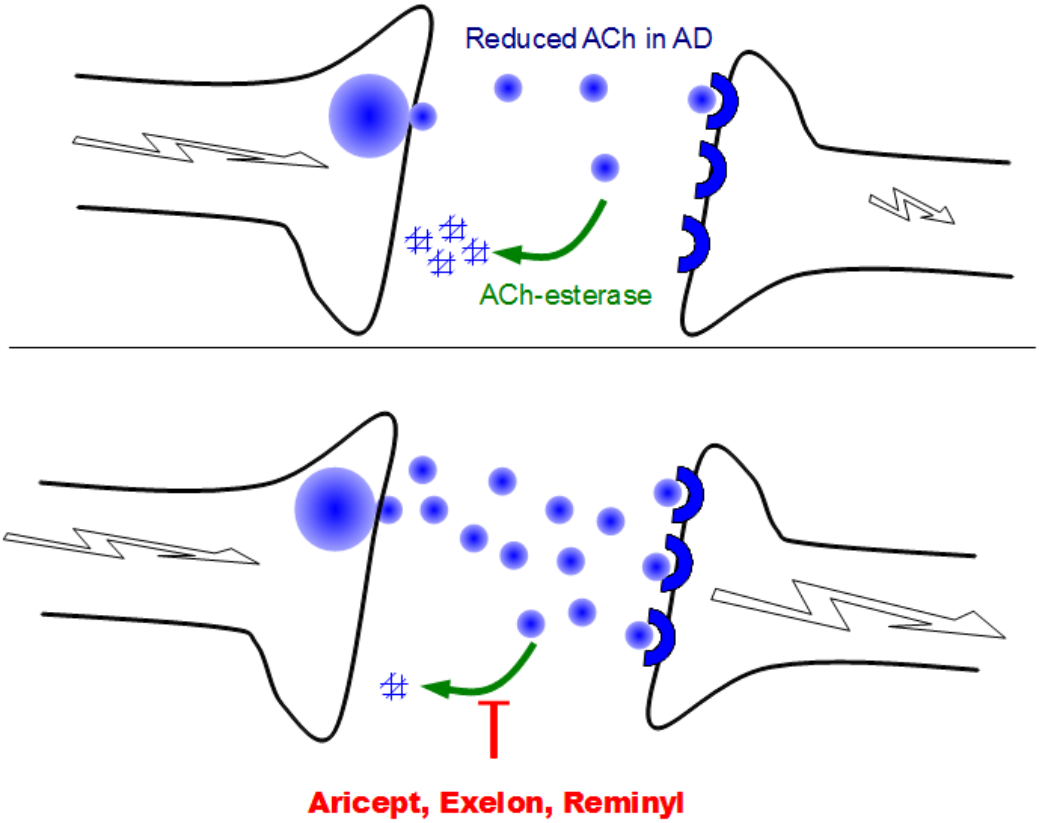

(a)

Figure 1.5: Mechanism of available AD drugs. (a) acetylcholinesterase-inhibitors increase the amount of the neurotransmitter acetylcholine (ACh, blue circles), thereby strengthening synaptic transmission between cholinergic neurons. Following page: (b) Aβ (yellow/red) inhibits glutamate recycling through glia cells (grey) and causes excess NMDA-R (dark blue) activation, thereby disturbing the transmission of new glutamate signals. Memantine (light green ovals) acts as non-competitive NMDA-R antagonist, reducing the effect of excess glutamate (green circles).

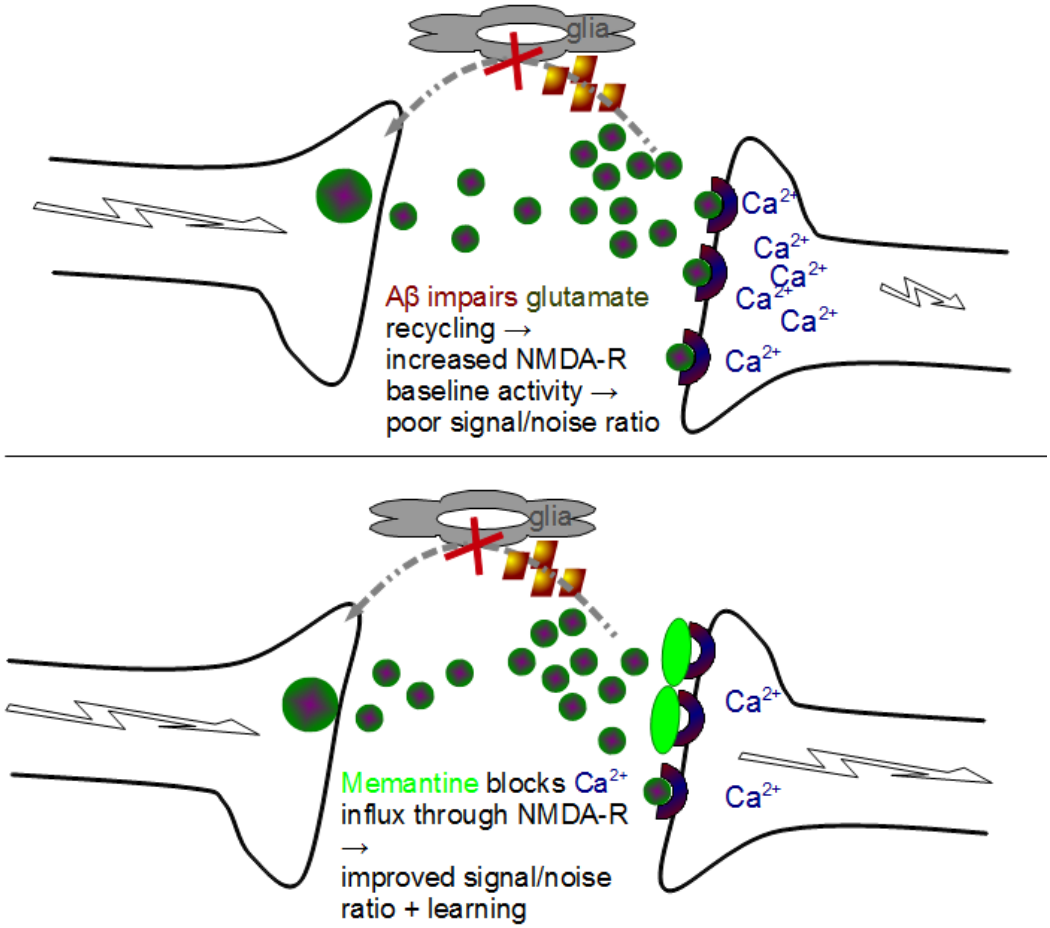

(b)

Figure 1.5: Mechanism of available AD drugs (continued).

1.2 The neuropathology of AD

There have been several major hypotheses proposed to explain aspects of the molecular mechanisms leading to the deterioration of the brain in AD. First, it has been noted that the anatomical structures of the brain affected in AD are regions occupied mainly by cholinergic neurons and their projections (Breese et al.,

1997; Perry et al., 1992) and that cholinergic neurons are specifically affected in the disease progress (Herholz et al., 2008). In line with this cholinergic hypothesis, it has been found that cholinergic neurons are specifically vulnerable in current *in vitro* models for AD because of an interaction between Aβ and the nicotinic acetylcholine receptor (Wang et al., 2000; Nagele et al., 2002). These findings have led to the introduction of cholinesterase-inhibitors for the treatment of AD, as mentioned before. Substantial research efforts have also focused on the two specific proteins related to histological hallmarks found in AD brains. This gave rise to the other main theories, which are the amyloid cascade-hypothesis (Hardy and Selkoe, 2002) and the tau-hypothesis, that regard either senile amyloid plaques or neurofibrillary tangles, respectively, as the factors initiating AD. Recently, more interactions between Aβ and tau-pathologies have been found and lead to an increasing awareness of their reciprocal effects on the neuropathology of AD (LaFerla and Oddo, 2005; Ittner and Gotz, 2011). Of note is that a link between normal aging, the specific effects of the neurotrophic factors nerve growth factor (NGF) and brain-derived neurotrophic factor (BDNF) on cholinergic neurons and the amyloid and tau-pathologies has recently been suggested (Schindowski et al., 2008; Costantini et al., 2005, 2006), adding to the complexity of the processes that are believed to occur in the brain during AD.

1.2.1 APP processing

The amyloid precursor protein (APP) is a type-I transmembrane protein belonging to the APP family, which also comprises two amyloid precursor-like proteins (APLP1/2), but the Aβ domain is unique to APP. All proteins belonging to this

family have been associated with synaptic function, cell adhesion and neuronal development (Coulson et al., 2000; Thinakaran and Koo, 2008). APP exists in several isoforms, with the three main isoforms containing 695, 751 or 770 amino acids, respectively (Kang and Mueller-Hill, 1990). APP^{695} was first identified in 1987 (Kang et al., 1987) and is the most abundant isoform in the brain (Kang and Mueller-Hill, 1990). The longer isoforms are also expressed in peripheral tissues as well and unlike APP^{695}, contain a Kunitz protease inhibitor (KIP) domain within their large extracellular domain (Tanzi et al., 1988b). Some reports have suggested that there is a relative increase in the production of the longer isoforms in AD, possibly leading to a shift towards the production of more pathological amyloid-β peptides (Matsui et al., 2007) (reviewed in Zhang et al. (2011)). It is also noteworthy that a study on human brains affected by head injury found increases in APP and Aβ immunohistochemical staining (Gentleman et al., 1993), indicating that APP or its cleavage products might play a physiological role in the neuronal response to cell or metabolic stress. This also points towards the increased risk for AD associated with those insults, which might be explained by the associated cellular/metabloic stress or the increased production of the amyloid peptides as a results of higher APP levels (see section 1.4).

APP mRNA is translated at the endoplasmic reticulum (ER) and transported through the Golgi complex to the trans-Golgi network (TGN), where most of the cellular APP can be detected (Vetrivel and Thinakaran, 2006; Zhang et al., 2011). APP can then be transported to the plasma membrane, where it is quickly internalised again due to its YENPTY internalisation motif (Selkoe et al., 1996; Haass et al., 1992). The cleavage of APP can be achieved in two ways (amyloidogenic or non-amyloidogenic) by consecutive action of different proteases (secretases) in-

and outside of the membrane and it is a disturbed balance between these two cleavage pathways which is believed to initiate the amyloid-cascade (Hardy and Selkoe, 2002) (Figure 1.6).

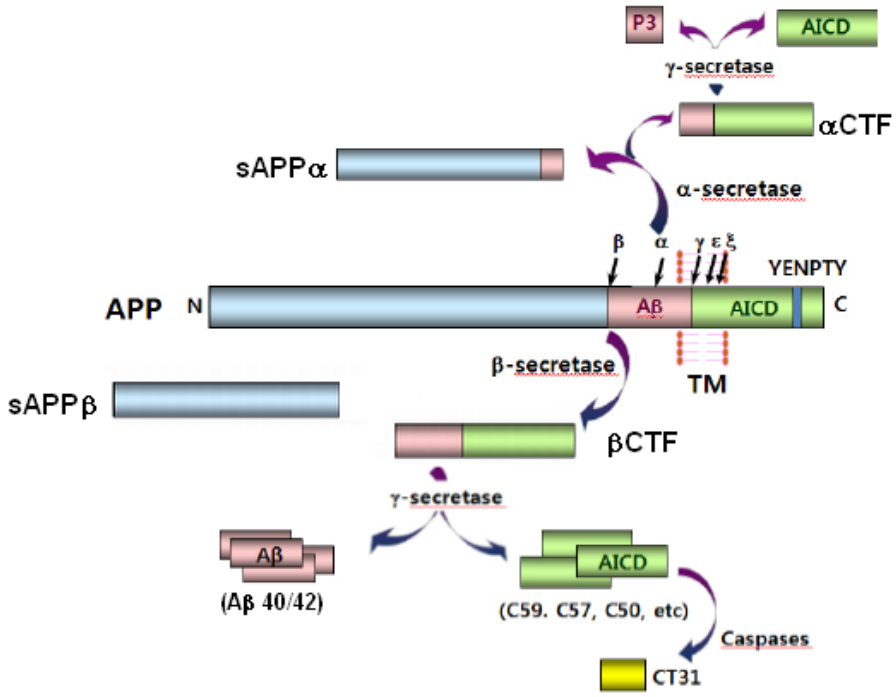

Figure 1.6: APP-processing. Full length APP (middle) can be processed in a non-amyloidogenic cleavage pathway by α- and γ-secretases (top) or in a amyloidogenic pathway by β- and γ-secretases. See text for detailed description and function of the fragments produced. Adapted with permission from Korean Society for Biochemistry and Molecular Biology (Chang and Suh, 2010).

1.2.1.1 Non-amyloidogenic pathway

If APP is first cleaved by the α-secretase, shedding the extracellular domain of the protein (sAPPα), it leaves the α-C-terminal fragment (αCTF) in the plasma membrane and precludes the production of Aβ, which has been cut between Lys^{16}

and Leu^{17} of its sequence. The α-secretase cleavage can be achieved by different proteins at the plasma membrane including the zinc metalloproteases A disintegrin and metalloproteinase domain-containing protein 17 (ADAM17; also: tumor necrosis factor-α converting enzyme, TACE), ADAM9, ADAM10 and metalloprotease disintegrin 9 (MDC9) as well as the aspartyl-protease beta APP cleaving enzyme 2 (BACE2) (Allinson et al., 2003). Recently, ADAM10 has been put forward as the physiologically relevant α-secretase in the brain (Kuhn et al., 2010). It has been found that the sAPPα fragment released from the N-terminus of APP has protective and growth promoting effects on both neuronal and non-neuronal cells and that release of this fragment might underlie the reported trophic functions of APP itself (reviewed in Chasseigneaux and Allinquant (2012)). Of note, fragments corresponding to this type of APP processing have been detected in various brain regions and throughout life and also inside neurons without any pathological implication (Wegiel et al., 2007).

α-Secretase in AD treatment: Following from these observations, stimulation of α-secretase activity has been considered as a therapeutic option for AD (Allinson et al., 2003). For example, it has been demonstrated that pharmacological activation of muscarinic acetylcholine receptors can activate α-secretase cleavage and have protective effects in a triple transgenic mouse model for AD (Caccamo et al., 2006). Similarly, activation of the purinergic receptor P2X7 can also induce α-secretase activity in a MAP-kinase dependent manner and could therefore be a therapeutic target in AD (Delarasse et al., 2011). It is important to note, however, that a possible caveat against the use of α-secretase activating agents could be the growth promoting and inflammatory effects of sAPPα, which could lead to tumorigenesis and promote neurotoxic inflammation (Chas-

seigneaux and Allinquant, 2012).

1.2.1.2 Amyloidogenic pathway

Production of the Aβ peptide requires its C-terminal end to be produced by β-secretase cleavage of APP at either Asp^{1} (β-site) or Glu^{11} (β'-site) of the Aβ sequence. This cleavage releases an extracellular sAPPβ fragment, which is 16 amino acids shorter than the corresponding sAPPα and does not possess all of its neuroprotective properties (Chasseigneaux and Allinquant, 2012). Instead, some reports have rather pointed towards a cytotoxic function of this fragment by binding to death receptor 6 (DR6) (Nikolaev et al., 2009). β-Site cleavage also leaves the β-CTF of APP inside the membrane, which is then processed by the γ-secretase complex (see below).

Several lines of evidence have indicated that an increase in β-secretase activity might be associated with the initiation of Aβ pathology. The function of this secretase is fulfilled by the beta APP cleaving enzyme 1 (BACE1), an aspartyl-protease. BACE1 is predominantly present in the Golgi complex/TGN and early endosomes (Zhang et al., 2011), where it is located in cholesterol-rich microdomains (lipid rafts) and its enzymatic activity requires the presence of cholesterol (Kaether and Haass, 2004). BACE1 expression is elevated in AD affected brain (Matsui et al., 2007; Fukumoto et al., 2002) but it has emerged that BACE1 could also be affected by normal aging. Experimental evidence exists from mouse models that production of ceramide, which is an important component of lipid rafts and stabilises BACE1 activity, increases with age as a result of enhanced p75^{NTR} signalling and can lead to a concomitant increase in the

production of Aβ with age (Costantini et al., 2005, 2006).

APP can reach BACE1 in lipid rafts as a result of cell signalling events, especially involving calpain, which can accordingly promote the production of Aβ (Saito et al., 1993; Mathews et al., 2002; Andersen et al., 2005; Liang et al., 2010). Furthermore, it has been revealed APP targeting can be influenced by phosphorylation of the APP intracellular domain at Thr^{668} (Selkoe et al., 1996; Lee et al., 2003) which probably acts as a sorting signal to these domains. Phosphorylation at this site can be mediated by the stress kinase c-Jun N-terminal kinase (JNK), which is therefore thought to be an important regulator of Aβ production in response to stress signals (Colombo et al., 2009). In addition, a stretch in amino acids 680-689 including the YENPTY motif of APP can interact with the scaffold protein JNK interacting protein 1b (JIP-1b) and enhance APP Thr^{668} phosphorylation (Taru et al., 2002; Matsuda et al., 2001; Scheinfeld et al., 2002). In agreement with this, reduced energy metabolism (Gabuzda et al., 1994; Velliquette et al., 2005) as well as oxidative stress (Tamagno et al., 2005, 2008) (an inducer of JNK activity) have been identified previously as factors increasing amyloid production and are both associated with the aging brain (Beal, 1995; Lin and Beal, 2006).

β-Secretase in AD treatment: Evidence suggests an essential role for β-secretase in Aβ production and causing neurodegeneration during AD as well as in normal aging. It follows that β-secretase inhibition as a potential therapeutic approach for AD has come into focus. Promising results were obtained from BACE1 knock out animals, which were protected against amyloid build up in the brain and no detrimental side effects caused by the deficiency could be detected. However, development of a BACE1 specific aspartyl-protease inhibitor as a drug

molecule has so far been challenging (Citron, 2004). Due to their negative effect on the levels of cholesterol in the blood and potentially the brain tissue, which is necessary for BACE1 function as mentioned above, lipid-lowering agents such as statins have been suggested to have a beneficial effect on the progression of AD. However, rigorous assessment of the different types of lipid-lowering agents currently available, considering their mechanism of action, blood-brain barrier permeability, effects on other apsects of cellular metabolism and efficacy at different stages of AD pathology is still outstanding (Shepardson et al., 2011).

1.2.1.3 The γ-secretase step

The shedding of the extracellular domain by either α- or β-secretase prepares APP for cleavage by γ-secretase. γ-Secretase is a multiprotein complex, consisting of presenilin-1 or presenilin-2, Aph-1 (anterior pharynx defective 1), PEN-2 (presenilin enhancer 2) and nicastrin, where the presenilins act as the catalytic subunits (Haass and Steiner, 2002). The enzyme and its activity have been detected in several compartments of the cell, including the ER, Golgi complex, TGN, plasmamembrane and endosomes (Thinakaran and Koo, 2008) and have also been found in association with mitochondria (Hansson et al., 2004; Area-Gomez et al., 2009). Cleavage of the remaining APP-CTF membrane stub occurs within its α-helical domain inside the membrane (Wolfe et al., 1999; Haass and Steiner, 2002) at different sites, producing, Aβ49 (ϵ-site), Aβ46 (δ-site) and Aβ40 or 42 (γ-sites) respectively following β-secretase cleavage or a p3 fragment (γ-site) following α-secretase cleavage. Some evidence has pointed towards a consecutive cleavage model, where δ- and ϵ-site fragments only exist as intermediates towards the production of Aβ40/42 (Zhao et al., 2007; Zhang et al., 2011). It has also been

proposed that changes in the membrane environment, e.g. by endocytosis, could affect the specificity of the γ-secretase cleavage at least at the ϵ-site (Fukumori et al., 2006).

Full proteolysis by the γ-secretase produces the more abundant Aβ40 and the Aβ42 peptides, which are released into the extracellular/lumenal space and are able to cause neurodegeneration. At the same time, Aβ peptides have been attributed contrasting functions under different conditions. It has been suggested early on that low concentrations of Aβ peptides, probably representing monomers, could act as neurotrophic factors (Yankner et al., 1990). This view has been supported by a more recent study, finding that picomolar concentrations of Aβ positively affect synaptic plasticity in hippocampal neurons (Puzzo et al., 2008). Interestingly, the study also revealed that the effect was mediated by the α7-containing nicotinic acetylcholine receptor (Puzzo et al., 2008), a previously identified binding site for Aβ42 peptides, which caused cytotoxicity at the higher Aβ concentrations (Wang et al., 2000). In contrast, the p3 fragment produced by non-amyloidogenic cleavage is believed to be degraded rapidly and have no further function (Zhang et al., 2011).

Cleavage of the CTF at the ϵ-site close to the cytosolic face of the membrane also results in the release of the APP intracellular domain (AICD). The AICD interacts with other proteins via its YENPTY motif, carries post-translational modifications (Figure 1.7) and its activity and turnover can be regulated by caspase cleavage and degradation by the insulin-degrading enzyme (IDE). A range of functions have therefore been proposed for the AICD. The most accepted model is that a complex comprising AICD, the adaptor protein Fe65 and the histone acetyl-transferase Tip60 acts as a transcriptional regulator which plays a role

in the induction of apoptosis and cytoskeletal re-arrangements involved during neuronal development and synaptic plasticity (Keita et al., 2009; Scheinfeld et al., 2002; Zhang et al., 2007; Mueller et al., 2008).

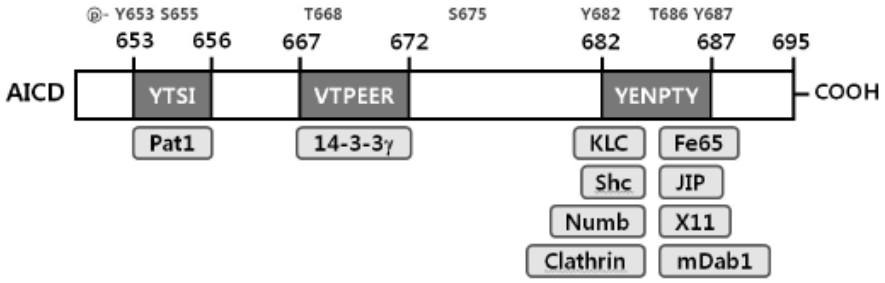

Figure 1.7: The APP intracellular domain (AICD). Motifs and binding partners are depicted. Phosphorylation sites in the sequence from APP^{695} are indicated above. Reproduced with permission from Korean Society for Biochemistry and Molecular Biology (Chang and Suh, 2010).

γ-Secretase in AD-treatment: Because of its pivotal role in generating the toxic Aβ peptides, much work has been done towards the development of γsecretase inhibitors. A problematic aspect of this approach is that APP is not the only γ-secretase substrate. The enzyme is also responsible for the release of intracellular domains from a number of other membrane proteins after they have undergone ectodomain shedding in response to ligand binding or stimuli activating second-messengers (Kopan and Ilagan, 2004). Amongst these are important molecules for neuronal development and function like the cell surface receptor Notch and its ligands Delta and Jagged, N-cadherin and the neurotrophin co-receptor $p75^{NTR}$ and release of their intracellular domains is a crucial part of their signalling function (Kopan and Ilagan, 2004). Failure of clinical phase studies on γ-secretase inhibitors, most prominently Elly Lilli's semagacestat, are probably down to effects on these molecules (Gravitz, 2011; Imbimbo and Giardina, 2011).

The focus has therefore now shifted towards achieving more subtle changes in γ-secretase activity, which would affect Aβ-production but not the processing of other substrates. Non-steroidal anti-inflammatory drugs (NSAIDs) are able to act as such modulators of γ-secretase cleavage and shift it towards the production of the less toxic Aβ38 peptide (reviewed in Selkoe and Wolfe (2007); Zhang et al. (2007)). So far, use of NSAIDs for clinical use has not been recommended because of the lack of proof of efficacy (NCCMH, 2006-2011; Imbimbo and Giardina, 2011), but it is conceivable that small molecule inhibitors with similar properties could be developed (Selkoe and Wolfe, 2007).

1.2.2 Amyloid production in AD

1.2.2.1 FAD mutations cause increased Aβ production

The mutation causing a substitution of Val^{717} to Ile in the APP gene, which is associated with familial AD had been identified long before its processing and the identity of the secretases had been elucidated (Goate, 1991). Many other mutations in APP have since been found, which are all clustered around the cleavage sites for the different secretases and favour either entry into the amyloidogenic cleavage pathway or the production of more Aβ42 compared to Aβ40 (Suzuki et al., 1994; Citron et al., 1992; De Jonghe et al., 2001; Haass et al., 1995). Some of this data also indicates that the production of Aβ from APP is shifted from endosomes towards the secretory pathway (TGN) by the Swedish mutation ($APP^{K595N/M596L}$) (Haass et al., 1995; Martin et al., 1995). Similarly, mutations in the genes encoding the presenilins also lead to an increased production of toxic Aβ42 (Borchelt et al., 1996) but effects of some PSEN mutations which

are independent from Aβ production, as no amyloid-pathology can be observed, have also been suggested in rare cases. They relate to defects in processing other γ-secretase substrates (Van Broeck et al., 2007).

1.2.2.2 Aβ oligomers, fibrils and plaques

The general hypothesis supported by experimental data is that under physiological conditions, Aβ aggregation is an ordered process of polymerisation with distinct steps (Figure 1.8) but is an unspecific aggregation at supranatural concentrations. The Aβ sequence is amphipathic with a hydrophilic N-terminus and a hydrophobic C-terminal segment, which can adopt an α-helical or a random coil structure depending on its environment. In contrast to the shorter Aβ variants, the monomeric Aβ42 version more rapidly adopts a β-sheet conformation in aqueous solutions at a physiological pH, which can then aggregate further. Residues 17–21 seem to be essential for further aggregation to happen and formation of a β-turn in segment 24–28 has been reported to help this process (reviewed in Finder and Glockshuber (2007)).

Small oligomers of Aβ consist of 3–50 subunits, while Aβ42 is thought to form intermediate unstructured paranuclei comprising 5–6 monomers, followed by 60 kDa Aβ24-globulomers which can also be found *in vivo*. **Aβ derived diffusible ligands** (ADDLs), which range in size from 17–42 kDa, can also be counted amongst them. These early aggregation species are believed to be the most cytotoxic forms of Aβ (Bucciantini et al., 2002; Walsh et al., 2002b; Stine et al., 2003). Their toxicity towards neurons has been established in a large number of studies and the detection of these soluble species has also been correlated with disease severity (Hoelscher et al., 2007; Klein, 2002; Walsh et al.,

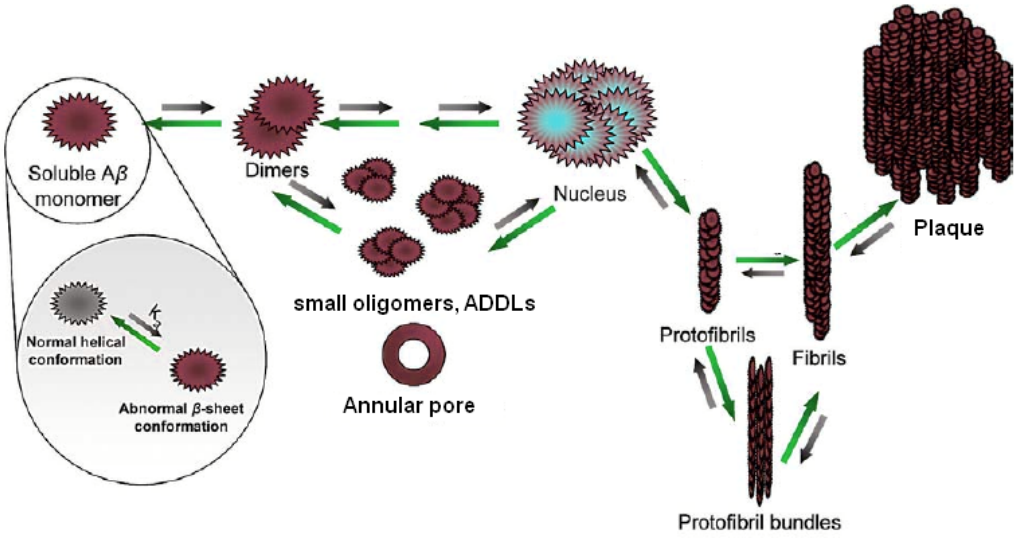

Figure 1.8: Aβ aggregation. Beginning with Aβ taking on a β-sheet conformation, different species with varying toxic properties (see text) are formed during the process of plaque formation. Most of these can also be detected *in vivo*. Adapted with permission from Karger (Finder and Glockshuber, 2007).

2002a; Klein, 2006; McLean et al., 1999).

Some data has indicated that Aβ can also disrupt calcium homeostasis of cells by inducing Ca^{2+} fluxes (Mattson et al., 1992) and disrupting membranes (Friedrich et al., 2010; Yang et al., 1998; Arispe et al., 1993). The formation of **annular pore**-like structures by Aβ has therefore been suggested but could not be demonstrated *in vivo* (Mueller et al., 2001; Arispe et al., 1993; Finder and Glockshuber, 2007).

Protofibrils are rod-like β-sheet containing structures made of arrays of Aβ-monomers, which can dissociate into oligomers or elongate depending on Aβ concentration, temperature, pH and ionic strength of the environment. They have been reported to quickly aggregate into various shapes of **fibrils** (Finder and Glockshuber, 2007), which are highly ordered assemblies of β-strands involving

the C-terminal part of Aβ. These can then aggregate into extracellular **plaques** (Finder and Glockshuber, 2007; Duyckaerts et al., 2009).

A recent study has shed some light on the process of Aβ-aggregation under physiological conditions. The results demonstrated that Aβ plaque formation in cell culture depends on living cells capable of endocytosis or phagocytosis (Friedrich et al., 2010), suggesting that all these species could be found inside cells and that the acidic endosomal pH facilitates their production. They also showed that the presence of pre-formed fibrils can have a strong seeding-effect (Friedrich et al., 2010). Immunohistochemical studies on human brain material from AD sufferers and patients with Down syndrome have also supported the view that intracellular assembly of Aβ aggregates precedes the formation of plaques (Gyure et al., 2001; Gouras et al., 2000) and this sequence has also been observed in AD animal models (Oddo et al., 2006).

1.2.3 Tau and neurofibrillary tangles

1.2.3.1 Tau structure and function

Tau belongs to the family of structural microtubule associated proteins (MAPs) type II and like the other group member MAP2, is mainly expressed in neurons (Dehmelt and Halpain, 2004). In humans there are 6 isoforms of tau which are built of an N-terminal projection domain of varying length (N), followed by two proline-rich domains, 3–4 microtubule binding repeats (R) and a C-terminal tail (Figure 1.9) (Kar et al., 2005; Morris et al., 2011; Mandelkow et al., 1995).

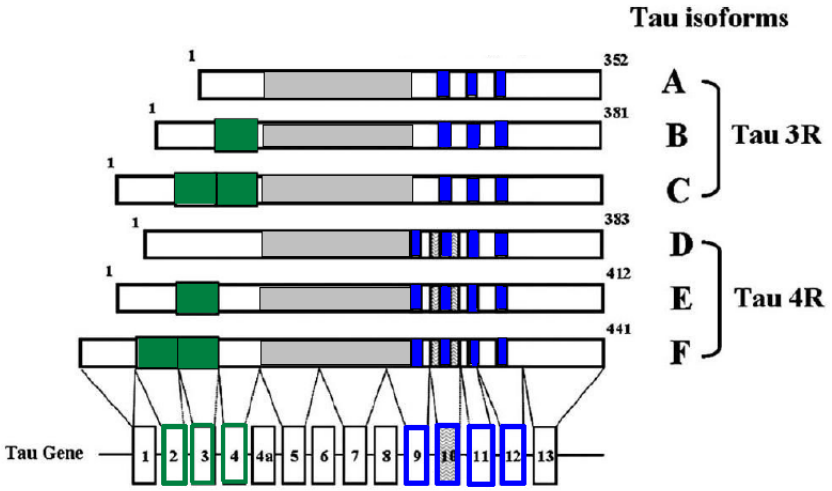

Figure 1.9: Human tau isoforms. The 6 most common isoforms A-F generated by alternative splicing are depicted. Isoform F with 441 amino acids corresponds to "htau40", the 4R isoform commonly used in the generation of transgenic animal models. Protein domains are indicated: Microtubule binding domains (blue), the proline rich domain (grey), N-terminal inserts (green). The alternatively spliced exon 10, included in 4R tau isoforms is shaded in gray. Corresponding exons in the tau gene are indicated below. Modified with permission from Lippincott Williams & Wilkins (Kar et al., 2005).

While there is only one 4R isoform in the adult mouse brain, human brain contains a 1:1 ratio of 3R to 4R tau proteins through alternative splicing of exon 10 and the balance between them seems to be crucial for neuronal function (Kar et al., 2005). Binding of tau along the microtubules has been thought to stabilise them by influencing the dynamics between shortening and lengthening of the tubulin rods, which occurs more efficiently by the 4R isoforms (Dehmelt and Halpain, 2004). Recently though, this view has been challenged in favour of microtubule based transport related functions of tau (Morris et al., 2011). *In vivo* experiments have demonstrated that it can influence axonal transport in cells and the detachment of motor proteins from their microtubule tracks (Dehmelt and Halpain, 2004; Morris et al., 2011). Tau carries a large number of post-

translational modifications, suggesting a high level of regulation of its function (Morris et al., 2011). Phosphorylation at sites within its microtubule binding domains regulates its ability to bind microtubules and is widely believed to play a part in NFT pathology (Mandelkow et al., 1995; Hanger and Wray, 2010) (see section 1.2.3.2). Addition of *N*-actetylglucosamine (GlcNAc) to serine and threonine residues has been found to inhibit its phosphorylation, thereby possibly stabilising its function at microtubules (Liu et al., 2004). In agreement with the important function of the microtubule network for neuronal development and function, tau is strongly expressed and phosphorylated at physiological sites in axons, cell bodies and dendrites of developing neurons (Brion et al., 1994) but is concentrated in axons at later stages of development (Dehmelt and Halpain, 2004). Furthermore, interaction of tau with actin filaments has also been reported, possibly pointing towards a function of tau in connecting actin with microtubule networks (Morris et al., 2011).

Functions of tau that are not directly mediated by its microtubule binding repeats but rather by interactions of its proline-rich domain with SH3-domain containing proteins have been identified. In neuronal cell lines, the src-kinase fyn has been shown to interact with and phosphorylate N-terminal Tyr residues in tau which is required for NGF-induced neurite outgrowth (Lee et al., 1998) and similar functions have also been allocated to tau in oligodendrocytes (Klein et al., 2002). In non-neuronal cells and neuronal cell lines, tau has been found to activate src and fyn kinases as well and play a role in growth factor induced actin remodelling independent from microtubule binding (Yu, 2006; Sharma et al., 2007). It has now emerged that tau also interacts with fyn during pathological NMDA-receptor signalling (Ittner et al., 2010). Other signalling related functions

of tau include possible activation of PLCγ and the cellular response to heat shock in neurons (Morris et al., 2011).

1.2.3.2 Hyperphosphorylated tau and tauopathy

Although phosphorylation of tau at some sites seems to be part of its normal function, hyperphosphorylation of tau has been observed in a number of models for metabolic and oxidative stress in animals and cell cultures, such as acute treatment with Aβ oligomers, hypoxia, glucose deprivation and heat shock (Zempel et al., 2010; Melov et al., 2007; Blurton-Jones and Laferla, 2006; Morris et al., 2011). In addition, the presence of hyperphosphorylated tau and neurofibrillary tangles has been detected in human brains after head injury (Omalu et al., 2011).

Co-localisation of hyperphosphorylated tau with NFTs and *in vitro* binding experiments have long suggested that hyperphosphorylated tau disengages from its interaction partners, most importantly the cytoskeleton, and eventually polymerises into paired helical filaments (PHF) which assemble into sarkosyl-insoluble aggregates, detectable with thioflavin dyes (Morris et al., 2011; Iqbal et al., 2010). Evidence for this proposed sequence of events stems from the finding that hyperphosphorylated tau can be detected before NFTs occur in human AD brain (Bancher et al., 1989). Phosphorylation of tau *in vitro* by GSK3β and CDK5 is also sufficient for its aggregation into filaments, while dephosphorylated tau disaggregates (reviewed in Iqbal et al. (2010)). Of note, phosphorylation of already assembled tau filaments by GSK3β can promote their aggregation into tangles *in vitro* (Rankin et al., 2008), suggesting that phosphorylation at certain epitopes can have effects at multiple stages of the aggregation process. The β sheet forming elements in tau are located in the microtubule-binding repeats R2

and R3 and phosphorylation at sites adjacent to these repeats appears to promote fibrillisation (Iqbal et al., 2010). Known phosphorylation sites in tau and the kinases able to phosphorylate these sites *in vivo* are listed in Table 1.1.

Site	**Foetal tau**	**Adult tau**	**PHF**	**Kinases**
Ser46			+	ERK2
Thr175			+	ERK2, p38, JNK, GSK3β
Thr188	+		+	ERK2
Ser184/185			+	p38
Ser198	+		+	?
Ser199	+		+	ERK2, GSK3β
Ser202	+	+	+	ERK2, p38, JNK, CDK5
Thr205			+	Erk2, p38, JNK
Ser208			+	?
Ser210			+	?
Thr212			+	ERK2, p38, JNK, GSK3β
Ser214			+	PKA, PKC
Thr217	+		+	ERK2, p38, JNK, GSK3β
Thr231	+	+	+	ERk2, p38, JNK, GSK3β, CDK5
Ser235	+		+	ERK2, p38, JNK, GSK3β, CDK5
Ser237			+	PK
Ser238			+	?
Thr245			+	p38
Ser262		+	+	GSK3β, PKA, PKC, MARK1, PK
Ser305				p38
Ser356			+	GSK3β, PKA, MARK1
Ser396	+		+	ERK2, p38, JNK, GSK3β
Ser400	+		+	GSK3β
Thr403			+	?
Ser404	+	+	+	ERK2, p38, GSK3β, CDK5
Ser409	+		+	PKA
Ser412			+	?
Ser413	+		+	GSK3β
Ser422			+	ERK2

Table 1.1: Tau-phosphorylation sites detected in foetal rat, adult rat brain and in PHF of human AD. Sites and *in vitro* phosphorylation by kinases of those sites found *in vivo* were identified in studies by Hanger et al. (1998), Morishima-Kawashima et al. (1995) and Reynolds et al. (2000) and references therein. ERK2: extracellular signal regulated kinase 2 (also p42-MAPK), JNK: c-Jun N-terminal kinase; p38: p38 mitogen activated kinase (p38-MAPK), GSK3β: glycogen-synthase kinase 3β, CDK5: cyclin dependent kinase 5, PKC: protein kinase C, PKA: protein kinase A, MARK1: microtubule affinity regulating kinase (formerly p110^{MARK})

The significance of these phosphorylation sites has been demonstrated recently in an *in vitro* study, which investigated their effect on aggregation and microtubule binding in different tau isoforms (3R and 4R). Introduction of mutations mimicking 7 of these phosphorylation events (Ser^{199}, Ser^{202}, Ser^{205}, Ser^{31}, Ser^{235}, Ser^{396} and Ser^{404}) enhanced the polymerisation of the 4R isoforms but inversely affected the 3R isoforms. At the same time the mutations interfered with microtubule stabilisation more in 3R isoforms than in 4R isoforms (Combs et al., 2011). This further highlights how phosphorylation of the different isoforms present in the human adult brain (but not the rodent brain) might lead to tauopathy.

Some research has suggested that not only phosphorylation but also proteolytic events have an impact on tangle formation, either by inducing direct conformational changes or by facilitating tau phosphorylation. Amongst the proteases involved in this cleavage are caspases 3, 6 and 7, calpain, cathepsin D and thrombin (Hanger and Wray, 2010). In a mouse model for tauopathy expressing the regulatable P301L tau mutant, activation of caspases precedes the formation of tangles following transgene expression but the authors found that both events do not lead to immediate cell death (de Calignon et al., 2010). The presence of

caspase cleaved tau has been confirmed in NFT in AD brain and cleavage of tau by calpain and caspases is also induced by exposure of cell cultures to Aβ (Morris et al., 2011; Hanger and Wray, 2010).

Some experimental results imply that tau species other than insoluble filaments are responsible for neurodegeneration (Morris et al., 2011; Iqbal et al., 2010). Comparing wild-type, soluble R406W mutant tau and P301L mutant tau revealed that wild-type and R406W mutant tau but not the more aggregation prone P301L mutant can promote Aβ toxicity in hippocampal slice cultures (Tackenberg and Brandt, 2009). Interestingly, dementia caused by the R406W tau mutation in tau has clinically been defined as a rare Alzheimer-mimicking type of frontotemporal dementia (Tolboom et al., 2010). This indicates that soluble tau is of particular importance in AD pathology and that the processes leading to frontotemporal dementia, e.g. caused by the P301L mutation, are not identical to those leading to tauopathy in AD.

Soluble tau was found to act in pathways of amyloid toxicity involving the NMDA-R, GSK3β and calcineurin in the mouse brain (Tackenberg and Brandt, 2009; Shipton et al., 2011). Phosphorylation and redistribution of endogenous tau from its normal location in axons to dendrites (rather than aggregation) has also been detected in primary hippocampal neurons exposed to oligomeric Aβ, which caused defects in spine morphology and microtubule assembly (Zhang et al., 2011). In dendrites, tau has been found to act together with the src kinase fyn, which had previously been associated with neurite outgrowth (Lee et al., 1998; Sharma et al., 2007; Klein, 2002; Ittner et al., 2010). It has been shown that tau can localise fyn to post-synaptic sites containing PSD95 and the NMDA-R in response to Aβ, thereby causing neurotoxicity (Ittner et al., 2010).

More information about the fyn–tau interactions comes from the JNPL3 mouse model for tauopathy (FTLD), expressing the human 4R P301L tau mutant. A strong interaction between tau and fyn and fyn-mediated Tyr^{18} phosphorylation of tau have been found in the JNPL3 mouse model just before the onset of pathology (Bhaskar et al., 2005). Importantly, the same study also showed that the 3R isoform of tau interacts stronger with fyn than the 4R isoform but that the interaction between fyn and 4R tau can be increased by disease related tau-phosphorylation (Bhaskar et al., 2005). This suggests that hyperphosphorylation of tau can lead to an increased interaction between 4R tau and fyn and possibly the re-distribution of fyn and tau, which is not seen under physiological conditions. More similarities between other tauopathies and human AD were revealed by studying the distribution of mitochondria. In human AD brain and a mouse model reversibly expressing the P301L tau mutant, disruption of mitochondrial trafficking has been found in neurons bearing tau pathology. However, this was reversed as soon as the expression of the tau mutant was stopped in the mice, which reduced soluble tau species but not NFT pathology (Kopeikina et al., 2011).

1.2.3.3 Tauopathy in AD

Mechanisms causing tauopathy which might be at play specifically in AD have been described by numerous studies, although evidence for their presence in the human brain *in vivo* has not been presented for all of them.

As pointed out, tau cleavage can promote its aggregation but whether or not this is actually toxic to neurons or a protective side effect leading to disposal of toxic soluble tau remains to be seen. Even though activation of caspases follow-

ing exposure to Aβ has been well documented (Umeda et al., 2011; D'Amelio et al., 2011), it is not clear if this happens as a result of Aβ mediated tau-phosphorylation causing toxicity or if Aβ activates caspases via other routes. The ability of Aβ exposure to activate caspases in models of tau deficiency has not been tested so far. Calpain, a calcium-activated protease which is able to cleave tau, has also been linked to AD, as its activation has been detected in human AD brain samples (Saito et al., 1993) and in cell cultures overexpressing APP (Kuwako et al., 2002). Similarly, the lysosomal protease cathepsin D can cleave tau and is also affected by AD pathology, as it leaks from defective lysosomes accumulating Aβ42 (Yang et al., 1998; Umeda et al., 2011). A point to consider is that phosphorylation of tau around the respective cleavage sites interferes with proteolysis and these phosphorylation events have also been detected in brains affected by AD (Hanger and Wray, 2010). This leads to the idea that increasing phosphorylation of tau might be able to overcome a possibly protective tau cleavage and thereby initiate pathology.

Most of the kinases involved in normal and pathological phosphorylation of tau have been found to be altered in AD and so it is conceivable that the delicate balance of tau-phosphorylation will be disturbed, contributing to tauopathy. Evidence for the involvement of the signal transduction pathways involving each of these kinases is summarised below.

- There is an increased expression of pERK1/2, p38 and JNK in AD and Down syndrome compared to control brains and higher expression of the CDK5 activator p25 in AD (Swatton et al., 2004). Fittingly, increases in tau-phosphorylation at sites that have been reported as target sites for

MAPKs and CDK5 have also been detected (Reynolds et al., 2000; Swatton et al., 2004).

- CDK5 also accumulates in neurons with early tangle pathology in AD brains (Pei et al., 1998).

- Phosphorylated (activated) JNK)(Lagalwar et al., 2006; Zhu et al., 2001) and its substrate, the transcription factor c-Jun (MacGibbon et al., 1997; Thakur et al., 2007; Pearson et al., 2006) are associated with tangles in AD brains. Also, Aβ treatment of cell cultures results in the activation of JNK in cell lines (Troy et al., 2001; Marques et al., 2003) and in neurons (Minogue et al., 2003; Morishima et al., 2001).

- The scaffolding protein p66shc is a target of JNK. p66shc is involved in the regulation of cellular oxidative stress and aging related dysfunction of organelles such as the mitochondria and its activation has, too, been found following Aβ exposure (Smith et al., 2005).

- Activated transcription factor NF-κB, which is a target of the MAPK signalling cascade, has been detected in neurons exposed to Aβ and in AD brain in affected regions. However, this activation is dependent on the production of reactive oxygen species (ROS) in response to Aβ (Kaltschmidt et al., 1997) and might therefore be secondary to the activation of other signalling molecules such as JNK and p66Shc.

- The Ser/Thr kinase Akt (PKB), which regulates GSK3β activity, is down-regulated in response to Aβ in cell cultures and also diminished in affected AD brain regions, which co-localise with areas of increased GSK3β activity

(Ryder et al., 2004). Accordingly, Akt isolated from Aβ expressing cells is deficient in its kinase activity towards GSK3β *in vitro* (Lee et al., 2009). In line with this, Aβ-exposure on neurons leads to GKS3β activation and inhibiting GSK3β blocks Aβ toxicity (Koh et al., 2008), as does the over-expression of Akt in cell lines (Martin et al., 2001).

- GSK3 and CDK5 not only phosphorylate tau but also cause hyperphosphorylation of the collapsin response mediator protein 2 (CRMP2), disturbing its function in the assembly of microtubules. This hyperphosphorylation is also present in AD mouse models and human AD brains but not in a mouse model lacking amyloid pathology (Cole et al., 2007).

- *N*-acetylglucosamine (GlcNAc) modifications on phosphorylation sites, which negatively regulate phosphorylation, are reduced in AD brains, which could contribute to the observed hyperphosphorylation of tau in these tissues(Liu et al., 2004).

Additionally, studies in transgenic mouse AD models confirmed the proposed cascade of events (Aβ pathology causing tau-pathology). They revealed an aggravation of tauopathy in APP/tau double transgenic animals compared to single transgenic mice (LaFerla, 2010; LaFerla and Oddo, 2005). Finally, clearance of intra- and extracellular Aβ in a triple transgenic mouse model APP_{Swe}/PSEN1_{M146V}/tau_{P301L} by an immunotherapy approach led to the reduction of hyperphosphorylated tau and NFTs as well as Aβ-pathology and upon removal of the therapeutic antibody, NFTs only reappeared after Aβ accumulation (LaFerla, 2010).

1.2.4 Prospective disease-modifying treatments for AD

1.2.4.1 Targeting amyloid-β

Research into the development of inhibitors of Aβ production has so far not resulted in a breakthrough in AD therapy. Other avenues such as the enhancement of Aβ clearance from the brain and interference with toxic Aβ aggregation are therefore being explored as therapies which could be used in place of or in combination with other potential therapeutics.

Inhibition of Aβ aggregation: A large amount of evidence is pointing towards Aβ aggregates as the culprits in amyloid-mediated neurotoxicity, so it is only logical to think of ways to stop this aggregation as a therapeutic approach. Still, Aβ aggregation is a complex and non-linear process, which leads to the production of not only one species of aggregate but many with entirely different properties. As mentioned, it is Aβ oligomers, rather than large aggregates and fibrils, which are believed to induce neurotoxicity (Walsh and Selkoe, 2007; McLean et al., 1999) and so it is of crucial importance to be aware of the dynamics of Aβ aggregation and how a potential inhibitor might affect relative levels of individual Aβ species. Meanwhile, some compounds have been tested for their therapeutic potential and for example, cyclohexanehexol inhibitors seemed to have beneficial effects in an AD mouse model (Van Broeck et al., 2007). Likewise, zinc-chelators and glycosaminoglycan mimetics have been tested for their potential to reduce Aβ aggregation in clinical trials but no significant improvement has been reported (reviewed in Citron (2004)). Interestingly, a differential effect of zinc-chelators on plasma Aβ levels (reduction only in less severe cases)

and cognition (improvement only in more severe AD cases) was noted during these studies (Citron, 2004), adding weight to the view that inhibition of aggregation can have opposing effects under different conditions.

Enhancement of Aβ clearance: One approach to increase the clearance of Aβ peptides from the brain is based on the ability of the endogenous peptidases insulin-degrading enzyme (IDE) and neprilysin to degrade Aβ (Qiu et al., 1998; Shirotani et al., 2001). An increased expression of both enzymes has been demonstrated in AD brains, possibly as a response to higher Aβ levels (Vepsalainen et al., 2008). Furthermore, systemically reduced levels of neprilysin in mice have been shown to affect Aβ degradation and build-up in brain regions typically affected by AD (Iwata et al., 2001) and variations in the IDE gene on chromosome 10 have also been associated with genetically linked cases of late-onset AD (Bjork et al., 2007; Kim et al., 2007; Vepsalainen et al., 2007). Ways to increase the activity levels of these enzymes as potential therapies are therefore being explored but have not reached the level of clinical trials yet (Miners et al., 2011).

More advanced studies have investigated the use of immunotherapy in AD. Trials using active vaccination based on aggregated Aβ preparations have proven very successful in AD mouse models, where reduction of amyloid load and cognitive improvement could be demonstrated (reviewed in Brody and Holtzman (2008)). Disappointingly, phase II clinical trials with patients suffering from mild to moderate AD had to be halted because of cases of meningoencephalitis and antibody titers were usually much lower than expected from the studies in animals. Even analysis of "responders" (with reasonable antibody-titers) without

encephalitis did not demonstrate any improvement in vaccinated patients, although autopsies revealed a specific reduction in amyloid pathology (Brody and Holtzman, 2008). Much hope has now been directed towards studies into the use of passive immunisation with monoclonal antibodies. Notably, results in mouse models have revealed that vaccination can improve behavioural deficits but also that there is no correlation with amyloid plaque clearance in those animals, similar to the observations made in human trials (Brody and Holtzman, 2008). This shows that the mechanism of amyloid directed immunotherapy has so far not been understood. Several mechanisms have been proposed, which in fact might work in concert (Brody and Holtzman, 2008; Citron, 2004). For example:

- phagocytosis of plaques by immune cells
- disruption of Aβ aggregates favouring their clearance
- capture and clearance of soluble Aβ species
- action as a peripheral sink by binding of Aβ and transport away from the brain
- stimulation of non-immunogenic cell mediated effects (phagocytosis)

1.2.4.2 Targeting tau-pathology

It appears that tau-pathology is a more downstream event in AD, probably brought about by processes involving Aβ together with other factors. Irrespective of the order of events leading to AD, there is little doubt that hyperphosphorylation and disengagement of tau from its interaction partners can cause neurotoxicity (Goetz, 2001) and as such it would be worthwhile preventing.

A modified version of methylene blue (TauRx) has been claimed to inhibit tau-aggregation and have a positive effect on AD progression but the results and

methodology of the phase II clinical study are controversial (Ballard et al., 2011; Gravitz, 2011). Other tested therapeutics targeting tau-tangles are inhibitors of the important tau-kinase GSK3β. Lithium has been reported to act as such an inhibitor and is being tested in clinical trials (Leroy et al., 2010; Gravitz, 2011), as well as other new inhibitors of GSK3 (Gravitz, 2011; Palmer, 2011). The stabilisation of microtubules alongside reduction of tau-phosphorylation is the proposed effect of another class of reagents tested in AD treatment (NAP and AL-108) but with unknown results so far (Morris et al., 2011).

1.3 Frontotemporal dementia and AD

As mentioned, mutations in the tau gene, leading to its aberrant processing and mostly increasing the amount of 4R tau (Hanger and Wray, 2010) are not characteristic of AD but more of frontotemporal dementia. However, tau-mutations and its aggregation are not defining for all cases of FTLD either as reviewed by Goedert et al. (2012). Instead, they characterise 5% of all FTLD cases which are together described as frontotemporal dementia and parkinsonism linked to chromosome 17 (FTDP-17) and manifest clinically as either dementia-dominant or parkinsonism-dominant types with different levels of atrophy in the frontotemporoparietal part or basal ganglia of the brain. Tau-inlusions are a feature of about 40 % of FTLD cases while only a small minority of them additionally bear amyloid pathology and then also present with AD-like neuropsychological symptoms (logopenic non-fluent aphasia). In those cases, the distribution of tau-pathology throughout the brain has also been linked to the specific clinical symptoms, as is has been described for AD (Goedert et al., 2012; Duyckaerts et al.,

2009). However, whereas tau-inlcusions in FTLD have mainly been described to contain the 4R tau-isoform, inclusions in AD have been described to contain a mixture of 4R and 3R tau aggregated in neurofibrillary tangels (Goedert et al., 2012; Duyckaerts et al., 2009; Goetz, 2001).

Most of the remaining cases of FTLD without tau-inclusions and cases of FTD presenting with motor neuron disease symptoms (FTD-MND) contain proteinous inclusions which stain positive for the transactive response-DNA binding protein-43 (TDP-43), encoded by the TARDBP gene, which is linked to some cases of FTLD and to MND. TDP-43 is a heterogenous nuclear ribonucleoprotein (hnRNP) which (when not aggregated in the cytoplasm) acts as a transcriptional repressor and splicing modulator (Goedert et al., 2012). Some other cases of tau-negative FLTD contain inclusions of another protein which has been genetically linked to familial amyotrophic lateral sclerosis (ALS), called fused in sarcoma (FUS), which also is a DNA/RNA binding protein invovled in transcriptional regulation. Genetically, FTLD cases not caused by mutations in the tau gene are sometimes associated with loss of function mutations in the gene encoding progranulin (PGRN), a secreted glycoprotein, which can act as a growth factor activating cytokine-type signalling pathways in neurons and immune cells. PGRN dysfunction has also been linked to the formation TDP-43 inclusions (Ahmed et al., 2007; Muynck and Damme, 2011). Other genes linked to FTLD include valosin-containing protein (VCP) which is involved in autophagosome formation and the charged multivesicular body protein 2B (CHMP2B), which is also part of the cellular response against aged/unfolded endocytic proteins by acting in the endosomal-sorting complex required for transport-III (ESCRT-III) (Goedert et al., 2012). In summary, while some overlap exists between FTLD and AD

in terms of tau-pathology and clinical and anatomical manifestation, different pathological mechanisms underlie most of the pathological features of both diseases. Figure 1.10 summarises the different variants of frontotemporal dementia and classifies them according to knowm mutations and protein inclusions.

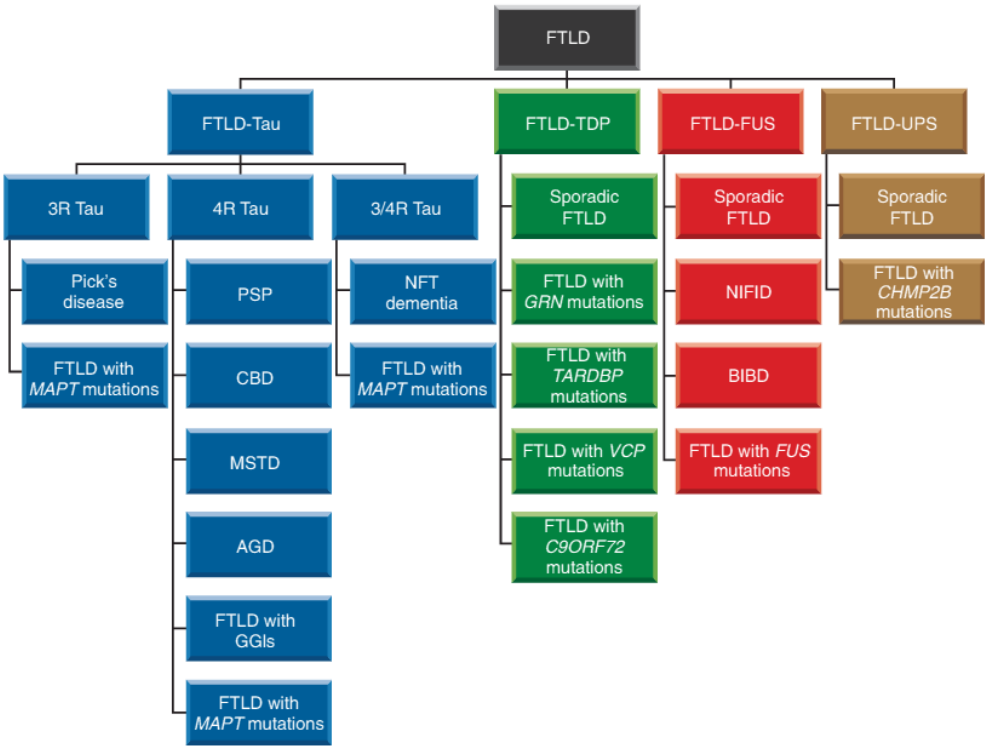

Figure 1.10: Types of frontotemporal dementia. There are four subtypes of FLTD (FTLD-Tau, FTLD-TDP, FTLD-FUS, and FTLD-UPS), based on the major components of the pathological deposits that can be detected (tau, TDP-43, FUS and unknown protein only identified by markers of the ubiquitin-proteasome system (UPS)). FTLD-Tau and FTLD-TDP are more common than FTLD-FUS and FTLD-UPS. Tau deposits are made of either 3R, 4R or all six (3/4R) isoforms of tau. Together, FTLD-TDP, FTLD-FUS, and FTLD-UPS make up FTLD-U, which is characterized by the presence of tau-negative, ubiquitin-positive inclusions. Abbreviations: PSP = progressive supranuclear palsy, CBD = corticobasal degeneration, MSTD = multiple system tauopathy with presenile dementia, AGD = argyrophilic grain disease, GGI = globular glial inclusion, NIFID = neuronal intermediate filament inclusion disease, BIBD = basophilic inclusion body disease. Reproduced with permission from Cold Spring Harbor Laboratory Press (Goedert et al., 2012).

1.4 Signalling processes in AD

The activation and inactivation of various intracellular signalling pathways by Aβ has been outlined above. Activation of JNK stress kinase signalling in particular appears to start a self-activating cycle. JNK phosphorylation and activity is enhanced in AD brains (Thakur et al., 2007; Zhu et al., 2001) and can be induced by Aβ in cell culture (Smith et al., 2005; Morishima et al., 2001; Minogue et al., 2003). At the same time, phosphorylation of APP at Thr^{668} by JNK, which is facilitated by JIP1b (Taru et al., 2002; Matsuda et al., 2001; Scheinfeld et al., 2002; Colombo et al., 2009) can enhance cleavage of APP by BACE1 (Lee et al., 2003; Colombo et al., 2009; Selkoe et al., 1996). Interestingly, a signalling complex containing APP, the MAP3K ASK1, JIP1 and JNK1 has been identified in neuronal cell cultures undergoing a metabolic stress response and in an mAPP transgenic mouse model (Galvan et al., 2007). It is not surprising then that the presence of phosphorylated JNK in the brains of AD patients correlates with the detection of intraneuronal Aβ accumulation (Shoji et al., 2000).

An important observation is also that many of the molecules activated or defective in AD (PDK, Akt, GSK3) are involved in insulin/insulin-like growth factor (IGF) signalling and are critical for the normal network function and survival of neurons. This feeds in with type II diabetes being one of the strongest risk factors for AD (Leibson et al., 1997; Cole et al., 2007). In fact, the IGF-receptor itself and its adaptor molecules insulin-receptor substrate (IRS) 1 and 2 have been found to be affected in late-onset AD and AD patients also tend to have aberrant insulin levels in CSF and plasma, pointing towards a potential insulin-insensitivity (reviewed in Hoelscher (2011); Cole et al. (2007)). The underlying reasons for these

changes are not yet known, but attempts to translate diabetes treatments into approaches for managing AD have been made. Stimulation of insulin signalling, for example by using troglitazones, ω-3 fatty acids, exercise and caloric restriction (Cole et al., 2007) has been suggested. Similarly, direct modulation of cell survival signalling via glucagon-like peptide (GLP) and glucose-dependent insulinotropic polypeptide (GIP), which is also used for diabetes treatment (Hoelscher, 2011), have been considered as options for AD treatment and such stimulation has already been shown to protect cell cultures from Aβ toxicity (Wei et al., 2002). Notably, signalling downstream from the IGF-1 receptor has also been associated with a switch from the NGF-receptor TrkA towards its co-receptor p75^{NTR}, which is observed in mouse models during aging and controls levels of Aβ production *via* BACE1. Experiments have shown that IRS2, PI3K/Akt and ceramide production were involved in the signalling cascade and interestingly, caloric restriction could prevent these age-related changes, which further validates the role of insulin-signalling in these processes (Costantini et al., 2006, 2005). It is not yet clear how these findings relate to the situation in the aging human brain and to the potential insulin-insensitivity in AD sufferers.

1.4.1 Dysregulation of calcium mediated processes in AD

Ca^{2+} is the most important second messenger in the cell, controlling a large number of processes *via* calcium-binding proteins (such as calmodulin, calbindin, calcineurin, calpain) and a resting concentration of 100 nM is therefore usually maintained. It is known that calcium levels in the cell have a reciprocal relationship with amyloid pathology, which can lead to a positive feedback of an

increasingly disturbed calcium-homeostasis and amyloid production (Berridge, 2010). Aβ can lead to pathological increases in the intracellular calcium concentration by affecting the internal stores the mitochondria (see below) and the ER (at InsP3 and ryanodine receptors, reviewed in Berridge (2010)) or *via* cell surface receptor calcium channels, such as the NMDA-R (Verdier et al., 2004; Pellistri et al., 2008; Zempel et al., 2010; Mattson et al., 1992). Decreased levels of the calcium buffer protein calbindin and elevated levels of the calcium dependent serine-phosphatase calcineurin and the kinase calpain, possibly due to AICD modulated gene expression in AD brain and AD animal models, have also been reported (Berridge, 2010). On the other hand, calcium signals influencing calpain can also regulate Aβ production through BACE1 as mentioned before (Liang et al., 2010).

An important player in mitochondrial dysfunction and calcium-homeostasis is the mitochondrial permeability transition pore (mPTP) (Figure 1.11). The mPTP is a non-specific pore consisting of proteins in the inner and outer mitochondrial membranes and plays a central role in neuronal cell death in response to oxidative and other cellular stresses (Halestrap, 2009; Leung and Halestrap, 2008). Opening of this pore collapses the membrane potential due to the uncoupled release of H^+ and influx of water from the cytosol causing mitochondrial swelling. This also facilitates the leakage of ROS from the electron-transport chain and can amplify apoptotic mechanisms by releasing Ca^{2+} as well as pro-apoptotic proteins from the intermembrane space (Halestrap, 2005). Opening of the mPTP is also thought to be behind very transient superoxide flashes in single mitochondria throughout the cell, which can be observed at a higher frequency during hypoxia and might therefore be an indicator of cellular stress

(Wang et al., 2008). The mPTP is believed to comprise of, at least, the adenine nucleotide translocase (ANT) and possibly the mitochondrial phosphate carrier (Basso et al., 2008) in the inner mitochondrial membrane, the voltage dependent anion channel in the outer membrane, as well as cyclophilin D (CypD) in the mitochondrial matrix (Leung and Halestrap, 2008; Halestrap, 2005) (see Figure 1.11). It is interesting to note that there is data suggesting a higher susceptibility towards mPTP formation in mitochondria from brain regions which are a more vulnerable during ischemia (hippocampus > cortex > cerebellum) and that this correlates with a lower adenine nucleotide content in these regions (Friberg et al., 1999). Higher vulnerability was also detected in synaptic mitochondria in comparison to mitochondria from other compartments of the cell (Du et al., 2010) and this could serve as an explanation for the selective damage of synapses in the hippocampus and cortex of the brain during aging and cellular stress. An important link between the mPTP and AD in particular is that CypD acts as a binding site for Aβ in mitochondria (see Section 1.4.4).

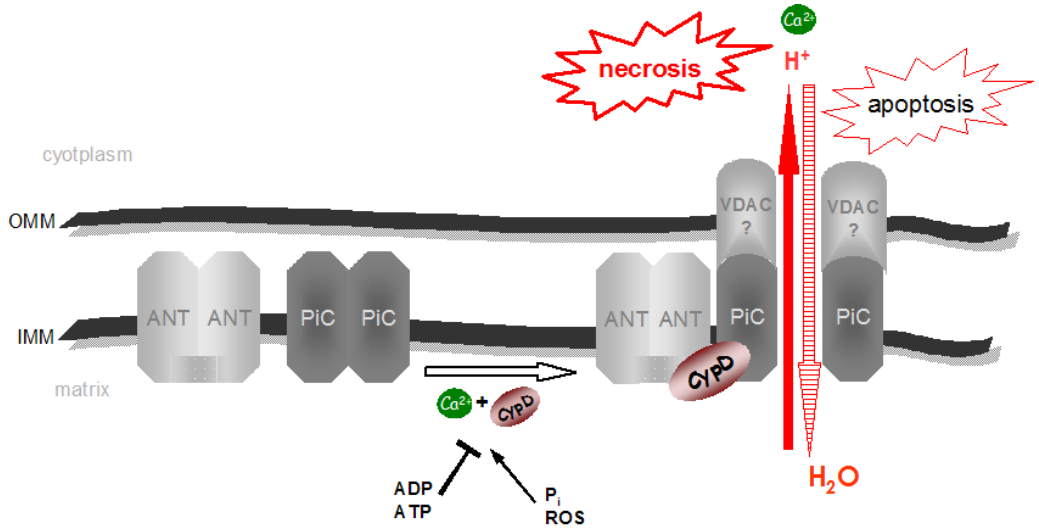

Figure 1.11: The mitochondrial permeability transition pore (mPTP). The formation of the pore containing the adenine nucleotide transporter (ANT) and the mitochondrial phosphate carrier (PiC) in the inner mitochondrial membrane (IMM) and the voltage dependent anion channel (VDAC) in the outer mitochondrial membrane (OMM) is promoted by high levels of calcium (Ca^{2+}) and dependent on the presence of cyclophilin D (CypD). mPTP formation causes the release of calcium and disturbs the membrane potential due to the efflux of protons (H^+) from mitochondria, which can cause necrosis. Mitochondrial swelling happens due to influx of water (H_2O) and results in the release of apoptotic proteins from the intermembrane space. Reproduced with permission from Portland Press (Muirhead et al., 2010)

1.4.2 The location and species of intracellular amyloid

In agreement with the proposed location of the β-secretase which initiates the amyloidogenic processing, the secretory and the endosomal compartments have been found to be the main sites of Aβ production within the cell (Selkoe et al., 1996; Khvotchev and Sudhof, 2004). Some familial forms of AD associated with mutations in APP such as the Swedish mutation $APP^{K595N/M596L}$, have been found to cause an increase of Aβ production in the secretory pathway (Martin et al., 1995; Haass et al., 1995). Likewise, Aβ produced in cells during over-

expression of wild-type APP is produced in the secretory pathway (Khvotchev and Sudhof, 2004), while cleavage of endogenous APP does not seem to take place there under normal conditions (Selkoe et al., 1996). This means that any pathological mechanism leading towards a strong increase in APP translation or modification of APP can shift Aβ production towards the Golgi or TGN. However, this might not be what is happening in all cases of AD, especially not late-onset AD, where e.g. targeting of APP to lipid rafts at the cell surface or BACE1 expression/activity itself could be affected first. The decrease of of sortilin-1 expression, which has been associated as a risk factor for late-onset AD (Rogaeva et al., 2007; Zhao et al., 2007; Dodson et al., 2008) also points towards a role of the endosomal compartment in these cases. Missorting of APP to the endosomal pathway, rather than its recycling by sortilin-1 could facilitate its accumulation and processing there (Andersen et al., 2005). Figure 1.12 summarises the various sites inside the cell where APP and Aβ can be found and the consequences of Aβ accumulation in these compartments, which will be described in more detail in the remainder of this section. It also highlights the best studied interaction partners of Aβ inside the cell.

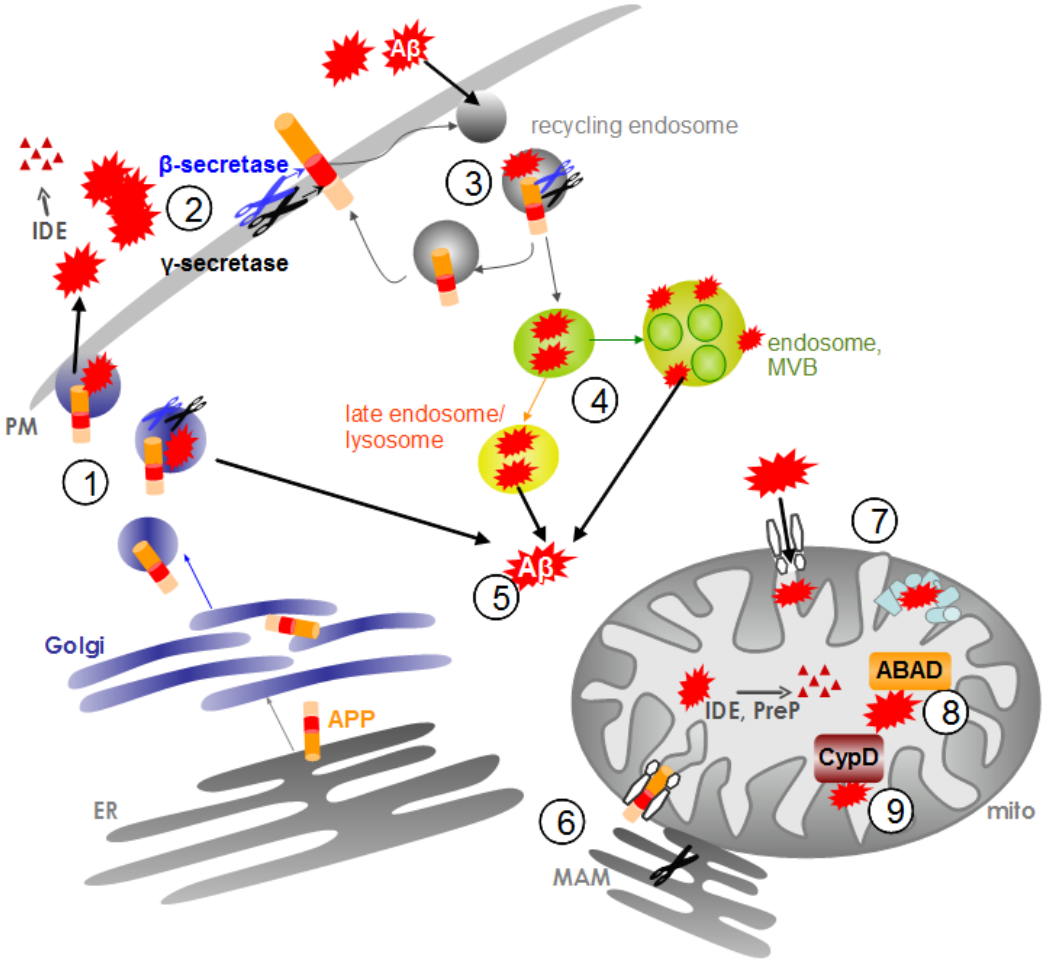

Figure 1.12: Intracellular amyloid and its effects. APP is synthesised in the ER and transported to the Golgi complex and TGN, where secretases are present and can process APP in the TGN to produce Aβ (1). Excess secreted Aβ contributes to plaque formation (2) and can also be taken up by the cell by endocytosis (3) and be found in endosomes, lysosomes and multivesicular bodies (MVB). Unprocessed APP travels to the plasmamembrane and can also be endocytosed and processed by β- and γ-secretase in the endosomal compartment (3). Endosomal Aβ (4) is important for plaque formation and causes disturbance of protein recycling and degradation. It can also impair vesicle integrity and cause cell stress through the leakage of "aged" proteins, lysosomal enzymes as well as Aβ itself. Cytosolic Aβ (5) can interact with other proteins and disturb ROS turnover and cell signalling processes. APP with its dual targeting sequence can reach the mitochondria and interfere with the mitochondrial import machinery (6). Cytosolic or locally produced Aβ can be imported into mitochondria and interact with parts of the electron transport chain (7), causing ROS production and disturbing ATP synthesis. In the matrix, Aβ can bind to ABAD (8) and interfere with its function. It can also bind to CypD (9), cause its translocation to the inner membrane and the opening of the mPTP. MAM: mitochondria associated membranes.

1.4.2.1 Aβ in endosomes and lysosomes

A large amount of evidence points towards the endosomal/lysosomal compartment as an important pathological site in late-onset AD, either by way of amyloid production or endocytosis. Experiments have demonstrated recently that *in vitro* plaque formation induced by the addition of exogenous Aβ requires the presence of cells capable of endocytosis and is accompanied by the leakage of fibrillar amyloid from multivesicular bodies (MVBs) (Friedrich et al., 2010). Uptake of Aβ added to the culture medium by receptor mediated endocytosis had been previously demonstrated, where it competed with ApoE for its LDL receptor with the help of cell surface glycoproteins (Winkler et al., 1999). Another Aβ binding receptor, which like the LDL-R is involved in transport processes through the blood–brain barrier is the receptor for advanced glycation end products (RAGE) (Deane et al., 2003, 2004). Finally, the α7 containing nicotinic acetylcholine receptor (α7-AChR) has been shown to help its receptor mediated endocytosis (Nagele et al., 2002; Wang et al., 2000). Once in endosomes, Aβ is believed to be able to damage them causing leakage from endosomes and lysosomes (Umeda et al., 2011; Zhang et al., 2002; Yang et al., 1998). MVBs are derived form early endosomes by membrane-invagination and acidification of the lumen. They are critical structures for the ubiquitin dependent recycling and degradation of membrane proteins and the silencing and recycling of cell surface receptors. The presence of Aβ in MVB has been implicated in the inhibition of the ubiquitin-proteasome system, disturbing the activity of membrane receptors and leading to the accumulation of "aged" proteins (Almeida et al., 2006). Aβ has also been found to accumulate in MVBs in transgenic animals and in the

human AD brain, especially in the post-synaptic compartment (Takahashi et al., 2002). The ability to impair the integrity of vesicular membranes can explain the presence of Aβ in the cytosol and interaction with cytosolic proteins (see below).

1.4.2.2 Mitochondrial Aβ

Another site of intracellular Aβ accumulation is the mitochondria. This location of Aβ was first described by Lustbader et al. (2004), who confirmed the interaction of Aβ with amyloid binding alcohol dehydrogenase (ABAD) and demonstrated their co-localisation inside the mitochondrial matrix in the human AD brain by immunoelectron microscopy. These findings were confirmed by other groups, for example Caspersen et al. (2005), who detected Aβ accumulation in the mitochondria of mAPP transgenic mice and brains from AD patients, which was more pronounced than in non-transgenic mice and brains from non-demented subjects. In agreement with previous studies, they found Aβ40 and Aβ42 co-localising with the mitochondrial matrix chaperone Hsp60 by immunoelectron microscopy and western blot analysis, although Aβ42 appeared to be the more abundant form (Caspersen et al., 2005). There has however been some controversy regarding these findings as Hansson Petersen et al. (2008) found Aβ only associated with the inner mitochondrial membrane but not the soluble (matrix) fraction in mitoplasts produced by osmotic shock (to remove the outer mitchondrial membrane and contaminating microsomal membranes) (Hansson Petersen et al., 2008). Whatever the submitochondrial location, most evidence has so far pointed towards a solely pathological role of the accumulation of Aβ within the mitochondria. A recent comparison of mitochondria from different brain regions in mAPP transgenic animals revealed that synaptic mitochondria are affected

by Aβ accumulation and impaired function earlier than mitochondria from other parts of the cell and before the onset of extracellular Aβ accumulation (Du et al., 2010). The synaptic pool of mitochondria also exhibited a lower threshold for mPTP formation, more oxidative stress and a more pronounced decline in respiratory function (Du et al., 2010), which could underlie a selective failure in synaptic transmission during the early stages of AD pathology. As descibed in Section 1.4.4, recent findings support the idea that specific interactions of Aβ with the mitochondrial proteins ABAD (amyloid-binding alcohol dehydrogenase) and CypD (cycolphilin D) could be important for Aβ induced mitochondrial dysfunction.

The origin of mitochondrial Aβ: There is experimental evidence for the local production as well as the import of Aβ from the cytosol as possible explanations for its occurrence in mitochondria. As outlined below, it is likely that both mechanisms are taking place.

APP can be targeted to mitochondria in cell culture systems and in the human brain due to its chimeric N-terminal targeting sequence, which causes the protein to translocate to the ER or the mitochondria (Anandatheerthavarada et al., 2003; Devi et al., 2006). This dual-targeting mechanism has previously been observed for other proteins (Anandatheerthavarada et al., 1999), however in the case of APP, co-staining, immunoblot and immunoprecipitation experiments only detected APP in a transmembrane-arrested form in contact with the mitochondrial translocases in an N-in C-out orientation (Anandatheerthavarada et al., 2003). Accordingly, this was associated with mitochondrial dysfunction (Devi et al., 2006) and interestingly, a correlation was noticed in AD patients be-

tween the amount of transmembrane arrested APP and the presence of the ApoE $\epsilon 4$ allele (Devi et al., 2006). The reason for this is unknown, but no physiological function of APP in mitochondria has so far been described, indicating that its presence there might be due to a missorting event, where altered cholestrol levels influencing membrane composition might play a role as well. This would be difficult to correct as mitochondria do not take part in normal antero- and retrograde vesicular traffic in the cell.

In support of the concept of local production of Aβ is the detection of all the components of the γ-secretase complex in mitochondria by immunoelectron microscopy (Hansson et al., 2004). However, a full explanation of the mechanism of mitochondrial cleavage of APP is still outstanding. β-Secretase, which is also crucial for Aβ production, has not been found in association with mitochondria. In addition, the topology of APP detected in mitochondria with the Aβ region located in the intermembrane space as reported by Anandatheerthavarada et al. (2003), would not be suitable for cleavage by the γ-secretase complex, which is an intramembrane cleaving protease.

One possibility around this topological problem would be the cleavage of APP by both secretases in mitochondria associated membranes (MAMs). These membrane compartments represent close contact points between the ER and mitochondria (Rusinol et al., 1994), where lipids and membrane proteins are thought to be exchanged directly between the organelles (Stone et al., 2009). Of note, presenilin 1 and 2 have been detected in this compartment (Area-Gomez et al., 2009) and the presence of active β-secretases in the secretory pathway (and hence also the ER) has been previously demonstrated (Khvotchev and Sudhof, 2004; LaFerla et al., 2007). Notably, dynamin like protein 1 (DLP1; also known as

Drp1) and mitofusin 1 and 2 (Mfn1/2), which are normally involved in mitochondrial fission and fusion processes, and are thought to modulate MAMs (Giorgi et al., 2009), have been reported to be down-regulated in AD (Wang et al., 2009). This could affect MAMs and cause changes in the way lipids and proteins, including APP, are distributed between the ER and mitochondria. The current data therefore supports two possible pathways. Firstly, APP might be fully cleaved while residing in the ER membrane and Aβ would subsequently be transported into mitochondria from the cytosol. Secondly, β-cleaved APP from the ER could transported to the mitochondrial outer membrane alongside other proteins and lipids in MAMs and then be cleaved by the γ-secretase in the mitochondrial membrane, thereby releasing Aβ directly into mitochondria.

In keeping with the first possibility, direct import of Aβ from outside the cell through the cytosol into mitochondria *via* the translocase system has been demonstrated (Hansson Petersen et al., 2008). Aβ has consequently been found within the mitochondrial cristae associated with the inner mitochondrial membrane and import of Aβ was independent of the mitochondrial membrane potential and involved the transporters of the outer membrane TOM20, TOM40 and TOM70 (Hansson Petersen et al., 2008). It is significant that this study found Aβ in mitochondrial preparations from *in vivo* human brain biopsies from non-demented patients, although it was present at lower levels compared to samples from demented patients (Hansson Petersen et al., 2008). Genetic studies have also produced evidence for a link between the mitochondrial import machinery and AD (Bekris et al., 2009; Yu et al., 2007). A single nucleotide polymorphism (SNP) in the TOM40 gene on chromosome 19 directly next to the APOE gene is linked to an increased risk for AD. However, the effect of this SNP on the TOM40

protein has not been explained so far.

Aβ degradation in mitochondria: Unlike in other compartments, there is evidence that Aβ can be rapidly degraded inside mitochondria, which could explain why it has been challenging to detect it in this location before. PreP is a thiol-sensitive metalloprotease located in the mitochondrial matrix, which is able to rapidly degrade Aβ (Falkevall et al., 2006). Another Aβ-degrading enzyme, the insulin degrading enzyme (IDE), has also been genetically linked to late-onset AD (Vepsalainen et al., 2008; Qiu et al., 1998) (see Section 1.1.2).

1.4.3 Mitochondrial dysfunction and dementia

Mitochondria take centre stage in the cellular metabolism. They contain the enzymes responsible for the β-oxidation of fatty acids as well as those making up the tricarboxylic acid (TCA) cycle and the electron transport chain for ATP production; they regulate the cellular Ca^{2+} homeostasis with the help of their powerful membrane potential, are involved in free radical (ROS) production and play an important role in the execution of apoptosis. For neurons, which are highly polarised cells with a high energy demand and rely on the efficient regulation of local currents and Ca^{2+} signals, mitochondria are vital. They play a key role together with the ER in the buffering of local calcium signals produced, for example at the NMDA and AMPA receptor ion channels during synaptic transmission. A link between the dysfunction of mitochondria and neurodegenerative conditions such as AD has therefore been recognised (Beal, 1995; Bowling and Beal, 1995). Bioenergetic deficits which can be measured in dementia patients using FDG-PET

(Foster et al., 1983; Duara et al., 1986) are also an indicator of problems involving mitochondria. Due to the proximity of mitochondrial DNA to ROS naturally produced in the electron transport chain, their DNA is prone to accumulation of mutations over time, which can cause increasing mitochondrial dysfunction and higher production of ROS with age (Richter et al., 1988; Liu et al., 2002). Accordingly, levels of the mitochondrial manganese-dependent isoform of superoxide disumutase (Mn-SOD), which is an important enzyme for the control of mitochondrial oxidative stress, have been linked to levels of amyloid-pathology and memory deficits in AD mouse models (Li et al., 2004; Dumont et al., 2009). Data demonstrating the impairment of specific mitochondrial enzymes in AD has also been produced. Parker et al. found reduced cytochrome C oxidase (COX) activity in platelets (Parker et al., 1994a) and the brains (Parker et al., 1994b) of AD patients and these findings were later confirmed by Cottrell et al. (2001). Diminished activity of the α-ketoglutarate dehydrogenase complex has also been found in association with AD (Gibson et al., 1999) and Bubber et al. (2005) subsequently measured the activity of other TCA cycle enzymes and confirmed the previous finding. This analysis also revealed a significant reduction in the activities of the pyruvate dehydrogenase complex and the isocitrate-dehydrogenase in AD brains (Bubber et al., 2005).

1.4.4 Intracellular binding partners of APP and Aβ

In order to understand the implications of the presence of intracellular Aβ for the development of AD, it is of interest to consider its interaction partners. A number of studies suggest direct interactions of mono- or oligomeric Aβ with in-

tracellular proteins and these specific interactions are likely to be critical events in AD, as they might represent early steps in the development of this disorder. Interestingly, some data suggests that not only the oligomerisation state but also the intracellular concentration of Aβ can determine which pathways are activated. For example, plasmids leading to the expression of APP with FAD mutations that cause moderate production of Aβ have been found to activate cAMP-response element (CRE) regulated gene expression, while this response was not observed when high levels of Aβ were produced (Arvanitis et al., 2007).

Phosphoinositide dependent kinase (PDK): As mentioned before, involvement of the PDK/Akt kinase pathway in AD had been suggested (Ryder et al., 2004). Lee et al. investigated the effect of Aβ on the expression and activity of PDK and its target Akt and demonstrated the inhibition of this signalling cascade by Aβ *in vitro* and the dissociation of Akt from PDK in the human AD-affected brain (Lee et al., 2009). Their study also revealed an increased association of Aβ with Akt and PDK in Aβ exposed cell cultures by co-immunoprecipitation and western blotting (Lee et al., 2009), although this effect could also be mediated by scaffolding proteins, as no direct binding studies with PDK or Akt and Aβ were performed.

Superoxide dismutase (SOD1): The Cu/Zn dependent SOD1 is a crucial enzyme in the cellular response to oxidative stress in the cytosol, which is known to be associated with neurodegeneration and memory deficits (Butterfield et al., 2001; Liu et al., 2002). A specific interaction between Aβ and SOD1 has been shown in a human neuroglioma cell line by co-immunoprecipitation and

co-localisation and this interaction resulted in the inhibition of SOD1 activity *in vitro* (Yoon et al., 2009). Interestingly, GFP-tagged Aβ and SOD1 eventually co-localised in aggregates in the perinuclear region of cells (Yoon et al., 2009) and similar Aβ aggregates have recently been reported to correlate with the attenuation of the actions of the proteasome and lead to apoptosis in neuronal cells (Park et al., 2009). Aggregates of SOD 1 have also been detected in brain tissue affected by AD and PD and SOD1 has also been found to be significantly up-regulated in these brains (Choi et al., 2005). Significantly, an oxidative modification of SOD1 on a Cys-residue was identified during this study, which is also relevant for the pathogenesis of amyotrophic lateral sclerosis (ALS) (Choi et al., 2005), potentially pointing towards common pathological mechanisms in these diseases.

Catalase: Catalase is another enzyme in the cellular defence against oxidative stress, which degrades H_2O_2 in peroxisomes and mitochondria and has been shown to interact with Aβ. Evidence has been brought forward for this by *in vitro* experiments with biotinylated Aβ peptides, which inhibited catalase activity (Milton, 1999; Milton and Harris, 2009). Narrowing in on the mechanism of this inhibition, it was reported that inhibition could be achieved by Aβ42 and Aβ(25-35) but not by Aβ(12-28) peptides, suggesting that the hydrophobic stretch in the peptide is needed. The inhibition was also observed in cell cultures and caused cytotoxicity which was aggravated by addition of 3-aminotriazole, a known inhibitor of catalase activity (Milton, 2001).

Amyloid binding alcohol dehydrogenase (ABAD): The most characterised intracellular Aβ binding protein has been ABAD. ABAD (also known as

ER-associated amyloid-binding protein (ERAB)) was first identified as an Aβ interaction partner using a yeast two-hybrid screen (Yan et al., 1997). ABAD acts as a short chain dehydrogenase/reductase (SDR) and catalyses the second step in the β-oxidation of fatty acids (He et al., 1998), thereby helping to produce energy through NAD^+ reduction and its activity has also been shown to protect cells against the effects of the toxic aldehydes 4-hydroxynonenal (HNE) and malondialdehyde (MDA) (Murakami et al., 2009). Studies in cell cultures as well as the brain showed that ABAD localises inside mitochondria as well as the ER (Yan et al., 1997; Oppermann et al., 1999; He et al., 1999; Frackowiak et al., 2001). In mouse brain, ABAD protein levels have been found to be elevated during the cellular response to glucose deprivation and hypoxia (Yan et al., 2000) and expression is also increased in brains from AD sufferers compared to non-demented controls (Yan et al., 1997).

Binding of a minimal sequence comprising amino acids 12–24 of Aβ to ABAD was found to inactivate its activity towards its usual substrates (Oppermann et al., 1999; Yan et al., 1999) and, interestingly, to enhance Aβ toxicity (Yan et al., 1997; Takuma et al., 2005), indicating that factors other than just binding and inhibition of ABAD were at play. Apoptosis and DNA fragmentation were greatly enhanced in COS cells exposed to Aβ when they overexpressed ABAD (Yan et al., 1997) and in neuroblastoma cells co-transfected with mAPP and ABAD plasmids compared to those transfected with mAPP or ABAD alone (Yan et al., 1999). The presence of ABAD and Aβ together also resulted in increased production of MDA and HNE (Yan et al., 1999) and consequently, addition of anti-ABAD antibodies abolished the negative effects of Aβ in the human neuroblastoma cells (Yan et al., 1997). Notably, an enzymatically inactive ABAD mutant expressed

in cell cultures could bind Aβ with similar affinity compared to the wild-type enzyme but was unable to enhance Aβ toxicity like active ABAD (Yan et al., 1999). ABAD also redistributes from its location inside the ER and mitochondria towards the plasma membrane in response to Aβ exposure (Yan et al., 1997, 1999) but the implications of this relocation have not yet been explained.

The toxic effect of increasing levels of ABAD together with Aβ has also been confirmed in an AD mouse model. Compared with neurons from non-transgenic mice and mice overexpressing ABAD or mAPP alone, cortical neurons cultured from mice mAPP/ABAD double transgenic mice exhibited higher levels of H_2O_2, impaired mitochondrial function and increased cell death (Takuma et al., 2005). Exacerbated mitochondrial dysfunction was also detected in these mAPP/ABAD double transgenic animals *in vivo* (Takuma et al., 2005). Moreover, the mAPP/ABAD transgenic animals presented with deficits in spatial and temporal memory and performed worse than non-transgenic mice as early as 4–5 months of age even before such deficits could be observed in mAPP single transgenic animals (Lustbader et al., 2004).

Cyclophilin D (CypD): Recently, another major interaction site for Aβ has been found within mitochondria. CypD is a peptidylprolyl isomerase F found in the mitochondrial matrix and during times of oxidative stress, it translocates to the inner mitochondrial membrane during the opening of the mPTP (Connern and Halestrap, 1994). By isomerising peptide bonds containing proline, it usually assists in the folding of other proteins (Schiene-Fischer and Yu, 2001; Freeman et al., 1996) and is thought to have this same function during mPTP formation and opening of the pore. Accordingly, genetic deficiency in CypD hinders opening

of the mPTP (Baines et al., 2005) and protects cells from Ca^{2+} and oxidative stress-induced death (Schinzel et al., 2005; Basso et al., 2005).

CypD levels have been found to be increased in an mAPP transgenic mouse model as well as in the human AD brain and this study also demonstrated that CypD can bind Aβ, especially oligomeric Aβ42 (Du et al., 2008). An association of Aβ with the inner mitochondrial membrane had been suggested by other groups (Hansson Petersen et al., 2008; Devi et al., 2006) and accordingly, Du et al. confirmed the co-localisation of CypD and Aβ in mitochondria by immunoelectron microscopy. Importantly, their study also revealed that the association between CypD and Aβ was increased in human AD brains and mAPP transgenic animals compared to controls (Du et al., 2008) and this resulted in enhanced translocation of CypD to the inner mitochondrial membrane, mPTP opening and increased ROS production causing cell death (Du et al., 2008; Singh et al., 2009). Consequently, neurons from the cortices of CypD deficient mAPP transgenic animals ($Ppif^{-/-}$/mAPP) were immune against cell death caused by oxidative stress (Du et al., 2008, 2009) and mitochondria isolated from the cortices of $Ppif^{-/-}$/mAPP transgenic mice were resistant to Aβ, Ca^{2+} induced swelling and opening of the mPTP (Du et al., 2008, 2009, 2011). Also, $Ppif^{-/-}$/mAPP transgenic animals performed better in learning and memory tests and exhibited less reduction of LTP compared to their $Ppif^{+/+}$ littermates at 12 (Du et al., 2008, 2009) and 24 months (Du et al., 2011) of age. Thus, the Aβ dependent activation of the mPTP directly links CypD to the cellular and synaptic perturbation relevant to the pathogenesis of AD.

1.4.5 Cellular consequences of the Aβ–ABAD interaction

Proteomic analysis has identified the increased expression of specific proteins in the brains of ABAD/mAPP transgenic animals, hinting at a more complex network of downstream effects resulting from the interaction of ABAD with Aβ.

The expression of peroxiredoxin-2 (Prx-2), a cytosolic enzyme which is part of the defence against protein associated peroxides, was found to be increased inmAPP transgenic and ABAD/mAPP double transgenic mice. Further analysis of ABAD/mAPP transgenic brains and human AD brains by western blotting and immunocytochemistry confirmed the increased expression of Prx-2 in the cerebral cortex (Yao et al., 2007). Overexpression of Prx-2 in cortical neurons was able to decrease Aβ toxicity, suggesting that its up-regulation in AD plays a protective role (Yao et al., 2007). Notably, Prx-2 has also been linked to Parkinsons disease (PD), where it was found to be phosphorylated and inactivated by CDK5 with its activator p25 although its expression levels remained normal (Qu et al., 2007). Similar to its effect in AD models, overexpression of Prx-2 in *in vitro* and *in vivo* models of PD protected against neuronal loss (Qu et al., 2007). In the light of these findings, the consequences of Prx-2 up-regulation in AD and its association with ABAD still require a more detailed investigation.

In a related study, endophilin A1 (Ep-1), was also identified as being up-regulated in ABAD/mAPP transgenic mice compared with ABAD transgenic and non-transgenic littermates (Ren et al., 2008). Ep-1 up-regulation was then also found in the hippocampus and cortex of ABAD/mAPP transgenic animals and in the temporal cortex of human AD brains by western blotting and immunohistochemistry (Ren et al., 2008). Ep-1 is a mainly presynaptic protein, which

has been known for its involvement in synaptic vesicle endocytosis (Ringstad et al., 1999). Research has also exposed a function of Ep-1 in the activation of c-jun N-terminal kinase (JNK) in cell lines (Ramjaun et al., 2001). The role of JNK-activation in AD pathogenesis has been explained in the beginning of this section and Ren et al. (2008) went on to show that Ep-1 overexpression is able to cause an increase in JNK activity and cell death in primary neuronal cultures. Thus, the increase in Ep-1 expression found in the AD brain could be another mechanism for the activation of the JNK signalling pathway but details of this have not been explained yet.

An important finding during further analysis of the observed proteomic changes was that the reported increases in Ep-1 as well as Prx-2 were directly due to the binding of ABAD and Aβ. Interfering with their interaction in living animals using a decoy peptide approach resulted in the expression of these proteins to be returned to normal (Ren et al., 2008; Yao et al., 2007). Using a similar approach, Yao et al. demonstrated that the behavioural deficits, which are exacerbated in the mAPP/ABAD transgenic mice compared to single transgenic animals (Yan et al., 1997; Takuma et al., 2005), are also alleviated by the treatment with this decoy peptide or the expression of a transgene encoding its sequence (Yao et al., 2011). This emphasises the importance of the ABAD–Aβ interaction *in vivo* and underlines its suitability as a drug target for the treatment of AD (Borger et al., 2011; Muirhead et al., 2010).

1.5 Conclusions

Despite a large effort in neurodegeneration research in recent years, the search for new truly disease modifying therapies for AD has so far not been successful. This is mainly due to a lack of understanding of the precise intracellular events that lead up to neuronal dysfunction in early and in late stages of the disease. An increasing awareness of the complex interactions between signalling pathways in AD, has led to the opening of new promising research avenues which are focused on the stabilisation of the neuronal networks during aging, the reduction of Aβ production and its clearance and the interactions of Aβ with intracellular targets. However, detailed knowledge of the intracellular situation will again be crucial in order to validate their effectiveness and assess potential long-term side effects of new innovative AD therapies.

1.6 Aims of this project

The aim of the research carried out for the production of this thesis was to investigate the cellular effects of proteins whose expression has been found to be increased in AD.

Firstly, the effects of endophilin-1 and peroxiredoxin-2, which are both up-regulated in response to the ABAD–Aβ interaction in neurons were investigated. To this aim, either protein was over-expressed in mouse primary cortical neurons and cell survival and the activation of the JNK-signalling cascade were assessed under different conditions.

Secondly, the role of the novel calcium-binding protein EFHD2 (EF-hand domain

family, member D2) was studied in cell cultures and primary neurons as a potential link between amyloid and tau pathologies and its expression in brains from patients with and without dementia (AD and FTLD) was further investigated. Finally, the protein and mRNA expression levels of Ep-1, Prx-2, ABAD and APP were investigated in human brains affected by dementia compared to non-demented controls. This was compared to the expression of these proteins in different mouse models for neurodegenerative diseases. It was hoped that this approach would shed new light on the roles of ABAD, Ep-1, Prx-2 and EFHD2 in neuronal cells and on the neuronal network as whole and lead to a characterisation of the biochemical processes that take place in the human brain affected by dementia.

CHAPTER 2

MATERIALS AND METHODS

2.1 Biochemical Methods

2.1.1 Protein extraction

2.1.1.1 Protein extraction

Small pieces (approximately 300 mg) of human brain tissue or mouse brain were broken up in a reaction tube on ice using micropistilles and 1 mL pipette tips after adding 5 volumes of lysis buffer (8.27 M urea, 4.7%(w/v) CHAPS, 1%(w/v) DTT, 2.5 mM phenylmethylsuflonylfluoride (PMSF)), supplemented with protease inhibitors (Roche, Burgess Hill, UK). Homogenised samples were then centrifuged at 13,000 × g for 10 min. The supernatant containing the protein extract was removed and the protein concentration was measured using Bradford reagent. 100 μl aliquots were snap frozen in liquid nitrogen and stored at -80 °C.

Protein from cell cultures grown in 35 mm dishes was extracted using the same lysis buffer. The culture medium was removed and dishes were washed 2 times with ice cold PBS (10 mM Na_2HPO_4, 2.7 mM KCl, 137 mM NaCl, pH 7.4, Sigma) before addition of 150–200 μl of ice cold lysis buffer. The cells were collected with a cell scraper, transferred to 1.5 mL reaction tubes and homogenised using a 200 μl pipette tip. Samples were centrifuged at 13,000 × g for 10 min. A Bradford test was performed to measure the protein concentration and the supernatant was snap frozen in liquid nitrogen and stored at -80 °C.

2.1.1.2 Extraction of phosphorylated proteins

If the phosphorylation state of proteins had to be maintained, cells and tissue samples were extracted as soon as possible following the dissection of the tissue sample and kept on ice at all times. Protein extracts were produced by addition 150–200 μl ice cold phospho-extraction buffer (50 mM Tris, 100 mM EGTA, 1 mM EDTA, 1% Triton-X-100, 1 mM Na_3VO_4, 50 mM NaF, 5 mM Na-PPO_4, 207 mM sucrose, 0.1% beta-mercaptoethanol, 2.5 mM PMSF; (all chemicals from Sigma, Gillingham, UK)) supplemented with protease inhibitors (Roche) to 35 mm cell culture dishes or 5 volumes of extraction buffer to tissue samples. Samples were homogenised using micro-pistilles and pipetting through a 1 mL pipette tip (tissue) or by pipetting through a 200 μl pipette tip (cell cultures). Samples were centrifuged at 13,000 $\times$ g for 10 min at 4 °C and the protein concentration in the supernatant was measured using a Bradford test before samples were used for SDS-PAGE and western blotting without delay.

For the extraction buffer, a 200 mM stock solution of sodium-orthovanadate (Na_3VO_4) was produced and adjusted to pH 10.00. The solution was activated by boiling it until colourless, cooling it to room temperature and adjusting to pH 10.00 again. This procedure was repeated until the solution remained stable and colourless at room temperature at pH 10.00.

2.1.1.3 Bradford test

The concentration of protein in extracts from tissue or cell cultures was measured by the absorbance of coomassie blue in the Bradford colorimetric assay.

First, a standard curve was prepared by measuring the absorbance of known dilutions of bovine serum albumine (BSA) (0–10 $^{\mu g}/_{ml}$) in disposable semi-micro cuvettes (VWR, Lutterworth, UK) at 595 nm in a UV-vis spectrometer (Shimadzu, Wolverton Mill South, UK). The protein concentration of appropriately diluted samples was then estimated by comparison to the standard curve. The protein concentrations of larger numbers of samples were measured using Bradford reagent in a microplate assay. For this assay, 5 μl of appropriatedly prediluted samples were distributed into the wells in duplicate and 250 μl Bradford reagent was added and incubated for 5 min in the dark. A standard curve was produced from known diltutions of BSA (0.2–1 $^{mg}/_{ml}$) pipetted in the same microplate.

2.1.2 SDS-PAGE

10% bis-tris polyacrylamide minigels were produced by preparing first the separating gel (375 mM Tris pH 8.8, 1% SDS, 10% Bis-Tris acrylamide (37.5:1), 0.1% ammoniumpersulfate, 0.04–0.08% TEMED) and then the stacking gel (125 mM Tris, pH 6.8, 1% SDS, 4% Bis-Tris acrylamide, 0.1% ammoniumpersulfate, 0.1% TEMED). The percentage of the separating gel was adjusted accordingly if smaller peptides were analysed (12.5–20 %). Samples were prepared by mixing an appropriate volume representing up to 40 μg of total protein with 4× protein sample buffer (106 mM Tris-HCl, 141 mM Tris-Base, 4% SDS, 40% Glycerol, 0.51 mM EDTA, 4% DTT, 0.05 $^{mg}/_{ml}$ bromphenol blue, pH 8.5) and denaturation for 5 min at 95 °C. Gels were run with SDS-running buffer (25 mM Tris

pH 8.3, 192 mM Glycine, 0.1% SDS) in a BioRad gel electrophoresis system at 120 V, 360 mA for 10 min followed by 160 V for 50 min. The prestained protein markers P7708 or P7710 or the protein ladder P7703 (NEB, Hitchin, UK) were separated in parallel to the samples.

2.1.3 Western blotting

Following the SDS-PAGE, the proteins were transferred to 0.2 μm supported nitrocellulose (Whatman) by blotting for 1 h at 30 V, 360 mA in Inivtrogen transfer buffer (25 mM Tris, 25 mM Bicine, 1 mM EDTA, 10% methanol pH 7.2) or self-made transfer buffer (25 mM Tris, 192 mM glycine, 20% methanol pH 8.0) using the Invitrogen X-Cell wet-blotting system. Blotting time was increased to 1 h 15 min if two gels where transferred in the same chamber.

Protein transfer to the nitrocellulose was confirmed by staining with Ponceau S (Sigma). After removal of the Ponceau staining by washing in TBS (50 mM Tris, 138 mM NaCl, 2.7 mM KCl, pH 8.3), non-specific antibody binding sites were blocked by incubating the membranes in blocking solution (50 mM Tris, 138 mM NaCl, 2.7 mM KCl, 0.1% Tween-20, 5% skimmed dried milk or 5% BSA) for 1 h at room temperature. Primary antibodies were diluted according to table A.1 in the appopriate blocking solution and incubated over night at 4 °C either using 10 mL of diluted antibody per blot in a tray or with 3–4 mL of diluted antibody per blot in a heat-sealed plastic foil. Excess primary antibody was removed by washing the membranes 3 x 5 min in TBS-T (50 mM Tris, 138 mM NaCl, 2.7 mM KCl, 0.1% Tween-20). Membranes were incubated with

the appropriate horse radish peroxidase (HRP) conjugated secondary antibodies diluted in blocking solution according to table A.2 for 1 h at room temerature. Immunostained bands were detected using enhanced chemiluminescence (ECL) peroxidase substrate (Millipore, Watford, UK) by repeatedly pipetting 2 mL of ECL mixture over the membrane for 1 min. Chemiluminescence images were taken in a LAS3000 detector (Fuji).

If a second antigen needed to be detected, bound antibodies were removed by washing the membrane 4 x 10 min in 10% acetic acid, followed by multiple washes in TBS (50 mM Tris, 138 mM NaCl, 2.7 mM KCl) for appoxmiately 30 min. Membranes were then blocked and probed with primary and secondary antibodies as described above.

2.1.4 Small induction of bacterial protein expression

Bacterial expression plasmids were transformed into chemically competent BL21 *E .coli* bacteria as described in section 2.2.12 and grown over night at 37 °C on LB-agar plates containing the appropriate antibiotic. Single colonies were picked the next day and grown in 10 mL of LB medium containing the appropriate antibiotic in a 50 mL falcon tube. On the following day, 10 mL over night culture were expanded in 1 L of LB-medium with antibiotic at 37 °C in a 3 L conical flask, shaking at 210 rpm until an OD(600 nm) of 0.5–0.9 was reached. A 1 mL sample of the culture was then removed and the bacteria pelleted at 13,000 × g for 10 min. The pellet was then resuspended in 100 μl 1x protein sample buffer and the sample denatured at 95 °C for 15 min and then left on the bench top for an analytical gel. Protein expression was induced in the remaining 9 mL culture by addition

of isopropyl β-D-1-thiogalactopyranoside (IPTG, Sigma) to a final concentration of 1 mM. The culture was incubated at 25 °C shaking at 180 rpm for 1 h and another analytical sample was taken. Further samples were removed after 2 h and 4 h of induction with IPTG. The samples were then subjected to SDS-PAGE on a 10% gel. Proteins were visualised in the gel by staining with Coommassie blue dye. The gel was incubated in Coommassie blue stain for 10–15 min and the staining solution was saved for re-use. Residual staining solution was removed with tap water and the gel was transferred to a microwavable container which was filled with tap water. Destaining was achieved by microwaving 2 times at full power for 5–7.5 min and the water was exchanged in between.

2.1.5 Purification of His-tagged proteins

Bacterial expression plasmids for the expression of 6×His-tagged proteins were transformed into chemically competent BL21 *E .coli* bacteria as described in section 2.2.12 and grown over night at 37 °C. Single colonies were picked the next day and grown over night in 10 mL LB-medium at 37 °C shaking at 210 rpm. On the following day, the culture was expanded in 1 L LB medium containing the same antibiotic and grown at 37 °C shaking at 210 rpm until an OD of 0.5–0.9 was reached. A 1 mL analytical sample was taken from the culture, the bacteria pelleted and resuspended in 100 μl protein sample buffer before boiling of the sample at 95 °C for 15 min. Protein expression was induced in the remaining culture by addition of IPTG to a final concentration of 1 mM and the culture was returned to the incubator and grown at 25 °C shaking at 180 rpm for 4 h. Another 1 mL analytical sample ws taken and processed as before. The bacteria

were harvested by centrifugation at 6500 rpm in a Beckman J2-M6 centrifuge for 10 min. The bacterial pellet was then removed from the centrifuge container and the weight of the pellet was determined. If not used on the same day, the bacterial pellet was stored at -80 °C. For lysis, the bacterial pellet was resuspended in 5 volumes (approximately 15 mL for a 1 L culture) of lysis buffer (50 mM Tris, pH 8.0, 0.5 M NaCl, 100 $^{\mu g}/_{mL}$ DNase I, 100 $^{mg}/_{mL}$ lysozyme, 10% glycerol, protease inhibitors without EDTA (all chemicals from Sigma)) per weight of bacterial pellet. The resuspended bacteria were then broken up by 6 times sonication for 10 s on ice. The lysate was cleared by centrifugation at 20,000 rpm at 4 °C for 20 min in a Beckman J26 centrifuge and filtered through a 0.45 μm syringe filter.

Proteins were then bound to Ni-NTa Agarose (QIAGEN) for purification of the 6 × His-tagged protein. For equilibration, 2 mL of Ni-NTA agarose slurry were transferred to a 15 mL falcon tube and spun at 500 × g for 1 min at 4 °C in a Heraeus tabletop centrifuge. The supernatant was removed and 4 mL lysis buffer were added and mixed with the agarose by inversion. The equilibrated agarose was centrifuged again at 500 × g for 1 min at 4 °C and the supernatant removed. The filtered bacterial lysate was then added to the Ni-NTA Agarose and mixed with it by inversion. The mix was transferred to a 50 mL falcon tube and incubated tumbling at 4 °C for 2 h. At the end of the incubation period, the agarose beads were collected by centrifugation at 500 × g for 3 min at 4 °C and the supernatant transferred to a fresh 50 mL tube and stored on ice for subsequent analysis on an analytical gel. The beads were then washed 5 times with 10 mL ($\geq$5 × the bead volume) wash buffer (50 mM Tris pH 8.0, 0.5 M NaCl, 10 mM

imidazol, 10% glycerol, protease inhibitors) followed by centrifugation and at 4 °C and each of the wash fractions was saved and stored on ice for subsequent analysis. Proteins were eluted from the agarose beads by 5 washes with 4 mL (2 times bead volume) of elution buffer (50 mM Tris pH 8.0, 0.5 M NaCl, 300 mM imidazol, 10% glycerol, protease inhibitors) at 4 °C and all the fractions were saved again for analysis. The protein concentration of all saved fractions was measured and an aliquot of the samples was mixed with an appropriate amount of 4x protein sample buffer and denatured for 10 min at 95 °C. 10 μl of the samples from all fractions were then analysed by SDS-PAGE and Coommassie staining.

2.2 Molecular Cloning

2.2.1 Polymerase Chain Reaction (PCR)

PCR reactions for molecular cloning were performed as 50 μl reactions with 25 ng template vector DNA using 2.5 U PfuTurbo polymerase (Agilent, Edinburgh), 200 μM dNTPs and 5 μl of 10x cloned Pfu reaction buffer (200 mM Tris, 20 mM $MgSO_4$, 100 mM KCl, 100 mM $(NH_4)_2SO_4$, 1% Triton-X-100, 1 $^{mg}/_{ml}$ nuclease-free BSA). Forward and reverse primers were added to a final concentration of 0.2 μM. The reactions were performed in the presence of 5% DMSO (Sigma) for EFHD2 cloning. The thermal cycles were run according to the protocol in Table 2.1 in a standard PCR machine (Biometra) using an appropriate annealing temperatures (AT) for the primers, which was determined by gradient PCR with varying annealing temperatures.

Standard PCR reactions were performed using a Taq DNA polymerase kit from

Step	Temperature	Duration [s]	
1	95 °C	180	
2	95 °C	30	repeat 35 x
3	AT	30	
4	72 °C	45–60	
5	72 °C	600	
6	4 °C	∞	

Table 2.1: Thermal cycle profile standard and cloning PCR reactions

Roche. 200 μM dNTPs, 0.8 U Roche Taq polymerase and 200 nM forward and reverse primers (all from Invitrogen, Paisley, UK) as well as 200 ng cDNA or 25 ng plasmid DNA were added to the reaction mix containing the appropriate amount of 10x reaction buffer (100 mM Tris-HCl, 15 mM $MgCl_2$, 500 mM KCl, pH 8.3) and the thermal cycles were run according to the protocol in Table 2.1.

2.2.2 Reverse transcription PCR (RT-PCR)

For reverse transcription PCR (RT-PCR) total RNA was extracted from tissue samples using Tri-reagent (Sigma). Before starting any RNA work, all surfaces and equipment were cleaned with autoclaved water containing 0.1% Diethylpyrocarbonate (DEPC, Sigma). 50–100 mg tissue was homogenised in 1 mL Tri-reagent using a micropistille and a 1 mL pipette tip at room temperature. The sample was then left at room temperature for 5 min for complete disintegration. 200 μl of chloroform were added per 1 mL of Tri-reagent used for the homogenisation inside the fume hood. The sample was shaken vigorously for 15 s and left at room temperature for 2 min followed by centrifugation at 12,000 $\times$ g for 15 min at 4 °C. The aqueous colourless phase containing the RNA was then transferred to a fresh reaction tube and 0.5 mL isopropanol were added per 1 mL of Tri-reagent

used. The samples were mixed by inversion and left 5 min at room temperature followed by centrifugation at 12,000 × g for 10 min at 4 °C. The RNA pellet was washed with 1 mL 75% ethanol and centrifuged at 7,500 × g for 5 min at 4 °C. The RNA-pellet was then air dried and resuspended in destilled DEPC-treated H_2O by incubation at 55–60 °C for 10 min. The RNA concentration was measured in a spectrometer at 260 nm and the total RNA was stored at -80 °C. Total RNA was digested with DNAse I. 5 U of RQI DNAse (Promega, Southampton, UK) were added to a mix of 5 μg total RNA and an appropriate amount of 10x RQI reaction buffer (Promega). The reaction mix was incubated at 37 °C for 45 min. 1 μl RQI DNAse Stop solution (Promega) was added per 10 μl reaction and the mix was incubated for 10 min at 65 °C.

cDNA was produced from the DNAse digested RNA using the Transcriptor First Strand cDNA Synthesis Kit (Roche) or the RevertAid Reverse Transcriptase (Fermentas, York, UK). 11 μl of the digested total RNA was mixed with 2 μl of random hexamer primers (60 μM final concentration) in a PCR reaction tube. RNA and primers were denatured for 5–10 min at 65 °C. 4 μl 5x reaction buffer (8 mM $MgCl_2$, 50 mM Tris-HCl, 30 mM KCl final concentration, pH 8.5), 20 U RNase inhibitor, 20 nmoles dNTPs and 10 U Transcriptor Reverse Transcriptase or 200 U RevertAid reverse transcriptase were added to the mix and made up to a final volume of 20 μl. The reaction mix was incubated at 25 °C for 10 min followed by 30 min at 55 °C (Transcriptor Reverse Transcriptse) or 60 min at 42 °C (RevertAid reverse transcriptase). The reverse transcriptase was then inactivated by heating to 85 °C for 5 min. 1 μl of the resulting cDNA was used for PCR reactions as described above using an appropriate PCR protocol.

2.2.3 Real time quantitative RT-PCR (qRT-PCR)

Real time quantitative RT-PCR reactions were performed on a MX3005P instrument (Agilent) and analysed using the MXPro QPCR software. qRT-PCR reactions were performed with 1 μl 1:2 diluted cDNA produced from DNAse digested total RNA from human brain using the Brilliant SYBR Green Mix (Agilent) adding gene specific primers to a final concentration of 100-200 nM. The qRT-PCR cycles were performed as described in Table 2.2.

Step	Temperature	Duration [sec]	
1	95 °C	600	
2	95 °C	10	repeat 35 x
3	AT	15	
4	72 °C	20	
5	95 °C	60	
6	55–95 °C (0.5 °C inc.)	5 sec/step	
7	4 °C	∞	

Table 2.2: Thermal cycle profile for qRT-PCR

Gene expression levels were calculated according to the ΔΔCt-Method, using actin-PCR as a housekeeping gene. Calculations were done using the following formula:

$$\Delta Ct = Ct_{GOI} - Ct_{actin}$$
$$\Delta\Delta Ct = \Delta Ct_{FTLD} - \Delta Ct_{Normal}$$
$$or: \Delta\Delta Ct = \Delta Ct_{AD} - \Delta Ct_{Normal}$$
$$Foldexpression(f.e.) = 2^{(-\Delta\Delta Ct)}$$
$$SE_{f.e.} = \sqrt{(ln(2)xf.e.)^2 xSE_{\Delta\Delta Ct}}$$

2.2.4 Restriction enzyme digest

Restriction digest reactions were performed on 5 μg template DNA using 50 U of high fidelity restriction enzymes (NEB) and NEB 10x restriction buffer 4 for 1 h or using 25–50 U of restriction enzymes (Promega) together with the appropriate 10x buffer (Promega) for 1–4 h at 37 °C. Restriction enzymes were then inactivated by incubation at 65 °C for 20 min. If possible, double restriction digests were performed at the same time. If enzymes were not compatible for double digest in the same buffer, the first restriction digest was performed, the product was cleaned up (see section 2.2.8) and the second restriction digest was performed as before.

2.2.5 Alkaline phosphatase treatment

DNA-samples were treated with calf intestine alkaline phosphatase (CIAP, Promega) in order to prevent the re-ligation of compatible ends. Following the restriction digest of typically 5 μg of vector DNA in a 20 μl reaction, 5 μl of 10x-CIAP-buffer (500 mM Tris, pH 9.3, 10 mM $MgCl_2$, 1 mM $ZnCl_2$, 10 mM spermidine) and 1 μl of 1 $^u/_{\mu l}$ CIAP were added and the mixture was incubated for 30 min at 37°C. These conditions usually approximated the use of 0.01 U of CIAP per picomole of DNA-ends. The treated DNA was then purified by agarose gel electrophoresis.

2.2.6 Agarose gel electrophoresis

Agarose gels were produced by melting the appropriate amount of agarose in 50 mL TBE buffer (89 mM Tris-Borate, 2 mM EDTA, pH 8.3 (Sigma)). Ethidium

bromide (Sigma) was added to the gel to a final concentration of 0.5 $^{\mu g}/_{ml}$ once it had cooled to about 60 °C and the gel was poured into a horizontal gel chamber (Hoeffer) and left to set for 20 min. DNA samples were prepared by adding an appropriate amount of 6x Orange G DNA sample buffer (45% glycerol, 89 mM Tris-Borate, 2 mM EDTA pH 8.3, 0.25% w/v Orange G) or Bromphenol Blue DNA sample buffer (62.5% glycerol, 0.625% SDS, 0.125% w/v Bromphenol Blue). DNA bands were separated at 70 V for 30–45 min. 5 μl Hyperladder I (Bioline) were separated in a seperate lane as a molecular weight marker. DNA bands were visualised by UV-transmission using a BioRad GelDoc system.

2.2.7 Polyacrylamide electrophoresis of DNA

Polyacrylamide gels for DNA electrophoresis were prepared with 5–8% of a 37.5:1 mixture of acrylamide:Bis-acrylamide, 0.07% APS and 0.04% TEMED in 1x TBE buffer. Vertical gels were poured between glassplates separated by a 1 mm spacer, appropriate combs were inserted and the gels were left to polymerise for 30 min–1 h. DNA samples were run at 50–60 V for 45 min–1 h and then stained with 0.5 $^{\mu g}/_{ml}$ ethidium bromide in TBE buffer for 15–20 min before gel bands were visualised by under UV-transmission using a BioRad GelDoc system.

2.2.8 Purification of DNA from agarose and neutral polyacrylamide gels

DNA bands were visualized under UV light and excised using a sterile razor blade. DNA bands were weighed and the DNA was purified from the agarose gel using a DNA gel-purification kit (QIAGEN) according to the manufacturer's protocol.

2.2.9 Ligation

Inserts were ligated into purified plasmids using 50 U T4 Turbo DNA ligase (Promega) together with the appropriate reaction buffer. Reactions were set up using different molar ratios of insert to plasmid (insert:plasmid, 0:1, 1:3, 1:6, 1:12), calculated according to the formula below and ligation reactions were performed at 16 °C over night or at room temperature over night or at 37 °C for 1 h.

$$\frac{(ng\ vector)x(kb\ insert)}{(kb\ vector)}x(molar\ ratio) = (ng\ insert)$$

2.2.10 Generation of chemically competent *E. coli*

DH5α bacterial cells were grown 16–18 h from a glycerol stock in 5 mL Luria Broth medium (Sigma)shaking at 210 rpm at 37 °C. 0.5 mL of this over night culture was then expanded in 50 mL LB medium until an OD(600 nm) of 0.3–0.5 was reached. Cells were pelleted for 10 min at 3,500 rpm and the bacterial pellet was resuspended in 20 mL sterile 100 mM $CaCl_2$. Cells were left on ice for 30 min and pelleted again by centrifugation at 1,500 rpm for 5 min. The resulting pellet was resuspended in 1 mL sterile 100 mM $CaCl_2$ and left on ice again for 30 min before they were used for transformations. For long-term storage, glycerol stocks were prepared according to the protocol in Section 2.2.14.

2.2.11 Generation of Magnesium-supercompetent *E. coli*

A frozen glycerol stock of STABL3 *E. coli* cells was streaked out on a LB-Agar plate containing 50 $^{\mu g}/_{ml}$ streptomycin and grown for 16–18 h at 37 °C. 10–12 large colonies were picked and used to inoculate 250 mL SOB medium (2% w/v bacto-tryptone, 0.55% w/v Bacto yeast extract, 10 mM NaCl, 10 mM KCl, 5 mM $MgSO_4$, 5 mM $MgCl_2$; prepared and sterilised without $MgCl_2$. Filter-sterilised $MgCl_2$ solution was added after autoclaving.) containing 50 $^{\mu g}/_{ml}$ streptomycin. The inoculated culture was incubated on ice for 10 min and then incubated at 18 °C (for up to 48 h) until an OD(600 nm) of 0.6 was reached. Cultures were placed on ice for 10 min and transferred to 50 mL centrifuge tubes. Cells were pelleted at 2500 × g for 10 min at 4 °C. Cells were then resuspended in 80 mL ice cold transformation buffer (TB: 10 mM PIPES, 55 mM $MnCl_2$, 15 mM $CaCl_2$,250 mM KCl; prepared without $MnCl_2$ and adjusted to pH 6.7 before $MnCl_2$ was added and the solution was filter-sterilised.), incubated on ice for 10 min and pelleted at 2500 × g for 10 min at 4 °C. Cells were resuspended in 20 mL TB and DMSO was added to a final concentration of 7%. The cell suspension was incubated on ice for 10 min and cells were split into 200–400 μl aliquots in cryogenic tubes and flash frozen in liquid nitrogen. Cells were stored at -80 °C and transformations were performed according to the standard transformation protocol.

2.2.12 Transformation of *E. coli*

10 μl of a 20 μl ligation product, 1–5 μl purified DNA or 5–10 μl of a recombination reaction was added to 200 μl chemically competent bacteria, gently mixed with a 1000 μl pipette tip and on ice for 30 min. Cells were then heat shocked for 45 s at

42 °C and subsequently left on ice for 1–2 min. 800 μl pre-warmed SOC medium (2% Tryptone, 0.5% yeast extract, 10 mM NaCl, 2.5 mM KCl, 10 mM $MgCl_2$, 20 mM glucose) were added and the mix was incubated in a 15 mL conical tube at 37 °C shaking at 210 rpm for 1 h. Luria Broth (LB) agar (1% Tryptone, 0.5% yeast extract, 0.5% NaCl, 1.5% Agar; Sigma) plates were prepared containing the appropriate antibiotic (ampicillin: 100 $^{\mu g}/_{ml}$; chloramphenicol: 34 $^{\mu g}/_{ml}$; kanamycin: 50 $^{\mu g}/_{ml}$, tetracycline: 10 $^{\mu g}/_{ml}$) and cells were spread and grown for 16–18 h at 37 °C. For transformations with pBlueScript plasmid, cells were grown on plates also containing 0.1 mM IPTG and 2% X-gal and only white colonies were picked the next day for over night culture.

2.2.13 Plasmid Purification

A single colony from an agar plate grown for 16–18 h at 37 °C was picked with a pipette tip and grown in LB medium (1% Tryptone, 0.5% yeast extract, 0.5% NaCl; Sigma) containing the appropriate antibiotic for 16–18 h at 37 °C, shaking at 210 rpm. DNA was then purified using a QIAGEN Miniprep Spin Column Kit (QIAGEN) according to the manufacturer's protocol and eluted from columns with nuclease-free water. Larger amounts of DNA were purified from 100–150 mL overnight cultures using the PureYield Plasmid Midiprep kit (Promega) according to the manufacturer's centrifugation protocol or from 250–500 mL over night cultures using the QIAGfilter Maxiprep kit (QUIAGEN). Nuclease-free water was produced by stirring with 0.1% Diethyl-pyrocarbonate (DEPC) over night followed by autoclaving in order to inactivate the DEPC. The DNA concentration was measured in a UV-1601 spectrophotometer (Shimadzu) by measuring

the absorbance at 260 nm. DNA purity was estimated by also measuring the absorbance at 280 nm and building the ratio of the absorbances at 260 nm and 280 nm. A ratio of 1.8–2.0 was regarded as pure. Purified DNA was stored at -20 °C in water or TE buffer (10 mM Tris, 1 mM EDTA, pH 8.0).

2.2.14 Generation of glycerol stocks

For long-term storage of bacterial cultures, glycerol stocks were prepared from fresh over night cultures by mixing 600 μl over-night LB-culture with 400 μl 50% glycerol (20% final concentration). Glycerol stocks were flash frozen in liquid nitrogen and stored at -80 °C.

2.2.15 Gateway® cloning

Lentiviral constructs were produced using the Gateway cloning system (Invitrogen) based on site specific recombination. For the first cloning step producing an entry clone, attB1 and attB2 site containing gene specific primers were created and PCR products were produced by conventional PCR using TurboPfu polymerase (Agilent). PCR products were purified after agarose gel electrophoresis and then cloned into the pDONR201 donor vector (Invitrogen) by recombination using the BP-Clonase II kit (Invitrogen). For the BP-reaction 50 fmol (150 ng) of supercoiled pDONR201 vector and 150 fmol of attB site containing PCR products were used. Reactions were performed over night at 25 °C using 0.5 μl of enzyme together with the appropriate amounts of vector and PCR product and made up to a final volume of 10 μl with TE-buffer. The amount of PCR product used in the reaction was calculated using the following formula:

$$ng = (fmol)x(N)x(\frac{660\ fg}{fmol})x(\frac{1\ ng}{10^6\ fg})$$

The recombination reaction was stopped by addition 1 μl of 2 $^{\mu g}/_{\mu l}$ Proteinase K solution and incubation at 37 °C for 10 min. 5 μl or all of the reaction was then transformed into STABL3 *E.coli* cells (Invitrogen) propagated and made chemically supercompetent as described in section 2.2.11. These cells do not contain the F1 episome encoding the ccdA gene and allow for negative selection with the ccdB gene product against failed recombination reactions. Transformants were plated on agar plates containing the appropriate antibiotic (kanamycin for pDONR201) and incubated over night at 37 °C. Colonies of different sizes were picked the next day and grown for 16–18 h at 37 °C and 210 rpm in 5 mL LB medium containing kanamycin. Purified entry clones were confirmed by analytical restriction digest and sequenced using pDONR201 specific primers (see Table C.1).

Expression clones were produced by recombination of the gene of interest from the entry clone into the destination vector (pSX69, a kind gift from Dr. Paul Reynolds/Prof. Richard Elliot) using the LR-clonase II kit (Invitrogen). Reactions were prepared on ice using 0.5 μl of LR clonase and 50 fmol of each pSX69 destination vector and the entry clone. The amount of DNA used for these reactions was calculated in the same way as for the BP-reaction. Reactions were made up to a total of 10 μl using TE-buffer and incubated at 25 °C over night. Reactions were stopped by addition 1 μl of 2 $^{\mu g}/_{\mu l}$ Proteinase K solution and incubation at 37 °C for 10 min. 5 μl or all of the reaction was then transformed into STABL3 cells and transformants were plated out on agar plates containing

the appropriate antibiotic (ampicillin for pSX69) and incubated over night at 37 °C. Colonies of different sizes were picked the following day and grown grown for 16–18 h at 3 °C and 210 rpm in 5 mL LB medium containing ampicillin. Purified expression clones were sequenced using psX69 specific primers (see Table C.1).

2.3 Cell culture

2.3.1 Culture of cell lines

The Human Embryonic Kidney (HEK293) cell line was cultured in high glucose modified Eagle's medium (MEM) (Sigma, ♯ M2279) supplemented with 10 % fetal calf serum (FCS, Seralab) and 2 mM L-glutamate (Sigma) as well as 100 $^{U}/_{ml}$ penicillin and 0.1 $^{mg}/_{ml}$ streptomycin (Sigma) and non-essential amino aicds (Sigma) at 37 °C and 5% CO_2. The SK-N-SH neuroblastoma and the 293T Lentigrade HEK cell lines were grown in Dulbecco's Modified Eagle's Medium (DMEM) (Sigma, ♯ D5671) supplemented with 10 % FCS and 2 mM L-glutamate (Sigma) as well as 100 $^{U}/_{ml}$ penicillin and 0.1 $^{mg}/_{ml}$ streptomycin (Sigma). Cells were thawed from liquid nitrogen quickly, resuspended in 10 mL of cold culture medium and pelleted before they were resuspended in culture medium and plated out in a culture dish or flask containing fresh culture medium and grown until confluent. For slow growing cell lines, 50% of the culture medium was changed every third day. Cells were subcultured 2 times per week in a class II sterile hood. The culture medium was removed and cultures were rinsed twice with 10 mL pre-warmed sterile PBS. All of the PBS was removed and 1 mL of sterile

0.025% Trypsin/EDTA solution (Sigma) was added. Cells were trypsinised at 37 °C, aspirated with 10 mL of pre-warmed culture medium containint 10% FCS and transferred to a 15 mL centrifuge tube. Cells were pelleted at 800 × g for 5 min and the cell pellet was resuspended in 5–10 mL of culture medium. An appropriate amount of cells was plated into a fresh culture dish or flask containing culture medium and cells were grown in a humidified Heraeus incubator at 37 °C and 5% CO_2.

2.3.2 Primary cortical neuron cultures

Primary neuronal cultures were prepared from embryonic day 14 mouse embryos. At day 14 of pregnancy the mother was sacrificed by cervical dislocation and the embryos were dissected from the uterus. Brains were dissected from the embryos using tungsten needles and placed in pre-warmed PBS. Meninges were removed and cortices were separated from the cerebellum and diencephalon. Cortices from one litter were transferred to a 15 mL centrifuge tube and rinsed with pre-warmed PBS. The tissue was then incubated for 5 min at 37 °C in PBS containing 50 $^{\mu g}/_{ml}$ trypsin (Worthington biochemical corporation, ♯ TRSEQII). At the end of the trypsinisation period, the tissue was allowed to settle and the trypsin solution was removed carefully. The cortices were then rinsed in 1 mL cortical plating medium (MEM (Sigma, ♯ M4655), 10% horse serum (HS), 10% FCS) and resuspended in 1 mL medium to produce a single cell suspension. Neurons were plated on culture dishes coated over night with 1–10 $^{\mu g}/_{ml}$ poly-D-lysine (30–70 kDa, Sigma) at a density of 2–2.5 × 10^5 cells per cm^2. The culture medium was changed 6–8 h after plating in cortical plating medium to cortical serum-free medium (MEM +

2% serum-replacement 2, 80 μM 5-fluorodeoxy-uridine, 24.5 μM KCl, 100 $^{U}/_{ml}$ penicillin and 0.1 $^{mg}/_{ml}$ streptomycin (Sigma)). Cells were cultured in cortical serum-free medium for another 48–72 h before 50% of the medium was replaced with fresh medium. Experimental procedures were conducted after 72 h *in vitro*. 50% of the cortical serum-free medium was replaced every 72 h.

2.3.3 Primary neuron transfection

Primary neuronal cells were transfected using the Amaxa nucleofection technique with the primary mouse nucleofector kit (♯ VPG1001) according to the manufacturer's protocol (Zeitelhofer et al., 2007). 6×10^6 cells were transfected in suspension in 100 μl nucleofection solution and cells were plated out in 35 mm culture dishes containing 2 mL of pre-warmed cortical plating medium. After 6–8 h incubation at 37 °C and 5% CO_2, the culture medium was replaced with cortical serum-free medium and cells were cultured for another 48–72 h before conducting other experimental procedures.

2.3.4 Cell line transfection

HEK293 cells were transfected using GeneJammer reagent (Stratagene). For a 35 mm culture dish, GeneJammer was diluted in a 1:3 ratio to the DNA transfected (i.e. 3 μl Gene Jammer per 1 μg of DNA) in Opti-MEM medium (Sigma) without antibiotics and incubated for 5 min at room temperature. 2 μg of DNA was added and the mix with a total volume of 100 μl was then incubated for 20 min at room temperature. The transfection mix was added drop wise to the cells plated to 80–90% confluency in 2 mL culture medium without antibiotics in

a 35 mm dish 24 h before. Cells were analysed 48 h post-transfection.
SK-N-SH neuroblastoma cells were transfected using Lipofectamine 2000 (Invitrogen) reagent. For a 35 mm cell culture dish, Lipofectamine 2000 was diluted in a 1:2.5 ratio to the amount of DNA transfected in 125 μl of serum-free DMEM or OptiMEM medium without antibiotics and incubated for 5 min at room temperature. 2 μg of DNA were diluted in 125 μl of serum-free DMEM, mixed with the Lipofectamine 2000 containing solution and incubated for 20 min at room temperature. The transfection mix was then added to the SK-NSH cells in 1.75 mL serum-free DMEM without antibiotics, which were plated in a 35 mm culture dish to 90% confluency 24 h before. Half of the medium was replaced with DMEM supplemented with 20% FCS and 4 mM L-glutamate (Sigma) after 4 h and cells were incubated in this medium for another 48 h before further analysis.

2.3.5 Lentivirus production and cell infection

HEK293T lentigrade cells were grown in DMEM medium supplemented with 10% FCS and 100 $^{U}/_{ml}$ penicillin and 0.1 $^{mg}/_{ml}$ streptomycin and seeded in a 96 mm culture dish to 80–90% confluency. The following day, cells were triple transfected with 1.2 μmol of plasmids encoding the viral packaging and polymerase genes (2.1 μg pSD11 and 6.3 μg pSD16, see Figure B.2) and an equimolar amount of the lentiviral expression vector encoding the gene of interest together with appropriate packaging signals as well as the VSV-G glycoprotein. Cells were transfected using 2.5 volumes of Lipofectamine 2000 reagent per 1 μg of DNA. The Lipofectamine 2000 and DNA mixtures were each prepared in 0.75 μl of Opti-MEM medium (Gibco) per 96 mm dish, vortexed and incubated for 5 min

at room temperature. The DNA and Lipofectamine 2000 were then mixed and incubated for 20 min at room temperature and then added drop wise to the cells cultured in 13.5 mL antibiotic-free DMEM medium containing 10% FCS. With the start of virus production 24 h after transfection, the transfection medium was removed, replaced by 4 mL normal DMEM growth medium and the cells were moved into designated viral incubators and handled in designated viral tissue culture hoods only. The cells were incubated for another 24 h and the lentiviral supernatant was collected the next day, stored at 4 °C and 4 mL of pre-warmed normal growth medium was again added to the cells which were incubated for further 24 h. The second batch of lentiviral supernatant was combined with the first one and the solution filtered through a sterile 0.45 μm syringe driven filter in order to remove debirs. Polybrene (Invitrogen) was added to the viral supernatant at a final concentration of 8 $^{\mu g}/_{\mu l}$. The viral supernatant was then added to the target cells for infection. After a 4 h incubation period, the viral supernatant was removed and replaced by normal growth medium. If primary cortical neurons were infected, the infection time was extended to a maximum of 8 h and the virus production was performed in DMEM supplemented with 0–1% FCS. Cells were analysed 48–72 h after viral infection.

2.3.6 Amyloid-β treatment of cell cultures

Monomeric amyloid-β peptides were prepared from lyophilised amyloid-β purchased from Innovagen (Sweden) or GenicBio (China) according to published protocols for Aβ oligomer and fibril formation (Stine et al., 2003). 0.1 mg lyophilised peptide (22 pmols Aβ42, MW 4514.1 $^{g}/_{mol}$; 23 pmols Aβ40, MW 4329.9 $^{g}/_{mol}$)

was dissolved in 1 mL ice cold hexa-fluoro-isopropanol (HFIP, Sigma) and left to dissolve for 1 h at room temperature in a closed reaction tube. Ten 100 μl aliquots were produced and the HFIP wa left to evaporate over night in a fume hood. Samples were then dried under vacuum for 1 h and subsequently stored at -20 °C.

For cell culture treatments a 0.1 mg aliquot of monomerised peptide was dissolved in sterile anhydrous dimethylsulfoxide (DMSO, Sigma) to a final concentration of 5 mM, vortexed and sonicated for 10 min. The peptide was then diluted with PBS to a final concentration of 1 mM and incubated at 37 °C (Aβ40) or 4 °C (Aβ42 for 24 h. Amyloid-β peptides were then added to 1 mL culture medium to produce a final concentration of 22-23 μM. Aggregated amyloid-β(25–35) peptides were also produced from lyophilised amyloid-β. A 1 mM solution of amyloid-β (25–35) in distilled sterilised water was produced and stored at - 20 °C. An aliquot was then thawed and mixed with 1 volume of sterile PBS and incubated at 37 °C for 3–5 days. Aggregated amyloid-β(25–35) was added to the cell cultures at a final concentration of 25–50 μM.

2.3.7 Cell survival and viability assays

Cell survival was assessed by cell counting. For this, phase-contrast pictures of 5 fields of view in a 20× or 40× objective were taken of each condition before and after the intended treatment and the number of cells was counted using the ImageJ software.

2.3.7.1 MTT assay

The reduction of 3-(4,5-dimethylthiazol-2-yl)-2,5-diphenyltetrazolium bromide (MTT) by mitochondrial dehydrogenases was measured in a 96-well plate format. 12.5 μl of a 5 $^{mg}/_{ml}$ solution of MTT in PBS was added per well to 50 μl culture medium. The cells were then incubated with the MTT for 4 h (cell lines) or up to 6 h (primary neurons) in a humidified CO_2 incubator at 37 °C. The medium and MTT solution were then removed and the cells were lysed by addition of 100 μl DMSO. The absorbance of the reduced formazan was then measured at 570 nm in a FLUOstar OPTIMA multidetection microplate reader.

2.4 Immunocytochemistry

Immunocytochemistry was performed on cells grown on glass-coverslips. Coverslips were placed on a piece of Nescofilm (VWR) and directly fixed with cold 4% PFA solution for 10 min (cytoskeleton stainings) or 15–20 min (cytoplasmic and organellar stainings) at room temperature. Cells were permeabilised with PBS-TT (PBS, 0.1% Tween-20, 0.1% Triton-X-100) for 15 min and non-specific antibody binding sites were blocked with ICC blocking solution (10% horse serum in PBS-TT) for 20 min. Primary antibodies were diluted in blocking solution as indicated in Table A.1 and incubated for 2 h at room temperature or overnight at 4 °C, followed by 3 times 5 min washes with PBS-TT. Secondary fluorochrome conjugated antibodies were diluted in ICC blocking solution as indicated in Table A.1 and incubated for 1 h at room temperature in the dark followed by 3 times 5 min washes with PBS-TT. 4',6-Diamidino-2-Phenylindole (DAPI, Sigma) was added to the secondary antibody solution at a final concentration of

1 $^{\mu g}/_{ml}$ as a nuclear counterstain. Coverslips were mounted on microscope slides in Mowiol-488 mounting medium (10% Mowiol-488, 2.5% glycerol, 100 mM Tris, pH 8.5) containing 1.5% propyl-gallate as an antifade or in ProlongGold mounting medium (Invitrogen).

2.5 Statistical analysis

Statistical analysis was performed using Prism statistical analysis softwaere (Graph Pad). 1-way analysis of variance (ANOVA) with Tukey's multiple comparison post-hoc test, 2-way ANOVA with Bonferroni post-hoc test or T-Test were performed as indicated in figure legends. Significance was denoted with stars accoring to $p \leq 0.05$ (1 star), $p \leq 0.01$ (2 star), $p \leq 0.001$ (3 star).

CHAPTER 3

ENDOPHILIN-1 CAN MODULATE STRESS KINASE SIGNALLING IN NEURONS

3.1 Introduction

3.1.1 c-Jun N-terminal kinase (JNK) in the CNS

c-Jun N-terminal kinases (JNK) are encoded by 3 genes (JNK1–3), giving rise to 10 isoforms of either 46 kDa or 54 kDa. They belong to the group of mitogen activated protein kinases (MAPK), which phosphorylate serine and threonine residues in their targets (Mehan et al., 2011). Similar to p38, JNK is a stress activated protein kinase (SAPK) and is activated by a wide range of extracellular signals which leads to the activation of the MAPK kinases MKK4 and MKK7, which phosphorylate JNK on specific tyrosine and threonine sites, causing its activation. MKK4/7 are activated themselves by a series of MAP-triple kinases (MAP3Ks), which are often activated by the small GTPases Ras and Rac, the Rho-family GTPase Cdc42 or the Ste20-family protein kinase GLK (Mehan et al., 2011; Diener et al., 1997). Known components of the JNK signalling cascade are depicted in Figure 3.1.

JNK-interacting proteins 1, 2 and 3 (JIP1/2/3) fulfil crucial functions in the activation of this signalling cascade by acting as scaffolding proteins for JNK and positioning it in the vicinity of specific activators, substrates or inactivators (Mehan et al., 2011). Their scaffolding function is also subject to regulation as, for example, cleavage of JIP1 by caspase 3 can cause its disassembly from JNK during apoptosis (Vaishnav et al., 2011).

As suggested by the name, the best described function of JNK is phosphorylation of the transcription factor c-Jun at its N-terminus. This phosphorylation has been reported to increase c-Jun's half-life and enhance its transcriptional activity by forming the important transcription factor complex activating protein

1 (AP-1) through homo- and heterodimerisation of c-Jun with c-fos or the activating transcription factor 1 (ATF-1) (Shaulian, 2010). Formation of the AP-1 complexes plays an important role in the context-dependent control of cell cycle progression, cell survival or p53-mediated cell death (Shaulian, 2010).

Apart from its role in stress-induced cell death, JNK signalling modulates a number of activities specifically in neurons, which are also summarised in Figure 3.1. As mentioned in Chapter 1, JNK is able to phosphorylate APP at Thr^{668}, thereby regulating its processing with the help of JIP1b (Colombo et al., 2009; Matsuda et al., 2001) and JNK has also been implicated in the phosphorylation of tau (Reynolds et al., 2000; Swatton et al., 2004). Other effects of JNK-signalling which are important for neuronal function include the stabilisation of microtubules through MAP1 and MAP2 phosphorylation (Chang et al., 2003) and the dissociation of kinesin proteins from their tubulin tracks (Stagi et al., 2006). In this respect, it is of interest that a differential effect of JNK isoforms on cell death (mainly JNK2 translocation to the nucleus) and microtubule dependent neurite outgrowth (dependent on all isoforms) in hippocampal neurons has been found (Eminel et al., 2008). A differential role of different JNK isoforms has also been suggested by studies in different JNK knockout animals where a mainly neuroprotective role for JNK1 in contrast to a cytotoxic effect of JNK3 has been described (Brecht et al., 2005). Positive effects of JNK-signalling on the formation of hippocampal LTP and LTD in neurons have also been reported and might be due to JNK-mediated modulation of the microtubule network or its proposed effects on AMPA receptor (AMPA-R) internalisation (reviewed in Mehan et al. (2011)). In contrast, JNK1 can also be involved in the inhibition of hippocampal LTP and cell death in response to Aβ exposure (Minogue et al., 2003). This underlines

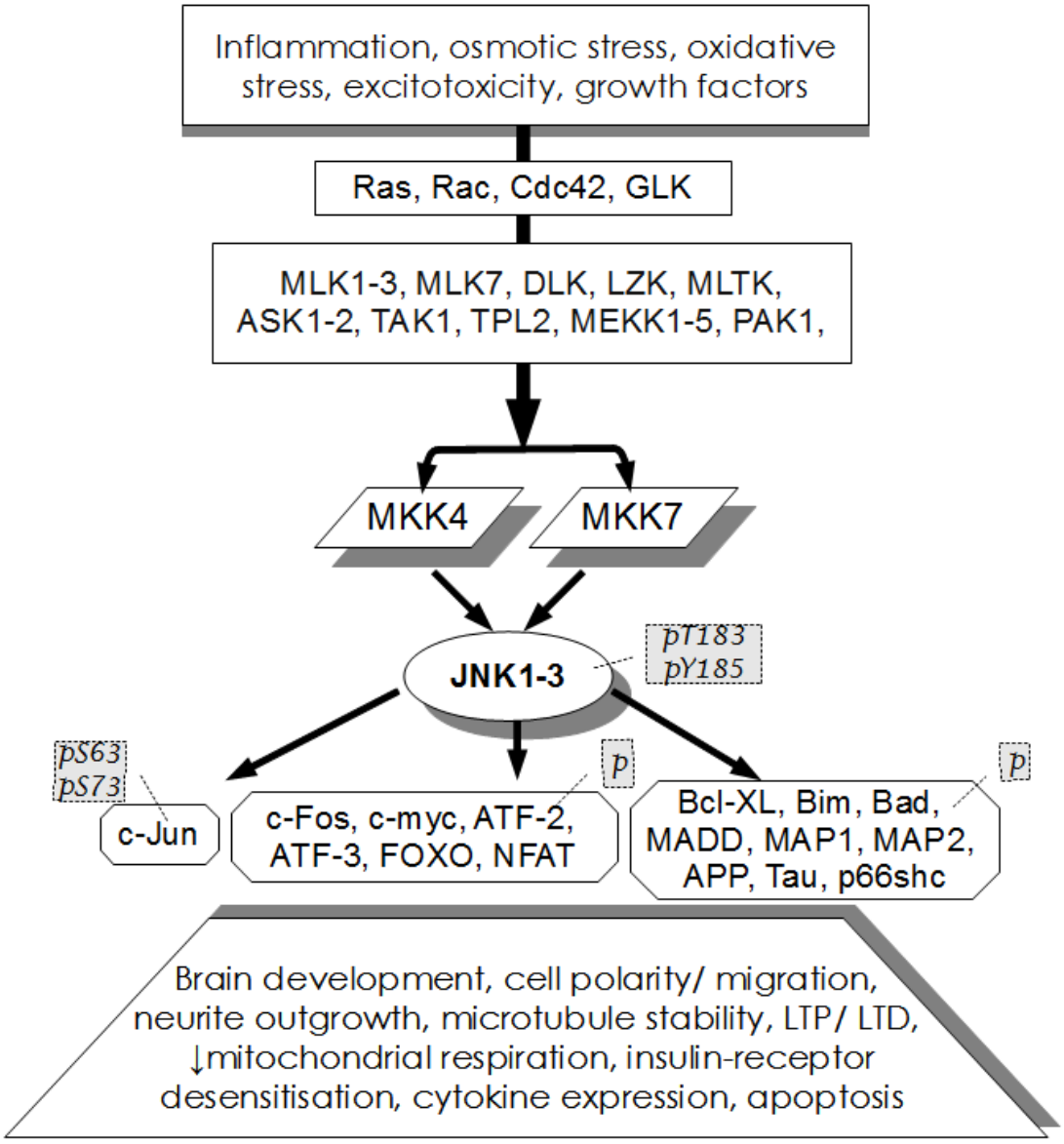

Figure 3.1: The SAPK/ JNK signalling cascade. ASK: apoptosis signal regulating kinase, ATF: activating transcription factor, Cdc42: cell division cycle 42, GLK: germinal center like kinase, LZK: leucine-zipper bearing kinase, MADD: MAP-kinase activating death domain, MAPK: mitogen activated protein kinase, MKK: MAPK kinase, MLK: mixed lineage kinase, MLTK: MLK-like mitogen activated protein triple kinase, PAK: p21 activated kinase, TAK: transforming growth factor β activated protein kinase, TPL: tumour progression locus. Modified with permission from Humana Press (Mehan et al., 2011).

the fact that the outcome of the activation of JNK in neuronal networks strongly depends on the specific context and the availability of the different isoforms.

3.1.2 Endophilin-1 function and its proposed role in AD

Endophilin A1 (Ep-1) is a plasma- and synaptic vesicle membrane associated protein. It contains an N-terminal Bin/Amphiphysin/Rvs (N-BAR) domain comprising α-helical structures, which allow its interaction with membrane lipids, induction of membrane curvature and homo- or heterodimerisation with other endophilins. The N-BAR domain is followed by a proline rich domain (PRD) and a C-terminal Grb2-like src homology 3 (SH3) domain for the interaction with specific PRDs in other proteins (see Figure 3.2). Ep-1 also contains a putative nuclear localisation sequence (NLS) but it has not been reported to localise to the nucleus in the literature (Reutens and Begley, 2002). Ep-1 is also known as Sh3p4, SH3GL2, CNSA2, EEN-1 or SH3DA2 and forms a unique group of SH3 proteins together with the closely related proteins endophilin A2 (SH3p8/ SH3GL1) and endophilin A3 (SH3p13/ SH3GL3). Of these isoforms, Ep-1 is expressed mainly in the brain, while Ep-3 is enriched in testes and the brain and Ep-2 is expressed ubiquitously (Giachino et al., 1997). In contrast to endophilin A proteins, endophilin B1 and B2 are associated with organelle membranes and have been reported to regulate mitochondrial morphology, apoptosis and autophagy (Kjaerulff et al., 2010).

Ep-1 was initially identified as a binding partner for the lipid phosphatase synaptojanin and for dynamin in synapses (Sparks et al., 1996; Micheva et al., 1997; Ringstad et al., 1997) and also found to co-localise and interact with synap-

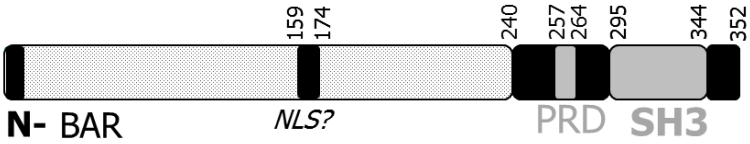

Figure 3.2: Endopohilin A1 structure. N-BAR: N-terminal Bin/Amphiphysin/Rvs domain, NLS: putative nuclear localisation signal, PRD: proline rich domain, SH3: src homology 3. Modified with permission from Nature Publishing Group (Gallop et al., 2006).

tophysin (Ringstad et al., 2001). Accordingly, a role for endophilin-1 in synaptic vesicle endocytosis, mediated by dimerisation and membrane interaction through its N-BAR domain, has been demonstrated *in vitro* and *in vivo* (Ringstad et al., 1999; Gallop et al., 2006; Bai et al., 2010). Furthermore, interaction of Ep-1 with voltage-gated Ca^{2+} channels (VGCC), has been shown to be important for coordinated synaptic vesicle endocytosis to occur (Chen et al., 2003). Notably, the study also demonstrated that the interaction with VGCCs was negatively regulated binding of Ca^{2+} to Ep-1 in a region around its PRD which occurred at increased levels of Ca^{2+}. The authors suggested that this might be a mechanism of targeting of Ep-1 to sites of synaptic activity, where VGCCs are located and regulating its function in response to Ca^{2+} fluxes (Chen et al., 2003). Data from a recent study by Weston et al. (2011) provided evidence that interactions *via* the Ep-1 SH3 domain can also modulate its endocytotic function. It has been found that Ep-1 can interact with the vesicular glutamate transporter VGLUT1 through its SH3 domain (Vinatier et al., 2006; De Gois et al., 2006). Using VGLUT1/2 knockout models, lentiviral overexpression and knock down of Ep-1, Weston et al. (2011) showed that inherent differences in the dynamics of glutamate release from VGLUT1 and VGLUT2 expressing synapses are caused by the binding of Ep-1 to VGLUT1 (but not VGLUT2). The authors therefore proposed

a mechanism by which binding of VGLUT1 reduces the amount of Ep-1 available for endocytosis and therefore VGLUT1 recycling, which results in a decreased probability of glutamate release in VGLUT1 expressing synapses.

Ep-1 also influences the enodcytic trafficking of a number of membrane proteins through direct or indirect interactions *via* its SH3 domain. Binding of Ep-1 to the G-protein coupled β1-adrenergic receptor has been shown to promote receptor internalisation and silencing (Tang et al., 1999) and similarly, interactions with CIN85 (Soubeyran et al., 2002) and ataxin-2 (Ralser et al., 2005; Nonis et al., 2008) link Ep-1 to ligand induced EGF-receptor internalisation and silencing and to actin remodelling. It has been proposed that Ep-1 could also modulate the transport, targeting or processing of ADAM9 and ADAM15, which act as metalloprotease disintegrins and are involved in cell–cell interactions (Howard et al., 1999).

It has emerged that Ep-1 can afurthermore have functions which are not directly related to its role in endocytosis. Two studies have linked Ep-1 to the regulation of the turnover of synaptic proteins and to BDNF-induced dendritic development. Trempe et al. found that all isoforms of endophilin A can interact with the ubiquitin E3 ligase parkin in a phosphorylation dependent manner and that Ep-1 can affect the ubiquitination of its PRD containing binding partners in synaptosomes (Trempe et al., 2009). Dendritic development is dependent on BDNF-induced signalling events and upon binding of BDNF, its receptor TrkB is internalised in a process that requires the transmembrane protein retrolinkin (Fu et al., 2011). The study by Fu et al. revealed that the subsequent activation of the MAP kinase ERK1/2 depends on the recruitment of Ep-1 by retrolinkin to early endosomes containing TrkB, rab5 and APP-like protein 1 (APPL1) (Fu

et al., 2011).

In addition, research has also revealed that Ep-1 is able to activate the SAPK/JNK signalling cascade. Expression of Ep-1 in cell lines can cause the phosphorylation of JNK and this depends on the interaction between the Ep-1 SH3 domain and GLK (Ramjaun et al., 2001). In synaptosomes from mouse cortex, Ep-1 has been found to be associated with the same endocytic vesicles as JIP3 (also known as Sunday Driver, syd) (Abe et al., 2009), which brings Ep-1 into the proximity of the JNK-signalling components. In 2008, Ren et al. showed that overexpression of Ep-1 also leads to the activation of JNK in primary cortical neurons and that this effect is abolished upon deletion of the Ep-1 SH3 domain (Ep-1ΔSH3) (Ren et al., 2008). Ren et al. also demonstrated that Aβ-induced activation of JNK is reduced to background levels when mutant Ep-1ΔSH3 was expressed, while there was a tendency towards higher levels of phosphorylated JNK in Aβ treated neurons expressing full length Ep-1 (Ren et al., 2008), suggesting that Ep-1 can facilitate JNK-activation. As mentioned in Chapter 1, the study also identified Ep-1 as specifically up-regulated in mAPP/ABAD double transgenic mice and confirmed this finding by western blotting and immunohistochemistry (Ren et al., 2008). Importantly, it was also found that Ep-1 protein levels are increased in the brains of AD patients compared to controls and concluded that this might point towards a new mechanism of how stress kinase signalling becomes activated during AD pathology.

3.2 Aims of this chapter

The cellular outcome of the up-regulation of endophilin A1 in AD has not been described in detail. Therefore, the aim of the work described in this chapter was to dissect out which components of the JNK-signalling cascade are activated in response to the overexpression of Ep-1 in primary neurons. It was first planned to confirm the activation of JNK and its downstream target c-Jun in human brain tissue affected by dementia. As a next step, JNK-activation was investigated in primary neuronal cultures overexpressing Ep-1 and subsequently it was hoped to identify which targets become phosphorylated as a result of JNK activation under these circumstances. Finally, the cellular effects of the activation of these downstream targets was be studied in primary neurons in more detail.

3.3 Activation of JNK and c-Jun in human AD

An increased activation of c-Jun-N-terminal kinase in Alzheimer's disease has been described before (see Chapter 1.4). In order to validate these previous findings, I analysed the status of c-Jun-N-terminal kinase (JNK) in samples of brains from human dementia sufferers by western blotting. Tissue samples from five individuals with diagnosis of AD, four individuals with diagnosed frontotemporal lobar degeneration (FTLD) and five age-matched non-demented control individuals were kindly provided by the Manchester brain bank through Prof. David Mann. From each individual, samples from the frontal cortex (FCx), the hippocampus (Hippo) and the cerebellum (Cere) were analysed. An assessment of amyloid plaque pathology and neurofibrillary tangle pathology in these brain

samples was performed by pathologists at the Manchester brain bank. Scores representing the extend of pathology found by histological stainings for Aβ and hyperphosphorylated tau (0 = no pathology detected; 4 = severe pathology with strong immunoreactivity) are given in Table 3.1.

ID	Diagnosis	FCx		Hippo		Cere	
		tau	amyloid	tau	amyloid	tau	amyloid
08/01	AD 1	4	4	3	3	0	1
09/15	AD 2	3	3	3	2	0	0
10/07	AD 3	4	4	3	3	0	1
10/08	AD 4	4	4	3	3	0	1
09/01	AD 5	3	3	2	2	0	0
94/13	FTLD 1 (PGRN)	0	0	0	0	0	0
96/14	FTLD 2 (Pick's)	4	0	4	0	0	0
98/04	FTLD 3 (Pick's)	4	0	4	0	0	0
01/01	FTLD 4 (exon10 +16)	4	1	4	0	0	0
03/06	FTLD 5 (Pick's)	3	0	4	0	0	0
09/18	FTLD 6 (exon10 +16)	4	0	4	0	0	0
07/13	control 1	0	0	0	0	0	0
08/04	control 2	1	2	1	2	0	0
08/28	control 3	0	2	1	2	0	0
08/29	control 4	1	3	1	2	0	0
09/05	control 5	0	1	1	0	0	0

Table 3.1: Pathological assessment of human brain samples with dementia from the Manchester brain bank. Scores refer to the amount of pathology (amyloid plaques or neurofibrillary tangles) detected by immuo-histochemistry against Aβ or hyperphosphorylated tau. Low scores mean little or no detection of amyloid or neurofibrillary tangles, high scores mean large amount of pathology. FCx: frontal cortex, Hippo: hippocampus, Cere: cerebellum. AD: Alzheimer's disease, FTLD: frontotemporal lobar degeneration with mutations in progranulin (PGRN), a mutation in the tau gene on chromosome 17 in the intron following exon 10 at position +16 (exon10 +16) or with Pick's disease (Pick's), control: age-matched non-demented individuals. The assessment was done by pathologists at the Manchester brain bank.

Proteins were extracted from 300 mg of human brain tissue from control individuals, AD sufferers or patients diagnosed with FTLD and 20 μg of protein

was subjected to SDS-PAGE as described in Chapter 2.1.1. Figure 3.3 shows the results of the western blot analysis and the quantification of the stained bands by densitometry. Staining for total JNK protein revealed a number of bands in the human brain samples corresponding to different isoforms and to phosphorylated species of JNK. A double band appeared at 40–45 kDa, another band separated at approximately 50 kDa, which was the only band detected by the antibody directed against Thr^{183}/ Tyr^{185}-phosphorylated JNK and a fourth band appeared at about 60 kDa. Significantly increased signals for phosphorylated JNK relative to total JNK protein could be detected in samples from brains affected by AD and FTLD compared to age matched non-demented controls. The strongest increase in JNK phosphorylation was detected in the hippocampus and cerebellum of these brains, while in the frontal cortex, only samples from FTLD patients showed a significant increase in phosphorylated JNK levels.

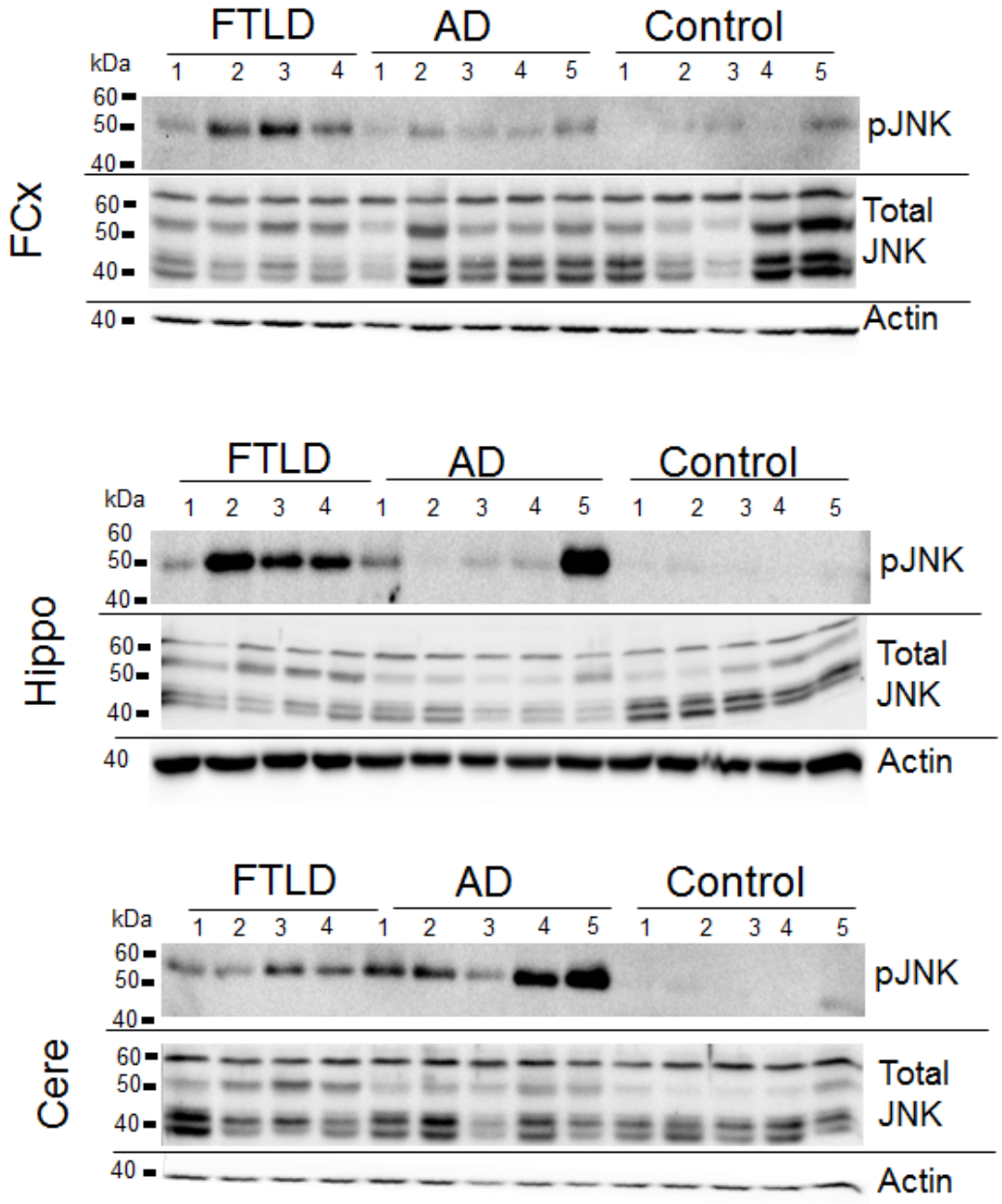

(a)

Figure 3.3: Phosphorylated JNK in human brains with dementia.

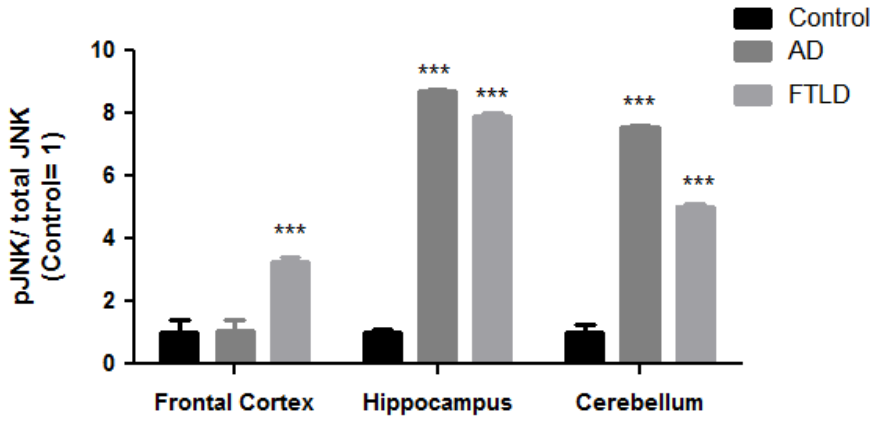

(b)

Figure 3.3: Phosphorylated JNK in human brains with dementia (continued). Levels of Thr^{183}/Tyr^{185} phosphorylated JNK in different brain regions from human dementia sufferers. a) FCx: frontal cortex, Hippo: hippocampus, Cere: cerebellum. Actin was used as a loading control. Approximate molecular weight sizes from a pre-stained protein marker are indicated on the left of each western blot. b) Quantification of stained bands by densitometry. Phosphorylated JNK bands were expressed as a ratio over total JNK levels and mean values were compared. Control = 1. Error bars show SEM. Significance was tested using 2-way ANOVA and Bonferroni post-hoc test. FTLD: Frontotemporal lobar degeneration, AD: Alzheimer's disease.

I then tested the levels of phosphorylated c-Jun at Ser^{63} in the same samples, as c-Jun is a target of JNK. Protein samples were prepared in the same way as before and total and phosphorylated c-Jun was detected by immuno-western blotting. The results of the western blot analysis and quantification by densitometry is shown in Figure 3.4. Compared to samples from non-demented control individuals, there was a significant increase in the levels of phosphorylated c-Jun in the frontal cortices from dementia patients. No significant changes of phosphorylated c-Jun could be detected in any of the other brain regions. Activated c-Jun is known to induce its own expression and c-Jun is also able to act as a transcription factor independent of its phosphorylation state, e.g. in response to Ca^{2+}-signals (Cruzalegui et al., 1999). I therefore also assessed the amount

of total c-Jun protein compared to actin, which served as a loading control. A significant increase in the levels of total c-Jun could be detected in the frontal cortices from patients with FTLD but not from patients with AD. In addition, there was a marked increase in the levels of total c-Jun in samples from the cerebellum from both AD and FTLD patients. However, there were again no changes in total c-Jun protein levels detected in the hippocampi from dementia patients.

It was noted that there was a high degree of variability in the levels of JNK and c-Jun as well as their phosphorylated species between samples of each group. However, in individual samples, levels of phosphorylated and especially total c-Jun correlated with levels of phosphorylated JNK, suggesting a link between the two, which was particularly apparent in the hippocampus and cerebellum samples (compare Figures 3.3(b) and (c) and Figure 3.4).

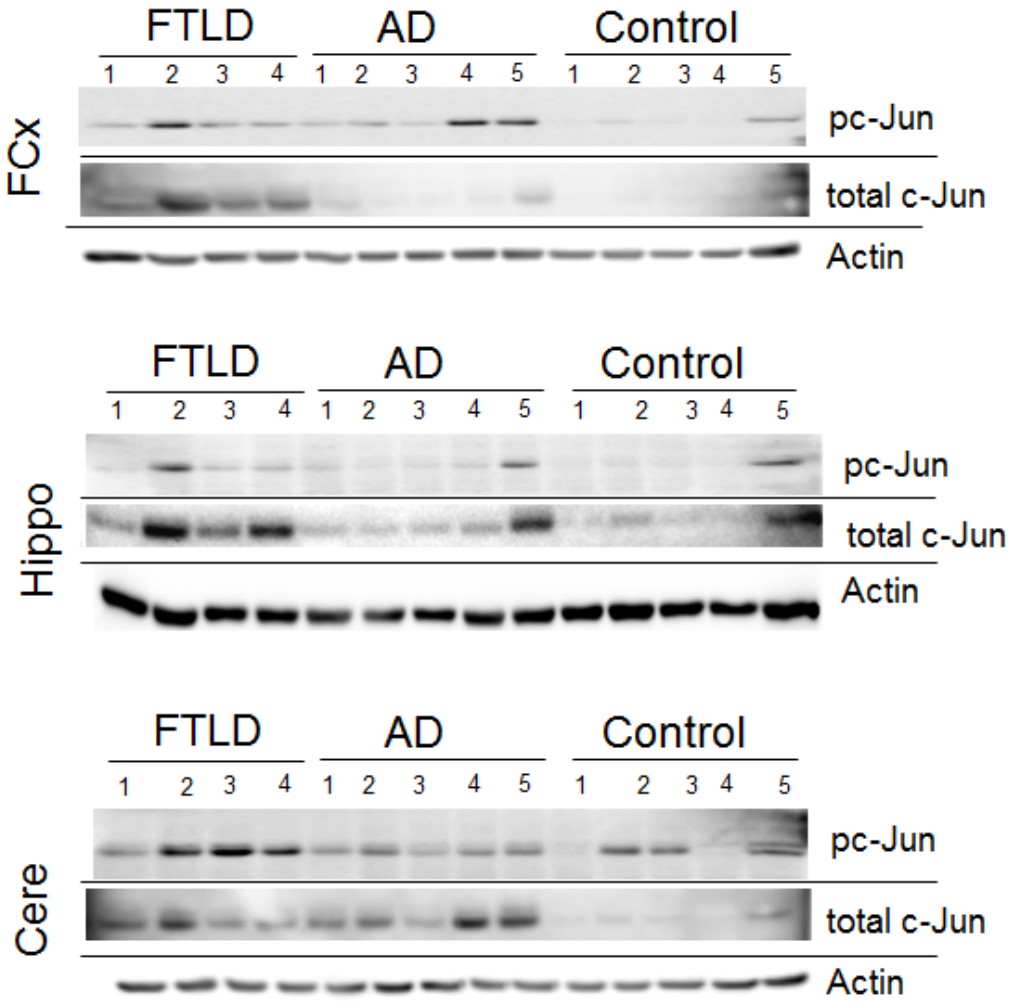

(a)

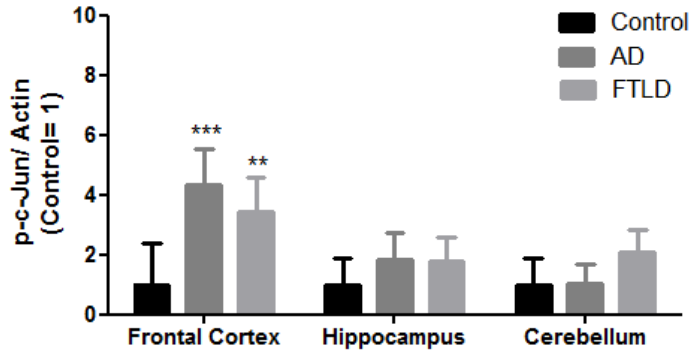

(b)

Figure 3.4: Total and phospho-Ser^{63} c-Jun protein in human brains with dementia.

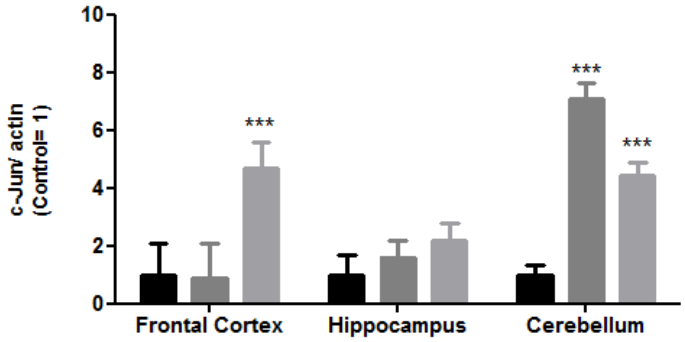

(c)

Figure 3.4: Total and phospho-Ser^{63} c-Jun protein in human brains with dementia (continued). a) Western blot of phosphorylated c-Jun (pc-Jun) and total c-Jun. Actin staining served as a loading control. FCx: Frontal Cortex, Hippo: Hippocampus, Cere: Cerebellum. b) Quantification of stained bands by densitometry. Phosphorylated c-Jun bands were normalised to actin levels and mean values were compared. c) Bands stained for total c-Jun were normalised to actin stained bands in order to quantify levels of total c-Jun. Error bars show SEM. Significance was tested using 2-way ANOVA and Bonferroni post-hoc test. Control = 1, FTLD: Frontotemporal lobar degeneration, AD: Alzheimer's disease.

Overall, the results confirmed the activation of JNK-signalling in the frontal cortex and hippocampus in *post-mortem* AD samples but this was not always accompanied by similarly strong phosphorylation of c-Jun and sometimes more by an up-regulation of total c-Jun levels, especially in those samples with the highest JNK-phosphorylation. This might be explained by the fact that activation of JNK measured by its phosphorylation might lead to only a transient phosphorylation of c-Jun while changes total levels of c-Jun are sustained. Another possibility is that the signal in the form of activated JNK is transmitted by retrograde transport in neurons (for example *via* JIP3 (Abe et al., 2009)) and leads to the activation of its target c-Jun in neuronal cell bodies in the frontal cortex and cerebellum, distant from the initial JNK-activation in the hippocampus. The AD brains used in this study also revealed a significant activation of JNK as well as c-Jun in the

cerebellum. This finding was not expected initially but could be explained by the progression of AD pathology throughout the brain in later stages of the disease as mentioned in Chapter 1.1.1. Of note, there were also particularly high levels of c-Jun phosphorylation in the cerebella of control samples (Figure 3.4(a)), while JNK-phosphorylation was absent, suggesting that other additional mechanisms of c-Jun phosphorylation might be at play here.

3.4 Activation of JNK-signalling in *in vitro* models of AD

3.4.1 Aβ exposure leads to phosphorylation of JNK and c-Jun in primary neurons

We proposed that there might be a link between the activation of JNK reported in response to Aβ exposure and JNK-activation as it is seen during overexpression of Ep-1. It was therefore first necessary to verify the experimental system by demonstrating the activation of the JNK-signalling cascade *in vitro* in primary neuronal cultures from the mouse cortex. Primary neuronal cultures were prepared from embryonic day (ED) 14 mouse embryos as described in Chapter 2.3.2. After 42–72 h the cells had established a neuronal network and virtually all surviving cells stained positive for the neuronal marker βIII-tubulin as seen in Figure 3.5.

Amyloid peptides were prepared as described in Chapter 2.3.6 and 72 h after plating, neurons were exposed to different concentrations of Aβ and phosphorylated JNK was analysed by western blotting after a 12 h incubation period. The

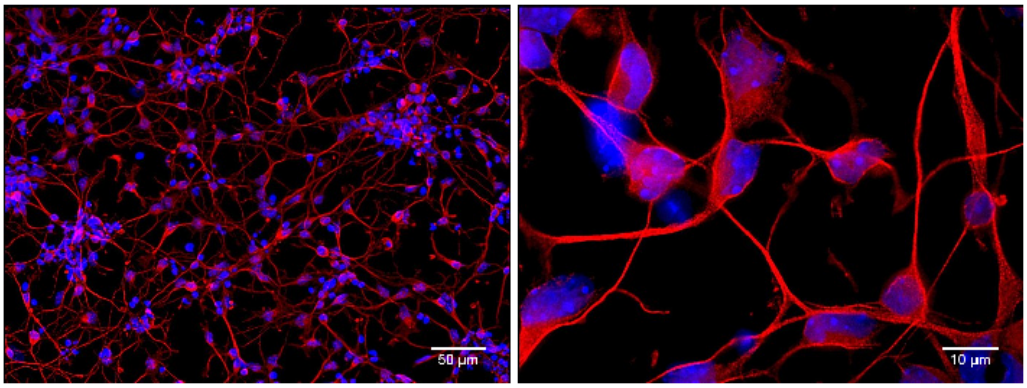

Figure 3.5: Primary neuronal cultures. Cultures were prepared from ED14 mouse embryos as described in Chapter 2. Images show immunocytochemistry against βIII-tubulin (red) in two different magnifications. Scale bars are 50 μm (left) and 10 μm (right). Nuclei were stained with DAPI (blue).

experiment was repeated several times and representative western blot images are shown in Figure 3.6. Both, Aβ40 and Aβ42 were able to cause modest but apparent phosphorylation of JNK (Figure 3.6(a) and (b)) after treatment for 12 h at concentrations of 22 and 25 μM respectively but exposure to 50 μM of Aβ40 did not appear to lead to an additional increase in JNK phosphorylation. It was noted however, that the results were very variable and highly dependent on the quality of the culture and the amyloid preparation. Exposure to Aβ40 or Aβ42 also led to an apparent induction of c-Jun phosphorylation and a modest increase in total c-Jun protein levels (Figure 3.6(c)–(d)).

These results demonstrate that both Aβ40 and Aβ42 can lead to an activation of JNK-signalling components in our primary neuronal cell cultures. It was noted, however, that there were subtle differences between the effects exerted by the different forms of amyloid, when the treatments were performed in parallel. First, Aβ40 caused phosphorylation of mostly the larger isoform of JNK (Figure 3.6(b)), while the smaller p46-JNK band in the phospho-JNK western blots seemed to

respond stronger to exposure of Aβ42 (Figure 3.6(a)). There were also differences in the effect on total and phosphorylated c-Jun. While Aβ40 strongly increased c-Jun-phosphorylation but caused only a modest up-regulation of total c-Jun levels, Aβ42 seeemed to cause only a small induction of c-Jun phosphorylation while total c-Jun levels increased visibly (Figure 3.6(c)). This could point towards differences in the isoforms of JNK activated by Aβ40 and Aβ42 respectively. Alternatively, it is possibly that there are differences in the dynamics of signalling events caused by exposure to either forms of amyloid (Aβ42 acting faster) which might be due to the different aggregation protocols used for this study. It would therefore be necessary to compare the two forms of amyloid under more controlled conditions (aggregation temperature) with larger sample numbers in order to draw any conclusion.

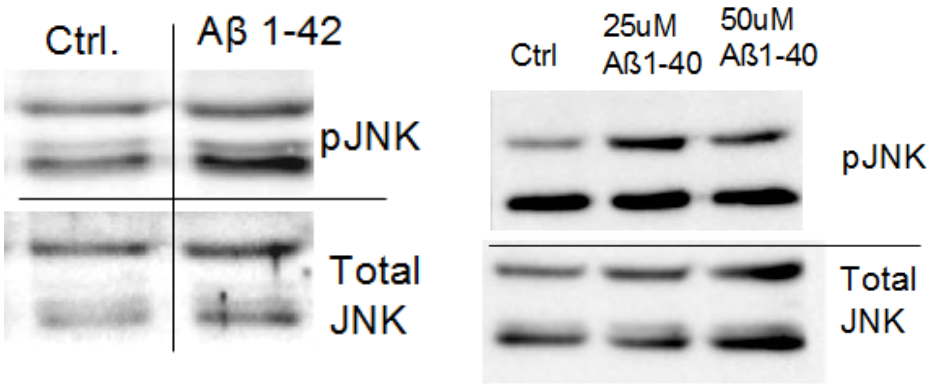

(a) **(b)**

Figure 3.6: Aβ-induced phosphorylation of JNK and c-Jun.

(c) **(d)**

Figure 3.6: Aβ induced phosphorylation of JNK and c-Jun (continued). Western blot analysis for phosphorylated JNK and c-Jun in protein extracts ED14 primary neurons treated with (a)/(c) 22 μM Aβ42 or (b)/(d) 25–50 μM Aβ40 for 12 h. Actin was used as a loading control in (c) and (d).

3.5 Endophilin-1 activates the JNK-signalling cascade *in vitro*

Data from the initial identification of endophilin A1–A3 indicated that Ep-1 is expressed in human fetal and adult brain (Giachino et al., 1997) and in rat hippocampal cultures (Ringstad et al., 2001). In order to investigate the role of Ep-1 in stress signalling pathways in mouse embryonic primary neurons, I next asked if Ep-1 is expressed in these cultures.

RNA from primary neuronal cultures was extracted after 72 h *in vitro* using Tri-reagent and DNase digestion and RT-PCR with mouse-specific primers for Ep-1 were performed as described in Chapter 2. The primer sequences used (see appendix, Table C.1) were specific to both the mouse and the human Ep-1 mR-

NAs and were expected to result in a 107 bp product. Separation of the PCR products on a 2% agarose gel and staining with ethidium bromide revealed a single product of the expected size but no product in a control reaction where no template was added at the reverse transcription step (Figure 3.7). Amplification of a non-specific product from potential genomic DNA contamination could be excluded due to the fact that the expected PCR product was overlapping an intron in the genomic sequence of Ep-1, which would therefore preclude the amplification of a product of the same size from genomic DNA. The RT-PCR results clearly demonstrate that Ep-1 is expressed in ED14 primary neurons and expressed stronger in adult mouse cortex. The same results were obtained using different intron-spanning primers, which only detected mouse Ep-1 mRNA.

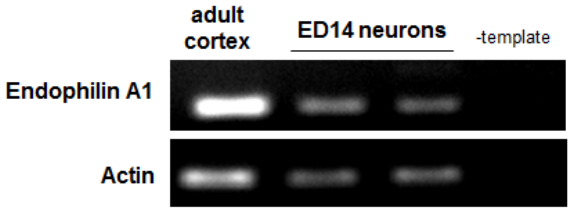

Figure 3.7: Ep-1 mRNA in primary neurons. RT-PCR on cDNA produced from two different ED14 primary cortical neuron cultures after 72 h *in vitro*. cDNA from adult mouse cortex served as a positive control. RT-PCR of actin was used as a loading control.

3.5.1 Ep-1 overexpression can lead to the activation of JNK-signalling

With the knowledge that Ep-1 is expressed in embryonic mouse neurons under physiological conditions, I now explored if overexpression of Ep-1 can influence the phosphorylation and expression of JNK and c-Jun as seen for Aβ. Overexpression

of Ep-1 in these cultures was achieved by transfection of 6×10^6 ED14 primary neurons with 2 μg of a plasmid containing Ep-1 in a pcDNA3 expression vector (a kind gift from Dr. Peter McPherson, McGill University, Montreal (Micheva et al., 1997), see also appendix, Figure B.1) or with 2 μg of an empty pcDNA3 plasmid by nucleofection and cells were plated on 3 poly-D-lysine coated 35 mm Petri dishes per transfection condition. The analysis of Ep-1 expression was performed after 72 h *in vitro* on protein extracts from the combined lysates of 3 dishes per condition and 30 μl of the combined protein lysate was separated by SDS-PAGE and transferred to nitrocellulose for immuno-staining. A strong band corresponding to Ep-1 was detected in Ep-1 transfected neurons but was weaker in vector controls (Figure 3.8). Quantification of the stained bands by densitometry as a ratio over actin staining intensity revealed a 2–3-fold increase in Ep-1 levels in Ep-1 transfected neurons. It was noted however, that nucleofection caused a large amount of cell death and affected the morphology of the cultures considerably with neurons building only a sparse network of cells and accordingly a low protein yield after extraction of cells in lysis buffer was obtained.

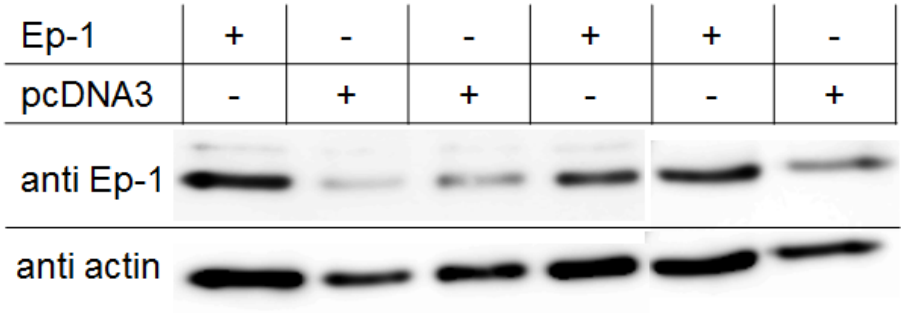

Figure 3.8: Ep-1 overexpression by nucleofection. Western blot of ED14 primary cortical neuron lysates after transfection with Ep-1 or an empty pcDNA3 vector as indicated. A monoclonal anti-SH3GL2 antibody (Abcam) was used for Ep-1 detection. Actin staining served as a loading control.

3.5.1.1 Ep-1 induced JNK-phosphorylation in primary neurons

I then analysed the activation of JNK in primary neuronal cultures transfected with Ep-1 after 72 h *in vitro*. Neurons were prepared and transfected in the same way as before and Figure 3.9 shows the results of the western blot analysis of total JNK and phosphorylated JNK. Compared to the empty vector control, neurons transfected with the Ep-1 expression vector exhibited significantly more phosphorylation of JNK, relative to the total amount of JNK present. This result is in line with the results presented by Ren et al. (2008) and it was concluded that the experimental system was suitable for studying the signalling pathways activated by Ep-1 in primary neurons in more detail.

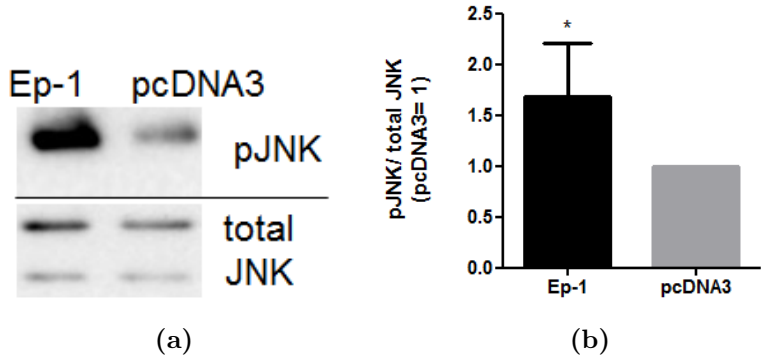

(a) (b)

Figure 3.9: JNK activation in Ep-1 transfected neurons. (a) Western blot analysis of JNK phosphorylation and total JNK expression in ED14 cortical neurons 72 h *in vitro* after transfection with Ep-1 or an empty pcDNA3 vector. (b) Quantification of bands by densitometry. The bar chart represents the ratio of the band intensities of phospho-JNK over total JNK. Error bars show SD. n = 4. Significance was tested with T-test.

3.5.1.2 Ep-1 overexpression leads to c-Jun phosphorylation

I next tested if Ep-1 will also lead to the phosphorylation of known targets of JNK in primary neurons, namely c-Jun. To this aim, Ep-1 was again overexpressed in ED14 primary neurons. 2 μg of Ep-1 expression plasmid or 2 μg of an empty pcDNA3 vector were transfected into 6×10^6 neurons by nucleoporation and cells were plated on 3 poly-D-lysine coated 35 mm Petri dishes. 30 μl of the combined lysates of 3 dishes per transfection condition were analysed by SDS-PAGE and western blotting 72 h after plating. As shown in Figure 3.10(a)(left), transfection of Ep-1 led to an increase in the phosphorylation of c-Jun. Total c-Jun protein levels were not changed significantly in Ep-1 overexpressing neurons in general (see Figures 3.10(a) and (b)). The increase in c-Jun phosphorylation could also be attributed to the activity of JNK, as inhibition of JNK activity by application of the ATP-competitive JNK-inhibitor SP600125 abolished the effect of Ep-1 on c-Jun phosphorylation (Figure 3.10(a), right). Also, deletion of the SH3-domain of Ep-1 resulted in the reduction of c-Jun phosphorylation to levels indistinguishable from vector controls (Figure 3.10(b) and (c)). Taken together with the observed phosphorylation of JNK following transfection of Ep-1, these results demonstrate that Ep-1 can activate several components of the JNK-signalling cascade in primary neurons *in vitro*. They also confirm that the Ep-1 SH3 domain is necessary for this activation to occur. This suggests that interaction of Ep-1 with other proteins is needed for canonical JNK signalling to succeed.

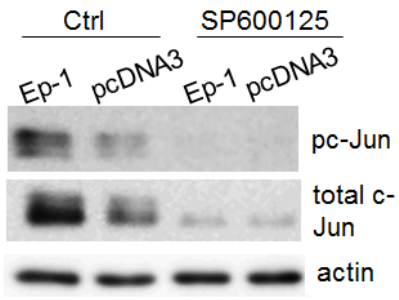

(a)

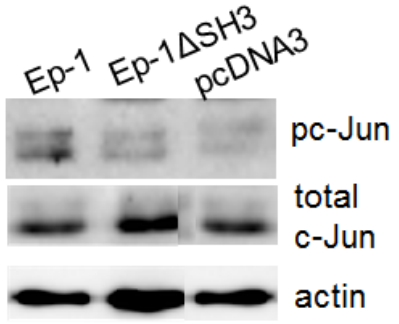

(b)

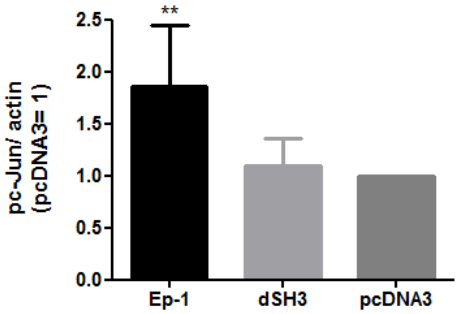

(c)

Figure 3.10: Ep-1 induces phosphorylation of c-Jun. Western blot analysis of c-Jun phosphorylation and total c-Jun levels in ED14 primary cortical neuron cultures. Actin was used as a loading control. (a) Transfection with Ep-1 or the empty pcDNA3 vector. Cells were treated with a vehicle control or 5 μM of JNK-inhibitor SP600125 and cells were analysed 72 h after plating. (b) Western blot after transfection with Ep-1, Ep-1ΔSH3 or the empty pcDNA3 vector. (c) Quantification of stained bands after transfection with Ep-1, Ep-1ΔSH3 (dSH3) or empty pcDNA3 vector. n = 8. Error bars show SD. Significance was tested using 1-way ANOVA.

3.5.2 Ep-1 overexpression alone does not activate JNK-signalling

3.5.2.1 Lentiviral transduction of of Ep-1 into primary neurons

Following from the observed activation of JNK-signalling components, I next aimed to shed light on up-stream events that link Ep-1 to JNK in primary neu-

rons. As previously mentioned, Ep-1 has been shown to interact with the upstream kinase GLK *via* its SH3 domain in human embryonic kidney cells (Ramjaun et al., 2001) and it is therefore conceivable that GLK might be the relevant kinase interacting with Ep-1 in primary neurons, which leads to the activation of JNK, possibly mediated by the JNK-interacting protein JIP3 (Abe et al., 2009).

In the light of the cell toxicity caused by the nucleofection technique and the variable transfection efficiency achieved by this method, I established a lentiviral infection protocol for the expression of full length Ep-1, Ep-1ΔSH3 from lentiviral expression vectors (kind gifts from Prof. Christian Rosenmund, Charité-Universitätsmedizin Berlin (Weston et al., 2011); see also appendix Figure B.2) or expression of EGFP from a control EGFP lentiviral vector (a kind gift from Prof. Chang-Duk Jun, GIST Gwangju, South Korea (Thylur et al., 2009); see also appendix Figure B.3(a)) in primary neurons. Transfection of constructs for the production of lentiviruses for each expression construct into the HEK293T packaging cell line was performed in 10 cm Petri dishes on the day when neurons were prepared as described in Chapter 2.3.5. 2×10^6 neurons from ED14 mouse cortices were plated in poly-D-lysine coated 35 mm dishes or 6-well plates and cells were infected 48–72h after plating as described in Chapter 2.3.5. Fluorescence images of infected cells 72 h after infection, expressing either red fluorescent protein (RFP), which is co-expressed from the Ep-1 and Ep-1ΔSH3 plasmids, or enhanced green fluorescent protein (EGFP) are shown in Figures 3.11 A–C. Together with the phase contrast images (Figures 3.11 D–F), they illustrate the high efficiency of lentiviral transduction and the good viability of the cultures. It was hoped that this improvement of cell viability and yield will facilitate the detection of upstream signalling components, which are typically less abundant.

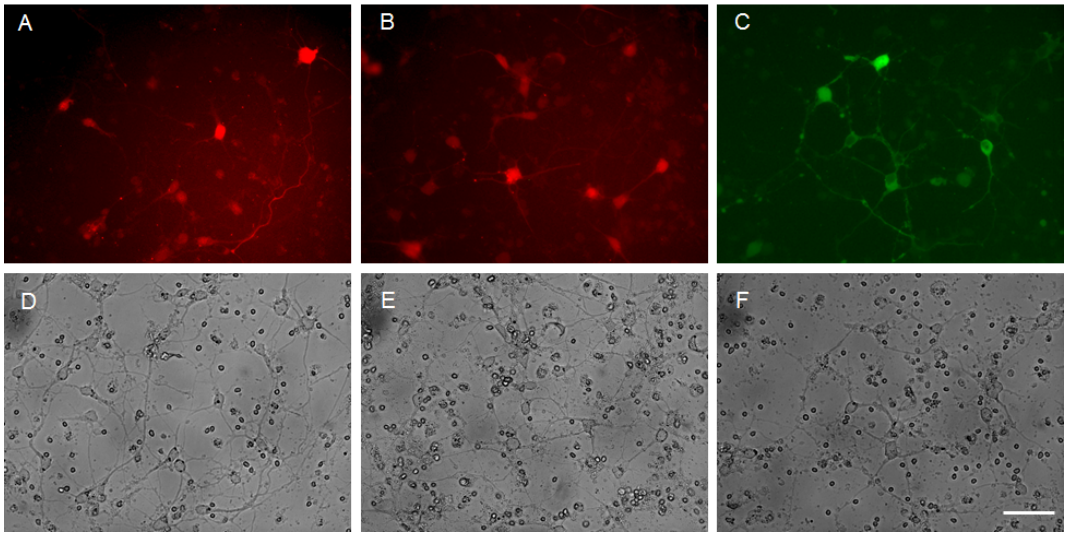

Figure 3.11: Fluorescence imaging of lentivirally infected of primary neurons. Red fluorescence images of A) Ep-1 B) Ep-1ΔSH3 expressing neurons co-expressing RFP or C) EGFP expressing cells. D–F) Phase-contrast images of the respective fluorescence images in A–C) above. Scale bar in F) = 50 μm

I also analysed the expression of full length Ep-1 or mutant Ep-1ΔSH3 in infected cultures by western blotting. For this analysis, neurons were grown in 2 wells of a 6-well plate for each experimental condition and infected 48 h after plating with lentiviruses for the expression of full length Ep-1, mutant Ep-1ΔSH3 or EGFP. 72 h later, cells from each well were lysed and the lysates analysed by western blotting. Figure 3.12 shows the results of the immunostaining, which demonstrates overexpression of Ep-1. Note the lower loading, indicated by the weaker actin staining, in the Ep-1 infected condition compared to the EGFP control vector. Densitometry of the the stained bands revealed an approximately 2-fold overexpression in the Ep-1 infected condition compared to the EGFP control when the intensities were normalised to actin as a loading control. The faster migrating truncated Ep-1ΔSH3 mutant could only be detected in lanes 3 and 4.

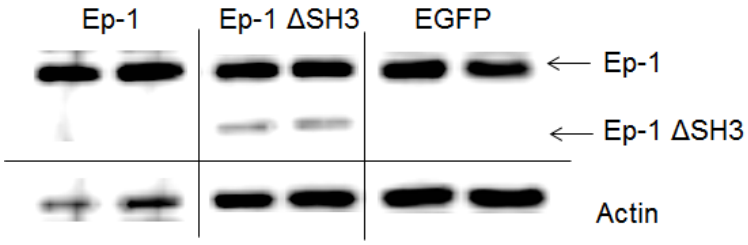

Figure 3.12: Western blot analysis of lentivirally infected primary neurons. 2 wells of ED14 primary neurons in a 6-well plate were infected with full length Ep-1, mutant Ep-1ΔSH3 or EGFP expression vectors. Arrows point to full length Ep-1 (top) or truncated Ep-1ΔSH3 (middle). Actin staining (bottom) served as a loading control.

Using the new lentiviral transduction technique, it was necessary to confirm that differences in JNK-activation in response to Ep-1 over-expression can still be detected in infected neurons. Therefore, 48 h after plating, primary neurons were infected with lentiviruses transducing Ep-1, Ep-1ΔSH3 and pHJ-EGFP plasmids into 2–3 35 mm dishes for each condition as described above and the cultures were analysed by western blotting 72 h after infection. Figure 3.13(a) (left) shows western blot images which are representative for 3 independent experiments. They demonstrate that Ep-1 was again able to cause changes in the phosphorylation status of JNK compared to the GFP-control or the Ep-1 construct lacking the SH3 domain (Ep-1ΔSH3). Quantification of stained bands from >3 repeats of the experiment revealed a significant increase in JNK-phosphorylation due to over-expression of Ep-1 (Figure 3.13(a), right), which matched with the increase in JNK-phosphorylation seen after nucleoporation (Figure 3.9). However, no changes in total c-Jun protein levels or c-Jun phosphorylation could be measured (Figure 3.13(b)) and quantification of phosphorylated c-Jun as shown in Figure 3.13(b) (right) demonstrated clearly, that there was no effect on c-Jun phosphorylation, despite the effect on JNK-phosphorylation seen in Figure 3.13(a).

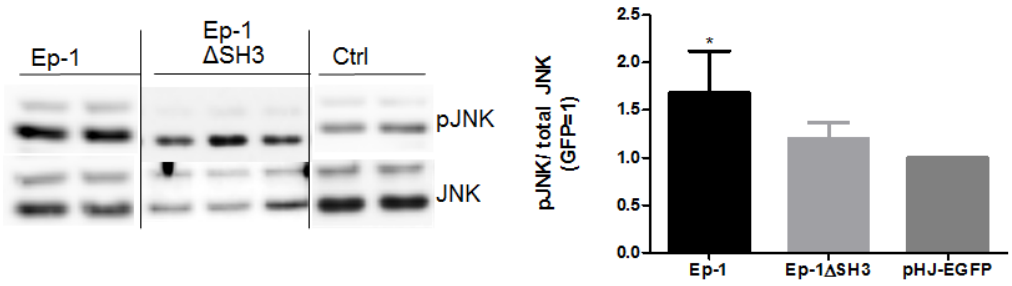

(a)

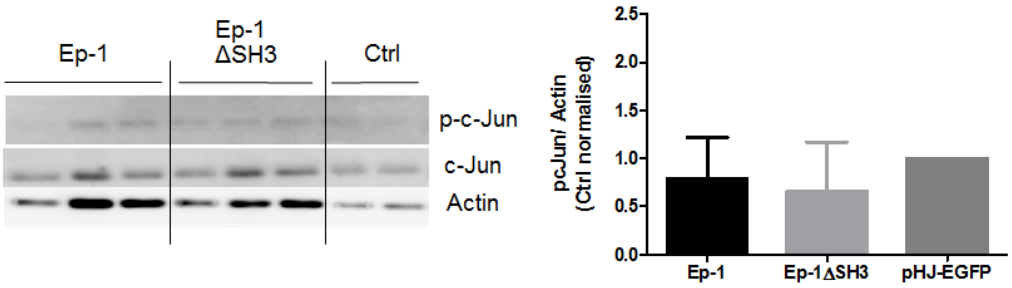

(b)

Figure 3.13: JNK-signalling after lentiviral transduction of Ep-1. (a) Left: Representative images of the western blot analysis of 3 samples of Ep-1, Ep-1ΔSH3 or pHJ-EGFP infected neurons, stained for phosphorylated and total JNK. Right: Quantification of stained bands by densitometry. The bar chart shows the ratio of phosphorylated JNK over total JNK, GFP-control = 1, n = 3. Significance was tested using 1-way ANOVA. (b) Left: Representative images of the western blot analysis of 3 samples of Ep-1, Ep-1ΔSH3 or pHJ-EGFP infected neurons, stained for phosphorylated c-Jun and total c-Jun. Right: The bar chart shows the ratio of phosphorylated c-Jun over actin. GFP-control = 1. Error bars show SD. n = 5.

The results obtained with the lentiviral transduction method were unexpected considering the results from earlier experiments using the nucleofection technique. Importantly, by using empty expression vectors of similar size as controls, which were delivered into the cells using the same technique, any effect seen in the Ep-1 overexpressing cells could be attributed specifically to expression of the Ep-1 in either case, rather than effects of the technique. It could therefore be concluded that the overexpression of Ep-1 compared to the Ep-1ΔSH3 mutant or the empty

control vector, did specifically cause phosphorylation of JNK and c-Jun when delivered by nucleoporation (Section 3.5.1) but was not able to exert the same effect when lentiviral expression was used as described in this section. This led to the hypothesis that other factors introduced by the nucleofection technique might facilitate the activation of JNK-signalling by Ep-1 in a way that is not present in the lentiviral technique.

Good viability of cultures transfected by nucleofection have been reported by some groups, who assessed the morphology and transgene expression in these cultures over a short-term culture period of 3–5 days (Zeitelhofer et al., 2007; Viesselmann et al., 2011). However, an assessment of the electrophysiological properties and cell stress kinase signalling in these cultures has not been published to this date. At the same time, some researchers have previously raised concerns about the electrophysiological properties of neuronal cultures transfected using nucleofection (Scottish Neuroscience Group Meeting 2011, personal communication). It is not difficult to imagine that neurons exposed to electrical pulses strong enough to disrupt their cell and nuclear membranes in order to deliver genetic material will respond to this treatment with the activation of stress signalling cascades, which might be enhanced by components of the nucleofection solution. Therefore, sustained changes in some signalling molecules could be caused and thus have implications for studies on the pathways these molecules are involved in. Meanwhile, this effect might not be relevant when investigating other properties of the neuronal cultures such as their overall morphology or transgene expression.

With this in mind, it is of interest that there are in fact subtle changes in the species of phosphorylated JNK between neurons transfected by nucleofection (Figure 3.9) and neurons infected with lentiviruses (Figure 3.13). In neurons

transfected using nucleoporation, it is consistently only the larger p54 isoform of JNK that can be detected using the phospho-specific antibody, which is the same isoform that has been detected in the human brains (Figures 3.3 and 3.9). However, in neurons infected using the lentiviral technique, mainly the the smaller p46 isoform of JNK is phosphorylated in response to Ep-1 overexpression (Figure 3.13) and this is more similar to the pattern of phosphorylated JNK detected in neurons that have not been transfected but exposed to Aβ (Figure 3.6). Robust changes are therefore present in neurons which have been exposed to the stress of nucleoporation, even 72 h after plating, which bear similarity to the situation present in samples from human AD patients. In conclusion, it was realised that Ep-1 might only be able to activate JNK-signalling in the presence of other stresses. In the case described above these stress factors are of an electrochemical nature but in an *in vivo* situation these stresses could be mitochondrial dysfunction, the deprivation of glucose, increases intra- and extracellular Aβ and changes in ABAD function.

3.6 Discussion and outlook

The data provided in this chapter demonstrates that Ep-1 is able to activate JNK in primary neurons *in vitro*. However, full activation of the canonical pathway appears to require the presence of other insults, which cause robust changes in signalling molecules possibly through the pre-assembly of protein scaffolds in the cell or aberrant targeting of Ep-1. This concept is corroborated by findings from our collaborator Prof. Shi Du Yan (Department of Pharmacology and Toxicology, University of Kansas), who could not detect any changes in the phos-

phorylation status of JNK or c-Jun in transgenic mice overexpressing Ep-1 alone. Behavioural testing for memory deficits did also not reveal any changes in animals overexpressing Ep-1 compared to their non-transgenic littermates. However, some behavioural deficits could be detected in double transgenic animals overexpressing Ep-1 together with mutant APP (mAPP) compared to their single-transgenic littermates (Prof. Shi Du Yan, unpublished results), indicating that Ep-1 has a negative effect on the AD pathogenesis in a situation of increased Aβ production.

Studies exploring the co-localisation of Ep-1 with proteins such as JIP3, GLK and JNK itself in these mouse models or neuronal cultures exposed to insults will shed light on the question of how and where JNK activation occurs under these conditions. The lack of any effect of lentiviral Ep-1 overexpression on c-Jun protein levels or phosphorylation, while some phosphorylation of JNK could still be detected (see Figure 3.13) also requires further investigation. Considering the distance of the synapse from the cell soma where c-Jun is located, JNK activated *via* Ep-1 in the synapse might be more likely to interact with other targets present in the neurites and dendrites, such as MAP1 and 2, tau or p66Shc, rather than with the transcription factor c-Jun. Probing the phosphorylation status of these targets in response to lentiviral Ep-1 overexpression will be able to resolve this question. In order to explain the effect of Ep-1 up-regulation in AD in more detail it will also be important to investigate the precise location of Ep-1 and JNK in AD models at high resolution. Accumulation of Ep-1 in the pre- or post-synaptic compartments will have different consequences depending on the interaction partners present and resolving the spatial distribution of Ep-1 under pathological conditions will inform future research into the function of Ep-1 during AD pathogenesis. A summary of the AD associated pathways which

would be affected by Ep-1 up-regulation is given in Figure 3.14.

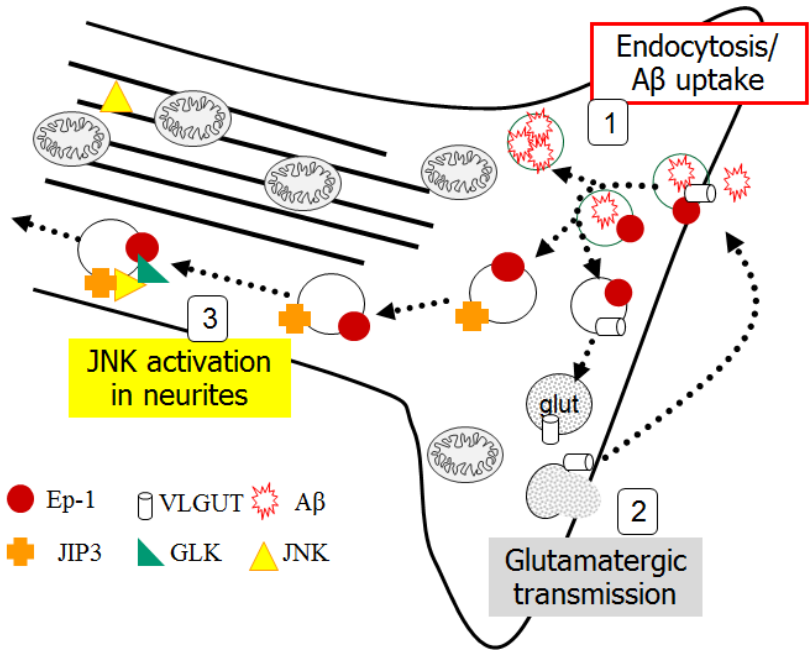

(a) pre-synapse

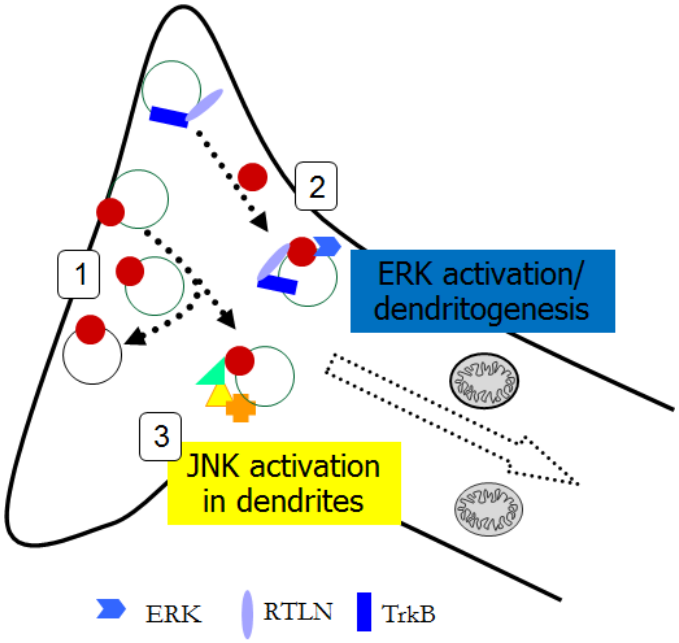

(b) post-synapse

Figure 3.14: Roles of Ep-1 over-expression at the synapse.

Figure 3.14: Roles of Ep-1 overexpression at the synapse (continued). (a) Ep-1 in the pre-synapse: 1) Ep-1 (red circle) functions in the endocytotic recycling of synaptic vesicles and membrane proteins like VGLUT1. Ep-1 would thereby also assist in the uptake of excess Aβ. 2) An increase in Ep-1 could disturb synaptic transmission by influencing VGLUT1 recycling and increasing the probability of glutamate release. 3) Excess Ep-1 could lead to the activation of JNK (yellow triangle) in neurites with the help of JIP3 (orange cross) and GLK (green triangle). (b) Ep-1 in the post-synapse: 1) Ep-1 also functions in endocytosis and the recycling of membrane receptors. 2) Ep-1 is involved in the activation ERK (blue chevron) after recruitment to TrkB carrying endosomes (blue rectangle) by retrolinkin (RTLN, light blue oval) which leads to dendritogenesis. 3) Ep-1, together with GLK and JIP3 could also activate JNK in dendrites.

A better understanding of the reasons for the up-regulation of Ep-1 in AD and ABAD/mAPP transgenic mouse models will also contribute to this field of research. Synaptic failure caused by the pronounced mitochondrial dysfunction in AD and the transgenic AD mouse models might be a causative factor, as Ep-1 could be up-regulated in order to increase synaptic transmission (at the pre-synapse) or synaptogenesis (at the post-synapse). Therefore, future research should address if Ep-1 levels change in response to metabolic stresses or changes in cellular Ca^{2+} levels in the presence or absence of Aβ, which is also known to affect ABAD activity (Allen, 2012).

An indication of how Ep-1 might become up-regulated during neurodegeneration comes from a proteomics study in schizophrenia patients, where Ep-1 has been found to be more abundant in the prefrontal cortices compared to control subjects (de Souza et al., 2009). This result has not been confirmed by other methods so far but there are intriguing parallels between AD and schizophrenia which could cause its up-regulation. Both AD and schizophrenia involve dysfunction of the prefrontal cortex and defects in synaptogenesis, synaptic plasticity and energy metabolism (de Souza et al., 2009; Goto et al., 2010; Schindowski et al., 2008).

In their analysis of proteins differentially expressed in schizophrenia, de Souza et al. point out that some of the proteins they identified also have implications for AD, such as ApoE and Prx-2 and fittingly, they also observed an up-regulation of EFHD2 and Ep-1 (de Souza et al., 2009). Furthermore, impairment of activity dependent BDNF secretion, TrkB signalling and the establishment of LTP and LTD are believed to play an important role in the pathogenesis of schizophrenia (Lu and Martinowich, 2008) and these processes are also impaired in AD mouse models (Chapman et al., 1999). As mentioned before, Ep-1 is also part of the TrkB signalling cascade. Ep-1 might therefore be up-regulated in both diseases in order to restore TrkB signalling in dendrites and synaptic plasticity. This could have far-reaching consequences, since Ep-1 also influences glutamate release in neurons through its interaction with VGLUT1 (Weston et al., 2011). An increase in Ep-1 levels during neurodegeneration as shown by Ren et al. (2008) and de Souza et al. (2009), leading to an increase in glutamate release at the synapse, could tip the balance of glutamatergic signalling, which is crucial for synaptic plasticity and learning. Taken together, Ep-1 is involved in several neuronal mechanisms, which are crucial for learning and memory as well as the modulation of stress kinases in neurons as depicted in Figure 3.14. Elucidating the physiological and pathological functions of Ep-1 and the time point of its up-regulation during neurodegenerative processes could thus be of major importance for the understanding of Alzheimer's disease as well as other neurological diseases such as schizophrenia.

CHAPTER 4

THE NOVEL CALCIUM-BINDING PROTEIN EFHD2 IS ASSOCIATED WITH FRONTOTEMPORAL DEMENTIA

4.1 Introduction

4.1.1 EFHD2 genetics and structure

The EF-hand domain family, member D2 (EFHD2), also known as swiprosin-1, is a 240 amino acid (33 kDa) protein. The gene encoding for EFHD2 is located on chromosome 1 in the human genome and on chromosome 4 in the murine genomes and homologs of EFHD2 have been found in a wide range of species including *C. elegans*, *Danio rerio* and *Drosophila melanogaster* as well as rodents (Duetting et al., 2011). EFHD2 expression has been identified in differentiating hematocytes and myoblasts in *Drosophila* (Hornbruch-Freitag et al., 2011), in mast cells and lymphocytes in mouse (Avramidou et al., 2007; Ramesh et al., 2009) and in lymphocytes and the brain in humans (Vuadens et al., 2004; Vega et al., 2008). In mice, EFHD2 expression has been found to be particularly high in the central nervous system (Avramidou et al., 2007).

The EFHD2 protein consists of a disordered N-terminus, followed by a region containing a proline-rich domain (PRD) for the interaction with SH3-domain containing proteins, two EF-hand domains (EF1 and EF2) and a C-terminal coiled coil domain, which can be involved in protein dimerisation (Figure 4.1). The calcium binding activity of purified EFHD2 has been demonstrated in an *in vitro* binding assay using radioactive ^{45}Ca (Vega et al., 2008). The N-terminal domain also contains an IAP-binding motif (IBM), which can interact with inhibitor of apoptosis (IAP) proteins and is found in pro-apoptotic proteins, which bind IAPs and therefore release caspases for activation during apoptosis. With regard to its IBM, it is interesting that one study found EFHD2 in protein complexes with pro-caspase 9 specifically before the induction of apoptosis in a human non-small lung

cancer cell line (Checiska et al., 2009) but the potential role of this interaction or involvement of the IBM in EFHD2 has not been studied so far.

Figure 4.1: EFHD2 domain structure. IBM: inhibitor of apoptosis (IAP) binding motif (aa 1–5), PRD: proline rich domain (aa 72–77), EF1/2: EF-hand domain 1(aa 96–124)/ EF-hand domain 2 (aa 132–160), CC: coiled coil domain, phosphorylation sites at serine 74 (S47), serine 76 (S76) and tyrosine 83 (Y83) are indicated by arrows. (Linear sequence analysis: http://www.elm.eu.org/)

Phosphorylation of EFHD2 at predicted sites in and around the PRD has also been shown. Blethrow et al. identified Ser^{74} as a phosphorylation site for CDK1 (Blethrow et al., 2008) and Ser^{76} also lies within the recognition domain for cyclin-dependent kinases, although its phosphorylation has not been detected in this assay. CDK5 has also been suggested to phosphorylate Ser^{74} (Irving Vega, personal communication). Phosphorylation of Tyr^{83} has been detected by Ballif et al. in a large scale screen for tyrosine-phosphorylation sites in the murine brain (Ballif et al., 2008). A potential role for this phosphorylation site in living cells comes from a screen for proteins phosphorylated in response to EGF-receptor activation in HeLa cells (Blagoev et al., 2004). This study identified EFHD2 as a protein specifically phosphorylated at a tyrosine residue in response to EGF-R activation, which, interestingly, coincided with the phosphorylation of known actin-modulators (Blagoev et al., 2004) (see Section 4.1.2).

The EFHD2 protein sequence is highly conserved between rodents and hu-

mans. An alignment of the protein sequences as shown in Figure 4.2 revealed only minor amino acid substitutions in the human sequence compared to the rodent sequences, which are not located in any of the major protein domains. This suggests that the various domains of EFHD2 are of crucial importance for its specific function in different organisms.

```
HUMAN      1   --------------------MATDELATKLSRRLQMEGEGGGETPEQPGL   30
MOUSE      1   --------------------MATDELASKLSRRLQMEGEGG-EATEQPGL   29
RAT        1   --------------------MATDELASKLSRRLQMEDEGG-EATEQPGL   29

          31   NG--AAAAAAGAPDEAAEALGSADCELSAKLLRRADLNQGIGEPQSPSRR   78
          30   NG-AAAAAAAEAPDETAQALGSADDELSAKLLRRADLNQGIGEPQSPSRR   78
          30   NG--AAAAAAEAPDETAQALGSADDELSAKLLRRADLNQGIGEPQSPSRR   77

          79   VFNPYTEFKEFSRKQIKDMEKMFKQYDAGRDGFIDLMELKLMMEKLGAPQ   128
          79   VFNPYTEFKEFSRKQIKDMEKMFKQYDAGRDGFIDLMELKLMMEKLGAPQ   128
          78   VFNPYTEFKEFSRKQIKDMEKMFKQYDAGKDGFIDLMELKLMMEKLGAPQ   127

         129   THLGLKNMIKEVDEDFDSKLSFREFLLIFRKAAAGELQEDSGLCVLARLS   178
         129   THLGLKSMIQEVDEDFDSKLSFREFLLIFRKAAAGELQEDSGLHVLARLS   178
         128   THLGLKSMIQEVDEDFDSKLSFREFLLIFRKAAAGELQEDSGLHVLARLS   177

         179   EIDVSSEGVKGAKSFFEAKVQAINVSSRFEEEIKAEQEERKKQAEEMKQR   228
         179   EIDVSTEGVKGAKNFFEAKVQAINVSSRFEEEIKAEQEERKKQAEEVKQR   228
         178   EIDVSTEGVKGAKNFFEAKVQAINVSSRFEEEIKAEQEERKKQAEEVKQR   227

         229   KAAFKELQSTFK   240
         229   KAAFKELQSTFK   240
         228   KAAFKELQSTFK   239
```

Figure 4.2: Homology of EFHD2 between human and rodents. Alignment of the amino acid sequences of EFHD2 from human (*Homo sapiens*, acc. no. NP 077305.2), mouse (*Mus musculus*, acc. no. NP 080270.2) and rat (*Rattus norvegicus*, acc no. NP 001026818.1) according to the NCBI database. The two EF-hand domains are marked by grey shading. Amino acids which differ in the human sequence (K138, C172 and S192) are underlined.

4.1.2 EFHD2 function in immune cells

EFHD2 was initially identified in lymphocytes as a protein specifically associated with cytotoxic CD8-expressing T-cells compared to their CD4+ and CD19+

counterparts (Vuadens et al., 2004). Most of the currently available functional data relating to EFHD2 therefore stems from studies in the field of immunology. Meng et al. identified it in a natural killer-like cell line associated with the cytoskeleton of these cells (Meng and Wilkins, 2005) and an association of EFHD2 with the actin cytoskeleton has also been proposed in mast cells (Ramesh et al., 2009). The reported concurrence of EFHD2 Tyr-phosphorylation with the phosphorylation of the known actin regulator ARP 2/3 in response to EGF-R activation in HeLa cells also suggests a function of EFHD2 in the modulation of the actin cytoskeleton (Blagoev et al., 2004). In mast cells, EFHD2 has been found to be an inducible protein under the control of Ca^{2+} signals via PKC-β/η and its expression has been associated with the induction of cytokine expression (Thylur et al., 2009). This activation of mast cell function has been shown to depend on a complex signalling cascade including PI3-kinase, association of EFHD2 with the actin cytoskeleton and activation of ERK- as well as p38-MAPKs and transcriptional regulation through the Ca^{2+} dependent transcription factors nuclear factor (NF)κB and NF-AT (Ramesh et al., 2009).

More functions of EFHD2 have been identified by Mielenz et al., who identified EFHD2 in the lipid rafts of an immature B-cell line (Mielenz et al., 2005). It was then demonstrated that the presence of EFHD2 in lipid rafts enhanced B-cell receptor (BCR) induced apoptosis by facilitating BCR-induced Ca^{2+} signals in these cells (Avramidou et al., 2007). Interestingly, Avramidou et al. also demonstrated that this apoptotic role of EFHD2 involved a reduction in transcription of the anti-apoptotic protein Bcl-XL, which is controlled by the NFκB-transcription factor. Accordingly, it turned out that EFHD2 caused the inhibition of NFκB by protecting its inhibitor IκB from degradation (Avramidou et al., 2007). These

findings are in direct contrast to the data presented by Ramesh et al. from mast cells (Ramesh et al., 2009) and suggest that EFHD2 has highly specialised functions in different cell types.

The mechanism of enhanced BCR-signalling by EFHD2 in immature B-cells has since been characterised in more detail. Kroczek et al. (2010) demonstrated that early BCR-induced Ca^{2+} release from intracellular stores coincided with increased phosphorylation and activity of the src-kinase Syk and also phosphorylation and targeting of the adaptor protein SLP65, the phospholipase PLCγ2, the BCR and Syk itself to lipid rafts. EFHD2 was found to interact with the SH3 domains of PLCγ2 as well as the src-kinases Lyn and Fgr and the authors suggested that binding of Lyn, which is located in lipid rafts, could be the key for EFHD2 to access these domains and regulate the Ca^{2+} signal *via* PLCγ2. Notably, Fgr and PLCγ2 shared the same interaction site in EFHD2 (amino acids 72–83) and binding occurred in a phosphorylation dependent manner, where phosphorylated EFHD2 preferentially bound to Fgr and *via* a different phospho-epitope to Lyn (Kroczek et al., 2010). Together, the studies in immature B-cells give the most detailed picture of EFHD2 function so far and indicate that it can act as a scaffold molecule in lipid rafts, interact with the SH3 domains of src kinases and that its function can be modulated by phosphorylation. Kroczek et al. noted the intriguing discrepancy that EFHD2 can increase intracellular Ca^{2+} but at the same time inhibit the Ca^{2+}-dependent transcription factor NFκB in B-cells. They concluded that EFHD2 is likely to bind the Ca^{2+} ions released from the ER and cause negative feedback to occur, which inhibits cell survival signalling from the BCR (Kroczek et al., 2010). The possible interactions of EFHD2 and its proposed function based on the above studies are illustrated in Figure 4.3.

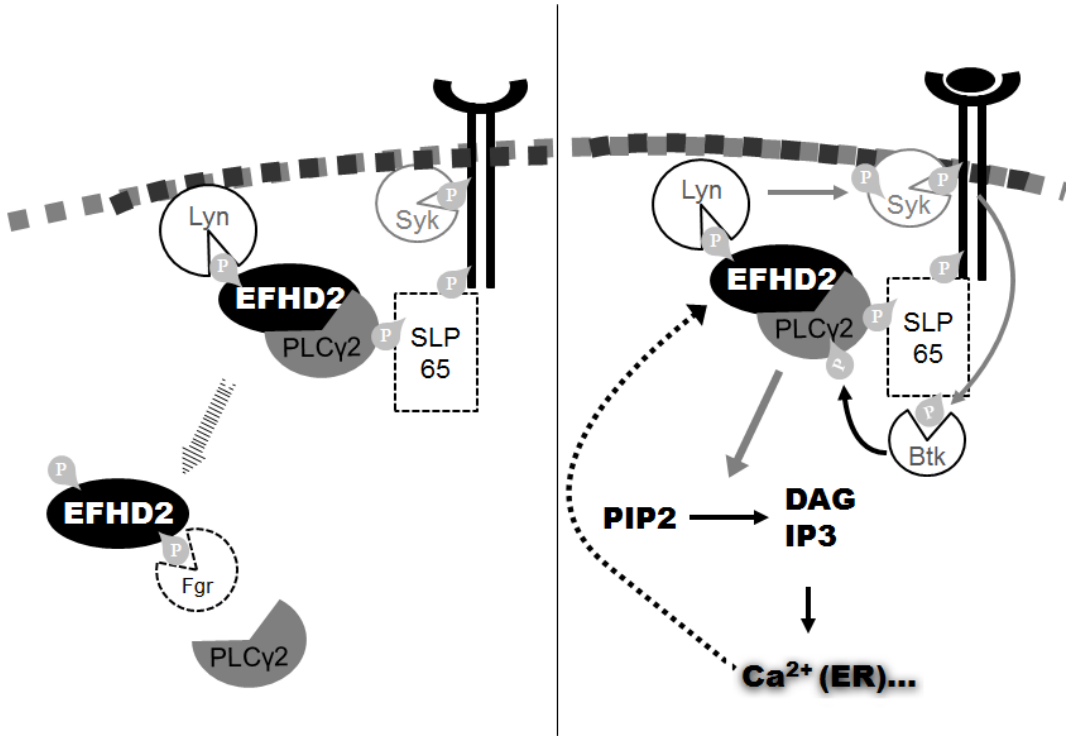

Figure 4.3: EFHD2 as a scaffold protein at the BCR. Left: EFHD2 can interact with the src-kinase Lyn and PLCγ2 and cause the association of the src kinase Syk, the adaptor protein SLP65 and PLCγ2 with the BCR in lipid rafts in unstimulated cells. The interaction of PLCγ2 and EFHD2 is reduced by EFHD2 phosphorylation, which enhances binding of the src kinase Fgr to the same motif in EFHD2. Right: Activation of the BCR induces phosphorylation of Syk and SPL65, binding of PLCγ2 to SLP65 and recruitment of the Bruton's kinase (Btk), which phosphorylates and activates PLCγ2. IP3 induced Ca^{2+} release from internal stores could cause negative feedback through binding of Ca^{2+} to EFHD2, which then counteracts BCR-induced cell survival signalling.

4.1.3 EFHD2 as a novel player in neurodegeneration

In addition to its role in immune cells, EFHD2 has recently been associated with neurodegeneration. In 2008, Vega et al. identified EFHD2 in a screen for proteins associated with insoluble tau-aggregates in the JNPL3 tauopathy mouse model for frontotemporal dementia (Vega et al., 2008). In their study, they

demonstrated that EFHD2 is associated with sarkosyl-insoluble (tangle forming) tau protein in the brains of terminally ill JNPL3 mice but not in younger mice lacking neuropathology. By immunoprecipitation from human brains affected by frontotemporal dementia (FTDP17), AD and non-demented control individuals, they also showed an increased association of EFHD2 with tau in an AD brain containing insoluble tau-aggregates but on in a brain affected by FTDP17 compared to age-matched controls. Furthermore, the study suggested an increased expression of EFHD2 in the temporal cortices of cases with AD, FTLD or progressive supranuclear palsy (PSP) compared to a non-demented brain. Although loading control was not shown in this context (Vega et al., 2008), unpublished data from studies on the temporal lobe tissue of more AD affected brains also pointed towards an up-regulation of EFHD2 protein level (Irving Vega, personal communication).

This is the first study linking EFHD2 to neuronal function and to neurodegeneration. As mentioned in Chapter 3, EFHD2 has since also been found to be up-regulated in the frontal cortices from human schizophrenia patients compared to control individuals (de Souza et al., 2009). This finding is interesting in the light of the parallels in synaptic dysfunction between AD and schizophrenia outlined in Chapter 3.6. However, the function of EFHD2 in neurons and its role in tauopathy or in synaptic function have not been described in detail to date.

EFHD2 has also been linked to amyotrophic lateral sclerosis, which is a form on motor neuron disease characterised by the degeneration of motor neurons in the motor cortex and associated spinal cord. Zhai et al. (2009) found an increased association of EFHD2 with lipid rafts in the spinal cords from transgenic mice expressing a mutant version of superoxide dismutase ($SOD1^{G93A}$) compared to

their wild-type SOD transgenic littermates using a proteomics approach. ALS can be caused by mutations in the Cu/Zn SOD1 gene on chromosome 21 such as the G93A mutation but interestingly, another gene which had been linked to ALS with dementia (C9orf72) has meanwhile, like EFHD2, also been linked to FTLD (Mayeux, 2003; Goedert et al., 2012), indicating possible common pathological mechanisms. It has been suggested, that the mutations in SOD1 leading to ALS cause a decrease in the enzyme's activity by unkown mechanisms, possibly involving misfolding of the protein and that similar defects, resulting in excess oxidative stress, might also underlie sporadic ALS cases (Deng et al., 1993; Bosco et al., 2010). As mentioned in Chapter 1.4.4, SOD1 has also been linked to amyloid pathology in AD (Yoon et al., 2009) and oxidative modifications of SOD1 which mimick known ALS-linked mutations have been identified in AD and PD affected human brains (Choi et al., 2005). However, a link between mutations in SOD1 and the development of FTLD, AD or PD could not be established, indicating that altered SOD function might be secondary to the underlying pathologies present in either of these diseases. It is therefore thinkable, that neurodegenerative processes, possibly involving oxidative stress and/or synaptic failure can lead to an up-regulation of EFHD2 or changes in its function in a similar way and that EFHD2 could represent a link between these diseases.

4.2 Aims of this chapter

Some evidence from proteomics studies performed our lab had pointed towards a possible up-regulation of EFHD2 protein levels in mAPP transgenic AD mouse models. The first aim of this chapter was therefore to verify an increased ex-

pression of EFHD2 protein and mRNA in AD mouse models and also in brains from human dementia sufferers. I then aimed to elucidate the effects of an up-regulation of EFHD2 in neuroblastoma cell cultures and embryonic mouse primary cortical neurons by studying cell survival and the activation of potential cell signalling cascades (see Section 4.1.2) in response to EFHD2 overexpression *in vitro*. Lastly, by studying the localisation of EFHD2 in cell lines and primary neuronal cultures under normal conditions or in response to cell stress, I hoped to shed light on dynamics of EFHD2 distribution in the cell and hence the cellular functions it is involved in in neuronal cells.

4.3 Human isoforms of EFHD2

In order to create specific primers for the mRNA expression analysis in human and mouse tissue and cells, it was first necessary to identify human and rodent mRNA sequences of EFHD2 and their potential splice variants. There is only one predicted isoform of EFHD2 in rodents, while in humans, three potential protein coding transcripts have been identified (see Figure 4.4). The longest isoform, EFHD2-001, produces the longest protein isoform with 240 amino acids (approximately 27 kDa) and isoforms EFHD2-002 and EFHD2-201 use an alternative start codon and contain an alternative exon after exon 3 (Figure 4.4(a)), which encodes a disordered protein domain and a stop codon. Due to these alterations, the resulting putative 177 amino acid (approximately 20 kDa) proteins from EFHD2-002 and EFHD2-201 comprise the EF-hand domains but lack the first 99 amino acids and do also not contain the coiled coil domain present in the longest isoform (Figure 4.4(b)). The expression of these isoforms has so far not

been verified in humans.

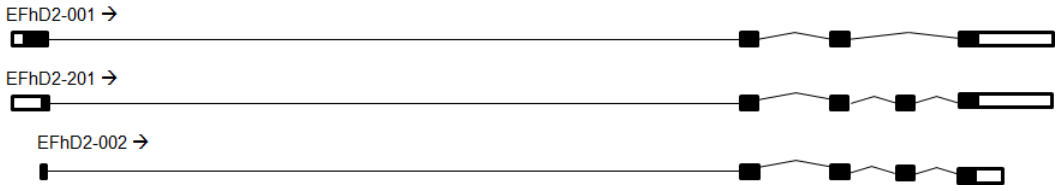

(a)

(b)

Figure 4.4: Human variants of EFHD2. a) The EFHD2-001 gene (top) and its predicted transcript variants EFHD2-201 (middle) and EFHD2-002 (bottom). Shown are introns (thin lines) and exons (black boxes) as well as 5'- and 3'-untranslated regions (white boxes). b) Alignment of the mRNA translation of EFHD2-001 (top line) and EFHD2-201/002 (bottom line), which are identical. Amino acid alignment is indicated by bold font and comprises the region containing the EF-hand domains EF1 and EF2, indicated by black boxes. The coiled coil domain present in EFHD2-001 but not in EFHD2-201/002 is indicated by a grey box.

In order to establish if all isoforms of EFHD2 are expressed in the human brain, specific primers were designed, which recognise either EFHD2-001 or EFHD2-002/201 specifically (Table C.1). To this aim, the forward primer 5-TCGACCTGATGGAGCTGAAACTCA-3 was designed so that it could be used for both pairs. For EFHD2-001, the reverse primer 5-GATGGCCTGGA

CCTTGGCCTCAAAG-3 was used, which would hybridise in the region spanning the exon border between exons 3 and 4, so that amplification from EFHD2-002 or EFHD2-201 or from genomic DNA would be precluded and it would produce a 269 bp product. A second reverse primer specific for the EFHD2-002 and 201 splice variants 5-GCAAAGCAAGGGCGCTCGA-3 was designed, so it would hybridise in a region inside the additional exon, which is present in these variants and produce a 351 bp product. These primers were used in RT-PCR reactions together with 1 μl cDNA produced from DNase I digested 5 μg of total RNA isolated from approximately 100 mg human hippocampus (Control 1) tissue as described in Chapter 2.2.2. The tissue was kindly provided by the Manchester brain bank through Prof. David Mann. Figure 4.5 shows a PCR product produced with the EFHD2-001 reverse primer that separated at the expected molecular weight indicated by a 1 kb DNA-ladder between 200 and 400 bp. The identity of the PCR product was also confirmed by ligation into a linearised pGEM-T-easy vector containing TA-cloning sites (Promega), which also allowed for blue-white screening after transformation of the ligated vector into DH5α *E.coli* bacteria (Chapter 2) and sequencing of the insert. This primer pair was subsequently used for quantitative real-time PCR analysis on human tissue (Section 4.5). At the same time, no PCR product could be produced using the alternative reverse primer EFHD2-002 under the same conditions (data not shown). Increasing the amount of cDNA (up to 5 μl), testing a sample from a different brain region, namely the cerebellum from FTLD patients, increasing the number of PCR cycles (up to 42 cycles) or the amount of primers (up to 1 μM) did also not result in the amplification of a specific product at the expected size. It was therefore concluded that the EFHD2-002 and EFHD2-201 splice variants are not expressed in the human

brain at a detectable level.

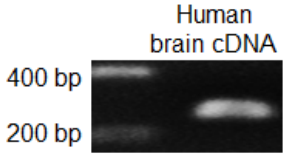

Figure 4.5: EFHD2-001 expression in human brain. Forward primer EFHD2-Fwd: 5-TCGACCTGATGGAGCTGAAACTCA-3 and reverse primer EFHD2-001-Rev: 5-GATGGCCTGGACCTTGGCCTCAAAG-3 were used together with 1 μl of cDNA produced from human hippocampus and a specific 269 bp product was amplified using Taq-polymerase (Roche) as described in Chapter 2.2.2.

4.4 Anti-EFHD2 antibodies

I planned to investigate EFHD2 protein levels in human and in mouse brain tissue by western blotting. Because of the limited number and quality of commercial anti-EFHD2 antibodies, I tested a mouse derived monoclonal anti-EFHD2 antibody which was kindly provided by Dr. Irving Vega (University of Puerto Rico) as well as a commercial anti-EFHD2 antibody raised in goat for the detection of transfected and endogenous EFHD2 protein in cell and tissue lysates. Phosphorylated cell lysates were prepared from SK-N-SH cells 72 h after infection with lentiviruses containing the pHJ-EGFP-SW1 plasmid or an empty pHJ-EGFP plasmid as described in Chapter 2.3.5. Expression from both plasmids (see Figure B.3) is driven by a CMV-promoter and in the case of pHJ-EGFP-SW1 this leads to the expression of a N-terminal fusion of human EFHD2 (swiprosin 1, SW1) with EGFP (expected size: 53 kDa). However, due to the cloning strategy used in the creation of the pHJ-EGFP-SW1 plasmid, untagged EFHD2 (expected size: 27 kDa) can also be expressed from this plasmid. This is, because the start

codon present in the EFHD2 sequence in the vector is preceded by a Sal 1 restriction site (recognition sequence GTCGAC) which together with the guanine in GCC triplet following the ATG codon, represents a strong Kozak consensus sequence (gccRccAUGG, where "R" at the -3 position from the AUG is a purine).

Tissue lysates were prepared from human frontal cortex as described in Chapter 3.3 and for this test, mixed samples with a protein concentration of 1 $^{mg}/_{mL}$ from all FTLD samples together or from control samples together were prepared. Mouse brain phosphorylated protein lysates were produced from 8 month old wild-type or mAPP expressing mouse brains or from embryonic day 14 (ED14) mouse cortices as described in Chapter 2.1.1 and diluted to 1 $^{mg}/_{mL}$ in protein sample buffer. 25 μl of the denatured protein samples were separated on a 12.5% SDS-PAGE and transferred to supported nitrocellulose membrane for immunostaining. Blots were incubated overnight at 4 °C with primary antibodies and detected the next day with a horse-radish peroxidase coupled anti-mouse antibody raised in goat (Abcam, see Table A.2). As a negative control, the mouse anti-EFHD2 antibody was pre-absorbed by mixing the antibody in a 1:1 ratio with purified His-tagged EFHD2 protein (see Section 4.4.1) for 3 h at room temperature. Figure 4.6 shows the result of the western blot analysis.

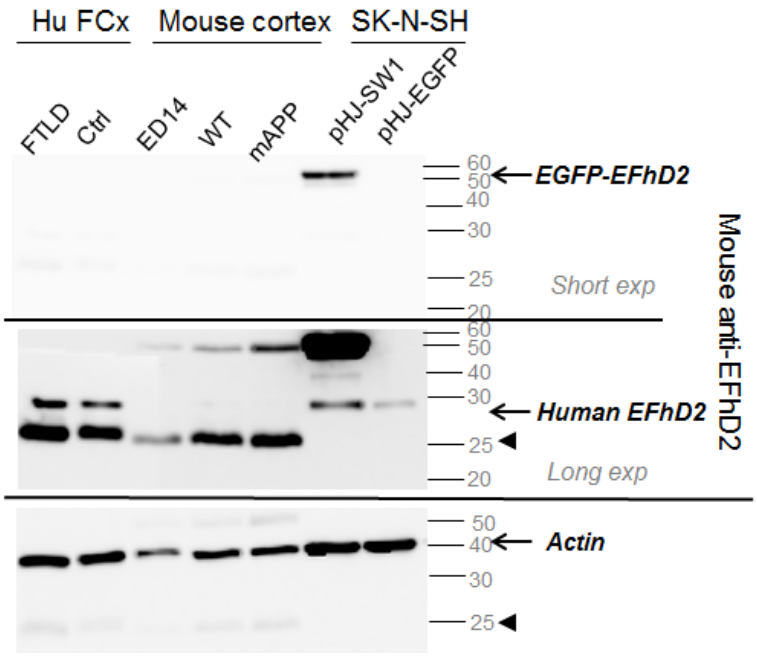

(a)

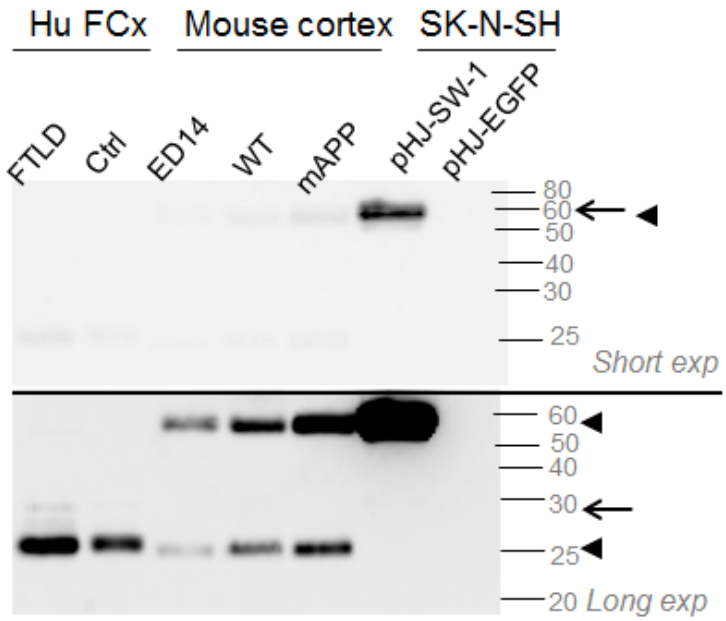

(b)

Figure 4.6: Evaluation of a Mouse anti-EFHD2 antibody.

Figure 4.6: Evaluation of a mouse anti-EFHD2 antibody (continued). (a) Western blot of samples from human frontal cortex (Hu FCx), mouse cortex from an embryonic day 14 (ED14) mouse embryo, adult wild-type (WT) and mAPP transgenic mice and from SK-N-SH cells infected with EFHD2 (pHJ-Sw-1) or EGFP (pHJ-EGFP) expressing plasmids. Images show staining with a monoclonal mouse anti-EFHD2 antibody after short exposure (top) and long exposure (middle). Staining with a monoclonal mouse anti-actin antibody served as a loading control (bottom). Arrows point to EGFP-EFHD2 or endogenous human EFHD2. Arrowheads point to a non-specific band caused by the secondary antibody. b) The same samples stained with pre-absorbed mouse anti-EFHD2 antibody. Top: short exposure, bottom: long exposure. Arrows and arrowheads point to EFHD2 or the non-specific band as in (a).

Staining with the monoclonal mouse anti-EFHD2 antibody revealed a strong band migrating above the 50 kDa molecular weight marker, which corresponds to the EGFP-EFHD2 (expected size 53 kDa) in infected SK-N-SH cells, which could not be detected in the control EGFP-infected SK-N-SH cells (Figure 4.6(a), top)). Longer detection times also revealed a band migrating at about 30 kDa, corresponding to untagged EFHD2 in these samples, which was stronger in the infected SK-N-SH cells due to overexpression of untagged human EFHD2 from the pHJ-Sw-1 plasmid (Figure 4.6(a), middle)). Equal loading between the SK-N-SH cell samples, the wild-type (WT) and mAPP mouse cortex samples and the human frontal cortex samples was indicated by comparable band intensity in the actin immunostaining below (Figure 4.6(a), bottom). In addition, strong bands separating at 25 kDa and above 50 kDa (arrowheads) were detected at longer detection times, which could however also be seen when the EFHD2 antibody was pre-absorbed with His-EFHD2 (arrowheads in Figure 4.6(b)) as well as in the blot stained with a monoclonal mouse anti-actin antibody (arrowhead in Figure 4.6(a), bottom). This indicated that these were non-specific bands, caused by the secondary antibody used in this experiment. A different goat anti-

mouse secondary antibody was therefore used in subsequent analyses of tissue samples. Bands migrating at approximately 30 kDa could also be detected in the samples from human frontal cortex but not in the samples from mouse cortex (Figure 4.6(a), middle). These bands were nearly abolished by pre-absorption of the primary antibody with purified His-EFHD2 protein (arrow in Figure 4.6(b), middle), indicating that they represented endogenous human EFHD2. Because of the strong overexpression of EFHD2 in the SK-N-SH cells, EGFP-EFHD2 could still be detected even after pre-absorption of the antibody (Figure 4.6(b), top).

Immunostaining with a commercial goat anti-EFHD2 antibody also revealed a strong band corresponding to EGFP-EFHD2 in infected SK-N-SH cells (arrow in Figure 4.7, top) and also endogenous and untagged overexpressed EFHD2 migrating at approximately 30 kDa (arrow in Figure 4.7, bottom). Human EFHD2 in frontal cortex as well as SK-N-SH cells was only weakly detected with this antibody, whereas endogenous murine EFHD2 in adult wild-type (WT) and mAPP mouse brains was stained efficiently (arrow in Figure 4.7, bottom). A strong non-specific band was caused by the primary goat anti-EFHD2 antibody at about 50 kDa. This part of the membrane was therefore removed when endogenous EFHD2 had to be detected in mouse derived samples in subsequent analyses in order to improve the staining result.

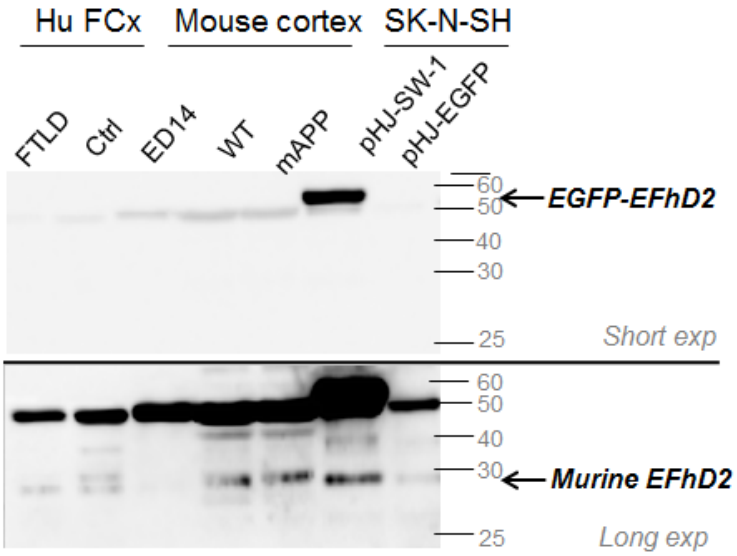

Figure 4.7: Detection of murine EFHD2. Western blot of samples from human frontal cortex (Hu FCx), mouse cortex from an embryonic day 14 (ED14) mouse embryo, adult wild-type (WT) and mAPP transgenic mice and from SK-N-SH cells infected with EFHD2 (pHJ-Sw-1) or EGFP (pHJ-EGFP) expressing plasmids. Images show staining of murine EFHD2 by the a goat anti-EFHD2 antibody after short exposure (top) and long exposure (middle). Arrows point to endogenous EFHD2 in adult mouse brain and overexpressed human EFHD2 in SK-N-SH cells.

In summary, both, the monoclonal mouse anti-EFHD2 antibody as well as the goat anti-EFHD2 antibody were able to detect overexpressed and endogenous EFHD2. However, the commercial goat derived antibody appeared to preferentially detect murine EFHD2, whereas the monoclonal mouse derived antibody detected human EFHD2. Interestingly, only a very faint protein band for EFHD2 could be detected in the sample from embryonic day 14 (ED14) mouse cortex, suggesting that the protein levels are lower in the embryonic compared to the adult mouse cortex.

I therefore performed semi-quantitative reverse transcription PCR (RT-PCR), in order to verify these difference in EFHD2 protein expression. I extracted total

RNA from ED14 and ED16 mouse cortices as well as from an adult wild-type mouse cortex and performed cDNA synthesis using random hexamer primers with a Roche cDNA synthesis kit. The PCR reaction as described in Chapter 2.2.2 was performed using the primer set EFHD2-Fwd and EFHD2-001-R for the EFHD2 reaction and actin specific primers as a loading control with an annealing temperature of 58 °C (see Table C.1). Figure 4.8, shows the results of the RT-PCR. It can be seen that despite equivalent cDNA loading demonstrated by similarly strong amplification of the actin PCR-product in all samples, the EFHD2 message was clearly less abundant in the embryonic samples than in the adult brain. Quantification of the band intensities by densitometry normalised to the band intensity of the actin RT-PCR product in each sample revealed that the band in ED16 mouse brain sample corresponded to 57% and the band in the ED14 mouse brain to only 27% of the PCR-product detected in the adult mouse brain. Further analysis will be necessary in order to explain the developmental regulation of EFHD2 expression. RT-PCR or real-time PCR analysis on a larger number of samples from embryonic, adult and early postnatal brains would be able to demonstrate when changes in EFHD2 expression levels occur. Furthermore, mapping of EFHD2 expression in the mouse brain at these developmental stages by immunohistochemistry or *in-situ* hybridisation might help to explain where EFHD2 is located and which cell types it is associated with in the brain.

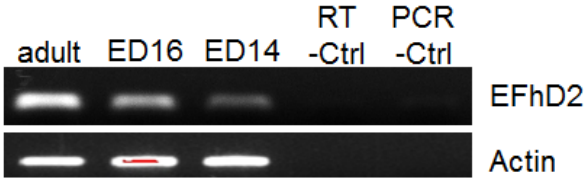

Figure 4.8: EFHD2 mRNA in murine brain.

Figure 4.8: EFHD2 mRNA in murine brain (continued). RT-PCR on cDNA produced from adult, ED14 and ED16 mouse brain tissue. Shown are PCR products for EFHD2 (top) and actin (bottom) as a house keeping gene. No-template controls were included in the RT-step and the PCR reaction.

4.4.1 Purification of 6 × His-tagged EFHD2

His-tagged EFHD2 protein was expressed in BL21 *E c.coli* bacteria and purified for experiments in which antibodies were pre-absorbed with the target protein as a negative control. A bacterial expression vector for the expression of 6 × His-tagged EFHD2 was kindly provided by Dr. Irving Vega (University of Puerto Rico). The EFHD2 sequence and presence of the histidine tag were confirmed by sequencing, which also revealed that the start codon was present in the EFHD2 cDNA sequence itself as well as the N-terminal His-tag. Like with the pHJ-EGFP-Sw 1 plasmid, this could lead to the expression of untagged protein, although only the AU-rich sequence of the N-terminal His-tag (codons CAT or CAG), bound by the S1 ribosomal protein in gram-negative bacteria, but no Shine-dalgarno sequence (AGGAGG) were present in the sequence.

Chemically competent BL21 bacteria were transformed with approximately 60 ng of the plasmid and plated on ampicillin containing LB-agar plates. Overnight cultures from individual colonies were grown in ampicillin containing LB-medium the following day, glycerol stocks were prepared from these cultures and a small induction experiment was performed as described in Chapter 2.1.4 in order to verify successful induction of protein expression from the plasmid. A fresh 10 mL overnight culture was prepared from the glycerol stock with best expressing clone and expression of the protein in a 1 L culture at OD(600 nm) =

0.6 and purification with Ni-NTA agarose were performed as described in Chapter 2.1.5. The only modifications to this protocol were that the lysis buffer (50 mM Tris, pH 8.0, 0.5 M NaCl, 100 $^{\mu g}/_{mL}$ DNase I, 100 $^{mg}/_{mL}$ lysozyme, protease inhibitors without EDTA), wash buffer (50 mM Tris, pH 8.0, 0.5 M NaCl, 10 mM imidazol, protease inhibitors) and elution buffer (50 mM Tris, pH 8.0, 0.5 M NaCl, 300 mM imidazol, protease inhibitors) did not contain any glycerol.

Figure 4.9(a) shows an image of a Coommassie stained gel containing all fractions sampled during the purification process. A strong band corresponding in size to His-EFHD2 could be detected in the 4 h induced sample but not in the uninduced bacteria. This band was again present in the lysate but depleted in the supernatant after incubation with the Ni-NTA agarose. The wash fractions (W1–W5) also contained some of the protein alongside other proteins, which were loosely attached to the beads. This indicates that a fraction of the His-EFHD2 bound only weakly to the Ni-NTA resin under these conditions, possibly due to misfolding of the protein or expression of EFHD2 without the His-tag. However, elution with 300 mM imidazol resulted in the retrieval of the majority of the protein in the first elution step. In order to concentrate the samples and to reduce the high NaCl concentration and imidazol from the elution buffer, the samples with the highest protein concentration and purity were concentrated on a spin column with a 10 kDa molecular weight cut-off (Amicon, Milipore) at 4000 × g until the samples were 5–10 fold concentrated. The desalted column retention was then mixed in a 1:1 ratio with a buffer containing 50 mM Tris, 350 mM NaCl and 5% glycerol, so that the resulting samples contained 25 mM Tris, pH 8.0, 150 mM NaCl and 2.5% glycerol. The final protein concentration of the samples was then measured with a Bradford microplate assay, and a 10 μl sample of

the protein was separated on a 10% SDS-PAGE for an analytical staining. The samples were finally snap frozen in liquid nitrogen and stored at -80 °C. Figure 4.9(b) shows a picture of the Coommassie stained gel after concentration of the samples in comparison to a sample from the un-induced bacterial culture and from the un-concentrated first eluate. It is apparent after the concentration of the samples that all elution fractions also contained proteins other than His-EFHD2. However, it was decided that the relative abundance of the protein was sufficient for the purpose of this study (pre-absorption of an antibody) and that further optimisation of the purification protocol was therefore not necessary at this stage.

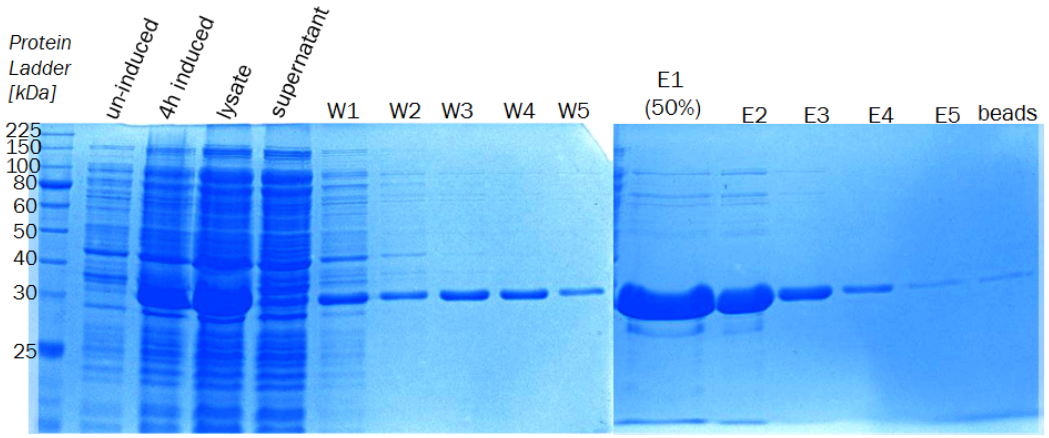

(a)

Figure 4.9: Purification 6 × His-tagged EFHD2.

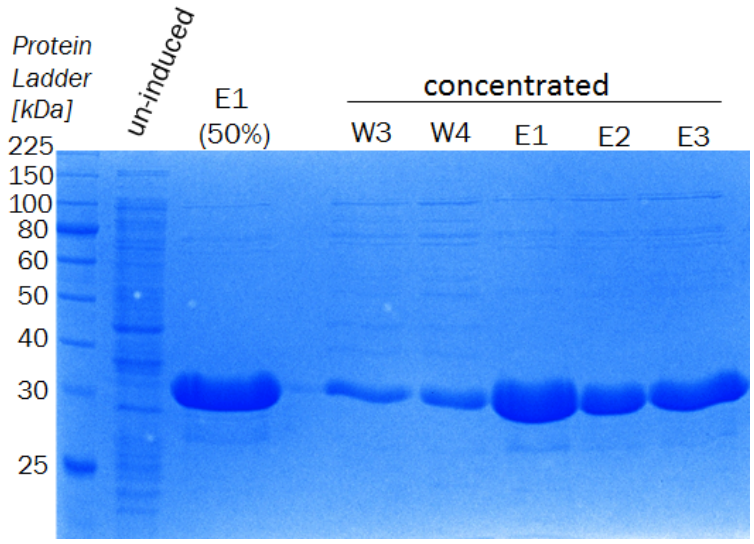

(b)

Figure 4.9: Purification 6 × His-tagged EFHD2 (continued). a) Fractions of the purification process shown on a Coommassie stained gel. W1–W5: wash fractions 1–5, E1–E5: elution fractions 1–5, beads: NiTA agarose after elution. b) Coommassie stained gel of fractions W3, W4 and elution fractions E1–E3 after concentration on a spin column with 10 kDa molecular weight cut off, compared to the uninduced sample and fraction E1 before concentration on the spin column.

4.5 EFHD2 expression levels are increased in human dementia

Following on from the findings by Vega et al. that EFHD2 associates more with hyper-phosphorylated tau in the AD brain (Vega et al., 2008), I investigated if total EFHD2 protein and mRNA levels were also changed in brains affected by AD or by FTLD compared to age-matched control individuals. Samples from the frontal cortices, hippocampi and cerebella from human brain with either a diagnosis of AD, FTLD or no dementia were provided by the Manchester brain

bank through Prof. David Mann. Table 3.1 gives histopathological scores for the brain regions from each individual the samples were obtained from. Phosphorylated protein samples for western blotting analysis from four FTLD patients, five AD patients and five age-matched control individuals were prepared by lysis of approximately 300 mg of brain tissue in 1 mL of phospho-lysis buffer as described in Chapter 2.1.1. Protein samples were diluted to a final concentration of 1 $^{mg}/_{mL}$ in 1 x protein sample buffer and 20 μl samples were separated on a 12.5% SDS-PAGE and subjected to western blotting and staining using the mouse monoclonal anti-EFHD2 antibody and a HRP coupled goat anti-mouse secondary antibody from Jackson Immunoresearch. Figure 4.10(a) shows the results of the immunostaining and Figure 4.10(b) shows a bar chart representing the quantification of the stained bands relative to actin of 3 repeats of the western blot analysis. This quantification revealed that there was a tendency towards higher levels of EFHD2 in all brain regions from FTLD sufferers and that EFHD2 levels were increased significantly in the hippocampi compared to controls. However, no changes in the levels of EFHD2 could be detected in AD cases.

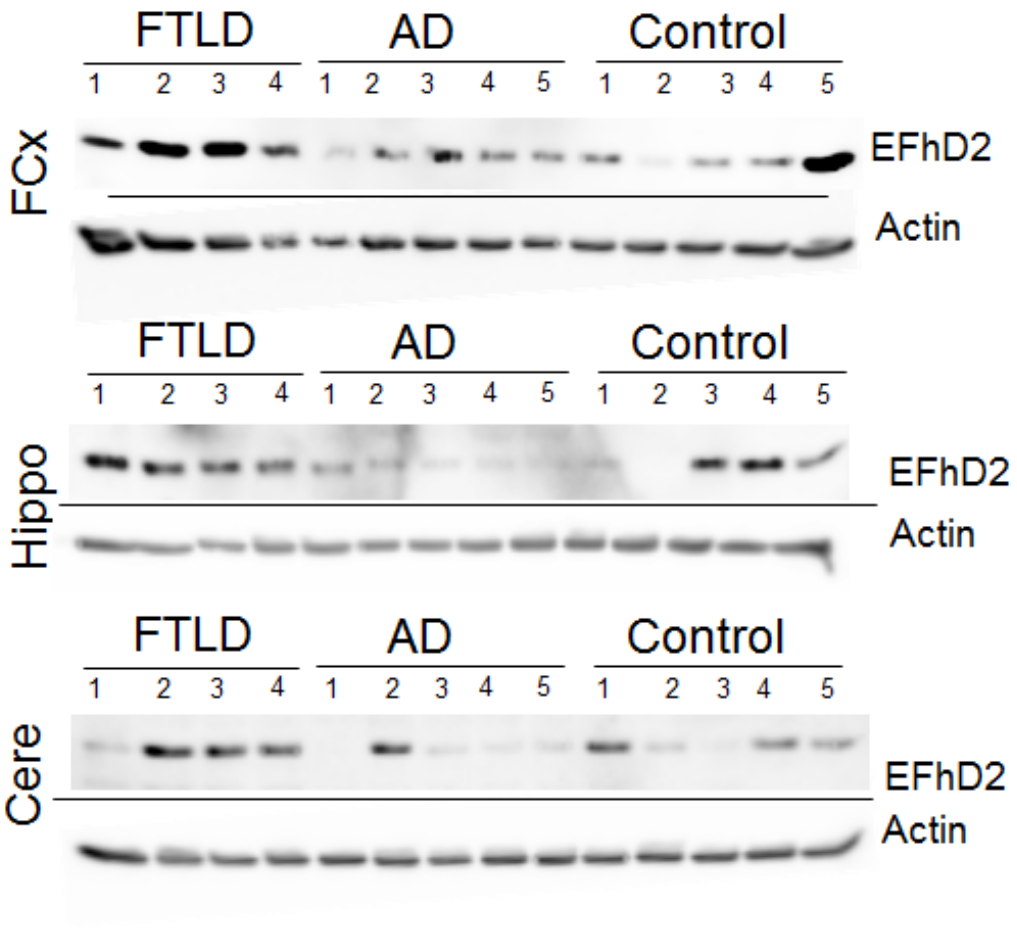

(a)

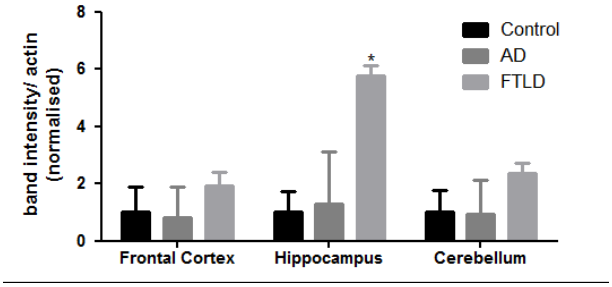

(b)

Figure 4.10: Levels of EFHD2 protein and mRNA in human tissue.

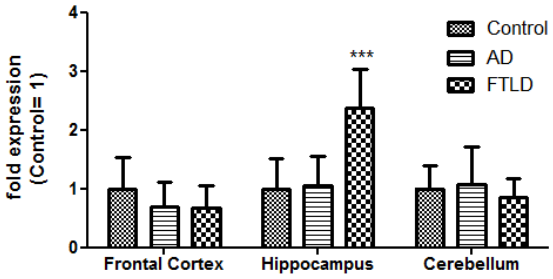

(c)

Figure 4.10: Levels of EFHD2 protein and mRNA in human tissue (continued). Human tissue from frontal cortex (FCx), hippocampus (Hippo) or cerebellum (Cere) from individuals with frontotemporal lobar degeneration (FTLD), Alzheimer's disease (AD) or age-matched non-demented individuals (Control) was analysed. a) Western blot analysis of EFHD2 protein levels. Actin was used as a loading control. b) Quantification of stained bands from 3 independent experiments by densitometry, normalised to actin. Mean values were calculated for FTLD, AD and control and groups were compared by 2-way ANOVA with Bonferroni post-hoc test. Error bars show SEM. n = 4–5 c) Quantification of EFHD2 mRNA levels by quantitative real time PCR. Three independent measurements were performed and each time expression levels were calculated relative to actin mRNA. Control = 1, n = 5–6. Error bars show SEM. Differences were compared using 2-way ANOVA and Bonferroni post-hoc test.

I then also analysed EFHD2 mRNA levels in brains with dementia compared to non-demented controls. In order to do this, I extracted total RNA from approximately 100 mg of frozen human brain tissue from all brain regions provided by the Manchester brain bank and removed potential DNA contamination by 45 min DNase I digestion and produced cDNA with the Revert Aid reverse transcriptase with reduced RNase H activity (Fermentas) as described in Chapter 2.2.2. For this analysis, I analysed all six cases diagnosed with FTLD, five cases with AD and five non-demented control cases. I then performed real-time qPCR analysis as described in Chapter 2.2.3 using Brilliant II or Brilliant III SYBR Green kits (Agilent) with 200 nM each of EFHD2-R-001 and EFHD2-Fwd primers (see Table C.1). As a loading control, qRT-PCR for actin was performed with the same

samples on the same PCR-plate and the analysis was repeated 3 times. The calculation of expression levels of EFHD2 compared to actin was done according to the ΔCC method (see formula described in Chapter 2.2.2). A bar chart illustrating the collated results normalised to the non-demented control samples is shown in Figure 4.10(c). The results are in line with the western blot analysis and reveal a significant increase in the EFHD2 mRNA levels in the hippocampi from FTLD cases but no changes in samples from AD cases compared to non-demented controls.

These expression changes (up-regulation in the hippocampus but not the frontal cortex of FTLD patients) might sound odd at first, given the name of the disease which suggests a more frontal location of the pathology in the brain. However, a biochemical marker for frontotemporal dementia does currently not exist and it has not been possible to say, which neuronal cell populatoins are affected by pathology in the FTLD brain and in fact how this exactly compares between the various different types of FTLD. To this date, FTLD has mainly been described as a spectrum of neurological symptoms characterised by atrophy in certain brain regions and specific protein inclusions as described in Section 1.3. As reviewed by Goedert et al. (2012), the hippocampus (in the temporal lobe) and is function are also affected by these processes and it is conceivable, that EFHD2 might mark a subset of neurons affected by FTLD in the hippocampus as part of the disease process at a later stage. It will therefore be very important to expand this study to more cases of different types of FTLD and to also include immunohistochemical analysis of EFHD2 expression in the future.

4.6 EFHD2 protein levels are increased in an AD mouse model

The tight regulation of calcium levels and calcium mediated signalling processes, partly through the mitochondrial permeability transition pore (mPTP), play a crucial role for neuronal function. Cyclophilin D (CypD) is an important component of the mPTP and ablation of the Ppif gene encoding CypD has been shown to be protective against Aβ toxicity and neurodegeneration in AD mouse models (Du et al., 2008, 2009, 2011). CypD has furthermore been shown to delay the onset of pathology in motor neurons in a mouse model for amyotrophic lateral sclerosis (ALS) (Martin et al., 2009), a disease which EFHD2 has been linked to as well (Zhai et al., 2009). I therefore tested if deficiency in the CypD gene has an influence on the protein levels of EFHD2. The CypD deficient mouse line had been cross-bred with the Tg2572 mAPP mouse line, which is characterised by amyloid pathology due to the overexpression of human APP_{695} harboring the Swedish mutation ($APP^{K595N/M596L}$). The pathology observed in the mAPP transgenic animals includes reduction of the mitochondrial calcium buffering capacity and cognitive dysfunction at the age of 6–8 month, while tau-pathology is absent. I analysed the levels of EFHD2 in protein samples from the brains of wild-type and transgenic mouse brains, which are either deficient for the Ppif gene ($CypD^{-/-}$), overexpressing mAPP or both ($mAPP/CypD^{-/-}$). To this aim, protein samples were used which had been prepared by lysis of 1 hemisphere of a mouse cortex in approximately 1 mL of protein lysis buffer as described in Chapter 2.1.1. The protein concentration of the pre-diluted samples was measured using a Bradford assay and 30 μg of protein were separated on a 4–12%

NuPAGE Bis-Tris acrylamide gel (Invitrogen).

In order to confirm the genetic background of the samples used in this study, protein levels of APP and CypD were analysed by western blotting as shown in Figure 4.11. Note the high levels of APP protein levels in one of the wild-type control samples.

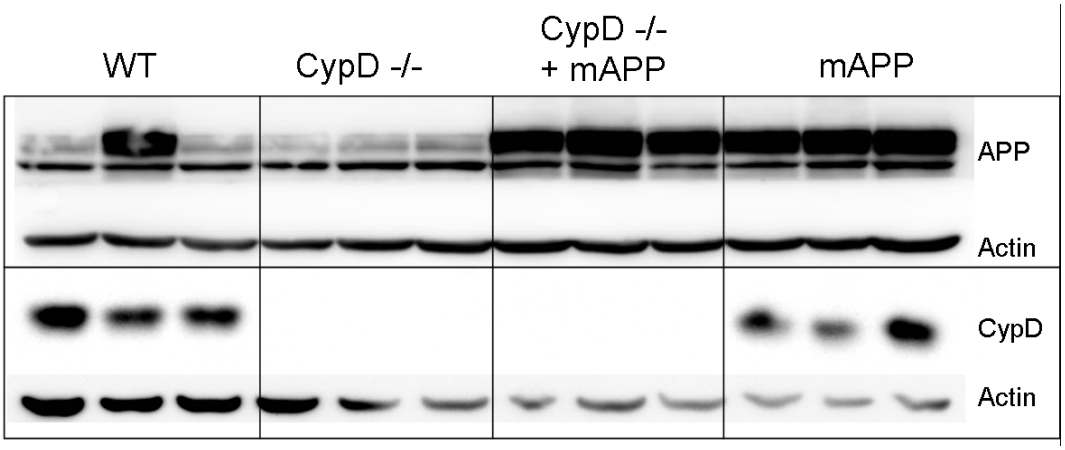

Figure 4.11: Cyclophilin D deficiency in a transgenic mouse model for AD. Western blot analysis of APP (upper panel) and cyclophilin D (lower panel) in protein extracts from whole mouse brains from wild-type (WT) animals or transgenic littermates as indicated. Actin was used as a loading control.

I then performed western blot analysis of the same samples with a goat anti-EFHD2 antibody and the results of the analysis are presented in Figure 4.12(a). Actin staining was used as a loading control by re-probing the membranes after removal of the first antigen as described in Chapter 2.1.3.

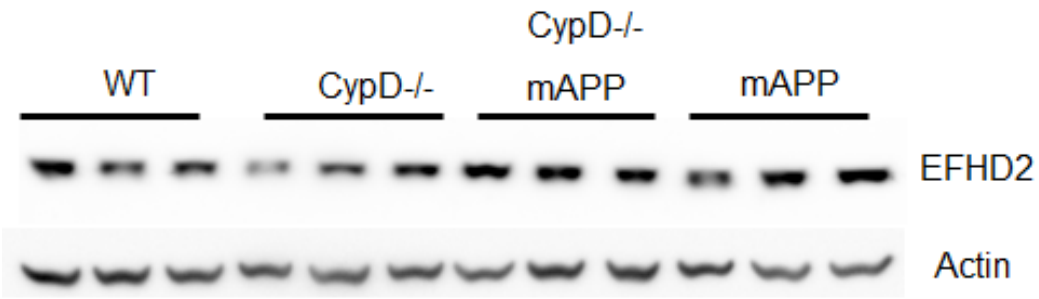

(a)

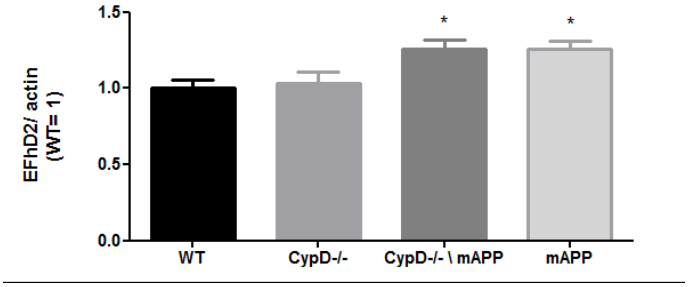

(b)

Figure 4.12: EFHD2 in mAPP transgenic and CypD-deficient mouse models. Levels of EFHD2 were measured in mouse brain tissue from wild-type (WT), mAPP overexpressing (mAPP), CypD-deficient (CypD -/-) and double transgenic (mAPP/CypD--/-) animals;. (a) Western blot for EFHD2 using a goat anti-EFHD2 antibody. Actin was used as loading control. (b) Quantification of stained bands by densitometry. WT = 1. Error bars show SEM; n = 3. Significance was tested using 1-way ANOVA and Tukey's post-hoc test.

The western blot analysis on three brains from each genetic background was repeated 3–5 times and the band intensities of the stained bands were quantified by densitometry. A bar chart summarising the results is shown in Figure 4.12(b). The results demonstrated that EFHD2 protein levels were not changed in brains from CypD-deficient animals with or without expression of mAPP (compare WT indicated by the horizontal bar to CypD$^{-/-}$ and mAPP to mAPP/CypD$^{-/-}$). This shows that the presence or absence of CypD and therefore regulation of mitochondrial calcium release had no effect on EFHD2 protein levels in these

mouse models. At the same time, quantification of the stained bands revealed that EFHD2 protein levels were increased 1.2-fold in mAPP overexpressing animals compared to their wild-type APP expressing littermates. This suggests that Aβ-pathology or overexpression of human APP_{695} in the transgenic mouse model in the absence of tau-pathology can affect EFHD2 protein levels.

The increase of EFHD2 in mAPP expressing animals is in line with previous findings by our group from a proteomics study on mAPP overexpressing or wild-type animals (Frank Gunn-Moore, unpublished data). Still, the increase was unexpected in the light of the results obtained from the human AD brain, where no such increase could be detected compared to non-demented controls. Because the transgenic mouse model used in the above study had been engineered to overexpress human APP protein, I tested if the up-regulation of EFHD2 protein and mRNA levels in the human FTLD affected brain also correlates with higher APP protein levels.

Western blot analysis and quantification of the stained bands of total APP protein were performed on the human brain samples used to study the protein and mRNA levels of EFHD2 (see Section 4.5). As shown in Figure 4.13, APP protein levels were indeed elevated in the human hippocampus of FTLD cases compared to non-demented controls but this up-regulation was not present in the sporadic AD cases studied here. Due to the small number of cases studied and the variable levels of APP within the groups, the increase was however only statistically significant when tested using a direct comparison to non-demented controls by T-test (see Figure 4.13(c)) rather than 2-way ANOVA (Figure 4.13(b)).

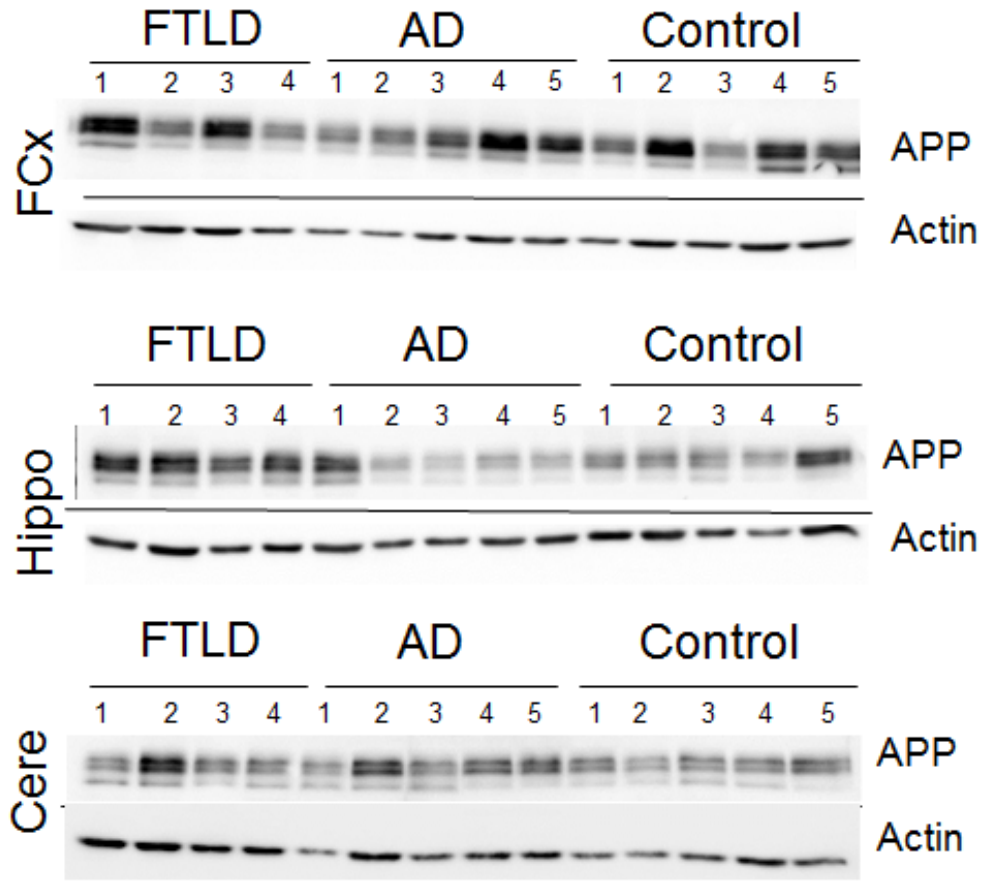

(a)

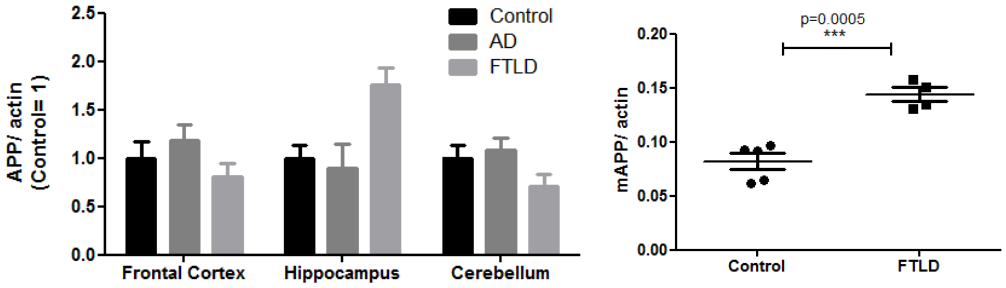

(b) (c)

Figure 4.13: APP protein levels in human dementia

Figure 4.13: APP protein levels in human dementia (continued). Levels of APP in different brain regions from human dementia sufferers (continued). (a) FCx: frontal cortex, Hippo: hippocampus, Cere: cerebellum. Actin was used as a loading control. (b) Quantification of stained bands by densitometry. APP bands were normalised to actin and mean values were compared. Error bars show SEM. Control = 1. n = 5(c) Quantification of APP stained bands by densitometry. Bands were normalised to actin as a loading control and mean values were compared. Significance was tested using T-Test. Error bars show SEM. FTLD: Frontotemporal lobar degeneration, AD: Alzheimer's disease.

4.7 The cellular location of EFHD2

4.7.1 EGFP-EFHD2 in SK-N-SH neuroblastoma cells reveals a cytosolic location.

The function and location of EFHD2 have not been investigated in neurons and neuronal cell lines so far. In order to get an insight into the location of EFHD2 in these cell types, I transfected plasmids expressing either full length murine Flag-tagged EFHD2 in a vector co-expressing EGFP controlled by an internal ribosomal entry site (pIRES-EGFP, see Figure B.4), or Flag-tagged EFHD2 lacking the coiled coil domain (EFHD2ΔCC) into SK-N-SH cells. Transfection was achieved by lipofection of 2 μg of plasmid into approximately 85% confluent SK-N-SH cells, which had been plated the day before in 35 mm Petri-dishes and expression of the transgene was checked by fluorescence imaging of EGFP 48 h after transfection. Cells grown on coverslips were then fixed with 4% PFA and permeabilised as described in Chapter 2.4 and stained with the monoclonal mouse anti-EFhd2 antibody or an M2 anti-Flag antibody (Sigma) overnight at 4°C. The following day, primary antibodies were detected with a goat anti-mouse IgG antibody coupled to the Dylight 594 fluorescent marker (see Table A.1) and nuclei were counter-

stained with DAPI. Figure 4.14 shows the result of the immunocytochemistry after imaging with a Zeiss Axiostar epifluorescence microscope. Cells successfully transfected by lipofection could be identified by their GFP-signal. Accordingly, those cells also stained with a mouse anti-EFHD2 antibody (Figure 4.14 (a)) and an anti-Flag antibody (Figure 4.14 (b)). At the same time no staining could be observed with either antibody in non-transfected cells identified by the absence of GFP-fluorescence, indicating that endogenous EFHD2 levels were too low for detection by ICC using this antibody. This is in agreement with the findings from the western blot analysis, where endogenous human EFHD2 could also not be detected efficiently using this antibody (see Figure 4.6). Compared to the evenly distributed cytosolic EGFP signal, staining of both the full length as well as the EFHD2ΔCC mutant appeared granular or punctate, which could be seen particularly well in cells with lower expression levels. This suggests an association with intracellular membranes. However, the identity of these potential membranes has not been investigated yet. Co-localisation studies with markers for intracellular compartments such as the Golgi complex and the endoplasmic reticulum or membrane domains such as lipid rafts will help to answer this question.

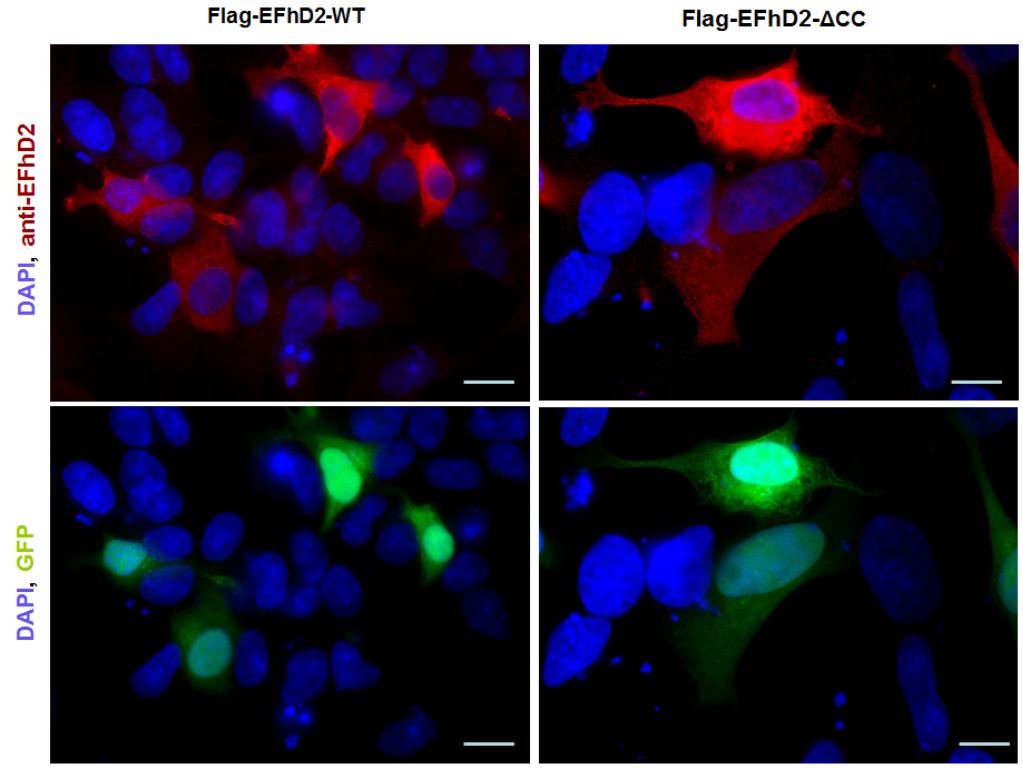

(a)

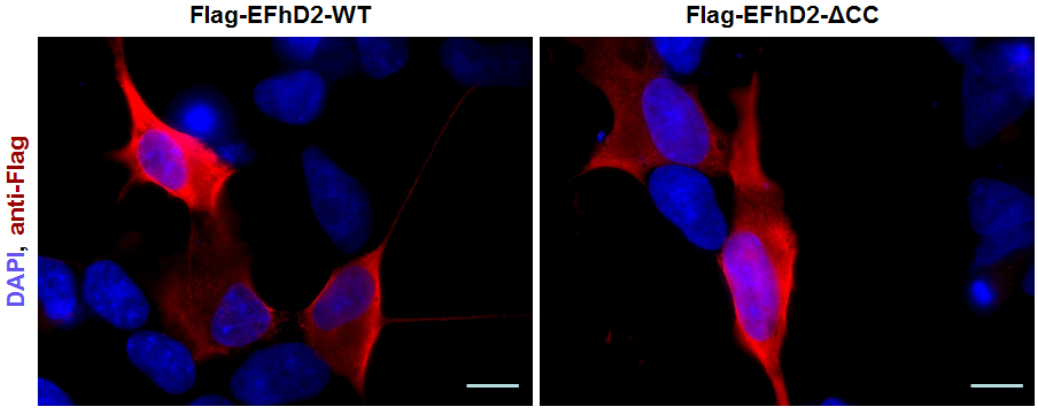

(b)

Figure 4.14: Flag-EFHD2 in SK-N-SH cells. (a) Top: ICC against EFHD2 in SK-N-SH cells 48 h after transfection with full length EFHD2 (left) or EFhd2ΔCC (right). Bottom: Imaging of EGFP co-expressed from the plasmid highlighting transfected cells. (b) Fluorescence images of an ICC against the Flag-tag in SK-N-SH cells 48 h after transfection with full length Flag-EFHD2 (left) or EFHD2ΔCC (right). Images show an overlay with DAPI. Scale bars = 10 μm.

4.7.2 EFHD2 in primary neurons

I aimed to investigate the function of EFHD2 in a more physiologically relevant system and therefore also studied the location of EFHD2 in mouse primary cortical neurons. For this, ED14 primary neurons were grown on glass coverslips and cultured for 72 h before fixation and staining of endogenous EFhd2 with either of the available anti-EFhd2 antibodies. Unfortunately, immunocytochemical staining with the goat anti-Efhd2 antibody could not be achieved. Immunocytochemistry using the monoclonal mouse anti-EFhd2 antibody resulted in a strong staining. However, it was realised that the staining pattern was significantly different from the pattern seen in the transfected SK-N-SH cell line and using a confocal microscope as well as a Deltavision deconvolution microscope the same signal could also be seen in areas on the coverslips without any cells or cell processes. It was therefore concluded that the staining pattern had derived from an interaction of the primary antibody with the poly-D-lysine coating of the coverslips used for the neuronal cultures.

In order to overcome this problem, I infected primary neurons with a lentiviral vector for the expression of GFP-tagged EFHD2 (pHJ-Sw-1) as described in Section 4.4. ED14 primary cortical neurons were infected 72 h after plating on poly-D-lysine coated coverslips and cells were fixed with 4% PFA, mounted in Prolong Gold mounting medium (Invitrogen) and imaged using a Deltavision deconvolution microscope 48 h after infection. Figure 4.15 shows deconvolved images of primary neurons expressing EGFP-EFHD2, one near the center of the cell soma (left) and another image of the cell near the cell membrane on the coverslip, where the cell processes can be seen as well (right). They illustrate

the distribution of EFHD2 throughout the cytoplasm of the cell, including all cell processes and sparing out the area of the cell nucleus. The pattern of the GFP-signal appeared granular, and with accummulations in some areas of the cell in a similar way to that detected in neuroblastoma cells (see Figure 4.14).

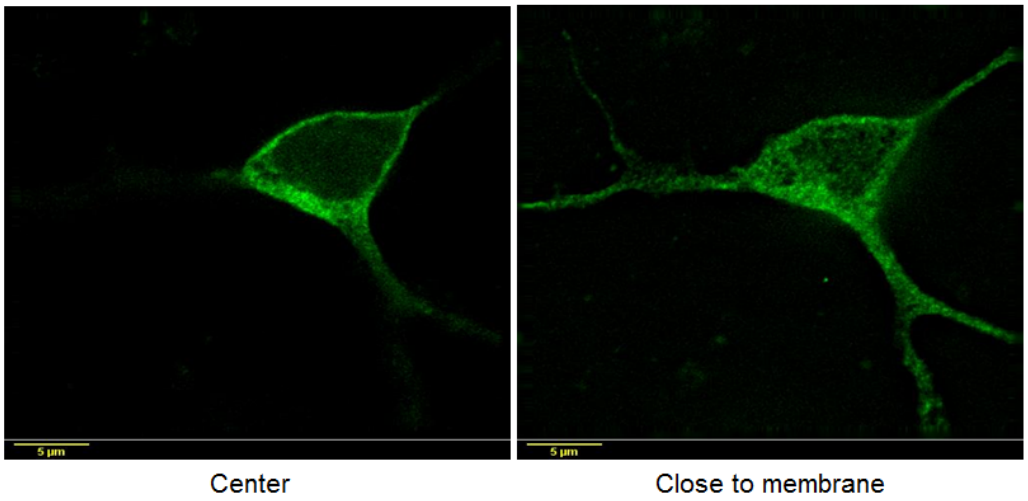

Figure 4.15: GFP-EFHD2 in primary cortical neurons. ED14 cortical neurons were imaged after 5 days *in vitro*, 48 h after after infection with a lentiviral vector for the expression of EGFP-EFHD2. Image stacks of 0.2 μm thickness were acquired with a Deltavision deconvolution microscope. Left: Image slice close to the cell center. Right: Image slice close to the cell membrane. Scale bar = 5 μm

Treatment of infected primary neurons before fixation with 22 μM Aβ(42), which is known to affect cell stress signalling, mitochondrial function and calcium signals in neurons, for 4 h, 12 h or 24 h did not affect this distribution of the EFHD2 signal. Again, co-localisation studies of EFHD2 with markers for cellular organelles and compartments will help to identify the exact location of EFHD2 in the cytoplasm. Also, immunoelectron microscopy of EFHD2 in SK-N-SH cell cultures or primary neurons will provide helpful information about the distribution of EFHD2 throughout neuronal cells.

4.8 The effect of EFHD2 overexpression in cell lines and primary cortical neurons

4.8.1 Cell viability in EFHD2 overexpressing cultures

I investigated if overexpression of EFHD2 had an impact on the viability of SK-N-SH cells or primary neurons. Constructs for the expression of full length Flag-EFHD2 in the pIRES-EGFP expression vector, mutant Flag-EFHD2ΔCC or empty pIRES-EGFP vector were transfected into SK-N-SH cells plated in 8 wells of a 96-well plate with an equal number of cells for each condition. Cell viability was assessed 48 h after transfection by MTT assay as described in chapter 2.3.7.1. The average absorption of the formazan product at 570 nm in all 8 wells per condition was normalised to the average value obtained by the empty pIRES-EGFP vector control. The results are presented in the bar chart in Figure 4.16(a). The MTT assay revealed no difference in cell viability between the Flag-EFHD2 transfected cells and cells transfected with the control vector.

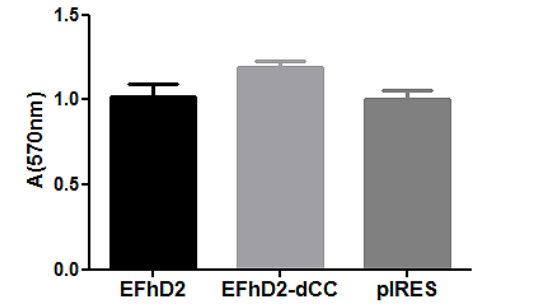

(a)

Figure 4.16: Cell viability in cells overexpressing EFHD2.

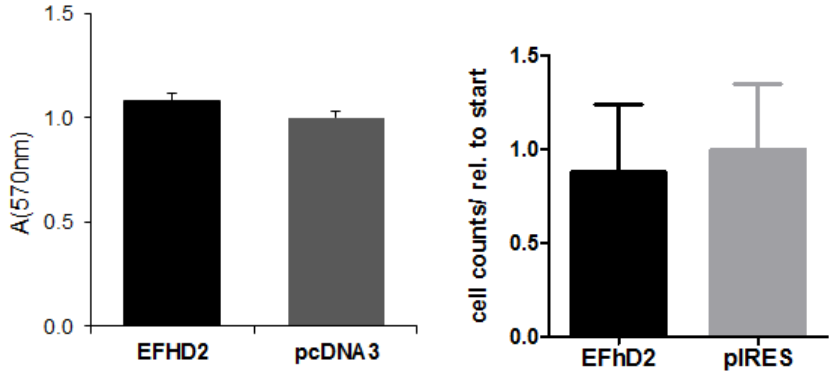

(b) **(c)**

Figure 4.16: Cell viability in cells overexpressing EFHD2 (continued). (a) SK-N-SH plated in a 96-well plate were transfected with a 0.2 μg per well of a pIRES-EGFP expression vector for Flag-EFHD2, Flag-EFHD2ΔCC mutant (EFhd2-dCC) or an empty pIRES-EGFP vector. Cell viability of 8 wells per condition was measured by MTT-assay and an average of absorbance at 570 nm was calculated (EGFP control = 1). n = 3; error bars show SEM. (b) ED14 primary neurons were nucleofected with a pcDNA3 expression vector for EFHD2 or an empty pcDNA3 vector at the time of plating in a 96-well plate. Cell viability was measured by MTT-assay 3 days after plating as in (a). n = 3; error bars show SEM. (c) Cell counts of primary neurons transfected as in (b). Cell numbers in 5 fields of view of a 40$\times$ phase contrast objective were counted 24 h after nucleofection and again 48 h after plating. The bar chart presents the ratio of cell numbers at 48 h over cell numbers at 24 h. n = 3; error bars show SEM.

I also explored the cell viability of primary neuronal cultures overexpressing EFHD2. ED14 mouse primary cortical neurons were transfected by nucleofection at the time of plating with full length EFHD2 in a pcDNA3 expression vector, which was created in collaboration with Ms Zoe Allen. Neurons were cultured in 8 wells of a poly-D-lysine coated 96-well plate for each condition and after 3 days *in vitro* the cell viability of the cultures was measured by MTT assay. Compared to the empty pcDNA3 vector, overexpression of EFHD2 had no effect on the reduction of MTT (Figure 4.16 (b)). Similarly, average cell counts on five phase contrast images of nucleofected neurons after 24 h, 48 h or 72 h in culture did

also not reveal any changes between EFHD2 expressing cells and empty vector controls (Figure 4.16 (c)). It was therefore concluded that overexpression of EFHD2 alone does not affect cell viability either in cell lines or primary neurons. EFHD2 or its ΔCC mutant might still be able to modulate the activation of pathways important for cell viability in response to extracellular signals.

A propidium iodide (PI) exclusion assay by FACS analysis of PI-fluorescence did not show any changes in cell viability between SK-N-SH cells transfected with either full length EFHD2, EFHD2ΔCC or pIRES-EGFP. This might indicate that the difference in MTT reduction measured previously did not represent changes in cell viability but rather mitochondrial dehydrogenase activity in cells transfected with the EFHD2ΔCC mutant or that the PI-exclusion assay is not sensitive enough to measure subtle changes of cell viability. In order to further address the question of cell viability in cultures overexpressing EFHD2 or its mutants, exposure of transfected cells to toxic agents or calcium modulators could be helpful in elucidating a potential effect. Exposure of the cell cultures to Aβ or the quinone-analogue and known oxidising agent menadione followed by measurement of cell viability were tested but later abandoned because of technical difficulties with the cell toxicity caused by the chemicals. An interesting alternative to this approach could be the measurement of intracellular calcium fluxes with calcium-indicators such as Fura-2 or the assessment of other mitochondrial properties such as the mitochondrial membrane potential with tetramethyl rhodamine dyes in transfected cell cultures. This approach might be able to clarify if EFHD2 or its ΔCC mutant are able to modulate intracellular calcium signals in neuronal cells and indirectly influence cell viability, similar to its function in B-lymphocytes described before (Avramidou et al., 2007; Kroczek et al., 2010).

4.8.2 Analysis of the PI3-kinase pathway

Studies in mast cells have linked EFHD2 to the activation of the PI3-kinase (PI3K)/Akt signalling pathway (Ramesh et al., 2009; Thylur et al., 2009). Because of the significance of this signalling pathway for cell survival as well as its involvement in the control of GSK3 activity, which is one of the main tau-kinases in the brain (see Chapter 1.2.3.2 and Hers et al. (2011)), I studied a potential influence of EFHD2 overexpression on the activation of PI3K signalling in neuronal cells.

Activation of PI3K leads to the phosphorylation and activation of Akt (also known as protein kinase B, PKB) by phosphorylation at Thr^{308} and Ser^{473} (facilitated by Thr^{308} phosphorylation) *via* 3-phosphoinositide-dependent protein kinase 1 (PDK-1) and the mammalian target of rapamycin complex 2 (mTORC 2) respectively. Active Akt then causes the phosphorylation and regulation of a large number of substrates, including GSK3, PRAS 40 and pro-caspase 9 (Hers et al., 2011). I investigated the activation of this pathway by western blotting for phosphorylated Akt and its substrate GSK3. Because of the high transfection efficiency that can be achieved by lentiviral infection, I used this method to deliver EGFP-EFHD2 (pHJ-SW1) or an empty EGFP vector (pHJ-EGFP) into SK-N-SH cells plated, so the cells would reach different cell densities during lentiviral infection and expression of the transgene (confluent, high cell density, low cell density). Cells were infected 24 h after plating in a 6-well plate and phosphorylated proteins from 3 wells per condition were extracted 48 h after infection as described in Chapter 2.1.1 and subjected to SDS-PAGE and western blotting. Figure 4.17 shows the results of the western blot analysis and bar charts

presenting the quantification of total Akt as a ratio over actin, phosphorylated Ser^{473}-Akt and phosphorylated Thr^{308}-Akt as ratios over the total amount of Akt.

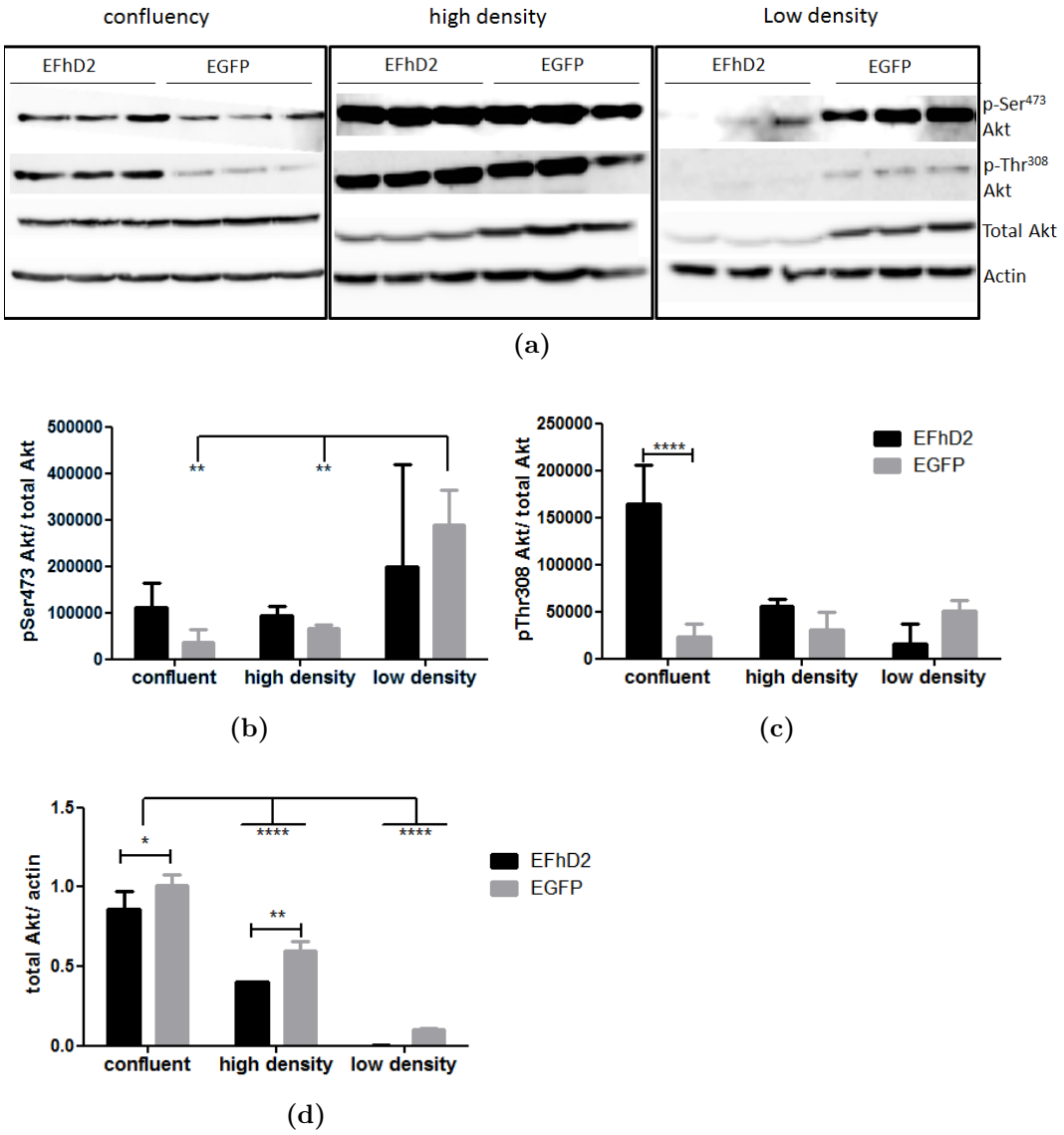

Figure 4.17: Akt signalling in SK-N-SH cells overexpressing EFHD2.

Figure 4.17: Akt signalling in SK-N-SH cells overexpressing EFHD2 (continued). (a) SK-N-SH cells were infected with lentiviruses delivering expression vectors for EGFP-EFHD2 or EGFP alone. Cell were plated so that they reached confluency (left), high cell density (middle) or low cell density (right) 48 h after infection. Western blotting for Akt phosphorylated at Thr^{308} (pThr308-Akt), at Ser^{473} (pSer473-Akt), for total Akt or actin was performed. (b)–(c) Quantification of phosphorylated Akt bands by densitometry. The bar charts show ratios of Ser^{473}-phosphorylated (b) or Thr^{308}-phosphorylated (c) Akt over total Akt protein (arbitrary units). (d) Quantification of total Akt by densitometry. The bar chart presents ratios of total Akt protein over actin stained bands. Significance was tested by 2-way ANOVA and Bonferroni post-hoc test. Error bars show SD.

In agreement with the studies performed in immune cells, SK-N-SH cells infected with full length EGFP-EFHD2 exhibited increased phosphorylation of Akt compared to cells infected with the vector expressing EGFP alone (Figure 4.17(a)). However, this effect was strongly dependent on the cell density of the infected cultures, so that phosphorylation of Akt could only be caused by EFHD2 at high cell densities and was only significant for the Thr^{308} site in confluent cultures, while in low density cultures, phosphorylated Akt levels tended to be reduced, although this effect was not significant (see Figure 4.17(a)–(c)). Interestingly, a similar reduction of phospho-Thr^{308} Akt and phospho-Ser^{473} Akt levels could be observed in SK-N-SH cells transfected with EFHD2 by lipofection, where the lower cell density was caused by toxicity of the lipofection reagent (not shown). Quantification of total Akt levels in lentivirally infected SK-N-SH cells revealed that EFHD2 also caused a reduction of total Akt protein compared to EGFP expressing cells (Figure 4.17(d)).

It was noted that cell density alone also had an effect on the levels of total and phosphorylated Akt protein. Total Akt protein levels increased significantly in high density cultures (Figure 4.17(d)), whereas levels of Ser^{473} phosphorylation

decreased (Figure 4.17(b)) and phosphorylation at the Thr^{308} site was not affected at all in control infected cultures (Figure 4.17(c)). Meanwhile, a strong increase of phosphorylation at Thr^{308} was seen the presence of EFHD2, indicating that EFHD2 facilitates the activation of Akt *via* PDK, possibly upon stimulation of cell adhesion molecules or neurotrophic factors in these cells.

Despite this effect on Akt phosphorylation, western blot analysis of GSK3α/β phosphorylation in the same cultures as above did not reveal any effect of EFHD2 overexpression (Figure 4.18).

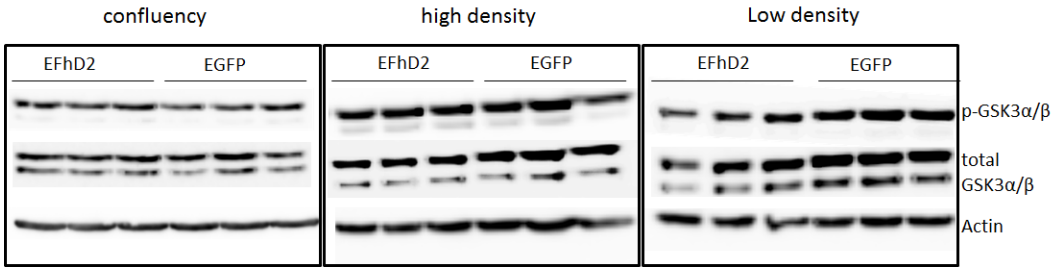

Figure 4.18: GSK3-phosphorylation in SK-N-SH cells overexpressing EFHD2. SK-N-SH cells were infected with lentiviruses delivering expression vectors for EGFP-EFHD2 or EGFP alone. Cell were plated so that they reached confluency (left), high cell density (middle) or low cell density (right) 48 h after infection. Western blotting for GSK3α/β phosphorylated at $Ser^{21/9}$, for total GSK3α/β or actin was performed

With the strong effect seen SK-N-SH cell line, the activation of the Akt-signalling pathway in primary neuronal cultures from ED14 mouse cortex was tested next. Primary neurons were plated on poly-D-lysine coated dishes and infected with the same lentiviral expression vectors for EGFP-EFHD2 or the EGFP control as used for the neuroblastoma cells. 72 h after infection, phosphorylated proteins were extracted from the neurons and SDS-PAGE and western blot analysis were performed.

The results of the analysis of Ser^{473} phosphorylated Akt from two independent

experiments are presented in Figure 4.19(a). As seen in lanes 1 and 3, overexpression of EGFP-EFHD2 did cause a significant reduction of Akt-phosphorylation at Ser^{473} compared to the empty EGFP vector infected neurons. Quantification of the stained bands of 5 repeats of the experiment revealed a 50% reduction of Akt phosphorylation at this site. Notably, a smiliar albeit not statistically significant effect had been detected in SK-N-SH cells overexpressing EFHD2 at low cell density (Figure 4.17(b)–(c)). EFHD2 overexpression had however no effect on the levels of total Akt in primary neurons compared to EGFP control infected neurons.

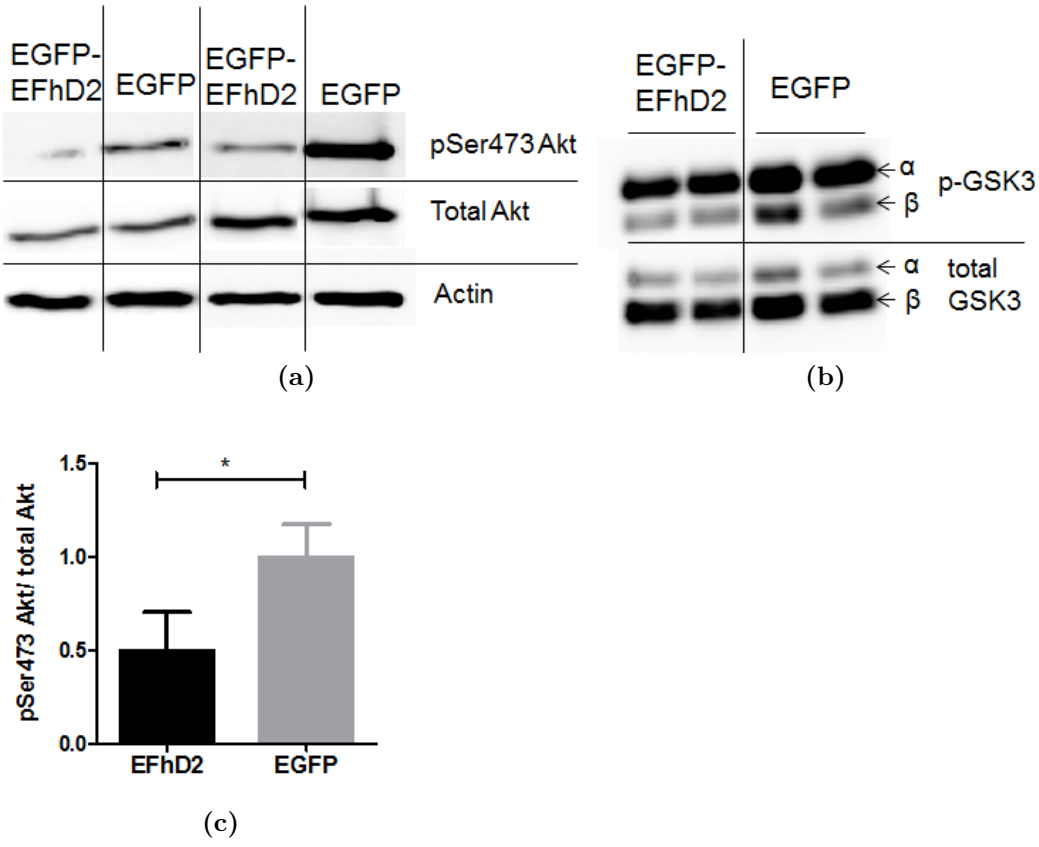

Figure 4.19: Akt signalling in primary neurons overexpressing EFHD2.

Figure 4.19: Akt signalling in primary neurons overexpressing EFHD2 (continued). (a) ED14 cortical neurons were infected with lentiviruses delivering expression vectors for EGFP-EFHD2 or EGFP alone. Phosphorylated proteins were analysed 72 h after infection by western blotting for Akt phosphorylated at Ser ^{473} (pSer473-Akt), total Akt or actin. (b) Western blot analysis of the same samples as in (a) for GSK3α/β phosphorylated at Ser $^{21/9}$ (p-GSK3α/β) or total GSK3α/β. (c) Quantification of phosphorylated protein bands by densitometry. The bar chart presents ratios of pSer^{473}-Akt over total Akt protein. Error bars show SD. Significance was tested by T-Test.

I also analysed the phosphorylation of GSK3α/β in primary neurons overexpressing EFHD2 by western blot analysis (Figure 4.19(b)). In agreement with the results obtained from the SK-N-SH cell line, I could not find any effect of EFHD2 overexpression on GSK3α/β phosphorylation, indicating that EFHD2 acts in a different branch of the Akt-signalling cascade in both SK-N-SH cells and embryonic primary neurons.

4.9 Discussion and outlook

4.9.1 EFHD2 in frontotemporal dementia and AD

With the work described in this chapter, I demonstrated that the EF-hand domain containing protein D2 (EFHD2) is linked to neurodegeneration and that its function might be especially relevant in the pathogenesis of frontotemporal dementia. I showed that protein and mRNA levels of EFHD2 are up-regulated in frontotemporal dementia compared to non-demented age-matched controls but unchanged in AD patient brains (Figure 4.10). These results fit together with the results presented by Vega et al. (2008), who discovered an increased association of EFHD2 with hyperphosphorylated (sarkosyl-insoluble) tau in a mouse model for

frontotemporal dementia and also implied an increase in EFHD2 protein levels in the temporal cortex from a human FTLD case, although no association with tau could be observed in this case (Vega et al., 2008). Vega et al. did find an increased association of EFHD2 with tau in a single human AD case, where insoluble tau-aggregates were present (Vega et al., 2008), however I could not find an increase in EFHD2 expression levels in the AD cases studied in the course of this project. In addition, I could also not find a correlation of EFHD2 protein or individual mRNA expression levels with the levels of tau-pathology detected in the individual human AD and FTLD brain samples (see Table 3.1) or with the tau mutations present in the FTLD cases studied. However, an association of EFHD2 with soluble or insoluble tau species by immunoprecipitation has not been studied in the course of this work. It would therefore be valuable to find out if the association of EFHD2 with tau in the AD brain is still maintained in the samples studied here. Furthermore, analysing the expression levels and association of EFHD2 with tau in more cases of FTLD with or without mutations in tau would be an important piece of the puzzle, as it is the first time that a protein has been linked to different variants of FTLD.

Together, the currently available data points towards a potential role for EFHD2 in neurodegenerative diseases which are accompanied by distinct types of tauopathy (like in FTLD compared to AD or the JNPL3 mouse model). As mentioned in Chapter 1.2.3.2, some experimental results have already pointed towards differences in the mechanism of tauopathy between these diseases, when different tau-mutations and their ability to form tangles and promote Aβ-toxicity were investigated (Tackenberg and Brandt, 2009). The question is therefore if EFHD2 could be one of the molecules manifesting these differences in the human

brain, possibly by changing tau-metabolism through its up-regulation in FTLD but not AD. Investigating the location of tau and EFHD2 in neurons overexpressing EFHD2 would be helpful in clarifying this matter. With respect to the findings from the JNPL3 mouse model expressing the more aggregation prone P301L mutant version of human tau, it would also be of interest to explore if mutant tau or hyperphosphorylated tau associated with late stage tau-pathology in the human AD brain has an increased affinity for EFHD2. This might explain why EFHD2 is not associated with tau in an FTDP17 brain not containing the same species of aggregated tau protein (Vega et al., 2008).

I also presented evidence that the up-regulation of EFHD2 coincides with a potential up-regulation of APP protein in the FTLD cases studied (Figure 4.13). Similarly, analysis of EFHD2 expression levels in an mAPP transgenic mouse model expressing mutant human APP_{695} revealed an up-regulation of EFHD2 in the mAPP transgenic mouse model. This hints at a potential role for an up-regulation of APP levels in the regulation of EFHD2 expression levels (see chapter 6).

4.9.2 EFHD2 influences PI3K signalling

One of the most important tau-kinases involved in tau-pathology is GSK3. Because of its signalling properties in other cell systems and the new link between EFHD2 and FTLD pathology, I investigated the phosphorylation of GSK3 and the activation of its upstream regulator Akt in response to EFHD2 overexpression in SK-N-SH cells and primary neuronal cultures (Figures 4.17, 4.18 and 4.19). I could not find any effect of EFHD2 overexpression on the phosphorylation of

GSK3α/β, indicating that EFHD2 is probably not involved in the regulation of its function in cell lines or embryonic primary neurons.

However, EFHD2 did have an impact on the PI3K/Akt signalling pathway, as the phosphorylation and therefore activation of Akt were increased in SK-N-SH cells (see Figure 4.17). Of note, EFHD2 overexpression mainly affected Thr^{308} phosphorylation at high cell density in these cells, implying that EFHD2 activates the pathway through PDK 1, which is the kinase responsible for phosphorylation at this site (Hers et al., 2011), and that a cell adhesion molecule or neurotrophic stimulation might be upstream of EFHD2. It will now be essential to decipher the activators and targets of this EFHD2 containing signalling cascade. A screen for interaction partners of EFHD2 is in progress in our lab and will be helpful in defining candidate proteins in neuronal cells. Furthermore, western blot analysis of known PI3K and Akt effectors other than GSK3 with a potential relevance for neuronal functions such as PRAS40 and pro-caspase 9 or IRS 1 and regulators of the actin cytoskeleton such as ARP 1/2, Rac or WASP will shed light on which other branches of the PI3K/Akt pathway might be modulated.

The role of EFHD2 in primary neurons, where a marked reduction of Akt-phosphorylation on Ser^{473} was detected, bears some similarity to the situation in low density SK-N-SH cultures but is markedly different from high density neuroblastoma cell cultures. These differences could be due to the trophic stimulation received by high density cultures, where EFHD2 acts as a facilitator of Akt signalling but the relative lack of such stimulation in low density cultures and differentiated primary neurons, where it appears to have the opposite effect. As mentioned in the introduction to this chapter, opposing effects of EFHD2 overexpression (on NFκB activation and Ca^{2+} signalling) have also been described for

B-cells (Kroczek et al., 2010) compared to mast cells (Ramesh et al., 2009) and between immature and mature B-cells (Avramidou et al., 2007). Future studies should therefore investigate a potential effect of EFHD2 overexpression on the stimulation of PI3K/Akt signalling in neurons above baseline, for example in response to exposure to neurotrophins. Additionally, determining the state of Akt-phosphorylation in human brains affected by FTLD, where EFHD2 levels are elevated and in non-demented control brains could provide some information about which direction EFHD2 might be working in in the adult human brain.

In conclusion, Figure 4.20 illustrates how EFHD2 might act as a scaffold or adaptor protein in the PI3K/Akt signalling pathway in a similar fashion to its role at the B-cell receptor. It will be the task for future research to identify other partners and upstream molecules of this potential scaffold.

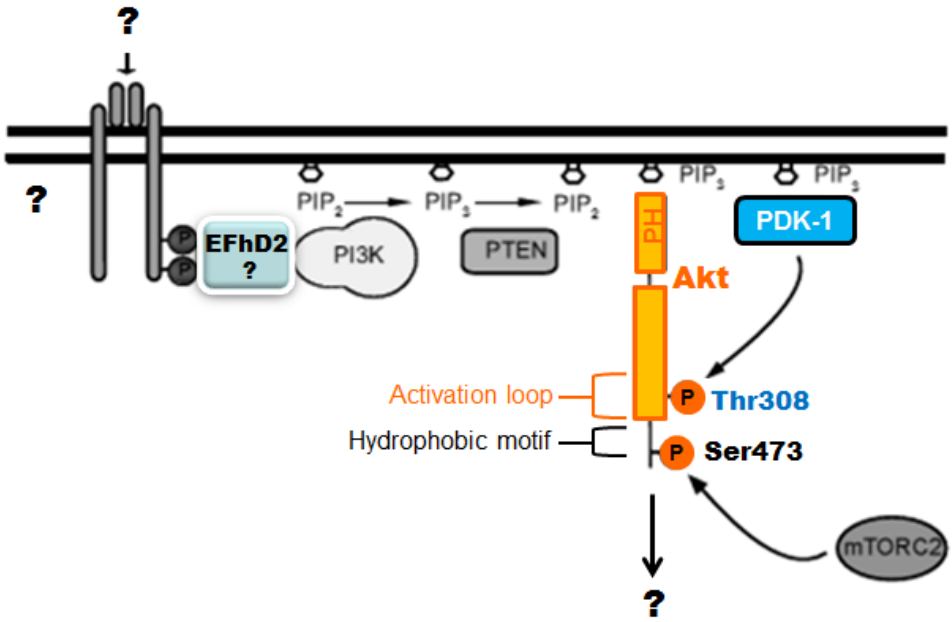

Figure 4.20: EFHD2 in PI3K/Akt signalling.

Figure 4.20: EFHD2 in PI3K/Akt signalling (continued). EFHD2 can lead to the activation of Akt and might therefore act as an adaptor protein for PI3-kinase (PI3K) at cell surface receptors or other membrane proteins, which then results in the production of phosphoinositol-trisphosphate (PIP3) from phosphoinositol-bisphosphate (PIP2) and the recruitment of PIP3-dependent kinase 1 (PDK 1), which phosphorylates Akt at Thr^{308} in its activation loop. The Phosphatase and tensin homolog protein (PTEN), can inactivate the pathway again by de-phosphorylating PIP3. The mammalian target of rapamycin complex 2 (mTORC 2) phosphorylates Ser^{473} in Akt at a hydrophobic motif, which facilitates Thr^{308} phosphorylation and might play a role in the regulation of Akt-specificity. Modified with permission from Elsevier B.V. (Hers et al., 2011).

CHAPTER 5

PEROXIREDOXIN-2 IN DEMENTIA AND *IN VITRO* MODELS FOR NEURODEGENERATION

5.1 Introduction

5.1.1 Peroxiredoxin-2 as an antioxidant and signalling modulator

Peroxiredoxin-2 (Prx-2) is a 198 aa cytosolic protein belonging to a group of antioxidant enzymes which possess peroxidase activity (ROOH + 2e $\rightarrow$ ROH + H_2O). Peroxiredoxins are a very abundant species in the cell and function to reduce hydrogen peroxide, organic peroxides and the very toxic peroxinitrite and thereby represent an important defense against damaging oxidation of proteins and lipids. In the case of Prx-2, which is a 2-Cys peroxiredoxin, the enzymatic mechanism involves 2 cysteine residues, a peroxidatic cysteine and a resolving cysteine, which react in two steps as depicted in Figure 5.1. The first step is the reduction of the peroxide through a nucleophilic attack by the peroxidatic cysteine residue, which leads to the formation of a cysteine sulfenic acid intermediate in Prx-2. The second step is the recovery of the Cys-sulfhydryl group. This involves Prx-2 homodimerisation and formation of a disulfide bond between the peroxidatic cysteine of one subunit with the resolving cysteine of the other subunit, followed by the recovery of both cysteins with the help of disulfide reductase together with thioredoxin. It has been proposed that redox-sensitive oligomerisation/decamerisation of Prx-2 also forms part of its normal catalytic cycle and enhances the catalytic activity of the subunits (Wood et al., 2003; Rhee et al., 2005).

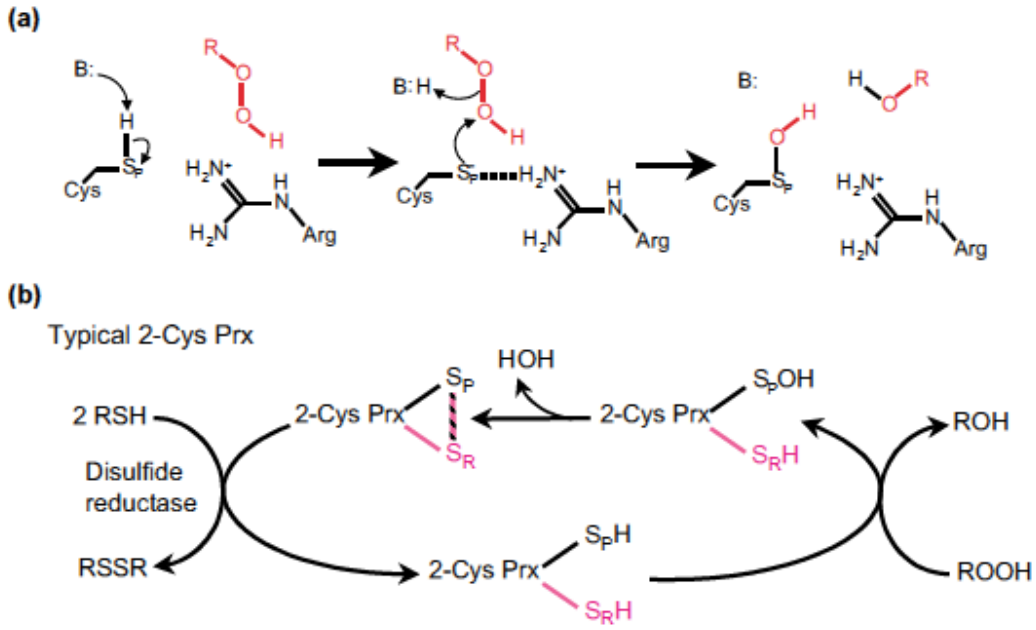

Figure 5.1: Mechanisms of 2-Cys peroxiredoxins. (a) First step: reduction of the peroxide (in red), by the peroxidatic cysteine residue. The peroxidatic cysteine is de-ionised by a catalytic base (B:) and stabilised by a conserved arginine residue. The outgoing ROO^- group is protonated by a catalytic acid (B:H). (b) Recovery of the oxidised enzyme. Formation of a disulfide bond between the peroxidatic cysteine sulfenic acid (black) and a resolving cysteine residue from another Prx-2 subunit (pink). Reduction of the cysteine residues is achieved by a disulfide reductase together with thioredoxin which is oxidized from a dithiol (2RSH) to a disulfide (RSSR). Reprinted with permission from Elsevier Science Ltd. (Wood et al., 2003).

High levels of ROS or low levels of Prx-2 have been shown to result in an overoxidation of the catalytic cysteine residue to a non-reactive sulfinic acid ($Cys\text{-}SO_2H$) and the inactivation of the enzyme (Wood et al., 2003). With regard to the rapid increase in ROS levels needed in order for H_2O_2 to act as a signalling molecule, this inactivation of 2-Cys peroxiredoxins has been proposed to play an important part in the facilitation of local H_2O_2 signalling events by delaying ROS degradation (Rhee et al., 2005). Notably, the inactivation of 2-Cys peroxiredoxins (but not other proteins containing cysteine residues which can be overoxidised)

can eventually be reversed by the actions of sulfiredoxin (Srx), which reduces the sulfinic acid back to the active thiol (Rhee et al., 2005).

An additional mechanism for regulating Prx-2 activity is its phosphorylation at Thr^{89} by cyclin-dependent kinases, which has been shown to diminish its enzymatic activity by interfering with the homodimerisation required for the recovery of the catalytic cysteine residues (Wood et al., 2003).

By controlling the diffusion of reactive oxygen species inside the cell, peroxiredoxins have also been recognised as modulators of signalling events mediated by H_2O_2. The main sources for reactive oxygen species in the cell are their leakage from the electron transport chain at complex I (NADH-oxidase) or NADPH oxidase in the cytosol, both of which produce the reactive superoxide anion that can then be converted to H_2O_2 by superoxide dismutase in the mitochondria and the cytosol. It has been shown that production of ROS by NADPH-oxidases can be enhanced for example in response PDGF- or TNFα exposure (Kang et al., 1998) and also plays a part in other cellular processes such as the EGF-receptor signalling, vascular endothelial growth factor (VEGF) and interleukin 1 (IL-1) signalling as well as oxidative events in the ER (reviewed in Hall et al. (2009)). Also, superoxide-flashes, caused by a transient opening of the mPTP in single mitochondria of cells under normal conditions and cells under stress (hypoxia) have been described (Wang et al., 2008) and could be an additional source for localised peroxide signalling.

One of the most important signalling molecules activated by ROS is JNK and intriguingly, Prx-2 has been given a role in the regulation of JNK activity in yeast as well as in mammalian cells (Veal et al., 2004; Lee et al., 2011). In yeast, this has been found to depend on the formation of a disulfide bond between Prx-2 and

the yeast specific JNK-homolog Sty1 in response to peroxides, which promotes its activation (Veal et al., 2004). In a human cancer cell line, Prx-2 has also been identified as an activator of JNK/c-Jun-signalling in response to DNA damage (Lee et al., 2011). Interestingly, this activation was found to be independent from oxidative stress caused by the compounds studied, as Prx-2 expression efficiently inactivated the oxidative species during exposure, but rather by a direct effect of Prx-2 on JNK in the nucleus (Lee et al., 2011). However, this does not exclude the possibility that peroxides are required to induce this interaction, as they induce changes in Prx-2 conformation and quaternary structure (Wood et al., 2003; Hall et al., 2009). Given this new function of Prx-2 in cellular signalling events it is not surprising, that Prx-2 has been found to be associated with the same pool of retrograde synaptic vesicles as Ep-1 and the JNK-interaction protein JIP3 in the mouse brain cortex (Abe et al., 2009). This introduces the interesting possibility that Prx-2 might be able to influence JNK-activation at the synapse or at retrogradely transported synaptic vesicles.

5.1.2 Peroxiredoxin-2 in neurodegeneration

The role of Prx-2 has also been studied in model systems for neurodegeneration. Like AD and FTLD, Parkinson's disease is a disease associated with aging manifesting with a pronounced resting tremor, slowing of simple movements (bradykinesia), an inability to move (akinesia) and rigid limbs, which can at a later stage also be accompanied by personality changes and dementia. Underlying PD is the degeneration of dopaminergic neurons in the substantia nigra of the brain and the formation of toxic Lewy body inclusions made of α-synuclein. This is often

associated with genetic mutations in the gene encoding for the ubiquitin-E3 ligase Parkin, which is thought to interfere with protein (sich as α-synuclein) degradation and lead to cell death (Mayeux, 2003). It is noteworthy though that some parallels between the pahtologies of AD and PD, especially with focus on mitochondrial dysfunction and oxidative stress have been identified (Beal, 1995) and that APP as well as α-synuclein have been found to be able to be transported to mitochondria causing their dysfunction (Devi and Anandatheerthavarada, 2010). Unsurprisingly then, overexpression of Prx-2 has been shown to protect dopaminergic neurons from oxidative stress induced by exposure to 6-hydroxydopamine (6-OHDA) as a model for Parkinson's disease *in vitro* and *in vivo*, where endogenous Prx-2 becomes inactivated by overoxidation (Hu et al., 2011). It was also revealed that the protection by Prx-2 was mediated by the inhibition of ASK-activation and downstream activation of the JNK and p38 signalling cascades (Hu et al., 2011) (see also Figure 3.1). Under normal conditions, ASK exists in a complex with thioredoxin (Trx), termed ASK-signalosome, which dissociates upon oxidation of Trx by cellular oxidants such as Prx-2 and leads to the release of active ASK (Fujino et al., 2007). Accordingly, Hu et al. (2011) demonstrated, that the oxidation of Trx was reduced and the association of ASK and Trx enhanced when the cells were exposed to 6-OHDA in the presence of surplus Prx-2, thereby inhibiting ASK release and activation.

Qu et al. (2007) employed a different mouse model for PD, where neurodegeneration is induced by exposure to 1-methyl-4-phenyl-1,2,3,6-tetrahydropyridine (MPTP), which can also cause Parkinsonism in humans (Qu et al., 2007). It had previously been shown, that activation of calpain and CDK5 are important mediators of MPTP induced toxicity on dopaminergic neurons (Smith et al., 2003).

In the course of their study, Qu et al. identified Prx-2 as an interacting partner of CDK5 through its activator p35, and showed that Prx-2 is phosphorylated by CDK5/p35 at Thr^{89} in MPTP exposed neurons *in vitro* and *in vivo*, decreasing its activity (Qu et al., 2007). In line with the study by Hu et al. (2011), wild-type Prx-2 as well as a Prx-2^{T89A} mutant, which can not be phosphorylated, both protected neurons against MPTP induced toxicity (Qu et al., 2007). In contrast, a Prx-2^{T89E} mutant mimicking constitutive phosphorylation of the protein, could not provide this protection. The importance of this posttranslational modification for the pathology of the human disease was demonstrated, when increased levels of phosphorylated Prx-2 could also be detected in human brains affected by PD (Qu et al., 2007).

This new link between calpain and CDK5 activation and the function of Prx-2 in neurons is particularly interesting as an increased activation of calpains and of CDK5 has also been implicated in AD as mentioned in Chapter 1. The calcium regulated protease calpain can regulate Aβ production *via* BACE1 activation (Liang et al., 2010; Mathews et al., 2002) and its activity is increased in the AD brain (Saito et al., 1993) as well as in APP overexpressing cell cultures (Kuwako et al., 2002). CDK5 is also up-regulated in AD (Pei et al., 1998; Swatton et al., 2004) and is one of the most important tau-kinases in the brain (see Chapter 1.2.3.2). Its activation has furthermore been linked to the production of intraneuronal Aβ (Cruz et al., 2006) and to the signalling events mediating amyloid toxicity (Wei et al., 2002; Zempel et al., 2010). At the same time, Prx-2 protein levels have been shown to be elevated in the AD brain (Krapfenbauer et al., 2003; Yao et al., 2007) and in the mAPP transgenic as well as the ABAD/mAPP double transgenic mouse models as a result of the ABAD–Aβ interaction (Yao et al.,

2007). This increase in Prx-2 expression could be due to the aggravated mitochondrial dysfunction and cellular stress seen in these mouse models (Takuma et al., 2005). However, the processes leading to this up-regulation have not been explained yet. The new findings in the mouse models for PD described above also beg the question, if the up-regulation of Prx-2 and the activation of the calpain/CDK5 system are linked in AD and if a phosphorylation of Prx-2 also plays a role in AD pathology.

5.2 Aims of this chapter

The aim of the work presented in this chapter was to further elucidate the role of Prx-2 in neurodegeneration. Hence, protein and mRNA expression levels of Prx-2 were analysed in human brain samples from patients with dementia (AD and FTLD) and compared to the levels found in non-demented controls. Taking their relationship in the mAPP/ABAD double transgenic mouse model into account, the expression levels of ABAD and Ep-1 were also analysed in human brains with dementia. Other mouse models for neurodegeneration were analysed in order to broaden the picture of how the expression of these proteins is linked to neurodegenerative disorders in general.

Finally, the the effect of Prx-2 on neuronal cell survival and the activation of the JNK-signalling cascade were studied in an *in vitro* model for AD. Mouse embryonic primary neurons were transfected with Prx-2 or its mutants and cell survival and the phosphorylation of components of the JNK-signalling cascade in response to exposure to amyloid were analysed.

It was anticipated that these studies would shed more light on the functions

of Prx-2 and also of ABAD and Ep-1 in different settings of neurodegeneration. A deeper understanding of their roles in the brain will also be necessary in order to validate ABAD as a potential drug-target for the treatment of Alzheimer's disease.

5.3 Expression levels of Prx-2 in human AD and AD mouse models

5.3.1 Analysis of Prx-2 protein levels in brains from human dementia sufferers

Protein and mRNA expression levels of Prx-2 were analysed in brain tissue samples from human dementia sufferers as described before in Chapters 3.3 and 4.5. Tissue samples from 4 patients diagnosed with FTLD, 5 cases diagnosed with AD and 5 non-demented control subjects were used for the analysis. For real-time PCR analysis 6 FTLD cases were analysed. Figure 5.2 shows the results of the western blot and qPCR analyses of Prx-2 expression. The western blot images 5.2(a) together with quantification of the western blots by densitometry shown in Figure 5.2(b) revealed that while there was a tendency towards higher levels of Prx-2 in the hippocampus of both, AD affected brains and the frontal cortex from FTLD cases, only the levels of Prx-2 in the hippocampus from FTLD patients were increased significantly compared to non-demented controls. No changes of Prx-2 expression could be measured by qRT-PCR (Figure 5.2(c)).

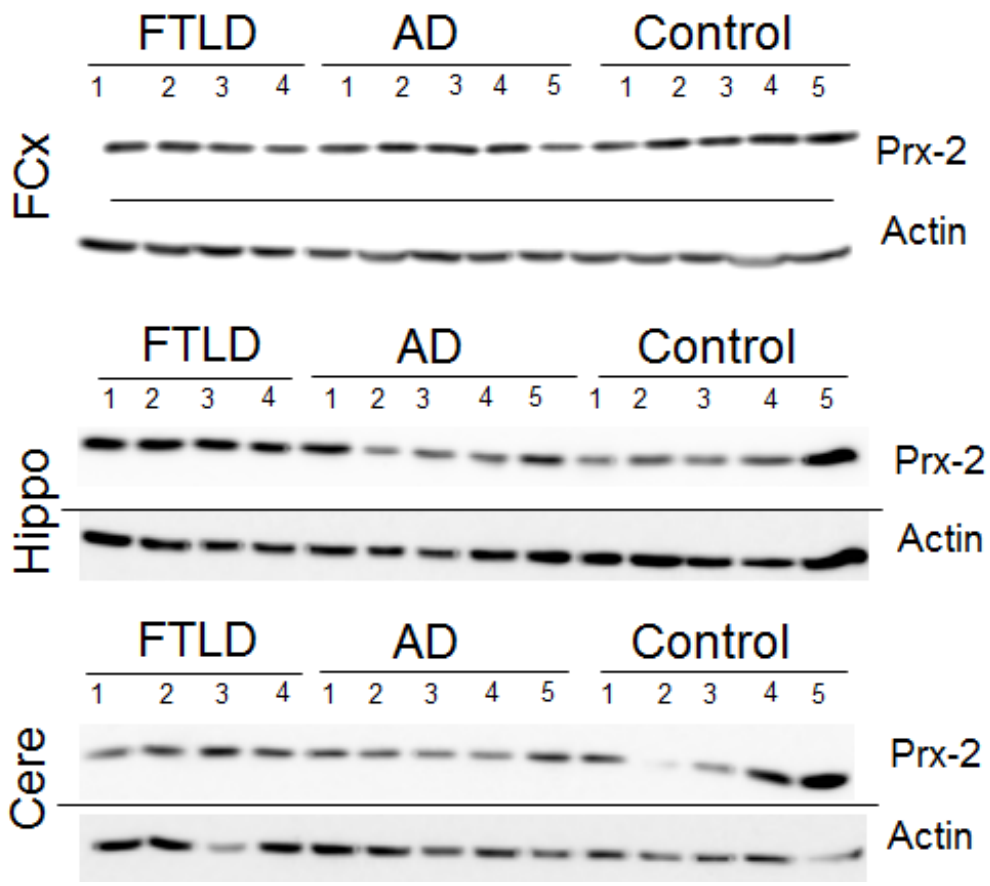

(a)

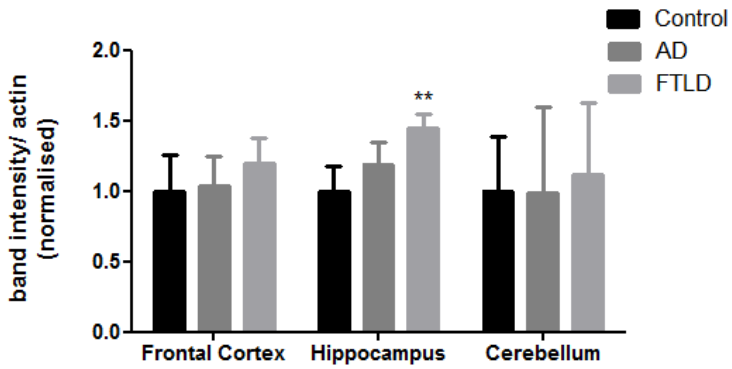

(b)

Figure 5.2: Prx-2 protein levels in human dementia.

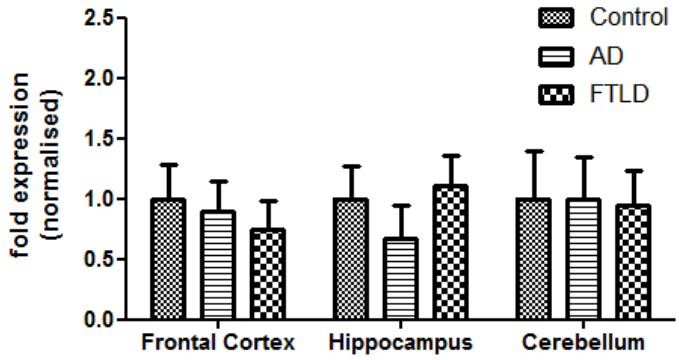

(c)

Figure 5.2: Prx-2 protein levels in human dementia (continued). Levels of Prx-2 in different brain regions from human dementia sufferers. (a) FCx: frontal cortex, Hippo: hippocampus, Cere: cerebellum. Actin was used as a loading control. (b) Quantification of stained bands by densitometry. Prx-2 bands were normalised to total actin and mean values were compared. Error bars show SEM. Control = 1, n = 5. Groups were compared using 2-way ANOVA and Bonferroni post-hoc test. FTLD: Fronto-temporal lobar degeneration, AD: Alzheimer's disease (c) Quantification of Prx-2 mRNA levels by quantitative real time PCR. 3 independent measurements were performed and each time expression levels relative to actin mRNA were calculated. Control = 1. Error bars show SEM. n = 5. Groups were compared using 2-way ANOVA and Bonferroni post-hoc test.

It was noted that this increase of Prx-2 expression correlated with the increased APP and EFHD2 expression (see Figures 4.10 and 4.13) detected in the hippocampus of FTLD cases, all of which have been linked to calcium controlled processes in the cell either directly or via calpain/CDK5. It was unexpected not to find increased expression of Prx-2 in the brain samples from human AD sufferers in this this study, as an increased expression of Prx-2 had been shown in AD previously (Ren et al., 2008; Krapfenbauer et al., 2003). This underlines the large amount of variability that is inherent in studies on the *post mortem* human brain and the need for sufficiently large samples sizes in order to detect more subtle changes in protein or mRNA expression. It might also reflect differences in

the cohorts studied by Yao et al. (Columbia Alzheimers Disease Research Center brain banks) and in this study (Manchester brain bank).

5.3.1.1 Analysis of ABAD, Ep-1 and protein and mRNA expression.

In their studies on the cellular effects of the interaction of ABAD and Aβ on neurons in the brain, Yao et al. and Ren et al. revealed that the increases in Prx-2 expression (Yao et al., 2007) and Ep-1 levels (Ren et al., 2008) were caused by the ABAD–Aβ interaction. Because of this link, I also analysed the mRNA and protein expression levels of ABAD and Ep-1 the same samples from human dementia patients. Figures 5.3(a) and (b) present the results of the analysis of ABAD protein expression, which did not reveal differences in ABAD protein levels between the different cases studied here. However, the analysis of ABAD mRNA levels shown in Figure 5.3(c) demonstrated an increase in ABAD mRNA expression in the hippocampi from AD and FTLD patients.

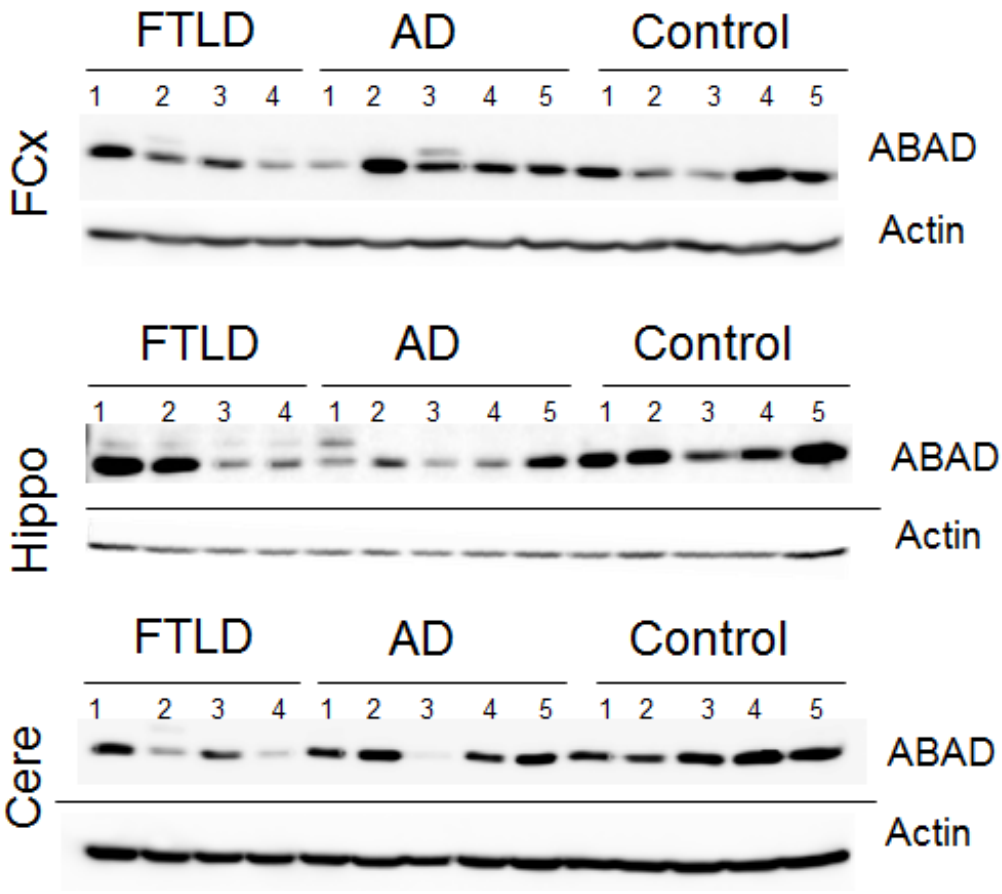

(a)

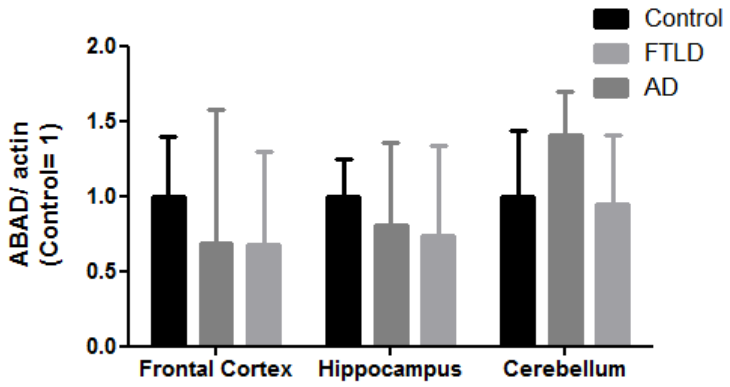

(b)

Figure 5.3: Levels of ABAD protein and mRNA in brain tissue from human dementia sufferers.

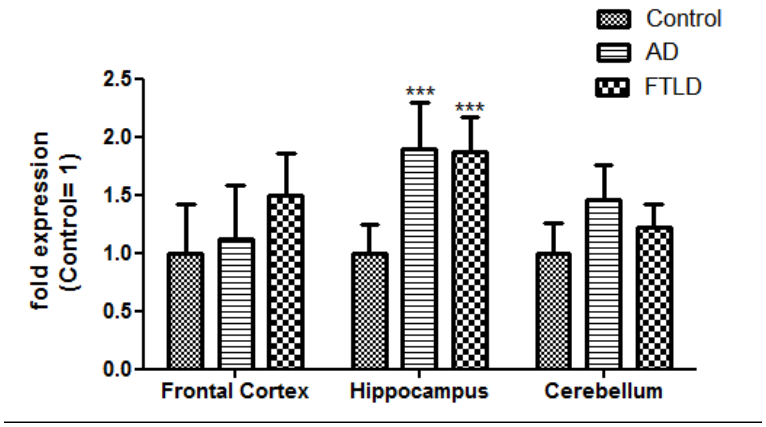

(c)

Figure 5.3: Levels of ABAD protein and mRNA in brain tissue from human dementia sufferers (continued). Human tissue from frontal cortex (FCx), hippocampus (Hippo) and cerebellum (Cere) from individuals with frontotemporal lobar degeneration (FTLD), Alzheimer's disease (AD) or non-demented control individuals was analysed. Analysis was performed as for Figure 5.2. (a) Representative images of ABAD western blots. (b) Quantification of stained bands normalised to actin by densitometry. Control = 1; n = 5 (c) Quantification of ABAD mRNA levels by quantitative real time PCR. Control = 1; n = 5

In the same way, Figure 5.4 shows the results of the analysis of Ep-1 expression in these brain samples. Surprisingly, despite the increased expression levels of ABAD mRNA and Prx-2 protein seen in the FTLD and AD affected hippocampi (Figures 5.2 and 5.3), no differences in the protein or mRNA levels of Ep-1 could be measured between the human AD, FTLD or non-demented control cases analysed in this study.

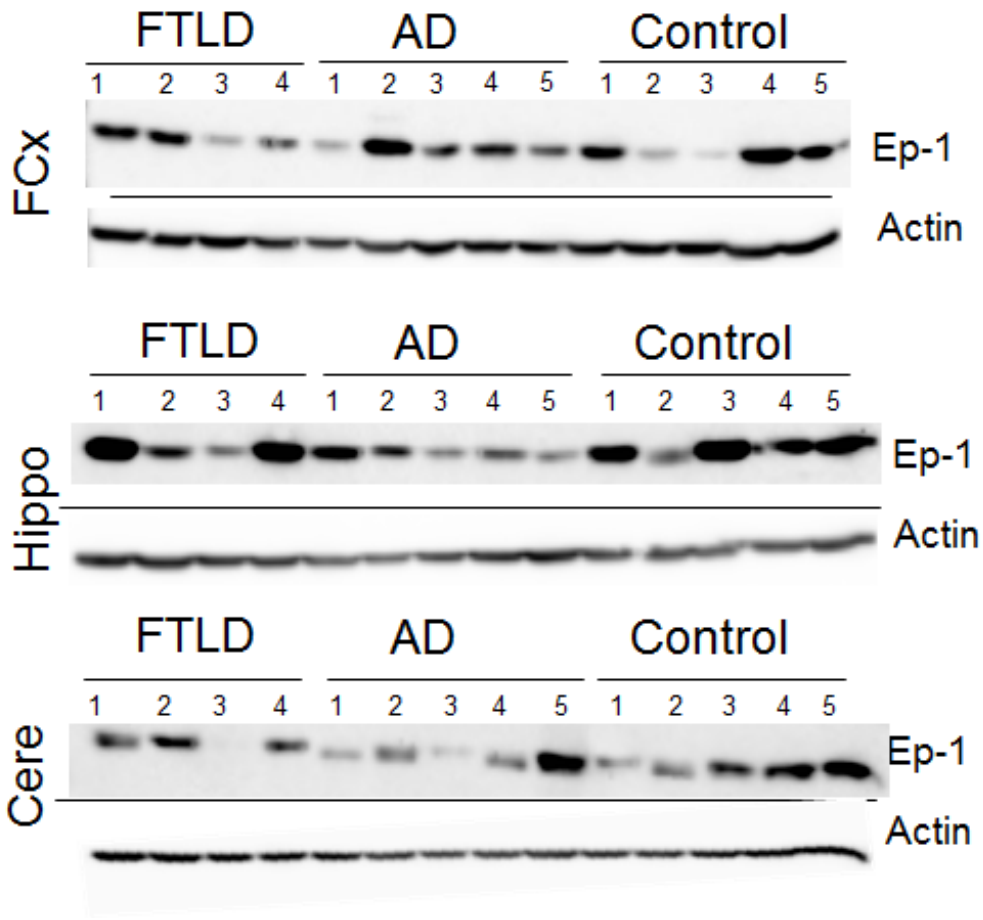

(a)

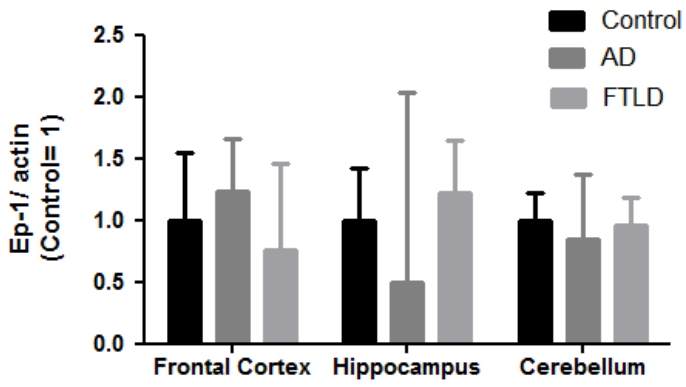

(b)

Figure 5.4: Endophilin-1 protein and mRNA in brain tissue from human dementia sufferers.

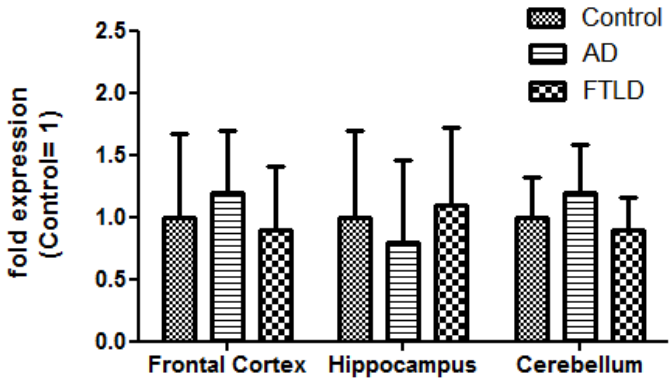

(c)

Figure 5.4: Endophilin-1 protein and mRNA in brain tissue from human dementia sufferers (continued). Human tissue from frontal cortex (FCx), hippocampus (Hippo) and cerebellum (Cere) from individuals with frontotemporal lobar degeneration (FTLD), Alzheimer's disease (AD) or non-demented control individuals was analysed. Analysis was performed as for Figure 5.2. (a) Representative images of Ep-1 western blots. (b) Quantification of stained bands by densitometry. Control = 1; n = 5. (c) Quantification of Ep-1 mRNA levels by quantitative real time PCR. Control = 1; n = 5

In summary, these results show an increase of Prx-2 protein and ABAD mRNA levels in the hippocampus from brains affected by FTLD, which has not been noted before.

Meanwhile, this analysis could not confirm previous findings by Ren et al. and Yao et al. , who had identified a link between the up-regulation of Ep-1 and Prx-2 in the AD brain and that of ABAD (Ren et al., 2008; Yao et al., 2007). Instead, the analysis shown in Figures 5.2–5.4 revealed no changes in the protein levels of Prx-2, ABAD or Ep-1 in the AD brain compared to non-demented controls, although an increase in ABAD mRNA levels was measured.

As mentioned before, the discrepancies to the previous findings might reflect inherent differences in the cohorts of donors studied or in the techniques used during tissue sampling and preparation for western blotting and qRT-PCR. They do

therefore point towards the high level of variability often seen when studying the aging human brain, especially when investigating dementia. Furthermore, the expression levels of these proteins have not been studied by immunohistochemistry during this study, which had been done by Yao et al. and Ren et al. to confirm their western blotting results (Yao et al., 2007; Ren et al., 2008). Information about the localisation and expression levels of these proteins in individual cells could provide important information about their relative expression levels on the cellular level which might be able to confirm a link between their expression levels which the biochemical analysis could not reveal.

Also, a link between the expression levels of ABAD and Ep-1 could still be found, even though it did not correlate with AD in the case of this study. Analysing the western blot results for the individual samples, it was noted that high levels of ABAD strongly correlated with high levels of Ep-1 protein, especially in samples from the frontal cortex and hippocampus. The findings of this experiment do therefore not undermine the role for the Ep-1, Prx-2 or ABAD in dementia pathology.

5.3.2 Prx-2 in a CypD-deficient mouse model for AD

The CypD deficient mouse model, crossed with mice overexpressing human mutant APP has proven to be a valuable model to study the effects of increased APP or Aβ levels and the impact of mPTP formation and mitochondrial calcium-homeostasis (see also chapter 4.6). I therefore also analysed the protein levels of Prx-2 in this mouse model by western blotting. Figure 5.5(a) shows the results of the western blot analysis. Quantification of the stained bands by densitometry

as shown in Figure 5.5(b) revealed that there was a significant increase in Prx-2 protein levels in those animals overexpressing mAPP compared to wild-type APP expressing mice. The reduction of oxidative stress in the CypD-deficient animals was however not sufficient to reduce Prx-2 levels back to the levels seen in wild-type animals (Figure 5.5(b)).

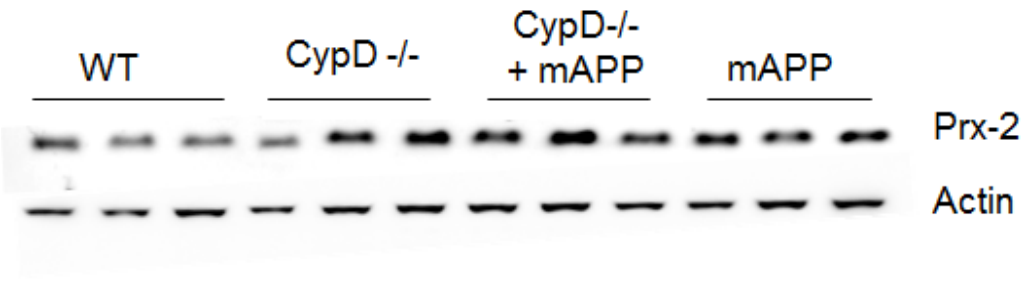

(a)

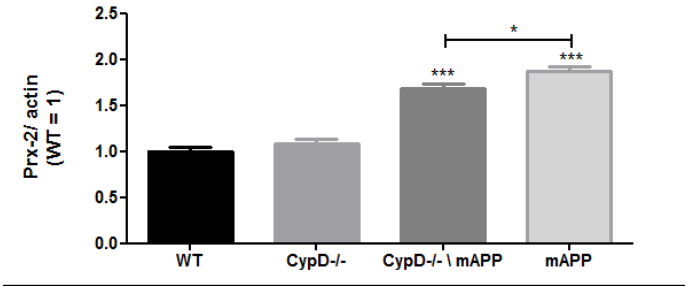

(b)

Figure 5.5: Peroxiredoxin-2 in the CypD-KO/mAPP transgenic mouse model. (a) Western blot analysis of Prx-2 in protein extracts from whole mouse brains from 3 Wild-type (WT), CypD-deficient (CypD-/-) or mAPP or mAPP transgenic (mAPP) littermates. (b) Densitometry of stained bands from 3 independent experiments. WT = 1, n = 3. Error bars show SEM. Groups were compared using 1-way ANOVA and Tukey's post-hoc test. Actin was used as a loading control.

In keeping with the logic applied when the EFHD2 expression levels were analysed (see chapter 4.6), up-regulation of Prx-2 levels could be detected in the mAPP overexpressing mouse model but not in the human AD brain. Amyloid pathology is an important feature of the human AD brain and its presence in

the mAPP transgenic mouse brain has been confirmed by numerous independent studies. This indicates that amyloid pathology does not correlate with increased expression levels of Prx-2 in the samples studied here. At the same time total APP protein levels have been found to be elevated in the FTLD-cases (see Figure 4.13) and are by definition increased in the mAPP transgenic mouse model (see Figure 4.11). It therefore appears that Prx-2 expression correlates with an increase in total APP protein levels, similar to what had been found for EFHD2 (see chapter 4.6).

5.3.2.1 JNK-activation in the CypD$^{-/-}$/mAPP transgenic mouse model

The human hippocampal tissue samples from FTLD-affected brains studied also harbored significantly increased levels of phosphorylated JNK. I therefore analysed the phosphorylation of JNK in the brains from littermates of the wild-type, CypD$^{-/-}$, mAPP/CypD$^{-/-}$ and mAPP transgenic mice. To do this, phosphorylated proteins from the brain of one animal per genotype were extracted in 1 ml of phospho-lysis buffer per cortical hemisphere as described in Chapter 2.1.1. Diluted protein samples were subjected to SDS-PAGE and western blot analysis for total and Thr^{183}/Tyr^{185} phosphorylated JNK. The results of the western blot analysis presented in Figure 5.6 and suggest an increase in phosphorylated JNK levels in the mAPP overexpressing animals (with or without CypD-deficiency) compared to their wild-type APP transgenic by visual insepction of the staining result. Activation of JNK in mAPP transgenic mouse models carrying the APP swedish mutation has been described before (Hwang et al., 2004) and supports the idea that JNK could be phosphorylated in the mouse model studied. How-

ever, quantification of phosphorylated JNK was not possible due to the shortage of brain samples from these transgenic animals.

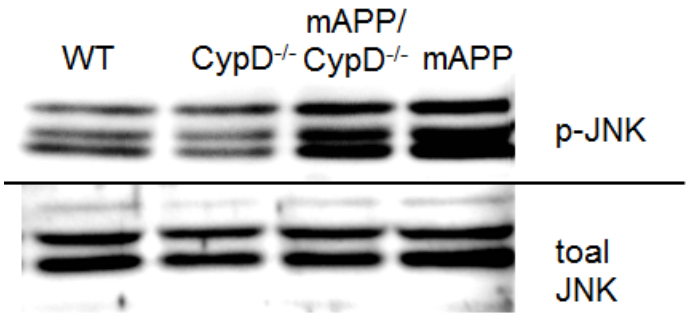

Figure 5.6: Phosphorylated JNK in the CypD$^{-/-}$/mAPP transgenic mouse model. Western blot analysis of JNK phosphorylated at Thr^{183}/Tyr^{185} (top) or total JNK (bottom) in protein extracts from whole mouse brain from a wild-type (WT), CypD-deficient (CypD$^{-/-}$), mAPP transgenic (mAPP) or double transgenic littermates (mAPP/CypD$^{-/-}$).

This demonstrates again a co-occurrence of Prx-2 up-regulation and the presence of active JNK in tissue overexpressing APP. However, it has to be taken into account that the animals studied here express the Swedish mutant of APP, which also causes excessive Aβ pathology that also leads to JNK-activation (Marques et al., 2003; Minogue et al., 2003; Morishima et al., 2001). Therefore the individual effects of APP and Aβ can not be dissected in this mouse model.

5.3.2.2 ABAD and Ep-1 in the CypD$^{-/-}$/mAPP transgenic mouse model

In line with the hypothesis that there is a link between increased levels of ABAD, Ep-1 and Prx-2, I next analysed the protein expression levels of ABAD and Ep-1, the in the CypD$^{-/-}$/mAPP transgenic mouse model. Figures 5.7 and 5.8 show the results of the western blot analysis of 3 brains from each genotype and

the quantification of the stained bands by densitometry. It is apparent that in contrast to its effect on Prx-2 expression, CypD deficiency has no effect on the expression levels of ABAD and Ep-1. Also, no changes in their expression could be detected in the mAPP transgenic animals compared to their wild-type APP expressing littermates.

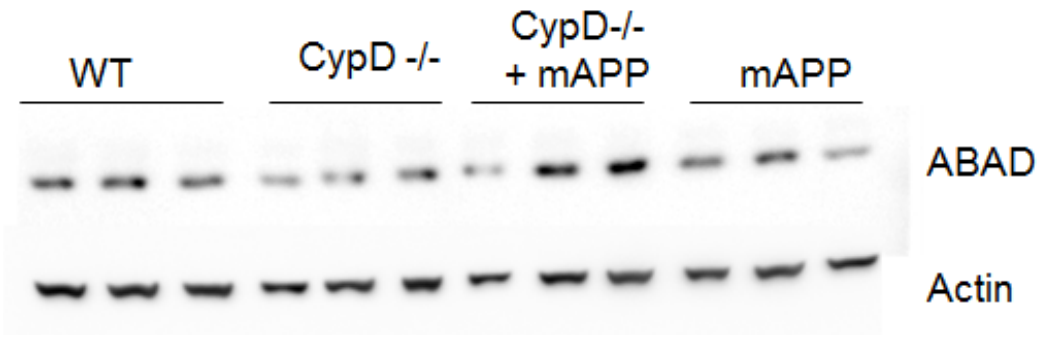

(a)

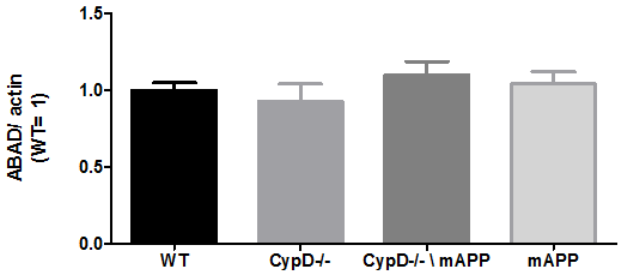

(b)

Figure 5.7: ABAD protein levels in the CypD$^{-/-}$/mAPP transgenic mouse model. Western blot analysis of ABAD in protein extracts from whole mouse brains from 3 wild-type (WT), CypD-deficient (CypD -/-) or mAPP or mAPP transgenic (mAPP) littermates. (a) Representative western blot images. (b) Densitometry of stained bands from 3 independent experiments. WT = 1, n = 3. Error bars show SEM. Actin was used as a loading control.

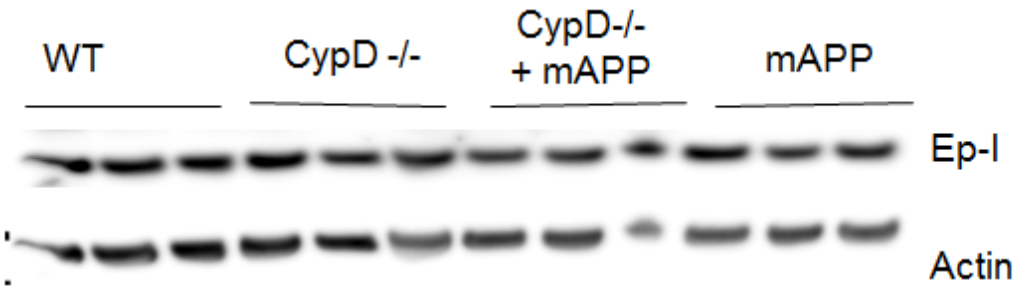

(a)

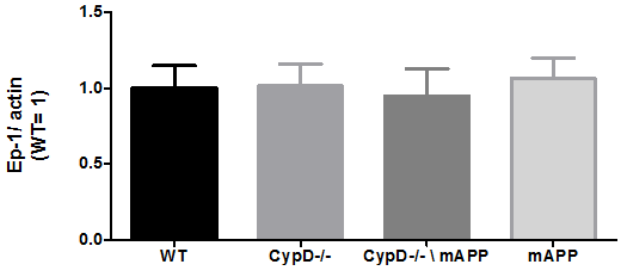

(b)

Figure 5.8: Ep-1 protein levels in the CypD$^{-/-}$/mAPP transgenic mouse model. Western blot analysis of endophilin-1 (Ep-1) in protein extracts from whole mouse brains from 3 wild-type (WT), CypD-deficient (CypD -/-) or mAPP or mAPP transgenic (mAPP) littermates. (a) Representative western blot images. (b) Densitometry of stained bands from 3 independent experiments. WT = 1, n = 3. Error bars show SEM. Actin was used as a loading control.

Previous studies had provided evidence that ABAD protein levels are increased in the brains of AD patients (Yan et al., 1997; Lustbader et al., 2004) and in a triple transgenic mouse model for AD, overexpressing mutant human APP, presenilin and tau, which leads to excessive amyloid pathology in these animals (Yao et al., 2009). However, no published study has investigated ABAD protein levels in the mAPP single transgenic mouse model. Ren et al. (2008) did also not reveal an up-regulation of Ep-1 in the mAPP transgenic mice but only in the mAPP/ABAD double transgenic animals. It appears therefore, that over-

expression of mAPP alone is not sufficient to cause the up-regulation of ABAD and Ep-1.

5.4 Peroxiredoxin-2 protects primary neurons *in vitro*

5.4.1 Prx-2 overexpression protects against Aβ toxicity

Prx-2 is an antioxidant protein and a such is expected to have protective effects on cells exposed to toxic agents. This has been demonstrated for cells exposed to 6OHDA (Hu et al., 2007) and to MPTP (Qu et al., 2007) and in an AD specific setting, Yao et al. (2007) demonstrated that overexpression of Prx-2 can protect primary neurons from cytotoxicity caused by Aβ exposure. In order to further investigate the protective function of Prx-2, I tested the effect of the overexpression of wild-type Prx-2 but also its phosphorylation mutant Prx-2^{T89E} in primary neurons exposed to Aβ. For these experiments, I chose to use the same method of Aβ preparation employed in the study by Yao et al. (2007), who used an aqueous solution of Aβ(25–35) aggregated at 37°C over 3 days at a final concentration of 50 μM (Yao et al., 2007) (see chapter 2.3.6).

At the time of plating, primary neurons were transfected by nucleofection with 2 μg of wild-type Flag-Prx-2, a mutant version, Flag-Prx-2^{T89E} (see Figure B.4 for a plasmid map) or the empty pcDNA3 vector and plateD in 2 wells of a ply-D-lysine coated 24 well plate (for cell counts) or 8 wells of a 96-well plate (for MTT-assays). 72 h after plating, cells were treated with 50 μM Aβ(25-35) or PBS as a control for 24 h and cell survival was assessed by counting cell numbers

in 5 fields of view at the start and the end of the incubation period for each condition or by MTT-assay. Figure 5.9 shows the results of the cell viability tests. The bar chart in Figure 5.9(a) reveals that transfection of primary neurons with wild-type Prx-2 prior to exposure to Aβ could provide a significantly higher level of protection against amyloid toxicity compared to the empty vector control. However, the Prx-2^{T89E} mutant did not have the same effect. Similar results were obtained when the cells were analysed by MTT assay as shown in Figure 5.9(b).

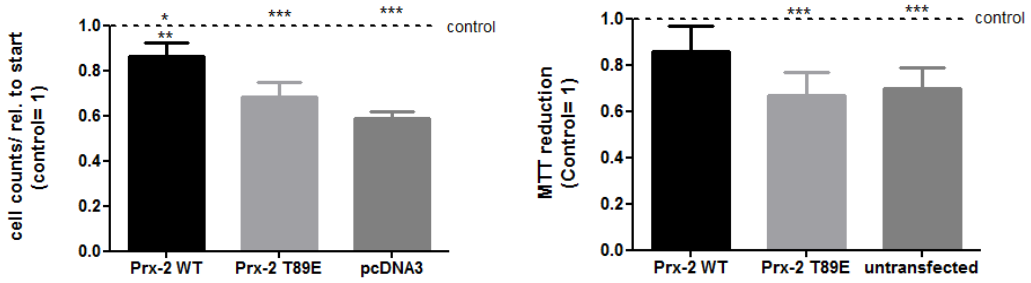

(a) **(b)**

Figure 5.9: Cell survival of primary neurons transfected with either wild-type Prx-2 (WT), mutant Prx-2^{T89E} or an empty pcDNA3 vector control. 72 h after nucleofection and plating, cells were treated with 50 μM Aβ(25-35) or PBS as a control for 24 h. (a) Analysis of cell viability by cell counts in 5 fields of view per time point. The bar chart presents the ratio of cell counts at the start over counts at the end of the incubation period; pcDNA3 = 1. Error bars show SEM. n = 5. (b) MTT-assay of 8 wells per transfection condition after exposure to 50 μM Aβ(25-35) or PBS for 24 h; PBS control = 1. Error bars show SEM. n = 5. Significance between groups was tested using 1-way ANOVA and Tukey's post-hoc test. Differences towards the pcNDA3 control were tested using T-Test.

5.4.2 Overexpression of Prx-2 modulates JNK-signalling in neurons.

As mentioned in section 5.1.1, Prx-2 has been linked to the activation of the JNK signalling cascade by direct interaction with JNK (Veal et al., 2004) and by indirect facilitation of ASK 1 activity through the oxidation of Trx (Hu et al., 2011). Hence, I asked if overexpression of Prx-2, in addition to improving the cell viability, also affected the activation of the JNK-signalling cascade in primary neurons at baseline levels or in response to Aβ exposure.

Primary neurons in were prepared as described in chapter 2.3.2 and nucleofected with Flag-tagged wild-type Prx-2, mutant Prx-2^{T89E}, mutant Prx-2^{T89A} or an empty pcDNA3 vector as control. 72 h after transfection and plating, the phosphorylation of JNK as well as of c-Jun were analysed by western blotting in protein extracts from 3 combined 25 mm dishes of transfected cells. As shown in Figure 5.10(a), staining for the Flag-tag expressed with Prx-2 confirmed successful transfection of the neurons with the plasmids, while no Flag antigen could be detected in the (pcDNA3) vector transfected cells. The figure also shows, that transfection with Prx-2 or its mutants had no effect on the amount of phosphorylated JNK detected (Figure 5.10(a)) and quantification of stained bands in (c)). However, a marked decrease in the levels of total and phosphorylated c-Jun was found in neurons overexpressing Prx-2 or its mutants (Figure 5.10(a)) and quantification of stained bands in (d)). This demonstrates a significant negative effect of Prx-2 overexpression directly c-Jun as a downstream effector of the JNK-signalling cascade, but not on the phosphorylation and activation of JNK itself.

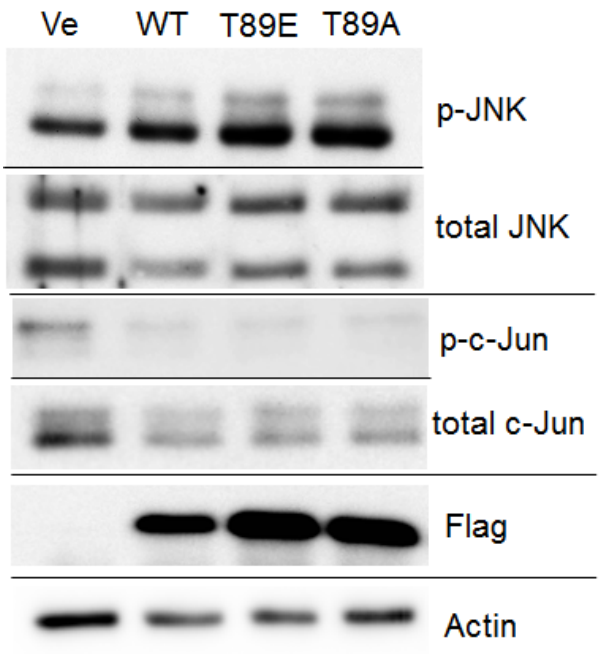

(a)

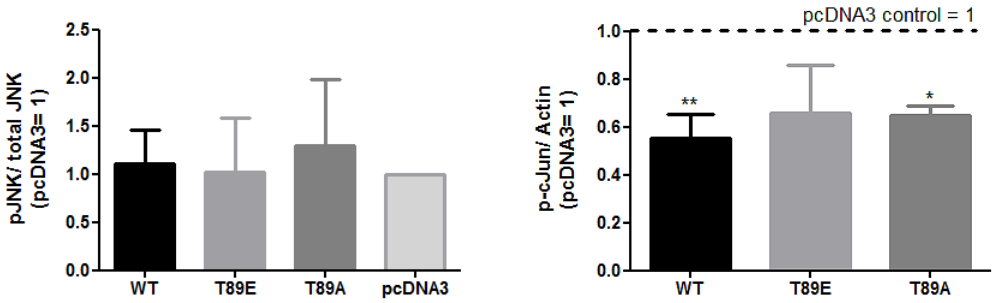

(b) (c)

Figure 5.10: Prx-2 effect on baseline JNK-signalling in neurons (continued). ED14 primary neurons were transfected by nucleofection with with 2 μg Flag-WT-Prx-2, Flag-Prx-2^{T89E}, Flag-Prx-2^{T89A} or an empty pcDNA3 vector (Ve) at the time of plating. (a) Western blot analysis of phosphorylated JNK, total JNK, phosphorylated c-Jun and total c-Jun 72 h after plating. Actin was used as a loading control. Anti-Flag staining was used to verify transfection. (b) Quantification of phosphorylated JNK by densitometry. The bar chart presents the ratio of p-JNK over total JNK. pcDNA control vector = 1 (dotted line), n = 4. Error bars show SD. (c) Quantification of phosphorylated c-Jun by densitometry. The bar chart presents the ratio of p-c-Jun over actin. pcDNA control vector = 1 (dotted line), n = 4. Error bars show SD. Significance was tested using T-test against the control.

Following from this result, I tested if Prx-2 overexpression could also interfere with the phosphorylation of c-Jun seen after exposure of the cells to Aβ. In line with the cell survival studies presented in Figure 5.9, Aβ(25–35) was again used in this experimental setup. It could be shown that exposure of primary neurons for 12 h to 25 μM of Aβ(25–35) caused the phosphorylation of JNK (Figure 5.11(a)) and the phosphorylation and up-regulation of c-Jun (Figure 5.11(b) and quantification in (c)). Note the lower levels of total JNK compared to the control in Figure 5.11(a), indicating a higher level of phosphorylated JNK relative to total JNK. These results are in agreement with what had been shown for Aβ42 and Aβ40 (see Figure 3.6), where activation of c-Jun, probably through JNK, could also be demonstrated.

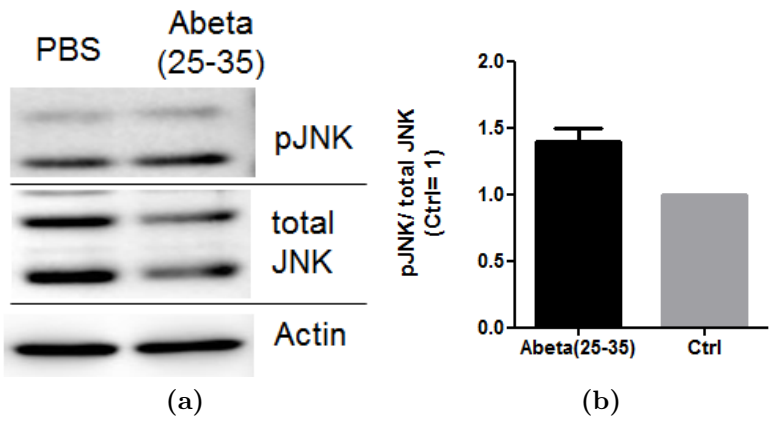

Figure 5.11: Activation of JNK by Aβ(25–35).

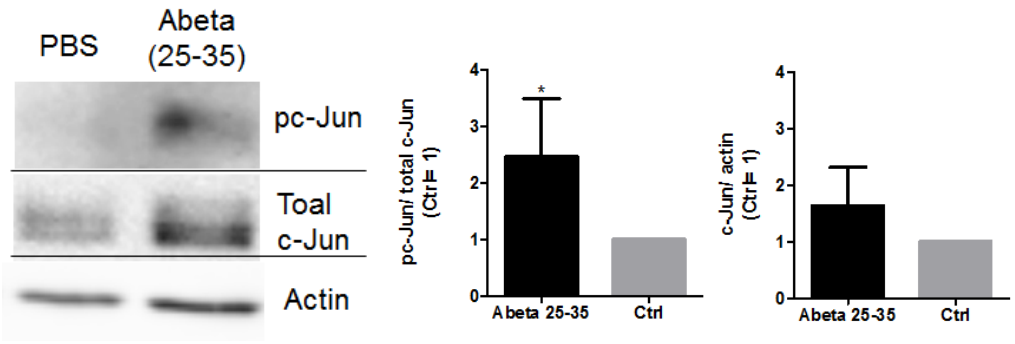

(c) (d)

Figure 5.11: Activation of JNK by Aβ(25–35) (continued). ED14 primary neurons were treated with 25 μM Aβ(25–35) or PBS as a control at 72 h *in vitro*. Phosphorylated proteins were analysed after 12 h exposure. (a) Western blot analysis of phosphorylated JNK and total JNK. Actin was used as a loading control. (b) Quantification of phosphorylated JNK by densitometry. The bar chart presents the ratio of pJNK over total JNK. PBS = 1, n = 3. Error bars show SD. (c) Western blot analysis of phosphorylated c-Jun and total c-Jun. Actin was used as a loading control. (b) Quantification of phosphorylated c-Jun (left) and total c-Jun (right) by densitometry. The bar charts present the ratio of pc-Jun over actin (left) or total c-Jun over actin (right). PBS = 1, n = 3. Error bars show SD. Significance was tested using T-test.

Primary neurons were then transfected as before with 2 μg of wild-type Flag-Prx-2, mutant Flag-Prx-2^{T89E} or mutant Flag-Prx-2^{T89A} and plated on 3 35 mm dishes per condition. 72 h after plating neurons were exposed for 12 h to either 25 μM Aβ(25-35), aggregated for 3 days at 37 °C in PBS or PBS only as a control. Phosphorylated proteins were extracted at the end of this incubation period and subjected to SDS-PAGE and western blotting without delay. Figure 5.12 shows the western blot images of c-Jun phosphorylation in the Prx-2 transfected and amyloid-treated neurons. Staining of the Flag-tag expressed with Prx-2 was again used to verify transfection. While virtually no phosphorylated c-Jun and only low levels of total c-Jun could be detected in wild-type or mutant Prx-2 transfected neurons exposed to the PBS control, overexpression of Prx-2 could not prevent the up-regulation of total c-Jun and phosphorylated c-Jun levels in response to Aβ

(Figure 5.12), which were up-regulated by visual inspection to the same extend as seen in Figure 5.11(c).

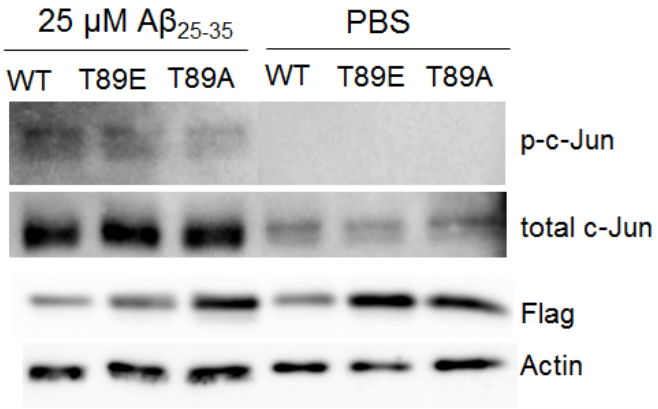

Figure 5.12: Activation of c-Jun in Prx-2 overexpressing neurons. ED14 primary neurons were transfected by nucleofection with with 2 μg Flag-WT-Prx-2 (WT), Flag-Prx-2^{T89E} (T89E), Flag-Prx-2^{T89A} (T89A) at the time of plating. 25 μM Aβ(25–35) or PBS as a control were added to the culture medium at 72 h *in vitro* for 12 h and total c-Jun levels and phosphorylated c-Jun were analysed by western blotting. Staining against β-actin was used as loading control. Anti-Flag staining was used to verify transfection.

The differential effects of wild-type Prx-2 and its mutants on cell viability (Figure 5.9) and on c-Jun phosphorylation (Figures 5.10 and 5.12), suggests that different molecular processes were at play in both experimental setups. A strong component of oxidative stress might lead to cell death in neurons exposed to amyloid, which could be counteracted by Prx-2 overexpression but not by over-expression of its T89E mutant. Meanwhile, no difference could be measured between neurons nucleofected with wild-type Prx-2 or its mutants on c-Jun phosphorylation at baseline or after exposure to amyloid. This indicates that Prx-2 enzymatic function was not needed for its negative effect on c-Jun activity, which appeared to be independent from JNK-phosphorylation (see Figure 5.10). In contrast, Aβ(25–35) exposure most likely caused c-Jun activation through JNK by

other means (see Figure 5.11) and was therefore still able to activate this transcription factor in Prx-2 overexpressing neurons. This also implies that Prx-2 was not able to act as a strong enough antioxidant in nucleofected primary neurons, which appeared to be more susceptible to the activation of the JNK-signalling pathway (see Chapter 3.5.2). It would be possible to answer if this is the case by measuring the amount of overoxidised Prx-2 in these cells, a method which has been used by Hu et al. (2011). Importantly, it will also be necessary to test if the same effects occur in cells infected with lentiviruses for Prx-2 expression, which is a more gentle and efficient way of gene delivery.

5.5 Prx-2, ABAD and Ep-1 in a mouse model for ALS

As mentioned in chapter 1.4.4, the Cu/Zn-dependent superoxide dismutase 1 (SOD1) has been identified as an amyloid binding molecule in cells (Yoon et al., 2009). SOD1 has also been found to be up-regulated in AD and PD brain tissue compared to non-demented controls and oxidation and aggregation of SOD 1 have been linked to senile plaques and neurofibrillary tangles in these brains (Choi et al., 2005). Yoon et al. (2009) also pointed out that the G93A mutant of SOD1 (SOD^{G93A}) which is linked to a familial form of amyotrophic lateral sclerosis (ALS), has a greater affinity to Aβ than wild-type SOD 1. Bosco et al. (2010) described that this SOD^{G93A} mutant shares conformational similarities with oxidised wild-type SOD1, which can be detected in the spinal cord of human sporadic ALS cases (Bosco et al., 2010). Of note, their investigation also revealed

that oxidatively modified SOD but not normal SOD 1 could inhibit kinesin-mediated fast axonal transport through an activation of p38-kinase. It is therefore possible that a similar mechanisms underlie the modification and aggregation of SOD1 seen in the AD and PD brain (Choi et al., 2005).

With this interesting link between AD and ALS in mind, I investigated whether proteins known to be affected in the AD brain are also affected in a mouse model for ALS expressing SOD^{G93A}. To this aim, cortices from 2 adult SOD^{G93A} transgenic mice and 2 wild-type SOD1 littermates were dissected and one hemisphere of each brain was lysed in 1 ml of protein lysis buffer as described in Chapter 2.1.1. The protein concentration of the lysates was determined and 30 μg of total protein was subjected to SDS-PAGE and western blotting. Figure 5.13 shows representative images of the western blot analysis. It revealed, that neither ABAD, Ep-1 or Prx-2 protein levels were altered in the SOD^{G93A} transgenic brains compared those from their wild-type SOD1 littermates. These results indicate that defects in axonal transport and cytosolic oxidative stress caused by overexpression of the mutant SOD1 in this mouse model are not sufficient to cause alterations in ABAD, Ep-1 or Prx-2 as seen in human AD.

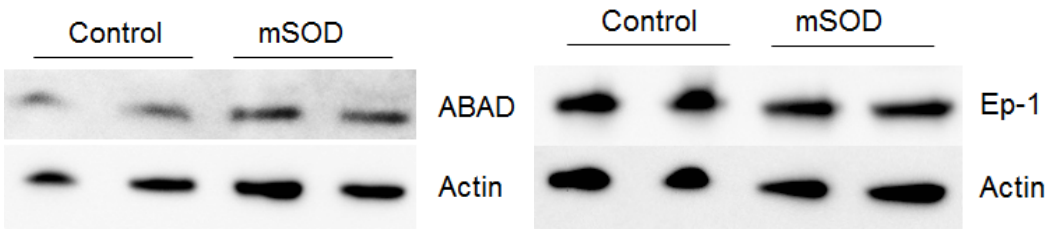

Figure 5.13: Protein levels of ABAD, Ep-1 and Prx-2 in a mouse model for ALS.

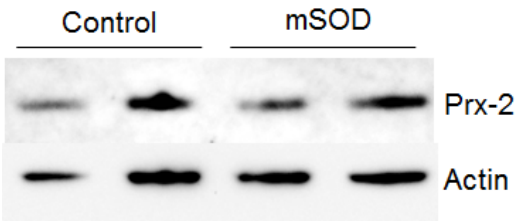

(c)

Figure 5.13: Protein levels of ABAD, Ep-1 and Prx-2 in a mouse model for ALS. Western blot analysis for (a) ABAD, (b) Ep-1 and (c) Prx-2 in brain cortex protein extracts from mutant SOD 1 (mSOD) overexpressing or wild-type control mice. Actin staining was used as a loading control.

5.6 Prx-2 in neurodegeneration. Discussion and outlook

The aim of the work presented in this chapter was to shed new light on the role of Prx-2 in neurodegeneration with special focus on AD, where Prx-2 had previously been found to be up-regulated (Yao et al., 2007).

5.6.1 Prx-2 in the human brain and transgenic mouse models

With the analysis of protein and mRNA expression levels of Prx-2 in human brain samples from patients with dementia (AD and FTLD) and non-demented controls, I could for the first time reveal an up-regulation of Prx-2 protein levels in the hippocampus from patients diagnosed with FTLD compared to the non-demented individuals (Figure 5.2).

In the course of this study, I did not find the previously reported up-regulation

of Prx-2 in the brains from AD patients and could also not measure increased protein levels of ABAD and Ep-1, as reported previously (Yan et al., 1997; Yao et al., 2007; Ren et al., 2008). This might be caused by technical differences in the sampling of the tissue, variations in the execution of the experiments and/or inherent differences in the cohorts studied (UK *versus* USA). Furthermore a large degree of variation of expression levels was observed within the different groups and this might have been possible to overcome with larger sample numbers and the use of immunohistochemistry, revealing potential changes at the cellular level. Especially the samples from FTLD patients represented a wide variety of underlying diagnoses which might have been a confounding aspect (see Table 3.1). Finally, it had been hypothesised that the levels of ABAD, Prx-2 and Ep-1 become up-regulated during the early stages of pathology, possibly due to synaptic failure, which implies that their elevated expression might not be detectable any longer in the *post-mortem* tissue studied here. Information regarding disease progression and length as well as the genetic background of the cases studied here been gathered but could not be compared to the data from previous studies which was not available.

5.6.2 The link to ABAD for Prx-2 and Ep-1

Despite the above described deviations, I could still observe a link between elevated levels of ABAD and higher levels of Ep-1, as individual samples with increased ABAD protein levels also exhibited high levels of Ep-1. This verifies the connection between these proteins as proposed by Ren et al. (2008). In contrast, I could not detect a similar correlation between ABAD protein levels and

Prx-2 expression, that had been predicted by its additional up-regulation in the mAPP/ABAD double transgenic mouse model compared to the mAPP transgenic animals (Yao et al., 2007). However, unlike Ep-1, Prdx-2 was also elevated in the mAPP transgenic animals alone, a finding, which I verified with the work described in this chapter (Figures 5.5 and 5.8). This suggests, that the additional mitochondrial and oxidative stress experienced in the double transgenic mouse model (Takuma et al., 2005) might have prompted the increase in Prx-2 expression.

Different mechanisms appear to be involved in the up-regulation of Ep-1 and its link to ABAD, as overexpression of mAPP alone was not sufficient to cause the up-regulation of ABAD and Ep-1 in the mAPP transgenic animals (Figures 5.7 and 5.8). This is even though Aβ pathology can be observed in these animals like in the human AD brain and it could be due to a potential effect of the overexpressed APP protein itself (that is the AICD) acting as a signalling molecule or transcriptional regulator (see Chapter 1.2.1.3). This effect might be outweighed by the exacerbated production of Aβ in the triple transgenic mouse model, where increased ABAD expression has been reported (Yao et al., 2009), so it would be interesting to see if Ep-1 levels are also elevated in these animals. Deciphering the mechanisms that underlie the link between ABAD and Ep-1 will be important for explaining the diverse roles of ABAD in neuronal networks and for synaptic function specifically.

5.6.3 Prx-2 in the JNK-signalling cascade

Finally, the the effect of Prx-2 on neuronal cell survival and the activation of the JNK-signalling cascade were studied *in vitro*. In agreement with earlier studies demonstrating a protective role for Prx-2 in neurons (Yao et al., 2007; Hu et al., 2011; Qu et al., 2007), I showed that overexpression of Prx-2 protected primary neurons form amyloid toxicity (Figure 5.9). The finding that an inactive mutant of Prx-2 (Prx-2^{T89E}) could not provide protection against Aβ(25–35) pointed towards oxidative stress as the main cause of cell death in Aβ exposed neurons.

Reactive oxygen species provoke an array of cellular responses and one of the main mediators of this reaction is JNK (see Chapter 3). I therefore studied the activation of the JNK-signalling cascade in Prx-2 overexpressing neurons and found that Prx-2 overexpression could in fact suppress the phosphorylation and activation of the JNK-target c-Jun (Figure 5.10). Surprisingly, no reduction of JNK-phosphorylation in response to Prx-2 overexpression was observed in these cell cultures and the Prx-2^{T89E} as well as the Prx-2^{T89A} mutants acted indistinguishable from wild-type Prx-2. This indicates that Prx-2 interferes with c-Jun activation without affecting ROS levels and either exerts a direct effect on c-Jun or modifies JNK activity without inhibiting its phosphorylation. Such a result could be achieved by direct interaction or Prx-2 with either of these proteins.

Notably, Prx-2 has already been found to directly bind to a JNK homologue in yeast through the formation of a disulfide bond between Prx-2 and Sty1 in response to peroxides (Veal et al., 2004). In addition, Prx-2 has been identified as an activator of JNK/c-Jun-signalling in human cancer cell lines (Lee et al., 2011). Although these studies describe activation of JNK-signalling rather than

its suppression, they demonstrate a direct interaction of Prx-2 and JNK which could have cell specific effects in neuronal cells.

In conclusion, the current experimental data strongly suggests a protective role for Prx-2 in neurons exposed to different types of cell stress. Also, up-regulation of Prx-2 in mouse models for neurodegeneration and in the human brain affected by dementia points towards a compensatory up-regulation of Prx-2 in order to cope with oxidative stress caused by neurodegenerative processes. At the same time, experimental evidence presented in this chapter points towards a more complex role for Prx-2 in the regulation of JNK-signalling in neurons, which goes beyond just the degradation of ROS and might involve direct interaction with JNK.

Figure 5.14 summarises the findings of this chapter in the light of other recent advances. It illustrates the current understanding of the function of Prx-2 in the defence against oxidative stress and JNK-signalling which are important factors in neurodegeneration.

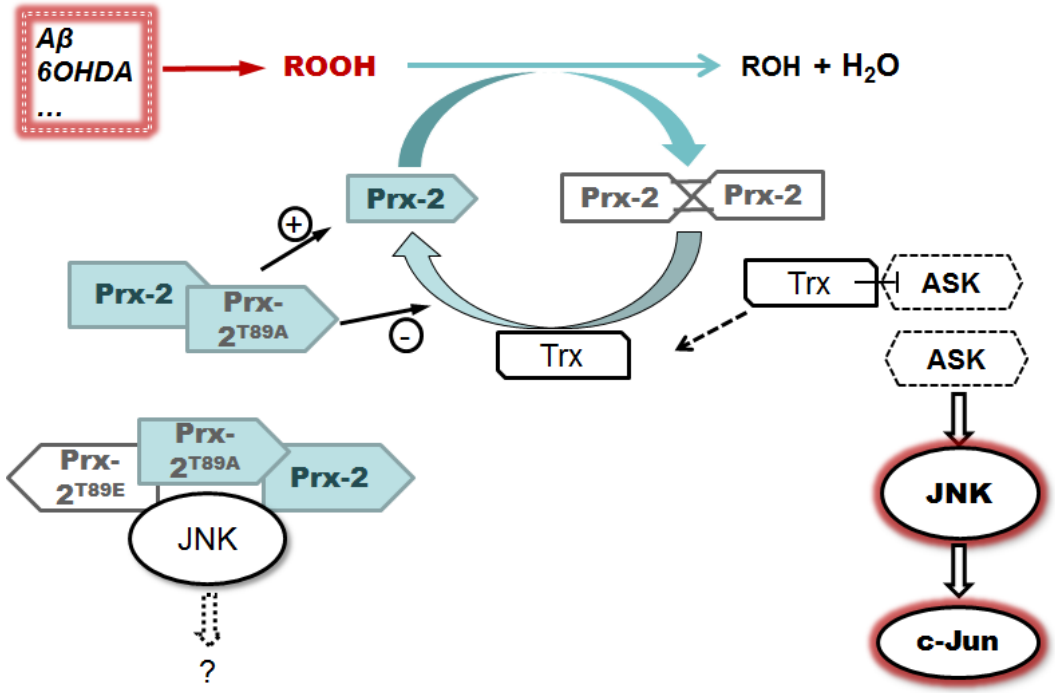

Figure 5.14: Prx-2 in oxidative stress defence and JNK-signalling.

Figure 5.14: Prx-2 in oxidative stress defence and JNK-signalling. Cell stress such as exposure to Aβ or 6OHDA can lead to the formation of peroxides (ROOH). Prx-2 degrades these to ROH and H_2O, whereby a disulfide bond is formed between two Prx-2 monomers. Thioredoxin (Trx) together with disulfide-reductase restores active Prx-2. Excessive oxidative stress can lead to the activation of JNK by releasing ASK (a MAP3K) from inhibition by Trx (Hu et al., 2011). Overexpression of Prx-2 or Prx-2^{T89A} can reduce JNK activation by increasing the antioxidant capacity and reducing the need for Prx-2 recycling and engagement of Trx. Prx-2 (as well as Prx-2^{T89A} and Prx-2^{T89E}) can also directly bind JNK and modulate its function, especially in times of reduced oxidative stress.

CHAPTER 6

CONCLUSIONS AND FUTURE PERSPECTIVE

6.1 The idea

Endophilin-1 (Ep-1), amyloid-binding alcohol dehydrogenase (ABAD), peroxiredoxin-2 (Prx-2) and the EF-hand domain family, member D2 (EFHD2) have all previously been found to be elevated in the human brain with dementia or in mouse models for frontotemporal lobar degeneration or Alzheimer's disease. With the work described in this thesis, I aimed to extend the current knowledge by investigating the expression of all of these proteins in human brains from AD or FTLD patients and by studying the cellular effects of the overexpression of Ep-1, Prx-2 or EFHD2.

6.2 Endophilin-A1: the key to synaptic function

In addition to its up-regulation in the human AD brain, elevated levels of Ep-1 have specifically been found in the mAPP/ABAD double transgenic mouse model as a result of the ABAD–Aβ interaction and so a link between ABAD expression or activity and Ep-1 expression has been suggested (Ren et al., 2008). As described in Chapter 5, I could also observe a link between high expression levels of ABAD and that of Ep-1 protein levels in the aged human brain. However, I could not verify the up-regulation of either protein in the human AD brain. This might be due to various effects caused by technical differences between the studies and importantly, the different number of cases studied as discussed in Chapter 5. This might have confounded the detection of potential expression changes detected by Lustbader et al. (2004) Ren et al. (2008). The detected changes of ABAD mRNA expression levels described in chapter 5 also indicate

that expression levels might in fact have been affected.

Ep-1 is a synaptic protein which functions in synaptic vesicle recycling (Ringstad et al., 1999), influences neurotransmitter release (Weston et al., 2011) and has also been given new roles in signalling processes associated with dendritogenesis (Fu et al., 2011) and JNK-activation (Ramjaun et al., 2001). ABAD is also important for synaptic function as it helps to supply energy through mitochondrial metabolism but can also interact with Aβ inside mitochondria when Aβ levels rise (Lustbader et al., 2004) and thereby cause extensive mitochondrial dysfunction, which synaptic mitochondria are exceptionally susceptible to (Takuma et al., 2005; Du et al., 2011). The synaptic dysfunction observed in the mAPP transgenic animals and in the AD brain is usually characterised by the loss of synaptic markers such as synaptophysin (Dodart et al., 2000; Heffernan et al., 1998; Reddy et al., 2005). Instead, Ep-1 levels increase in AD and the mAPP/ABAD double transgenic mouse model, suggesting that Ep-1 acts as a key multifunctional modulator of synaptic activity and that its up-regulation is a compensatory response to synaptic deficiency, Ca^{2+}-dysregulation or changes in lipid metabolism due to an altered ABAD activity. Direct proof for this sequence of events in AD has not been produced so far, however, it would be possible to address this question by investigating Ep-1 expression levels and its precise location (pre-synaptic or post-synaptic) for example by immunoelectron microscopy in brain tissue from Aβ overproducing mouse models challenged with metabolic/nutritional stress (known to increase ABAD levels (Yan et al., 2000)) compared to tissue from control animals. A similar approach could be taken in *in vitro* models using media deprived of glucose and exposure of primary neurons to Aβ with or without the increased expression of ABAD.

The fact that Ep-1 can also lead to JNK-activation and neuronal death *in vitro* (Ramjaun et al., 2001; Ren et al., 2008) seems at odds with the idea of its synaptic function at first. However, as shown in Chapter 3, I demonstrated that although Ep-1 is in principle capable of activating the JNK-signalling cascade, this signalling function is conditional in that it requires other insults. In line with this hypothesis, preliminary data has shown that lentivirus mediated over-expression of Ep-1, but not its SH3-domain deficient mutant is able to boost the activation of JNK and c-Jun in primary neurons exposed to Aβ. It remains to be seen what the consequences of this are for the synapse where c-Jun is absent. Are there local effects of this activation in the synapse or does the activated JNK-signal only get transmitted back to the neuronal cell body? This question could be addressed in the recently created mAPP/Ep-1 double transgenic mouse line, where the localisation of activated JNK could be determined at high resolution and electrophysiological measurements could answer if increased Ep-1 levels can positively influence synaptic strength in these animals. Furthermore, the effect of increased Ep-1 on TrkB-signalling and dendritogenesis, which are known to be dysregulated in AD (Schindowski et al., 2008) and mAPP transgenic animals (Wu et al., 2006), could also be investigated in these animals. The results of these studies will be important steps towards a better understanding of how the neuronal network reacts to the challenges its faces in AD and other neurodegenerative conditions and how modulating the activity of ABAD as a potential drug target (and therefore Ep-1) might change these processes.

Figure 6.1 summarises the proposed pathological link between the accumulation of Aβ inside synaptic mitochondria and the altered activity of ABAD, leading to the up-regulation of Ep-1, Prx-2 and synaptic dysfunction.

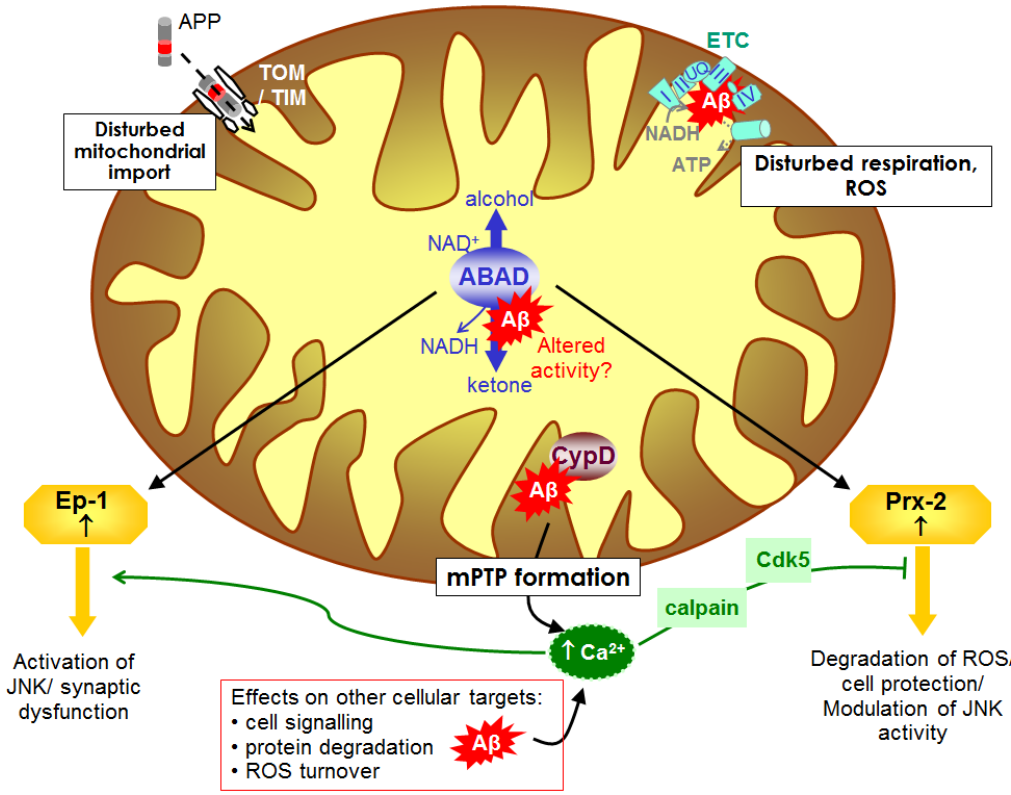

Figure 6.1: Effects of the ABAD–Aβ interaction in AD. APP can be transported to mitochondria, where it interacts with TOM/TIM (translocase of the outer/inner membrane), disturbing mitochondrial protein import. Aβ can be imported into mitochondria via TIM and TOM and is found associated with the inner mitochondrial membrane, disrupting mitochondrial respiration and leading to excess production of ROS. Aβ has been found to interact with ABAD in the mitochondrial matrix, inhibiting or altering the enzyme activity. The ABAD–Aβ interaction leads to the up-regulation of Ep-1 and Prx-2. At the inner mitochondrial membrane, Aβ can bind to CypD, which is involved in the formation of the mPTP and Ca^{2+}-release from mitochondria. In the cytosol, Aβ can disturb cell signalling, protein degradation and cause ROS production, also leading to an increase in cytosolic Ca^{2+}. Ca^{2+} mediated Cdk5 activation has been found to inhibit Prx-2 function and Ca^{2+} levels also influence in targeting and function of Ep-1. Modified with permission from Portland Press Ltd (Borger et al., 2011).

6.3 EFHD2, Prx-2 and APP and tau in frontotemporal dementia

The increased expression of Prx-2, ABAD and EFHD2 protein or mRNA levels in the hippocampus of FTLD affected brains is paralleled by changes in the levels of total APP protein supporting the possibility that their up-regulation in FTLD might be linked to common mechanisms involving calcium-homeostasis and mitochondrial function.

Notably, the increase of Prx-2 and EFHD2 protein levels in the mAPP transgenic mice overexpressing human mutant APP, together with the results from the human FTLD cases lends support to the hypothesis that up-regulation of APP itself (being a common factor between the mAPP transgenic mouse model and the FTLD-affected brain) could cause the increased expression of these proteins independent from amyloid pathology, possibly through actions of its intracellular domain (see Chapter 1.2.1.3). Increased levels of Aβ production in the secretory pathway (Khvotchev and Sudhof, 2004) in cells overexpressing wild-type APP have been observed, however, amyloid-pathology has not been reported as one of the main features in the FTLD brain. Instead, it is known that APP protein expression can be enhanced in situations of cellular stress in cell cultures and mediate ER-stress induced cell death via the AICD (Keita et al., 2009). Increased expression of APP has also been found in the human brain after head injury (Gentleman et al., 1993). Hence, increased levels of APP caused by metabolic dysfunction or ER-stress could be a crucial factor in the up-regulation of Prx-2, EFHD2 and ABAD in the mAPP transgenic mice and the FTLD affected brain. This hypothesis could be tested in cell culture models, for example using SK-N-

SH cells or primary neurons with stable or transient overexpression of wild-type APP or the ACID alone and could reveal a new cellular function of APP with relevance for FTLD and the analysis of mAPP transgenic mouse models.

Some experimental evidence also exists for a potential mechanism of this proposed APP mediated pathology. In primary neurons deprived of neurotrophic factors as well as in the mAPP transgenic mouse model, a complex comprised of of APP, JIP1, ASK and JNK1 has been found (Galvan et al., 2007). This might promote both, amyloidogenic cleavage of APP (Colombo et al., 2009) as well as downstream signaling and gene transcription by the AICD (Mueller et al., 2008). However, earlier work points towards AICD signaling as a potential mediator of this response, as it has already been implicated directly in neuronal cell death *via* ASK1 and JNK activation in neuronal cells (Hashimoto et al., 2003).

The JNK-signaling pathway is crucially important in regulating cell stress related protein transcription and function and has been analysed in the course of this study (see Chapter 3). It is noteworthy that increased levels of phosphorylated JNK (Figure 3.3) were indeed found in the hippocampus samples from FTLD patients compared to non-demented controls but were not accompanied by an increase in phosphorylated or total c-Jun (Figure 3.4), which were predominantly found elevated in the frontal cortices of FTLD patients. This might mean that the JNK/c-Jun signalling cascade is not involved in pathologically relevant transcriptional regulation in neurons in the hippocampus. However, as mentioned in Chapter 1.1.1, it is known that disease symptoms often spread along anatomical tracts in the brain. This therefore leaves the possibility that a phosphorylated JNK-signal, originating from nerve terminals in the hippocampus is retrogradely transported to neuronal cell bodies in the frontal cortex, where it activates c-Jun.

In line with this idea is the study by Abe et al. who found JIP3 in association with retrograde synaptic vesicles (Abe et al., 2009).

A similar dissociation of the phosphorylated JNK and c-Jun signals, has been found in the AD brains studied in the course of this work. Amyloid and tau pathologies are known to spread from the hippocampus to the frontal cortex during disease progression (Duyckaerts et al., 2009). Fittingly, it has also been reported that activated JNK associates more with neurofibrillary structures in neuronal processes in more advanced cases of AD in the human brain, rather than the cell nuclei, where it can be found in earlier stages (Zhu et al., 2001). Hence, it is possible, that JNK-mediated signalling events play a major role in disease progression in both AD and FTLD.

Figure 6.3 illustrates where the proteins studied here have been found up-regulated in the human brain affected by FTLD and AD on protein or mRNA level.

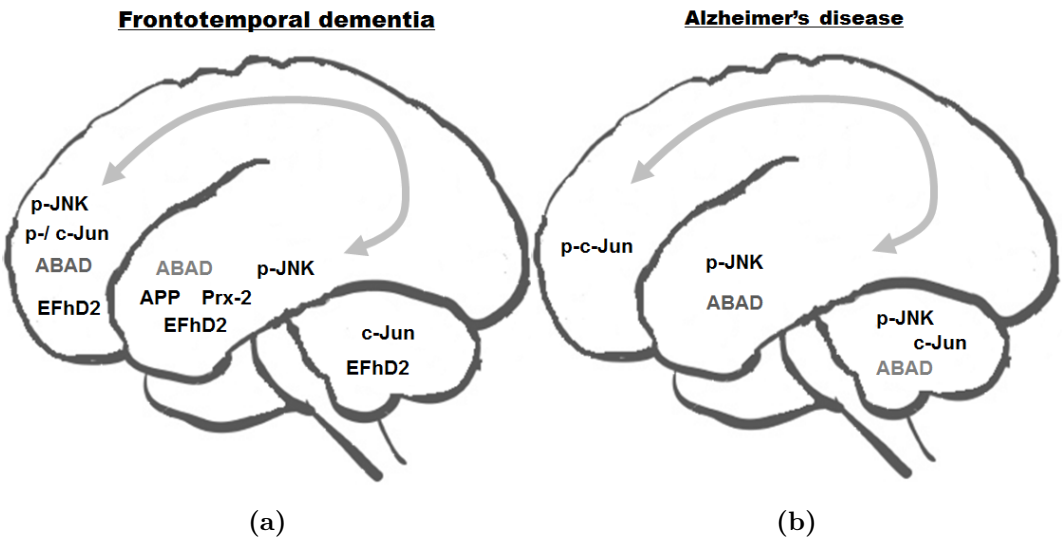

Figure 6.2: Proteins and mRNA levels up-regulated in the human dementia brain.

Figure 6.3: Proteins and mRNA levels up-regulated in the human dementia brain (continued). Increased expression of proteins found in the course of this work are mapped onto the human brain structure. (a) Frontotemporal dementia (b) Alzheimer's disease. Increased mRNA expression is indicated in grey, increased protein expression in black writing. The double arrows denote anatomical tracts between the temporal lobe/hippocampal formation and the frontal cortex.

In the course of this project, I confirmed that an up-regulation of Prx-2 has beneficial effects on neuronal survival, when cells are exposed to toxic agents inducing ROS production such as Aβ and that it can also suppress the effects of JNK activity in these cells. At this point, it is not clear how this relates to the situation in the FTLD brain. However, in keeping with the idea that APP up-regulation might be at least partly responsible for the activation of JNK in this situation, this could be investigated further in cell culture models of wild-type APP or AICD overexpression and resolve if Prx-2 up-regulation, knock-down or inhibition (using Conoidin A (Haraldsen et al., 2009)) could modulate the activation of JNK-signalling in these cultures.

As mentioned in Chapter 4, I did not find a correlation between the presence of tau-pathology in the human FTLD or AD cases and the up-regulation of EFHD2 protein or mRNA levels. Notably, all AD cases presented with high scores for tau-pathology, when the immunoreactivity for phosphorylated tau was assessed (see Table 3.1), but did not have increased levels of EFHD2. The report first linking EFHD2 to neurodegenerative processes in dementia did also not describe an association of EFHD2 with tau in a case of FTD and Parkinsonism linked to chromosome 17 (FTDP17) but only in a single AD case and in the JNPL3 mouse model, where sarkosyl insoluble tau species were detectable (Vega et al., 2008). Differences in the nature of tau-aggregates found in the brains of FTLD patients

and those patients with AD have be recognised before (van Eersel et al., 2009) and could be behind the difference in the association of EFHD2 with tau in these diseases implicated by the study by Vega et al. (2008). Together with the finding that EFHD2 overexpression did not affect the regulation of the important tau-kinase GSK3 (see Chapter 4.8.2), the current data contradicts a role for EFHD2 in the pathologically relevant processing of tau in the human brain. However, this does not rule out a potential function of EFHD2 in physiological tau-metabolism, which might in fact prevent tau from forming sarkosyl-insoluble aggregates in the case of its up-regulation in FTLD. Further deciphering the signalling pathways modulated by EFHD2 in cell cultures and correlating those with their activity in the FTLD brain and effect on tau-phosphorylation/cleavage of the different tau isoforms will be invaluable for answering this question.

6.4 From mouse to man

The current work has highlighted new intracellular mechanisms, which are linked to dementia and might contribute to the development of new diagnostic tools and treatments. Many aspects described in this thesis would however not have been recognised without the careful and open-minded comparison of cell culture and animals models used in this study to the situation in the human brain.

The high level complexity of the processes that feature in the human brain during neurodegeneration and aging, in particular, results in a large degree of variability between individuals and in fact whole study groups. It is therefore challenging to mimic all aspects of these processes in the mouse and *in vitro* models widely used to represent these neurodegenerative diseases. The use of

mouse models gives precious insights into the activity of the brain under physiological and pathological conditions, which would remain undetectable otherwise but there are limitations to their applicability to humans which are of particular importance for the aspects which ave been studied here.

Firstly, the mouse genome only encodes for one single confirmed isoform of tau with 4 microtubule binding domains (4R tau), whereas the human tau gene produces at least 6 isoforms as shown in Figure 1.9 by alternative splicing, so that an equal amount of 3R and 4R tau proteins is produced. As mentioned in Chapter 1.2.3.1, this ratio of tau isoforms is important for neuronal function and affects its interactions with other proteins. It is therefore easy to understand that the endogenous murine tau protein, will not be able contribute to the pathological processes in the same way as it happens in the human brain. This potentially explains, why single mAPP transgenic mice do not develop the same tauopathy that is seen in human AD. Double and triple transgenic mouse models which express mutant human P301L tau protein, do produce neurofibrillary tangles (LaFerla and Oddo, 2005) and Vega et al. could show that JNPL3 mice expressing this version of human tau produce sarkosyl-insoluble tau, which is similar to the tau-aggregate found in human AD (Vega et al., 2008). However mutations in the tau gene are genetically linked to frontotemporal lobar degeneration and not AD (Crawford et al., 1999; Goedert et al., 2012). Differences in the behaviour of tau during tauopathy in AD and FTLD (with Pick's disease) have been described (van Eersel et al., 2009) and are further exposed by the finding that the aggregation prone P301L mutant tau version is not able to promote amyloid-pathology in neurons (Tackenberg and Brandt, 2009). As another example, Vega et al. (2008) demonstrated association of EFHD2 with tau in a *post mortem* human AD brain

but not in a brain from an FTLD case linked to tau (FTDP17).

Secondly, overexpression of AD related proteins in these animal and cell culture models might itself pose a problem as mentioned in Section 6.3. Although, mAPP mice have synaptic dysfunction (Chapman et al., 1999) and the mutant APP is known to increase the amount of amyloid peptide produced (Haass et al., 1995; Citron et al., 1992), human AD is not normally characterised by a significant up-regulation of APP (or tau) protein levels but rather by their aberrant processing and targeting. Therefore, mouse models that better represent the genetic background of human AD sufferers for example by genetic-targeting of the endogenous mouse APP gene (Reaume et al., 1996), should be the preferred system to study.

Finally, cell culture models using human or murine cell lines or mouse primary neurons are a good system for studying cellular signaling pathways and the effects of the amyloid peptide in detail. However, limitations apply here as well. For example, the primary neurons used extensively in the current work derive from embryonic mouse cortices which potentially have a different biochemical setup from neurons in later embryonic stages, as has previously been reported for cerebellar granule cells (Oldreive et al., 2008). Similarly, I showed that expression levels of EFHD2 also vary between the embryonic and the postnatal mouse brain (see Figure 4.7(b)) and an effect of cellular maturation on the function of EFHD2 has been reported in B-cells (Avramidou et al., 2007). Recently refined culture systems for neurons derived from induced pluripotent stem cells (Shi et al., 2012b,a) could be an advance into the right direction for overcoming these potential problems.

The result of maturation on neurons in particular is an extreme level of com-

partmentalisation of the cell between the cell body and the synapse, where APP is located and Aβ peptides of varying length are secreted. Therefore, an additional problem is that topical administration of Aβ peptides to cell cultures might evoke responses, which do not naturally occur in the brain, especially when applied at supranatural concentrations and when only one type of peptide is used.

In conclusion, the increasing knowledge about the above mentioned caveats should result the development of according experimental paradigms and results obtained from transgenic animal models and cell culture systems should be analysed with caution and compared to other *in vivo* and *in vitro* models as well as to the human condition.

APPENDICES

APPENDIX A

ANTIBODY DILUTIONS AND SOURCES

A.1 Primary antibodies

Antigen	**Supplier** (product code)	**Host**	**Dilution (WB)**	**Dilution (IF)**
ABAD	Abcam (♯ ab52243)	rabbit	1:7500	NA
Akt (pan) (C67E7)	Cell Signalling (♯ 4691)	rabbit	1:2000	NA
phospho-(Ser473)-Akt (587F11)	Cell Signalling (♯ 4051)	mouse	1:1000	NA
phospho-(Thr308)-Akt	Cell Signalling (♯ 9275)	rabbit	1:1000	NA
Amyloid Precursor Protein (APP)	Sigma (♯ A8967)	rabbit	1:10,000	NA
β-Actin	Sigma (♯ A1978)	mouse	1:10,000	NA
CD95	Abcam (♯ ab82419)	rabbit	1:5000	NA
c-Jun (60A8)	Cell Signalling (♯ 9165)	rabbit	1:1000	NA

phospho-(Ser63)-c-Jun	Cell signalling (♯ 9261)	rabbit	1:1000	1:100
CypD	Abcam (♯ ab54496)	mouse	1:10,000	NA
Ep-1	Invitrogen (♯ 36-3000)	rabbit	1:2500	1:100
Ep-1	Abcam (♯ ab55702)	mouse	1:1000	NA
EFHD2	kind gift from Dr. Irving Vega	mouse	1:1000	1:100
EFHD2	Abcam (♯ ab24368)	goat	1:1000	NA
Enoyl-CoA-hydratase (ECHS)	Aviva (♯ ARP45699)	rabbit	1:1000	NA
Flag	Sigma (♯ F1804)	mosue	1:1000	NA
GSK3α/β	Upstate (♯ 05-903)	rabbit	1:1000	NA
phospho-(Ser21/9)-GSK3α/β	Cell Signalling (♯ 9331)	rabbit	1:1000	NA
SAPK/JNK	Cell Signalling (♯ 9252)	rabbit	1:1000	NA
phospho-(Y83/T89) -SPK/JNK	Cell Signalling (♯ 9251)	mouse	1:2000	1:100
Prx-2	Abcam (♯ ab71533)	rabbit	1:3000	NA
β3-tubulin	Promega (♯ G7121)	mouse	NA	1:7,500

Table A.1: Primary antibody dilutions for western blotting (WB) and immunofluorescence (IF)

A.2 Secondary antibodies

Antigen	Supplier	Host	Dilution (WB)	Dilution (IF)
rabbit IgG -HRP	Abcam (♯ ab97051)	goat	1:50,000	NA
mouse IgG -HRP	Abcam (♯ ab6709)	rabbit	1:20,000	NA
mouse IgG -HRP	Jackson Immunoresearch (♯ 115-035-062)	rabbit	1:10,000	NA
goat IgG -HRP	Sigma	rabbit	1:20,000	NA
rabbit IgG -FITC	Vector Laboratories	goat	NA	1:1000
mouse IgG - Texas-Red	Vector Laboratories	goat	NA	1:2000
mouse IgG -DylLight 594	Jackson Immunoresearch (♯ 115-515-062)	goat	NA	1:500
mouse IgG -DylLight 488	Jackson Immunoresearch (♯ 115-486-003)	goat	NA	1:500
rabbit IgG -DyLight 488	Jackson Immunoresearch (♯ 111-486-003)	goat	NA	1:500
goat IgG -DyLight 594	Jackson Immunoresearch (♯ 205-515-108)	goat	NA	1:500

Table A.2: Secondary antibody dilutions for immuno-western blotting (WB) and immuno-fluorescence (IF)

APPENDIX B

GENE SEQUENCES AND PLASMIDS

B.1 Mouse Endophilin A1

Accession number: NM 019535.2

Coding sequence: bp 122–1180

```
0001 GCGCCGCGCC CCCGCGCCAG CAGCTCCCGC GGTCGCACGA CCAGCGGCGG CCCGGCGACC
0061 CCAGCCGCCT CTCCGCATCT GCATCTGCAT CTGCCGGCCG CGCAGCCTCC CGCATCCCAT
0121 CATGTCGGTG GCAGGGCTGA AGAAGCAGTT CCACAAAGCC ACTCAGAAAG TGAGTGAGAA
0181 GGTGGGAGGA GCGGAAGGCA CCAAGCTCGA TGATGACTTC AAAGAGATGG AGAGGAAAGT
0241 GGATGTCACC AGCAGGGCTG TGATGGAGAT AATGACAAAA ACGATTGAAT ACCTCCAACC
0301 CAATCCAGCT TCCAGGGCTA AGCTCAGTAT GATCAACACC ATGTCGAAAA TCCGCGGCCA
0361 AGAGAAGGGG CCAGGCTACC CTCAGGCGGA AGCACTGCTG GCAGAGGCCA TGCTCAAGTT
0421 CGGCAGGGAG CTGGGTGATG ATTGCAACTT TGGTCCTGCT CTCGGTGAGG TGGGAGAAGC
0481 CATGAGGGAG CTCTCGGAGG TCAAGGACTC ATTGGACATG GAAGTGAAGC AGAATTTCAT
0541 CGACCCCCTT CAGAATCTTC ATGACAAGGA TCTGAGGGAG ATTCAGCATC ATCTGAAAAA
0601 GCTGGAAGGC CGACGCTTAG ACTTTGATTA TAAGAAGAAG CGACAAGGCA AGATTCCAGA
```

0661 TGAAGAACTC CGCCAAGCTC TGGAGAAATT CGATGAGTCT AAAGAAATCG CCGAGTCGAG

0721 CATGTTCAAC CTCTTGGAGA TGGATATAGA ACAGGTGAGC CAGCTCTCCG CACTTGTTCA

0781 GGCTCAGCTG GAGTACCACA AGCAGGCAGT GCAGATCCTG CAGCAGGTCA CTGTCAGACT

0841 GGAAGAAAGA ATAAGACAAG CTTCATCTCA GCCAAGAAGG GAATATCAGC CCAAACCACG

0901 GATGAGCCTA GAGTTTGCCA CTGGAGACAG TACTCAGCCC AACGGGGGTC TCTCCCACAC

0961 AGGCACACCC AAACCTCCAG GTGTCCAAAT GGATCAGCCC TGCTGCCGAG CTCTGTATGA

1021 CTTTGAACCT GAAAATGAAG GGGAATTGGG TTTTAAAGAG GGCGATATCA TCACACTCAC

1081 TAATCAGATT GACGAGAACT GGTATGAGGG GATGCTTCAT GGCCAGTCTG GCTTTTTCCC

1141 CATCAACTAT GTAGAAATTC TGGTTGCTCT GCCCCATTAG GATCCTGTGC TGGCTGGCTC

1201 ACCTCCTTCT GACCCAGATA GTTAAGTTTA ACCACTGCTT TGGTAATGCT GCTTCCAATA

1261 CATCACGAAT GCAGGCCGCA GTGGATGAGT CACCAAGCCC ACACGTGCCC TGGGTTGACC

1321 CGTGTGCTCC TCCAGGAGAC GCGGTGATAG ATGGTATCTT CCAAGGCCAG TGGGCCTGGT

1381 ACATGCTTTA AAACACCATC TGAGACTAGC CAGGAGTCCC AGAACTGGCT TCACAGTTCT

1441 CAGGAGGCTG TGGTTCCTGG TAACATGCCT GTGAACCACA TGGCAGAAAA ACTCTCCTCA

1501 CTGAAGATAT TGTCTCTCAC CCAGGGGCCA TCTCAAGGTC TCCAGTTCTC CATTTACAGA

1561 GGAGAAAGTC CTTTTTGTTG CACTTTCCCT TCCTAAATAT GTGAGTCACA GAATTGTTGG

1621 CAAAAACATC CCCTCACCAG CAAGATGTCT GCTGGTTTAA GCAACTTGGT CTCTTGATGC

1681 CATTAGCAAA AGTATTAATT GTCCAAAGCA CCTTTGTTCA CTAATATCTA TCTATCTATC

1741 TATCTATCTA TCTATCTATC TATCTATCTA TCTATCTATC TATCATCTAT CTACCTACCT

1801 ATCTACCTAT CATCTATCTA TCTATCATCT ATTATCTATC TATCTATCTA TCTATCTATC

1861 TATCTATCTA TCTATCCATC TATCTATCCA TCATCTATCT ACCTACCTAT CTACTATCCA

1921 TCTATCTATC TATCCATCAT CTATCTACCT ACCTATCTAC TATCCATCCA TTTATCTATC

1981 TATCTATCTA TCTATCTATC TATCTATCTC CCTCATACTT CTGAGACATG GCCAGTTTTC

2041 TTCCCTCCCT GCTGTTAAGC ACTTGGCAGA TGAGGGGGGG GGTCCCATTT ATTTCTGAGT

2101 GAGATGGTGA GCAATCTGTA TGTTGGCTGA AAAGAAAAAA AAATCTCCAG TCTGAATTGG

2161 GAAGAAATCT GGTCTCTAAG CTCAGATTCC TTGCTGTACA GAAGCTGTGT ATATACGTAG

```
2221 CCCGTTTCTG AAGGGTACAG GAAGGGGGCA CGGCTGTCTT CCCTTCTCTG TTTACTTACC
2281 CAGGAATCAG TCCATTCCCT GAGTCCCTTT ACCACAAAGA CGTAGGAGAG AAACACTAGT
2341 AAGCATTTCC CACTCCATAG AACAAGACAG TGAGCATCGC TCCTTCCCAC GTTTACTTGT
2401 TTGTGTTCCT TGAACATCAT TTGTGCATAT TCTGCCCTCA ATGAGGACCA AATAAAGATG
2461 ATTTTTGTGC TTAGCAGTTT AAGGTATGTG GCTGCATATG CAAACCCCTT TTCCACTCCA
2521 GTCATTACTT TGAACGCCTC CCTTCCTCAT TTTGTGTGTA CAGTGCTGTG TACGCTGATC
2581 AGTGTTGGGT TTTCGTTTTG TTCTCCTTTC AGTTATGGAA GTCCCGATAG GCACCCAGAG
2641 TTCTATTTAT CTAGCTGTAC AGGCTCCTTC AGAGGTTTAG CGTGCTGCTT CCGATATGCC
2701 ACTTGCGGTA GTGGATCGTG TGGAGTGAAA GGCAAATCTT CCTGCTTAAT GTATAAACTC
2761 ACCACGGGAA GCACTGCTGT TTCCAATAAA CATTGCTGAA GACGAAAAAA AAAAAAA
```

Wild-type and mutated endophilin A1 constructs (Figure B.1) in pcDNA3 vectors were kindly provided by Dr. Peter McPherson. Deletion of the SH3 domain of endophilin A1 (bp 885–1038) was accomplished by introducing the mutation C869T and therefore creating a stop codon (TAG) after amino acid 291 (Micheva et al., 1997).

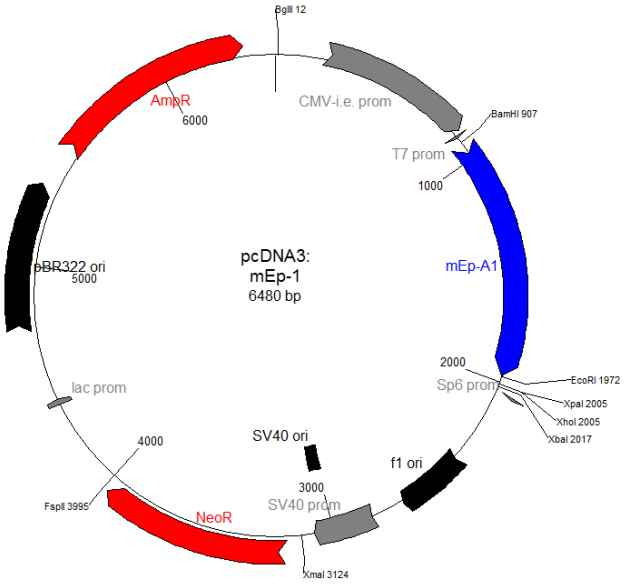

Figure B.1: Plasmid map of Endophilin A1 in the pcDNA3 vector.

Wild-type and mutated endophilin A1 lentiviral constructs with red fluroescent protein (RFP) (Figure B.2) co-expression were kindly provided by Prof. Matthias Rosenmund (Weston et al., 2011).

Wild-type endophilin A1 was cloned into the pSX69 lentiviral destination vector by recombination using the Gateway® cloning system in collarboration with Mr. Christopher Owen (Figure B.3).

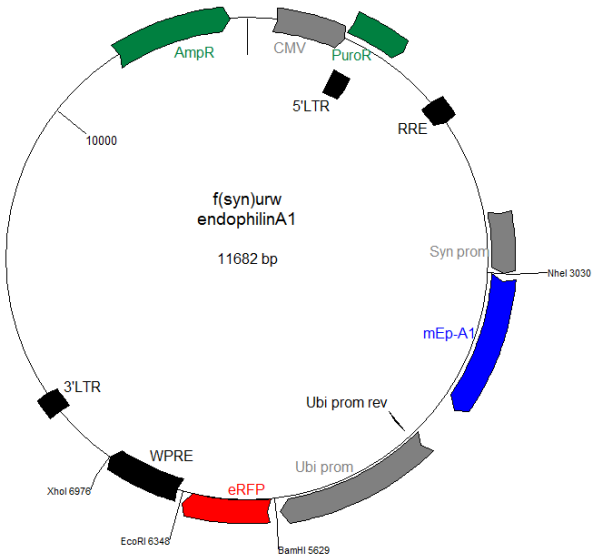

Figure B.2: Plasmid map of Endophilin A1 lentiviral constructs with RFP co-expression.

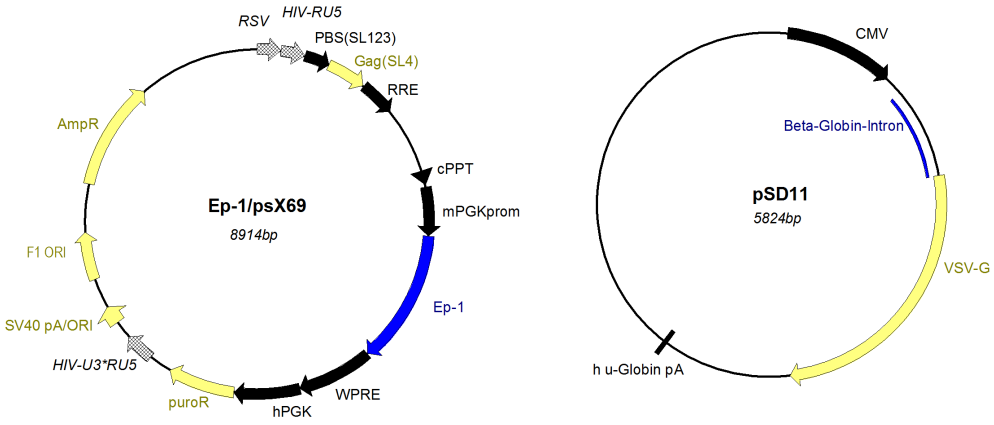

(a) Ep-1 psX69 lentiviral constructs

(b) VSV-G envelope protein expression plasmid

Figure B.3: Ep-1 lentiviral expression constructs and lentiviral production vectors.

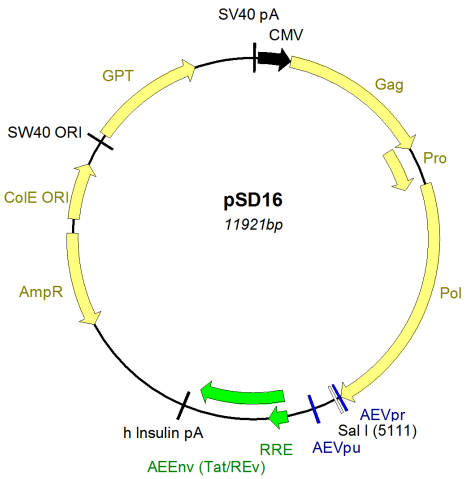

(c) Gag, pol, Rev, expression plasmid

Figure B.3: Plasmid maps of Endophilin A1 lentiviral psX69-constructs (continued).

B.2 Human Peroxiredoxin-2

Accession number: NM 005809

Coding sequence: bp 151–747

```
0001 GCTCGTCCGC TCCCTCCCCC GCGCCGTGCA CGTCTTGGTT CGGGCCGGGC ATAAAAGGCT
0061 TCGCGGCCCA GGGCTCACTT GGCGCTGAGA ACGCGGGTCC ACGCGTGTGA TCGTCCGTGC
0121 GTCTAGCCTT TGCCCACGCA GCTTTCAGTC ATGGCCTCCG GTAACGCGCG CATCGGAAAG
0181 CCAGCCCCTG ACTTCAAGGC CACAGCGGTG GTTGATGGCG CCTTCAAAGA GGTGAAGCTG
0241 TCGGACTACA AAGGGAAGTA CGTGGTCCTC TTTTTCTACC CTCTGGACTT CACTTTTGTG
0301 TGCCCCACCG AGATCATCGC GTTCAGCAAC CGTGCAGAGG ACTTCCGCAA GCTGGGCTGT
0361 GAAGTGCTGG GCGTCTCGGT GGACTCTCAG TTCACCCACC TGGCTTGGAT CAACACCCCC
0421 CGGAAAGAGG GAGGCTTGGG CCCCCTGAAC ATCCCCCTGC TTGCTGACGT GACCAGACGC
0481 TTGTCTGAGG ATTACGGCGT GCTGAAAACA GATGAGGGCA TTGCCTACAG GGGCCTCTTT
0541 ATCATCGATG GCAAGGGTGT CCTTCGCCAG ATCACTGTTA ATGATTTGCC TGTGGGACGC
0601 TCCGTGGATG AGGCTCTGCG GCTGGTCCAG GCCTTCCAGT ACACAGACGA GCATGGGGAA
0661 GTTTGTCCCG CTGGCTGGAA GCCTGGCAGT GACACGATTA AGCCCAACGT GGATGACAGC
```

```
0721 AAGGAATATT TCTCCAAACA CAATTAGGCT GGCTAACGGA TAGTGAGCTT GTGCCCCTGC
0781 CTAGGTGCCT GTGCTGGGTG TCCACCTGTG CCCCCACCTG GGTGCCCTAT GCTGACCCAG
0841 GAAAGGCCAG ACCTGCCCCT CCAAACTCCA CAGTATGGGA CCCTGGAGGG CTAGGCCAAG
0901 GCCTTCTCAT GCCTCCACCT AGAAGCTGAA TAGTGACGCC CTCCCCCAAG CCCACCCAGC
0961 CGCACACAGG CCTAGAGGTA ACCAATAAAG TATTAGGGAA AGGTGTGAAA AAAAAAAAAA
1021 AAAAAAAAAA AAAAAAAAA
```

Wild-type and mutated human Peroxiredoxin-2 constructs (Figure B.4) were kindly provided by Prof. David Park. The mutation A415G was introduced to produce the T89A mutant of peroxiredoxin-2. A mutation of bp 415–417 (ACC) to GAG accordingly lead to the production of the T89E mutant of peroxiredoxin-2 (Qu et al., 2007).

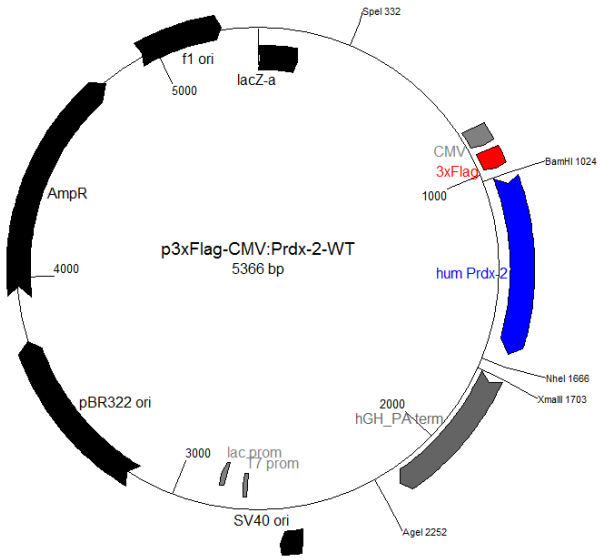

Figure B.4: Plasmid map of Prx-2 in the N-terminal p3xFlag-CMV vector.

B.3 Human EFHD2

Accession number: NM 024329

Coding sequence: 78–800

```
0001 AGGAAGAGGA AGAGCGCGGC CGGCGGCGCT GCGCTGAGAG CAGGGGCCCG GCCAAGGCGA
0061 GTGCCGCGCG GGCCACCATG GCCACGGACG AGCTGGCCAC CAAGCTGAGC CGGCGGCTGC
0121 AGATGGAGGG CGAGGGCGGC GGCGAGACCC CGGAGCAGCC CGGGCTGAAC GGGGCAGCGG
0181 CGGCGGCGGC GGGGGCACCC GACGAGGCGG CCGAGGCGCT GGGCAGCGCG GACTGCGAGC
0241 TGAGCGCCAA GCTGCTGCGG CGCGCAGACC TCAACCAGGG CATCGGCGAG CCCCAGTCGC
0301 CCAGCCGCCG CGTCTTCAAC CCCTACACCG AGTTCAAGGA GTTCTCCAGG AAGCAGATCA
0361 AGGACATGGA GAAGATGTTC AAGCAGTATG ATGCCGGGCG GGACGGCTTC ATCGACCTGA
0421 TGGAGCTAAA ACTCATGATG GAGAAACTTG GGGCCCCTCA GACCCACCTG GGCCTGAAAA
0481 ACATGATCAA GGAGGTGGAT GAGGACTTTG ACAGCAAGCT GAGCTTCCGG GAGTTCCTCC
0541 TGATCTTCCG CAAGGCGGCG GCCGGGGAGC TTCAGGAGGA CAGCGGGCTG TGCGTGCTGG
0601 CCCGCCTCTC TGAGATCGAC GTCTCCAGTG AGGGTGTCAA GGGGGCCAAG AGCTTCTTTG
0661 AGGCCAAGGT CCAGGCCATC AACGTGTCCA GCCGCTTCGA GGAGGAGATC AAGGCAGAGC
0721 AGGAGGAAAG GAAGAAGCAG GCGGAGGAGA TGAAGCAGCG GAAAGCGGCC TTCAAGGAGC
0781 TGCAGTCCAC CTTTAAGTAG CGGGGGCTGC AGCCGACCGC CCTGCTCCGG CCCCAGTGTG
0841 GTGGGCGAGG GTGGCGCATG GGAGGCCGAG CCTGAATCCT TGCCTGTGTC TGACGGGACC
0901 ACTACTAAAA ACCTAAAAAT ATCTGTGAAT GGAGCAAGTT CAGGGGTCTT ATGGAGGTGG
0961 CCCGGCCCCT CCCCGCTCCC TTCCACTCTG CACGAGGCCG CCACACCGGC GCTGGCTCCC
1021 TGCCCGGCCC GGCCCTCCCT GGCAATCCCT GGGCTCTCTT GCACCCCTAA CTGCCCCCTG
1081 CCTGCTCCGG CACTGCCCCA GGCCCAGCTC CTGGCCCTAG GTCCCTCCCA GCCCCATGTG
1141 CCTGCCGCCT GCCCTCCACA CATCCCTGTC CCCCCAACCC GGGAACCCCT GCCCTCCTCC
1201 AGCAGGCCGC ACCGCCCCTG GGGCCCCCTG CCAGCCCCTT CCCAGGCTGG GAGACGGCAG
1261 AAGAGATAGA ATCAGGGCTG CCCCCACAGA GTGGGACCCA AGGGGCTAAT TGGAGGCACG
1321 AGGGGACCCC TCCCCAGGGC CTTTTCCTCC TCTGCGTCTT CCATCTACTG AAATGGGAGA
```

```
1381 GGGGGTGGGG AGCTTCTGTT CTGGTGAAGG GACCCGGGCA GGCCCCCAGC ACCCCATGCT
1441 GACTTGGAGA ACCCCAGATC TCTGGGGCCC AGCCAGGCAG GGTGTGGGGG CAGCTGTGCC
1501 AATCTACCTC ACAGGCCCAC CCCCTGCCGG GCATGCCGTG GGATCATGGG CAGGGAAGGC
1561 TCTGGGGGTC GGAGACACCG CTGCTTAGCA CCCCCAGCCA GAACACCCTG AGGGTCTCGG
1621 GGCTCTGGAG AGAGTGGGGC GGGAGGAAGA ATTGGCACCT TCCTAGGGAA GGAGACGAGC
1681 GCTTCGCCTT GATTCTCCGA GAAGCCTCCG AGAAGTGCTT TAAGTGTGTT TGCATGCGCC
1741 AGGCGGTGGG CAGCGGGGGC CTGTCCAGCC CTCTCCCGCC ATCCTTCCCC AAGTGACGTC
1801 CACTGCCTTG TCACCAGCGA CCTGCCTGTC ATGCCCACCC CCTGAGGAAG CATGGGGACC
1861 CTAACACCCT GGTGCCCTGC ACCAGACAGG CCGTGGTCAG GCCCAGGCCA CCGGCCGGGT
1921 TCTGCCACAG CTTCCCACGT GCTTGCTGAC ATGCGTGTGC CTGTGTGTGG TGTCTGTTGC
1981 TGTGTCGTGA AACTGTGACC ATCACTCAGT CCAAACAAGT GAGTGGCCCT CGAGGCCACA
2041 GTTATGCAAC TTTCAGTGTG TGTCATAACG ACGTCACTGC TTTTTAAACT CGATAACTCT
2101 TTATTTTAGT AAAATGCCCA GGAGTCCTGG AAGCTACGCG GACTTGCAGA GGTTTTATTT
2161 TTTGGCCTTA GAATCTGCAG AAATTAGGAG GCACCGAGCC CAGCGCAGCA GCCTCGGACC
2221 CGGATTGCGT TTGCCTTAGC GGATATGTTT ATACAGATGA ATATAAAATG TTTTTTTCTT
2281 TGGGCTTTTT GCTTCTTTTT TCCCCCCCTT CTCACCTTCC CTTCTCCCCG ACCCCACCCC
2341 CCAAAAAAGC TACTTCTTCA TTCCGTGGTA CGATTATTTT TTTTAACTAA AGGAAGATAA
2401 AATTCTATAT TCTTATGTGA AAAA
```

Wild-type GFP-tagged human EFHD2 in a lentiviral expression vector and a lentiviral for GFP expression only were kind gifts from Prof. Chang-Duk Jun (GIST, Gwangju, South Korea) (Thylur et al., 2009) (Figure B.3).

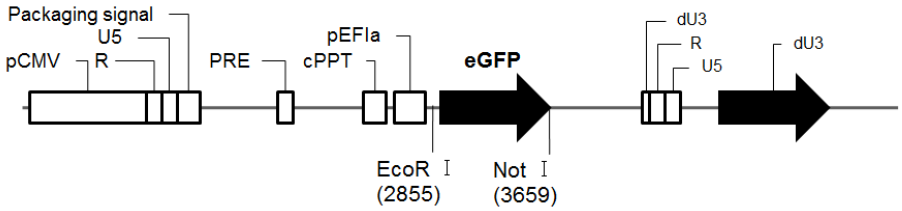

(a) pHJ-EGFP

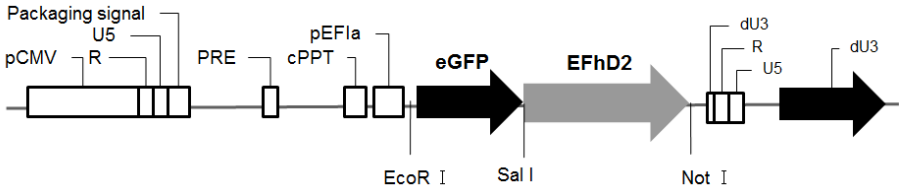

(b) pHJ-EFHD2

Figure B.5: EFHD2 lentiviral expression constructs. The pHJ-EGFP lentiviral vector is 7162 bp (a) and pHJ-EFHD2 based on the same vector and including the mouse EFHD2 coding sequence fused to GFP (b). The vector includes the CMV IE promoter (98bp), ampicillin resistance and the EGFP gene (2938bp–3657bp) and has no multiple cloning site.

B.4 Mouse EFHD2

Accession number: NM 025994

Coding sequence: 54–776

```
0001 GGGAGCGCGG CGCAGAGCAG GGGCCCGGCC GAGGCAGCGC TGCGCGGGCC ACCATGGCCA
0061 CGGACGAGTT GGCCAGCAAG CTGAGCCGGA GGCTGCAGAT GGAGGGCGAA GGCGGCGAGG
0121 CGACGGAGCA GCCGGGGCTC AACGGGGCGG CGGCGGCGGC GGCGGCCGAG GCTCCCGACG
0181 AGACTGCCCA GGCGTTGGGC AGCGCGGACG ACGAGCTGAG CGCCAAGCTG CTGCGGCGCG
0241 CGGACCTCAA CCAGGGCATC GGCGAGCCAC AGTCGCCCAG CCGCCGCGTC TTCAACCCCT
0301 ACACCGAGTT CAAGGAGTTC TCCAGGAAGC AGATCAAAGA CATGGAGAAG ATGTTCAAGC
0361 AGTATGATGC CGGCAGGGAT GGCTTCATCG ACCTGATGGA GCTGAAACTC ATGATGGAGA
0421 AGCTGGGGGC CCCCCAGACA CACTTGGGCC TCAAGAGTAT GATCCAGGAG GTGGACGAGG
0481 ATTTCGACAG CAAACTCAGC TTCCGGGAGT TCCTTCTGAT CTTCCGCAAG GCAGCAGCAG
```

```
0541 GGGAGTTGCA GGAAGACAGC GGCTTGCACG TCCTGGCCCG CCTGTCCGAG ATCGATGTCT
0601 CCACAGAGGG CGTTAAGGGT GCCAAGAACT TCTTCGAGGC CAAGGTACAG GCCATCAACG
0661 TGTCCAGCCG CTTTGAGGAA GAGATCAAAG CTGAGCAAGA GGAAAGGAAG AAGCAGGCTG
0721 AGGAGGTGAA GCAGCGGAAA GCGGCCTTTA AGGAGCTGCA GTCCACGTTC AAGTAGCCAG
0781 AGCCAAGGCC GAGACCTGGC CCTGCCCCGT GTGCGGTCTG GGGGCACGGG TGGGTACAGG
0841 GGATCTGTGG GAGACTAGCT CCCAGGTCCT GCTCTCTGTG CCCGGACCAC TACTAAAAAC
0901 CGCAAACGAT ATGTGACCCG ATCTCATTCA GGAGTCTCCT CGGTGGTTGG TCCCTGCCCT
0961 GCCCTCTCCT GCGGTTCATG CGGCTGTGAT GCCAGCCAGC AGCATCCTCT CTGGCCATCC
1021 CTACGTGTCT TGTTCTCTGG CCACCTTGCT GCCTGCTCTA GCCCAACTTC AGCCCATTCA
1081 CGCCCCTGCC TTTGGTACCA GCTACTTTCT CCACCCACCC AACTCCCCTT AACTATAGGC
1141 CGCCCTGCCA TGGTCCAGCA GAGAGTGAGA CCCTCCCCAG GACGCTTCCT TTCAGATCAG
1201 GCCCCATCTC TGATGGAAGT GGAGAGACTC TTCTATTAGT GAGGAGATCC GGGGACTCCT
1261 ACATTAGTGA GGAGATCCAG GCCCTAGCAC TCTAAGCTGA TTTCAATGGG GCCCAGCCAG
1321 GCAGGGTGAA GGCCACTGTG CGAATCTACC TCACAGGCTA CACTCTGCCA GGCATGCCTT
1381 GGGGATGTGA GTGATAGGGT TCCGAGGGGA GGGGCAGAAA TGTCACCCTC TGACAGCCTA
1441 CCCCCGCAGC AAGCTGAGGG TCCCAAGGGG CTGTGGAGAG AGGGGTGGGG TCCCTAAGGG
1501 ATTGGCCTTT TCAGGGTGGA CCTCAGCACT CTGCCTTGAC TCCCCAAGGA GTGCCTGACG
1561 TGTTTATGTT CACTGGCAGT AGGACTCGGG GCCGGCACCC CTTTCACACT CTCCTTCCTT
1621 GGGTTTGTCA CCCGTGATGG CACCAGCCTG TCGTGCCCAC CCGTAGACTC GCATGGGGAC
1681 TCCCCAGGCC ACAGTGAAAC CCGTGCCGTT CCTCTATAGC TCCATGTGCT TGCTCACGTG
1741 TGTGTATGTG CGTGTCCGTT GCTGTGTTGT GAAACTGTGA CGTCACCCAG TCTAAGTGAA
1801 TGGCCACCGG GGCCACCGTT ATGCAATGTT CAGCGTGTCA CTGCTTGTGA AGCTCGATAA
1861 CTCTTTATTT TACTACAATG TCCCCAGAGT CCCTGGGACC CCTGTGGGAC TTGCAAAGGT
1921 TTTATTTTTT CGGTCTTAGA ACCTATGAGA ATCGGAGGGG CCGAGCCAAG CCCAGCCCAG
1981 CCCAGCTGCC GTGGCCTTGG CTTGCGTTTG CCTCAGCGGA TATGTTTATA CAGATGAATA
2041 TAAATTCTCT TTACTTTTGG CTGTTTGCAT TTTATTTTTG GTTCCCCCTC TCAGTACCTC
```

```
2101 CCAAAAAAAG AAAAAAAGAA AAAAACTACT TCTTCATTCG GTGGTACGAT TATTTTTTTT
2161 AACTAAAATG AGATAAAATT CTATATTCTT ATGTGTGTGT GGTTTTTGAT GACTAACTAG
2221 AAACAAAGGT GGACAGGATC AGGATGAGGT CGCTGGATCT GGGCCGTCAC ATCAGGAGCC
2281 TGGGGAGGAA GGCACTCCTG CTGGAGAGCT CTGTCCCTTA GCATCTACAA ACACTCCTGA
2341 TCTAAGCACT ACCTGTATTA AACTCATTTC ATCCTTAAAG G
```

Wild-type and mutated EFHD2 constructs were kindly provided by Dr. Irving Vega (University of Puerto Rico) (Vega et al., 2008). Deletion of the c-terminal coiled coil domain of EFhD2cing was accomplished by introducing the mutation C648T, thereby producing a a stop codon in the EFHD2 coding sequence.

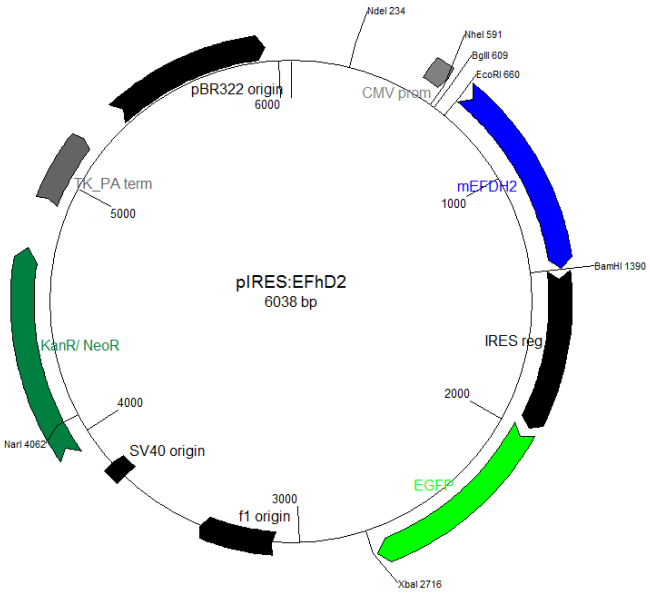

(a)

Figure B.6: EFHD2 expression construct in pIRES-EGFP.

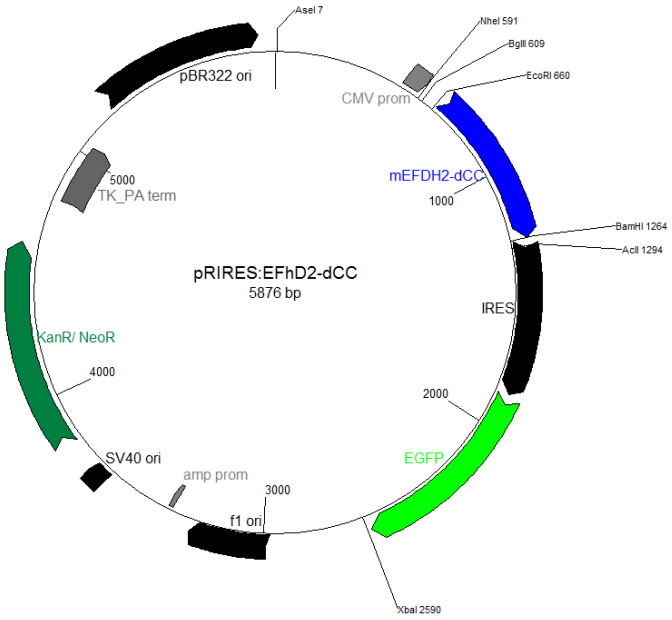

(b)

Figure B.6: EFHD2 expression construct in pIRES-EGFP (continued).

APPENDIX C

PRIMER SEQUENCES FOR PCR AND MOLECULAR CLONING

Name	Acc. No	Target	Sequence(5'→3')	Product
ABAD-fwd	NM004493	308–328	GGCATCGCG... GTGGCTAGCAAG	321 bp
ABAD-rev	NM004493	628–606	ACCTGGGGCA.. ATGGTCATCACCC	AT:60°C
Actin-fwd	NM007393.3	526–545	AGGCATTGTGATGGACTCCG	301 bp
Actin-rev	NM007393.3	826–807	AGTGATGACCTGGCCGTCAG	AT:56°C
EFHD2-Fwd	NM025994.3	335–358	TCGACCTGATG...	276 bp
	NM024329.5	412–435	AGCTGAAACTCA	AT:56°C
EFHD2-Rev	NM025994.3	610–589	CACGTTGATG...	
	NM024329.5	687–666	GCCTGTACCTT	
EFHD2-001R	NM024329.5	680–656	GATGGCCTGGACCTTGGCC...	269 bp
	NM025994.3		TCAAAGCTTGGCCTCAAAG	AT:58°C
EFHD2-002R	NM024329.5	526-508	GCAAAGCAAGGGCGCTCGA	351 bp
Ep-1-fwd	NM019535.2	287–308	GAATACCTTCA...	107 bp
	NM003026.2	454–475	ACCCAATCCAG	AT:60°C
Ep-1-rev	NM019535.2	393–375	GCCTCTGCCT...	
	NM003026.2	560–542	GAGGATAGC	
Ep-1-fwd (mouse)	NM019535.2	269–318	GCCTCTGC... CTGAGGATAGC	141 bp AT:60°C
Ep-1-rev (mouse)	NM019535.2 NM019535.2	393–375 437–418	GCCTCTGC... CTGAGGATAGC	
Prx-2 fwd	NM005809	418–439	CCCCGGAAAGA... GGGAGGCTTGG	200 bp
Prx-2 rev	NM005809	617–597	AGAGCCTCAT...	AT:60°C

			CCACGGAGCGT	
pSX69-fwd	–	–	CTGTGACCGAATCAC	seq
pSX69-rev	–	–	GCGTAAAAGGAGCAACATAG	
Syn-fwd	–	–	GCTGCCTCAGTCTGCGGTGG	seq
Ubi-rev	–	–	CCCTTCGTCT...	seq
Ubi-rev			GACGTGGCAGCG	

Table C.1: Nucleotide primers used for molecular cloning, RT-PCR and sequencing.

APPENDIX D

ETHICAL APPROVAL

I am familiar with the UTREC Guidelines for Ethical Research http://www.st-andrews.ac.uk/utrec/guidelines/ for Research practices, and have discussed them with other researchers involved in the project.

STUDENTS ONLY

My Supervisor has seen and agreed all relevant paperwork linked to this project **YES** ☒ **NO** ☐

Print Name:	Eva Borger
Signature	
Date:	15th Jan 2010

SUPERVISOR(S)

The Supervisor must ensure they have read both the application and the guidelines, and also has approved the project and application, before signing below, with clear regard for the balance between risk and the value of the research to the School/Student. (Supervisors should provide this on a separate sheet or supply to the student to insert below) Please, if you wish, add comments in no more than 200 words:

Print Name:	Dr. Frank Gunn-Moore
Signature	
Date:	15 Jan 2010

STAFF **YES** ☐ **NO** ☐

Print Name:	
Signature	
Date:	

SCHOOL ETHICS COMMITTEE OFFICIAL USE ONLY

STATEMENT OF ETHICAL APPROVAL

This project has been considered using agreed University Procedures and has been:

x Approved

☐ Not Approved pending:

- ☐ More Clarification Required
- ☐ New Submission Recommended
- ☐ Discussed with Supervisor
- ☐ Referred to UTREC
- ☐ Referred to Fieldwork Subcommittee

Convenor's Name	Keith T Sillar
Signature	
Date:	3rd February 2010

Please use the space below and additional pages to attach any supporting documents i.e. Participant Information Sheets, Consent Forms, Debriefing Forms, Questionnaires, Letter to Parents etc.
We recommend you refer to the sample documents provided at http://www/st-andrews.ac.uk/utrec/forms/

Approval Code:
(official Use Only)

UNIVERSITY OF ST ANDREWS TEACHING AND RESEARCH ETHICS COMMITTEE (UTREC)

ETHICAL APPLICATION FORM

Please Tick: Staff ☒ Postgraduate ☒ Undergraduate ☐ (**Module Code**):

double click on the box then click 'Checked' for a cross to appear in the box)

Researchers Name(s):	Dr Frank Gunn-Moore and Eva Borger		
Project Title:	Revealing the early biochemical events in dementia		
School/Unit: (Please indicate)	School of Biology	Supervisor:	Dr. Frank Gunn-Moore
Emails	eb427@st-andrews.ac.uk fjg1@st-andrews.ac.uk	Date Submitted	15th Jan 2010

Applications must be submitted electronically to the School Ethics Committee Secretary. Please submit directly to the S.E.C convenor only if the S.E.C has no appointed secretary – please refer to the web link for information, http://www.st-andrews.ac.uk/utrec/sec/schools/ Please DO NOT submit directly to UTREC. The Ethical Applications must contain all relevant supporting documents, added to the end of this document. Please include the Researcher(s)' name in the email subject box e.g. 'Smith-Ethical Application' One original hard copy must also be submitted with the signatures of all applicants and supervisors.
(Please do not type out with text boxes provided, note that the Text Boxes are fixed in size and will not allow any viewing beyond the word limit permitted.

Rationale: Please detail the project in 'lay language'. *This summary will be reviewed by UTREC and may be published as part of the reporting procedures. DO NOT exceed 75 Words (for database reasons).* Elucidation, if required can be given in Q.31

We are trying to reveal the chemical changes that take place in the brains of people who have died with dementia. Previously using transgenic animal models, we identified potential disease markers for the progression of Alzheimer's Disease. We will use human material supplied from the Manchester Brain Bank to confirm whether these potential markers also change in humans. We will therefore identify novel markers for the progression of dementia and identify possible new drug targets.

Ethical Considerations: Please detail the main ethical considerations raised by the project, concentrating on any issues raised specifically in the red sections, and addressing, where appropriate, the issue of whether basic ethical criteria has been met in all supporting documentation and if not why not. *This summary will be reviewed by UTREC and may be published as part of its reporting procedures. DO NOT exceed 75 words (for database reasons).* Elucidation, if required can be given in Q.31

There are no major ethical considerations raised by this project because it involves the use of human brain tissue from the Manchester Brain Bank. As such there have already been measures put in place to ensure confidentiality by anonymised brain donations. Additionally, we will not require to know who the donators were but only the pathological status of their brain i.e. whether they had dementia and of what type.

If ethical approval has been obtained from the University of St Andrews for research so similar to this project that a new review process may not be required, please give details of the application and the date of its approval.
Approval Code:
Date Approved:
Project Title:
Researchers Name(s):

RESEARCH INFORMATION

1. Estimated Start Date: 01.02.2010

2. Estimated Duration of Project: 12 months

3. Is this research funded by any external sponsor or agency? **YES** ☐ **NO** ☒

If YES please give details:

For projects funded by ESRC please be aware of the Ethical and Legal Considerations found at http://www.esds.ac.uk/aandp/create/ethical.asp

4. Does this research entail collaborative with other researchers? **YES** ☒ **NO** ☐

If YES state names and institutions of collaborators: Professor David Mann, Cerebral Function Unit, Greater Manchester Neuroscience Centre, Salford Royal NHS Foundation Trust, Salford M6 8HD

5. If the research is collaborative has a framework been devised to ensure That all participants are given appropriate recognition in any outputs? **N/A** ☐ **YES** ☒ **NO** ☐

6. Where projects raise ethical considerations to do with roles in research, intellectual property, publication strategies/authorship, responsibilities to funders, research with policy or other implications etc., have you taken appropriate steps to address these issues? **N/A** ☐ **YES** ☒ **NO** ☐

7. Location of Research Fieldwork to be conducted: Bute Buildings and Interdisciplinary Medical Research Institute, University of St. Andrews.

8. Is this research solely concerned with
   a. Published secondary data sources? **YES** ☐ **NO** ☒
   b. Unpublished data but with appropriate permissions, e.g. an archive curator? **YES** ☐ **NO** ☒

RESEARCH INFORMATION

9. a. Who are the intended Participants (e.g. students aged 18-21) and how will your recruit them (e.g. advertisement)	Patient material will be obtained via the Manchester Brain Bank from patients who donated tissues for research purposes.
b. Estimated duration of Participant Involvement.	N/A

If you have answered YES to Q8a or Q8b but the project has other Ethical Considerations please go to Q12, Q30 & Q31. If there are no other Ethical Considerations please sign and submit.

ETHICAL CHECKLIST

10. Have you obtained permission to access the site of research? **N/A** ☐ **YES** ☐ **NO** ☐

If YES please state agency/authority etc. & provide documentation.
If NO please indicate why

University of St. Andrews, School of Biology

11. Where appropriate has ethical approval been sought and obtained from any external body e.g. NRES/LEC or other UK Universities? If YES, please attach a copy of the external application and approval. **N/A** ☐ **YES** ☐ **NO** ☐

12. Will you tell participants that their participation is voluntary? **YES** ☐ **NO** ☐

13. Will you describe the main project/experimental procedures to participants in advance so that they can make an informed decision about whether or not to participate? **YES** ☐ **NO** ☐

14. Will you tell participants that they may withdraw from the research at any time and for any reason, without having to give an explanation? **YES** ☐ **NO** ☐

15. Please answer either a. or b.
    a. Will you obtain written consent from participants? **YES** ☐ **NO** ☐
    b. *(Social Anthropology Geography/Geosciences & Biology ONLY)* Will you obtain written consent from participants, in those cases where it is appropriate **YES** ☐ **NO** ☐

16. Please answer either a. or b.
    a. If the research is photographed or videoed or taped or observational, will you ask participants for their consent to being Photographed, videoed, taped or observed? **N/A** ☐ **YES** ☐ **NO** ☐
    b. *(Social Anthropology & Biology ONLY)* Will participants be free to reject the use of intrusive research Methods such as audio-visual recorders and photography? **N/A** ☐ **YES** ☐ **NO** ☐

17. Will you tell participants that their data will be treated with full confidentiality and that if published, it will not be identifiable as theirs? **YES** ☐ **NO** ☐

18. Will participants be clearly informed of how the data will be stored, who will have access to it, and when the data will be destroyed? **YES** ☐ **NO** ☐

19. Will you debrief participants at the end of their participation, i.e. give them a brief explanation in writing of the study? **YES** ☐ **NO** ☐

20. With questionnaires and/or interviews, will you give participants the option of omitting questions they do not want to answer? **N/A** ☐ **YES** ☐ **NO** ☐

If you have answered NO to any question 11- 20, please give a brief explanation in the statement of Ethical Considerations on Page 1 and expand in Q31 if necessary. If you have answered YES, it must be clearly illustrated in the relevant paperwork which must be attached i.e. Participants Information Sheet, Consent Form, Debriefing Form, Questionnaire, Letters etc……

WORKING WITH CHILDREN / VULNERABLE PEOPLE

Do participants fall into any of the following special groups? If they do, please tick the appropriate answer, refer to the relevant guidelines and complete Q31. Please see http://www.st-andrews.ac.uk/utrec/children/

21. a. Children (under 18 years of age) **YES** ☐ **NO** ☐

b. People with learning or communication difficulties **YES** ☐ **NO** ☐

c. Patients (including carers of NHS patients) **YES** ☐ **NO** ☐

d. People in custody **YES** ☐ **NO** ☐

e. Institutionalised persons **YES** ☐ **NO** ☐

f. People engaged in illegal activities e.g. drug-taking **YES** ☐ **NO** ☐

g. Other vulnerable groups **YES** ☐ **NO** ☐

If you have answered YES to Q 21 you must obtain Enhanced Disclosure Scotland Approval. Furthermore, you may need to obtain permission from the local Education Authority, Police, LREC (NHS) clearance

22. If working with children, institutionalised person(s) or vulnerable people, do you have:

1. Enhanced Disclosure Scotland Certificate? **YES** ☐ **NO** ☐

2. If you have been in the UK for less than a year, equivalent Documentation from the countries you have resided in? Information on what is required can be obtained from UTREC **N/A** ☐ **YES** ☐ **NO** ☐

If YES a copy (or copies) must be submitted with this application to be retained by the School. If NO please explain in Q31.

23. If working with children or vulnerable people, have you constructed appropriate letters to i.e. parents, children, head teachers, carers, institutions, police etc. **YES** ☐ **NO** ☐

RISK AND SAFETY

This section is for ethical use only and does not replace the University official procedures on Risk and Safety measures. In addition to completing this section you must review the following http://www.st-andrews.ac.uk/utrec/riskassessment/ and http://www.st-andrews.ac.uk/staff/policy/Healthandsafety/Publications/Fieldwork/ and follow the relevant procedures.

24. Are any of the participants in a dependant relationship with the investigator e.g. lecturer/student? If YES, give explanation in Q31. **YES** ☐ **NO** ☐

25. Will you project involve deliberately misleading participants in any way? If YES, give details in Q31 and state why it is necessary and explain how debriefing will occur **YES** ☐ **NO** ☐

26. Is there any significant risk to any paid or unpaid participant(s), field assistant(s), helper(s) or student(s), involved in the project, experiencing either physical or psychological distress or discomfort? If Yes, give details in Q31 and state what you will do if they should experience any problems e.g. who to contact for help. **YES** ☐ **NO** ☐

27. Is there any significant risk to the investigator? If YES, have the appropriate risk assessment forms been submitted to the appropriate Safety Committee(s)? **N/A** ☐ **YES** ☐ **NO** ☐

28. *(Bute Medical School and Biology only)* Have appropriate chemical, Radiation and biological (including GMAG) risk assessments been Submitted to the appropriate Safety Committee for approval? **N/A** ☐ **YES** ☐ **NO** ☐

30. Do you think the processes, including any results, of your research have the potential to cause any damage, harm or other problems for People in your study area? If YES, please explain in Q31 and indicate how you will seek to obviate the effects **YES** ☐ **NO** ☐

There is an obligation on the Lead Researcher & Supervisor to bring to the attention of the School Ethics Committee (SEC) any issues with ethical implications not clearly covered by the above checklist.

ETHICAL STATEMENT

31. Write a clear but concise statement of the ethical considerations raised by the project and how you intend to deal with them. It may be that in order to do this you need to expand on the Ethical Considerations section on page 1. (continue on additional pages if necessary)

DOCUMENTATION CHECKLIST		
Ethical Application Form	**YES** ☐	**NO** ☐
Participant Information Sheet	**YES** ☐	**NO** ☐
Consent Form	**YES** ☐	**NO** ☐
Debriefing Form	**YES** ☐	**NO** ☐
External Permissions	**YES** ☐	**NO** ☐
Letters to Parents / Children / Head Teachers etc…..	**YES** ☐	**NO** ☐
Enhanced Disclosure Scotland and or Equivalent (as necessary)	**YES** ☐	**NO** ☐
Advertisement	**YES** ☐	**NO** ☐
Other (please list):		

DECLARATION

APPENDIX E

PUBLICATIONS

Owing to copyright restrictions, the electronic version of this thesis does not contain the text of the following two articles.

Biochem. J. (2010) 426, 255–270 (Printed in Great Britain) doi:10.1042/BJ20091941

The consequences of mitochondrial amyloid ß-peptide in Alzheimer's disease

Kirsty E. A. MUIRHEAD*[1,2], Eva BORGER*[2], Laura AITKEN*, Stuart J. CONWAY† and Frank J. GUNN-MOORE*[1]

*School of Biology, Bute Medical Building, University of St Andrews, Westburn Lane, St Andrews, Fife KY16 9TS, U.K., and
†Department of Chemistry, Chemistry Research Laboratory,
University of Oxford, Mansfield Road, Oxford OX1 3TA, U.K.

Biochemical Society Transactions (2011) Volume 39, part 4. doi:10.1042/BST0390868

Mitochondrial ß-amyloid in Alzheimer's disease

Eva Borger*, Laura Aitken*, Kirsty E.A. Muirhead*, Zoe E. Allen*, James A. Ainge†, Stuart J. Conway‡ and Frank J. Gunn-Moore*[1]

*School of Biology, Biological and Medical Sciences Building, University of St Andrews, North Haugh, St Andrews, Fife KY16 9TF, U.K., †School of Psychology,
St. Mary's College, University of St Andrews, South Street, St Andrews, Fife KY16 9JP, U.K., and ‡Department of Chemistry, Chemistry Research Laboratory,
University of Oxford, Mansfield Road, Oxford OX1 3TA, U.K.

BIBLIOGRAPHY

Abbott A. Dementia: a problem for our age. *Nature*, 475(7355):S2–S4, Jul 2011.

Abe N., Almenar-Queralt A., Lillo C., Shen Z., Lozach J., Briggs S., Williams D., Goldstein L., and Cavalli V. Sunday driver interacts with two distinct classes of axonal organelles. *J Biol Chem*, 284(50):34628–34639, 2009.

Ahmed Z., Mackenzie I., Hutton M. L., and Dickson D. W. Progranulin in frontotemporal lobar degeneration and neuroinflammation. *J Neuroinflammation*, 4:7, 2007.

Allen Z. The activity of amyloid beta binding alcohol dehydrogenase in alzheimers disease. Master's thesis, University of St Andrews, School of Biology, 2012.

Allinson T. M., Parkin E., Turner A., and Hooper N. Adams family members as amyloid precursor protein -secretases. *J Neurosci Res*, 74(3):342–352, 2003.

Almeida C. G., Takahashi R. H., and Gouras G. K. Beta-amyloid accumulation impairs multivesicular body sorting by inhibiting the ubiquitin-proteasome system. *J Neurosci*, 26(16):4277–88, 2006.

Alzheimer A. Ueber einen eigenartigen schwaeren krankheitsprozess der hirnrinde. *Neurol Centralbl*, 25:1134, 1906.

Alzheimer A. Ueber eine eigenartige erkrankung der hirnrinde. *Allg Zeitschr Psychiatr Psych Gerichtl Med*, 64:146–148, 1907.

Anandatheerthavarada H. K., Biswas G., Mullick J., Sepuri N. B., Otvos L., Pain D., and Avadhani N. G. Dual targeting of cytochrome p4502b1 to endoplasmic reticulum and mitochondria involves a novel signal activation by cyclic amp-dependent phosphorylation at ser128. *EMBO J*, 18(20):5494–504, 1999.

Anandatheerthavarada H., Biswas G., Robin M., and Avadhani N. Mitochondrial targeting and a novel transmembrane arrest of alzheimer's amyloid precursor protein impairs mitochondrial function in neuronal cells. *J. Cell Biol.*, 161(1):41–54, 2003.

Andersen O. M., Reiche J., Schmidt V., Gotthardt M., Spoelgen R., Behlke J., von Arnim C. F., Breiderhoff T., Jansen P., Wu X., Bales K., Cappai R., Masters C., Gliemann J., Mufson E. J., Hyman B. T., Paul S., Nykjaer A., and Willnow T. Neuronal sorting protein-related receptor sorla/lr11 regulates processing of the amyloid precursor protein. *Proc. Natl. Acad. Sci. U.S.A.*, 102(38):13461–13466, 2005.

Area-Gomez E., de Groof A. J., Boldogh I., Bird T. D., Gibson G. E., Koehler C. M., Yu W. H., Duff K. E., Yaffe M. P., Pon L. A., and Schon E. A. Presenilins are enriched in endoplasmic reticulum membranes associated with mitochondria. *Am J Pathol*, 175:1810–1816, 2009.

Arispe N., Rojas E., and Pollard H. B. Alzheimer disease amyloid beta protein forms calcium channels in bilayer membranes: blockade by tromethamine and aluminum. *Proc Natl Acad Sci U S A*, 90(2):567–571, 1993.

Arvanitis D. N., Ducatenzeiler A., Ou J. N., Grodstein E., Andrews S. D., Tendulkar S. R., Ribeiro-da Silva A., Szyf M., and Cuello A. C. High intracellular concentrations of amyloid-beta block nuclear translocation of phosphorylated creb. *J Neurochem*, 103(1):216–228, 2007.

Avramidou A., Kroczek C., Lang C., Schuh W., Jack H. M., and Mielenz D. The novel adaptor protein swiprosin-1 enhances bcr signals and contributes to bcr-induced apoptosis. *Cell Death Differ*, 14(11):1936–1947, 2007.

Bai J., Hu Z., Dittman J., Pym E., and Kaplan J. Endophilin functions as a membrane-bending molecule and is delivered to endocytic zones by exocytosis. *Cell*, 143(3): 430–441, Oct 2010.

Baines C. P., Kaiser R. A., Purcell N. H., Blair N. S., Osinska H., Hambleton M. A., Brunskill E. W., Sayen M. R., Gottlieb R. A., Dorn G. W., Robbins J., and Molkentin J. D. Loss of cyclophilin d reveals a critical role for mitochondrial permeability transition in cell death. *Nature*, 434(7033):658–62, 2005.

Ballard C., Gauthier S., Corbett A., Brayne C., Aarsland D., and Jones E. Alzheimer's disease. *Lancet*, 377(9770):1019 – 1031, 2011.

Ballif B. A., Carey G. R., Sunyaev S. R., and Gygi S. P. Large-scale identification and evolution indexing of tyrosine phosphorylation sites from murine brain. *J Proteome Res*, 7(1):311–8, 2008.

Bancher C., Brunner C., Lassmann H., Budka H., Jellinger K., Wiche G., Seitelberger F., Grundke-Iqbal I., Iqbal K., and Wisniewski H. Accumulation of abnormally phosphorylated precedes the formation of neurofibrillary tangles in alzheimer's disease. *Brain Res*, 477:90–99, 1989.

Basso E., Fante L., Fowlkes J., Petronilli V., Forte M. A., and Bernardi P. Properties of the permeability transition pore in mitochondria devoid of cyclophilin d. *J Biol Chem*, 280(19):18558–61, 2005.

Basso E., Petronilli V., Forte M. A., and Bernardi P. Phosphate is essential for inhibition of the mitochondrial permeability transition pore by cyclosporin a and by cyclophilin d ablation. *J Biol Chem*, 283(39):26307–11, 2008.

Beal M. F. Aging, energy, and oxidative stress in neurodegenerative diseases. *Ann Neurol*, 38(3):357–66, 1995.

Bekris L., Galloway N., Montine T., Schellenberg G., and Yu C. Apoe mrna and protein expression in postmortem brain are modulated by an extended haplotype structure. *Am J Med Genet B Neuropsychiatr Genet*, 153B:409–417, 2009.

Berridge M. J. Calcium hypothesis of alzheimer's disease. *Pflugers Arch*, 459(3):441–9, 2010.

Bhaskar K., Yen S. H., and Lee G. Disease-related modifications in tau affect the interaction between fyn and tau. *J Biol Chem*, 280(42):35119–25, 2005.

Bjork B. F., Katzov H., Kehoe P., Fratiglioni L., Winblad B., Prince J. A., and Graff C. Positive association between risk for late-onset alzheimer disease and genetic variation in ide. *Neurobiol Aging*, 28(9):1374–80, 2007.

Blagoev B., Ong S., Kratchmarova I., and Mann M. Temporal analysis of phosphotyrosine-dependent signaling networks by quantitative proteomics. *Nat Biotech*, 22(9):1139–1145, Sep 2004.

Blethrow J., Glavy J., Morgan D., and Shokat K. Covalent capture of kinase-specific phosphopeptides reveals cdk1-cyclin b substrates. *Proc Natl Acad Sci U S A*, 105 (5):1442–1447, 2008.

Blurton-Jones M. and Laferla F. Pathways by which abeta facilitates tau pathology. *Curr. Alzheimer. Res.*, 3(5):437–48., 2006.

Borchelt D., Thinakaran G., Eckman C. B., Lee M., Davenport F., Ratovitsky T., Prada C., Kim G., Seekins S., Yager D., Slunt H., Wang R., Seeger M., Levey A., Gandy S., Copeland N., Jenkins N., Price D., Younkin S., and Sisodia S. Familial alzheimer's diseaselinked presenilin 1 variants elevate a142/140 ratio in vitro and in vivo. *Neuron*, 17(5):1005–1013, 1996.

Borger E., Aitken L., Muirhead K. E., Allen Z. E., Ainge J. A., Conway S. J., and Gunn-Moore F. J. Mitochondrial beta-amyloid in alzheimer's disease. *Biochem Soc Trans*, 39(4):868–73, 2011.

Bosco D. A., Morfini G., Karabacak N. M., Song Y., Gros-Louis F., Pasinelli P., Goolsby H., Fontaine B. A., Lemay N., McKenna-Yasek D., Frosch M. P., Agar J. N., Julien J. P., Brady S. T., and Brown J., R. H. Wild-type and mutant sod1 share an aberrant conformation and a common pathogenic pathway in als. *Nat Neurosci*, 13 (11):1396–403, 2010.

Bowling A. C. and Beal M. F. Bioenergetic and oxidative stress in neurodegenerative diseases. *Life Sci*, 56(14):1151–71, 1995.

Braak H J. B., Braak E. Staging of alzheimer-related cortical destruction. *Eur. Neurol.*, 33(6):403–8., 1993.

Brecht S., Kirchhof R., Chromik A., Willesen M., Nicolaus T., Raivich G., Wessig J., Waetzig V., Goetz M., Claussen M., Pearse D., Kuan C. Y., Vaudano E., Behrens A., Wagner E., Flavell R. A., Davis R. J., and Herdegen T. Specific pathophysiological functions of jnk isoforms in the brain. *Eur J Neurosci*, 21(2):363–77, 2005.

Breese C., Adams C., Logel J., Drebing C., Rollins Y., Barnhart M., Sullivan B., DeMasters B., Freedman R., and Leonard S. Comparison of the regional expression of nicotinic acetylcholine receptor 7 mrna and [125i]--bungarotoxin binding in human postmortem brain. *J Comp Physiol*, 387(3):385–398, 1997.

Brion J.-P., Octave J., and Couck A. Distribution of the phosphorylated microtubule-associated protein tau in developing cortical neurons. *Neuroscience*, 63(3):895–909, Dec 1994.

Brody D. and Holtzman D. Active and passive immunotherapy for neurodegenerative disorders. *Annu. Rev. Neurosci.*, 31(1):175–193, 2008.

Bubber P., Haroutunian V., Fisch G., Blass J. P., and Gibson G. E. Mitochondrial abnormalities in alzheimer brain: mechanistic implications. *Ann Neurol*, 57(5):695–703, 2005.

Bucciantini M., Giannoni E., Chiti F., Baroni F., Formigli L., Zurdo J., Taddei N., Ramponi G., Dobson C. M., and Stefani M. Inherent toxicity of aggregates implies a common mechanism for protein misfolding diseases. *Nature*, 416(6880):507–11, 2002.

Butterfield D. A., Drake J., Pocernich C., and Castegna A. Evidence of oxidative damage in alzheimer's disease brain: central role for amyloid beta-peptide. *Trends Mol Med*, 7(12):548–54, 2001.

Caccamo A., Oddo S., Billings L. M., Green K. N., Martinez-Coria H., Fisher A., and LaFerla F. M. M1 receptors play a central role in modulating ad-like pathology in transgenic mice. *Neuron*, 49(5):671–82, 2006.

Caspersen C., Wang N., Yao J., Sosunov A., Chen X., Lustbader J., Wei Xu H., Stern D., McKhann G., and Yan S. Mitochondrial aβ: a potential focal point for neuronal metabolic dysfunction in alzheimer's disease. *FASEB J.*, n/a:05–3735fje, 2005.

Chang K. A. and Suh Y. H. Possible roles of amyloid intracellular domain of amyloid precursor protein. *BMB Rep.*, 43(10):656–63., 2010.

Chang L., Jones Y., Ellisman M. H., Goldstein L. S., and Karin M. Jnk1 is required for maintenance of neuronal microtubules and controls phosphorylation of microtubule-associated proteins. *Dev Cell*, 4(4):521–33, 2003.

Chapman P. F., White G. L., Jones M. W., Cooper-Blacketer D., Marshall V. J., Irizarry M., Younkin L., Good M. A., Bliss T. V., Hyman B. T., Younkin S. G., and Hsiao K. K. Impaired synaptic plasticity and learning in aged amyloid precursor protein transgenic mice. *Nat Neurosci*, 2(3):271–276, Mar 1999.

Chasseigneaux S. and Allinquant B. Functions of a, sapp and sapp : similarities and differences. *J Neuro*, 120:99–108, 2012.

Checiska A., Giaccone G., Rodriguez J., Kruyt F., and Jimenez C. Comparative proteomics analysis of caspase-9-protein complexes in untreated and cytochrome c/datp stimulated lysates of nsclc cells. *J Proteomics*, 72(4):575–585, May 2009.

Chen J. and Yan S. Role of mitochondrial amyloid- in alzheimer's disease. *J Alzheimers Dis*, 20:569–578, May 2010.

Chen K. H., Reese E. A., Kim H. W., Rapoport S. I., and Rao J. S. Disturbed neurotransmitter transporter expression in alzheimer's disease brain. *J Alzheimers Dis.*, 26(4):755–66., 2011.

Chen Y., Deng L., Maeno-Hikichi Y., Lai M., Chang S., Chen G., and Zhang J. Formation of an endophilin-ca2+ channel complex is critical for clathrin-mediated synaptic vesicle endocytosis. *Cell*, 115(1):37–48, Oct 2003.

Cho D. H., Nakamura T., Fang J., Cieplak P., Godzik A., Gu Z., and Lipton S. A. S-nitrosylation of drp1 mediates beta-amyloid-related mitochondrial fission and neuronal injury. *Science*, 324(5923):102–5, 2009.

Choi J., Rees H. D., Weintraub S. T., Levey A. I., Chin L. S., and Li L. Oxidative modifications and aggregation of cu,zn-superoxide dismutase associated with alzheimer

and parkinson diseases. *J Biol Chem*, 280(12):11648–55, 2005.

Citron M. Strategies for disease modification in alzheimer's disease. *Nat Rev Neurosci*, 5(9):677–85, 2004.

Citron M., Oltersdorf T., Haass C., McConlogue L., Hung A., Seubert P., Vigo-Pelfrey C., Lieberburg I., and Selkoe D. Mutation of the [beta]-amyloid precursor protein in familial alzheimer's disease increases [beta]-protein production. *Nature*, 360(6405): 672–674, Dec 1992.

Cole A. R., Noble W., van Aalten L., Plattner F., Meimaridou R., Hogan D., Taylor M., LaFrancois J., Gunn-Moore F., Verkhratsky A., Oddo S., LaFerla F., Giese K. P., Dineley K. T., Duff K., Richardson J. C., Yan S. D., Hanger D. P., Allan S. M., and Sutherland C. Collapsin response mediator protein-2 hyperphosphorylation is an early event in alzheimer's disease progression. *J Neurochem*, 103(3):1132–44, 2007.

Colombo A., Bastone A., Ploia C., Sclip A., Salmona M., Forloni G., and Borsello T. Jnk regulates app cleavage and degradation in a model of alzheimer's disease. *Neurobiol Dis*, 33(3):518–525, 2009.

Combs B., Voss K., and Gamblin T. Pseudohyperphosphorylation has differential effects on polymerization and function of tau isoforms. *Biochemistry*, 50(44):9446–9456, 2011.

Connern C. P. and Halestrap A. P. Recruitment of mitochondrial cyclophilin to the mitochondrial inner membrane under conditions of oxidative stress that enhance the opening of a calcium-sensitive non-specific channel. *Biochem J*, 302(2):321–324, 1994.

Cordes C. M., Bennett R., Siford G., and Hamel F. Nitric oxide inhibits insulin-degrading enzyme activity and function through s-nitrosylation. *Biochem Pharmacol*, 77(6):1064–1073, 2009.

Costantini C., Weindruch R., Della Valle G., and Puglielli L. A trka-to-p75ntr molecular switch activates amyloid beta-peptide generation during aging. *Biochem J*, 391(Pt 1):59–67, 2005.

Costantini C., Scrable H., and Puglielli L. An aging pathway controls the trka to p75ntr receptor switch and amyloid beta-peptide generation. *EMBO J*, 25(9):1997–2006, 2006.

Cottrell D., Blakely E., Johnson M., Ince P., and Turnbull D. Mitochondrial enzyme-deficient hippocampal neurons and choroidal cells in ad. *Neurology*, 57(2):260–264, 2001.

Coulson E. J., Paliga K., Beyreuther K., and Masters C. L. What the evolution of the amyloid protein precursor supergene family tells us about its function. *Neurochem Int*, 36(3):175–1784, 2000.

Crawford F., Freeman M., Town T., Fallin D., Gold M., Duara R., and Mullan M. No genetic association between polymorphisms in the tau gene and alzheimer's disease in clinic or population based samples. *Neurosci. Lett.*, 266(3):193–196, 1999.

Cruz J., Kim D., Moy L., Dobbin M., Sun X., Bronson R., and Tsai L. p25/cyclin-dependent kinase 5 induces production and intraneuronal accumulation of amyloid beta in vivo. *J. Neurosci.*, 26(41):10536–10541, 2006.

Cruzalegui F. H., Hardingham G., and Bading H. c-jun functions as a calcium-regulated

transcriptional activator in the absence of jnk/sapk1 activation. *EMBO J*, 18(5): 1335–1344, Mar 1999.

Dahiyat M., Cumming A., Harrington C., Wischik C., Xuereb J., Corrigan F., Breen G., Shaw D., and Clair D. S. Association between alzheimer's disease and the nos3 gene. *Ann Neurol*, 46(4):664–667, Oct 1999.

D'Amelio M., Cavallucci S., Vand Middei, Marchetti C., Pacioni S., Ferri A., Diamantini A., De Zio D., Carrara P., Battistini L., Moreno S., Bacci A., Ammassari-Teule M., Marie H., and Cecconi F. Caspase-3 triggers early synaptic dysfunction in a mouse model of alzheimer's disease. *Nat Neurosci*, 14(1):69–76, Jan 2011.

de Calignon A., Fox L., Pitstick R., Carlson G., Bacskai B., Spires-Jones T., and Hyman B. Caspase activation precedes and leads to tangles. *Nature*, 464(7292):1201–1204, Apr 2010.

De Gois S., Jeanclos E., Morris M., Grewal S., Varoqui H., and Erickson J. Identification of endophilins 1 and 3 as selective binding partners for vglut1 and their co-localization in neocortical glutamatergic synapses: Implications for vesicular glutamate transporter trafficking and excitatory vesicle formation. *Cell Mol Neurobiol*, 26:677–691, 2006.

De Jonghe C., Esselens C., Kumar-Singh S., Craessaerts K., Serneels S., Checler F., Annaert W., Van Broeckhoven C., and De Strooper B. Pathogenic app mutations near the gamma-secretase cleavage site differentially affect abeta secretion and app c-terminal fragment stability. *Hum. Mol. Genet.*, 10(16):1665–1671, 2001.

de Souza D. M., Gattaz W., ASchmitt , CRewerts , Maccarrone G., Dias-Neto E., and Turck C. Prefrontal cortex shotgun proteome analysis reveals altered calcium homeostasis and immune system imbalance in schizophrenia. *Eur Arch Psychiatry Clin Neurosci*, 259(3):151–163, Apr 2009.

Deane R., Du Yan S., Submamaryan R. K., LaRue B., Jovanovic S., Hogg E., Welch D., Manness L., Lin C., Yu J., Zhu H., Ghiso J., Frangione B., Stern A., Schmidt A. M., Armstrong D. L., Arnold B., Liliensiek B., Nawroth P., Hofman F., Kindy M., Stern D., and Zlokovic B. Rage mediates amyloid-beta peptide transport across the blood-brain barrier and accumulation in brain. *Nat Med*, 9(7):907–13, 2003.

Deane R., Wu Z., and Zlokovic B. V. Rage (yin) versus lrp (yang) balance regulates alzheimer amyloid beta-peptide clearance through transport across the blood-brain barrier. *Stroke*, 35(11 Suppl 1):2628–31, 2004.

Dehmelt L. and Halpain S. The map2/tau family of microtubule-associated proteins. *Genome Biol*, 6(1):204, 2004.

Delarasse C., Auger R., Gonnord P., Fontaine B., and Kanellopoulos J. The purinergic receptor p2x7 triggers -secretase-dependent processing of the amyloid precursor protein. *J Biol Chem*, 286(4):2596–2606, 2011.

Deng H. X., Hentati A., Tainer J. A., Iqbal Z., Cayabyab A., Hung W. Y., Getzoff E. D., Hu P., Herzfeldt B., Roos R. P., and et a. Amyotrophic lateral sclerosis and structural defects in cu,zn superoxide dismutase. *Science*, 261(5124):1047–1051, 1993.

Devi L. and Anandatheerthavarada H. K. Mitochondrial trafficking of app and alpha

synuclein: Relevance to mitochondrial dysfunction in alzheimer's and parkinson's diseases. *Biochim Biophys Acta*, 1802(1):11–19, 2010.

Devi L., Prabhu B., Galati D., Avadhani N., and Anandatheerthavarada H. Accumulation of amyloid precursor protein in the mitochondrial import channels of human alzheimer's disease brain is associated with mitochondrial dysfunction. *J. Neurosci.*, 26(35):9057–9068, 2006.

Diener K., Wang X. S., Chen C., Meyer C. F., Keesler G., Zukowski M., Tan T. H., and Yao Z. Activation of the c-jun n-terminal kinase pathway by a novel protein kinase related to human germinal center kinase. *Proc Natl Acad Sci U S A*, 94(18): 9687–92, 1997.

Dodart J. C., Mathis C., Saura J., Bales K. R., Paul S. M., and Ungerer A. Neuroanatomical abnormalities in behaviorally characterized app(v717f) transgenic mice. *Neurobiol Dis.*, 7(2):71–85., 2000.

Dodson S., Andersen O., Karmali V., Fritz J., Cheng D., Peng J., Levey A., Willnow T., and Lah J. Loss of lr11/sorla enhances early pathology in a mouse model of amyloidosis: Evidence for a proximal role in alzheimer's disease. *J. Neurosci.*, 28 (48):12877–12886, 2008.

Du H., Guo L., Fang F., Chen D., Sosunov A. A., McKhann G. M., Yan Y., Wang C., Zhang H., Molkentin J. D., Gunn-Moore F. J., Vonsattel J. P., Arancio O., Chen J. X., and Yan S. D. Cyclophilin d deficiency attenuates mitochondrial and neuronal perturbation and ameliorates learning and memory in alzheimer's disease. *Nat Med*, 14(10):1097–105, 2008.

Du H., Guo L., Zhang W., Rydzewska M., and Yan S. Cyclophilin d deficiency improves mitochondrial function and learning/memory in aging alzheimer disease mouse model. *Neurobiol. Aging.*, 2009.

Du H., Guo L., Yan S., Sosunov A., McKhann G., and Yan S. Early deficits in synaptic mitochondria in an alzheimer's disease mouse model. *Proc Natl Acad Sci U S A*, 107 (43):18670–18675, 2010.

Du H., Guo L., Zhang W., Rydzewska M., and Yan S. Cyclophilin d deficiency improves mitochondrial function and learning/memory in aging alzheimer disease mouse model. *Neurobiol Aging*, 32(3):398–406, Mar 2011.

Duara R., Grady C., Haxby J., Sundaram M., Cutler N. R., Heston L., Moore A., Schlageter N., Larson S., and Rapoport S. I. Positron emission tomography in alzheimer's disease. *Neurology*, 36(7):879–87, 1986.

Duetting S., Brachs S., and Mielenz D. Fraternal twins: Swiprosin-1/efhd2 and swiprosin-2/efhd1, two homologous ef-hand containing calcium binding adaptor proteins with distinct functions. *Cell Commun Signal*, 9:2, 2011.

Dumont M., Wille E., Stack C., Calingasan N., Beal M., and Lin M. Reduction of oxidative stress, amyloid deposition, and memory deficit by manganese superoxide dismutase overexpression in a transgenic mouse model of alzheimer's disease. *FASEB J.*, 23:2459–2466, 2009.

Duyckaerts C., Delatour B., and Potier M. Classification and basic pathology of alzheimer disease. *Acta Neuropathol*, 118(1):5–36, Jul 2009.

Eminel S., Roemer L., Waetzig V., and Herdegen T. c-jun n-terminal kinases trigger both degeneration and neurite outgrowth in primary hippocampal and cortical neurons. *J Neurochem*, 104(4):957–969, 2008.

Falkevall A., Alikhani N., Bhushan S., Pavlov P., Busch K., Johnson K., Eneqvist T., Tjernberg L., Ankarcrona M., and Glaser E. Degradation of the amyloid beta-protein by the novel mitochondrial peptidasome, prep. *J. Biol. Chem.*, 281(39):29096–29104, 2006.

Finder V. H. and Glockshuber R. Amyloid-beta aggregation. *Neurodegener Dis*, 4(1): 13–27, 2007.

Foster N. L., Chase T. N., Fedio P., Patronas N. J., Brooks R. A., and Di Chiro G. Alzheimer's disease: focal cortical changes shown by positron emission tomography. *Neurology*, 33(8):961–5, 1983.

Frackowiak J., Mazur-Kolecka B., Kaczmarski W., and Dickson D. Deposition of alzheimer's vascular amyloid-beta is associated with decreased expression of brain l-3-hydroxyacyl-coenzyme a dehydrogenase (erab). *Brain. Res.*, 907(1-2):44–53, 2001.

Freeman B. C., Toft D. O., and Morimoto R. I. Molecular chaperone machines: chaperone activities of the cyclophilin cyp-40 and the steroid aporeceptor-associated protein p23. *Science*, 274(5293):1718–20, 1996.

Friberg H., Connern C., Halestrap A. P., and Wieloch T. Differences in the activation of the mitochondrial permeability transition among brain regions in the rat correlate with selective vulnerability. *J Neurochem*, 72(6):2488–97, 1999.

Friedrich R. P., Tepper K., Ronicke R., Soom M., Westermann M., Reymann K., Kaether C., and Fandrich M. Mechanism of amyloid plaque formation suggests an intracellular basis of abeta pathogenicity. *Proc Natl Acad Sci U S A*, 107(5):1942–7, 2010.

Fu X., Yang Y., Xu C., Niu Y., Chen T., Zhou Q., and Liu J. Retrolinkin cooperates with endophilin a1 to mediate bdnf-trkb early endocytic trafficking and signaling from early endosomes. *Mol Biol Cell*, 2011.

Fujino G., Noguchi T., Matsuzawa A., Yamauchi S., Saitoh M., Takeda K., and Ichijo H. Thioredoxin and traf family proteins regulate reactive oxygen species-dependent activation of ask1 through reciprocal modulation of the n-terminal homophilic interaction of ask1. *Mol Cell Biol*, 27(23):8152–63, 2007.

Fukumori A., Okochi M., Tagami S., Jiang J., Itoh N., Nakayama T., Yanagida K., Ishizuka-Katsura Y., Morihara T., Kamino K., Tanaka T., Kudo T., Tanii H., Ikuta A., Haass C., and Takeda M. Presenilin-dependent -secretase on plasma membrane and endosomes is functionally distinct. *Biochemistry*, 45(15):4907–4914, 2006.

Fukumoto H., Cheung B. S., Hyman B. T., and Irizarry M. C. beta-secretase protein and activity are increased in the neocortex in alzheimer disease. *Arch Neurol*, 59(9): 1381–1389, 2002.

Gabuzda D., Busciglio J., Chen L. B., Matsudaira P., and Yankner B. A. Inhibition of energy metabolism alters the processing of amyloid precursor protein and induces a potentially amyloidogenic derivative. *J Biol Chem*, 269(18):13623–13628, 1994.

Gallop J., Jao C. C., Kent H., Butler P. J. G., Evans P., Langen R., and McMahon

H. Mechanism of endophilin n-bar domain-mediated membrane curvature. *EMBO J*, 25(12):2898–2910, Jun 2006.

Galvan V., Banwait S., Spilman P., Gorostiza O., Peel A., Ataie M., Crippen D., Huang W., Sidhu G., Ichijo H., and Bredesen D. Interaction of ask1 and the [beta]-amyloid precursor protein in a stress-signaling complex. *Neurobiol Dis*, 28(1):65 – 75, 2007.

Gentleman S. M., Nash M. J., Sweeting C. J., Graham D. I., and Roberts G. W. Beta-amyloid precursor protein (beta app) as a marker for axonal injury after head injury. *Neurosci Lett*, 160(2):139–44, 1993.

Giachino C., Lantelme E., Lanzetti L., Saccone S., Bella Valle G., and Migone N. A novel sh3-containing human gene family preferentially expressed in the central nervous system. *Genomics*, 41(3):427–434, May 1997.

Gibson G. E., Park L. C., Zhang H., Sorbi S., and Calingasan N. Y. Oxidative stress and a key metabolic enzyme in alzheimer brains, cultured cells, and an animal model of chronic oxidative deficits. *Ann N Y Acad Sci*, 893:79–94, 1999.

Giorgi C., De Stefani D., Bononi A., Rizzuto R., and Pinton P. Structural and functional link between the mitochondrial network and the endoplasmic reticulum. *Int J Biochem Cell Biol*, 41(10):1817–27, 2009.

Goate A. Segregation of a missense mutation in the amyloid beta-protein precursor gene with familial alzheimer's disease. *J Alzheimers Dis*, 9(3 Suppl):341–347, 1991.

Goedert M., Ghetti B., and Spillantini M. G. Frontotemporal dementia: implications for understanding alzheimer disease. *Cold Spring Harb Perspect Med.*, 2(2):a006254., 2012.

Goetz J. Tau and transgenic animal models. *Brain Res Brain Res Rev*, 35(3):266–86, 2001.

Goto Y., Yang C., and Otani S. Functional and dysfunctional synaptic plasticity in prefrontal cortex: Roles in psychiatric disorders. *Biol Psychiatry*, 67(3):199–207, Feb 2010.

Gouras G. K., Tsai J., Naslund J., Vincent B., Edgar M., Checler F., Greenfield J. P., Haroutunian V., Buxbaum J. D., Xu H., Greengard P., and Relkin N. R. Intraneuronal abeta42 accumulation in human brain. *Am J Pathol*, 156(1):15–20, 2000.

Gravitz L. Drugs: a tangled web of targets. *Nature*, 475(7355):S9–11, 2011.

Gyure K. A., Durham R., Stewart W. F., Smialek J. E., and Troncoso J. C. Intraneuronal abeta-amyloid precedes development of amyloid plaques in down syndrome. *Arch Pathol Lab Med*, 125(4):489–92, 2001.

Haass C. and Steiner H. Alzheimer disease gamma-secretase: a complex story of gxgd-type presenilin proteases. *Trends Cell Biol*, 12(12):556–62, 2002.

Haass C., Koo E., Mellon S., Hung A., and Selkoe D. Targeting of cell-surface beta-amyloid precursor protein to lysosomes: alternative processing into amyloid-bearing fragments. *Nature*, 357(6378):500–503, 1992.

Haass C., Lemere C. A., Capell A., Citron M., Seubert P., Schenk D., Lannfelt L., and Selkoe D. J. The swedish mutation causes early-onset alzheimer's disease by beta-secretase cleavage within the secretory pathway. *Nat. Med.*, 1(12):1291–6, 1995.

Halestrap A. Biochemistry: a pore way to die. *Nature*, 434(7033):578–9, 2005.

Halestrap A. P. What is the mitochondrial permeability transition pore? *J. Mol. Cell. Cardiol.*, 46(6):821–31, 2009.

Hall A., Karplus P. A., and Poole L. B. Typical 2-cys peroxiredoxins–structures, mechanisms and functions. *FEBS J*, 276(9):2469–77. Epub 2009 Mar 24., 2009.

Hanger D. and Wray S. Tau cleavage and tau aggregation in neurodegenerative disease. *Biochem Soc Trans*, 38(0300-5127 (Linking)):1016–20, 2010.

Hanger P., Betts J., Loviny T. F., Blackstock W., and Anderton B. New phosphorylation sites identified in hyperphosphorylated tau (paired helical filament-tau) from alzheimer's disease brain using nanoelectrospray mass spectrometry. *J Neurochem*, 71(6):2465–2476, 1998.

Hansson C. A., Frykman S., Farmery M. R., Tjernberg L. O., Nilsberth C., Pursglove S. E., Ito A., Winblad B., Cowburn R. F., Thyberg J., and Ankarcrona M. Nicastrin, presenilin, aph-1, and pen-2 form active gamma-secretase complexes in mitochondria. *J Biol Chem*, 279(49):51654–60, 2004.

Hansson Petersen C. A., Alikhani N., Behbahani H., Wiehager B., Pavlov P. F., Alafuzoff I., Leinonen V., Ito A., Winblad B., Glaser E., and Ankarcrona M. The amyloid beta-peptide is imported into mitochondria via the tom import machinery and localized to mitochondrial cristae. *Proc Natl Acad Sci U S A*, 105(35):13145–50, 2008.

Haraldsen J. D., Liu G., Botting C., Walton J., Storm J., Phalen T., Kwok L., Soldati-Favre D., Heintz N., Muller S., Westwood N., and Ward G. Identification of conoidin a as a covalent inhibitor of peroxiredoxin ii. *Org Biomol Chem*, 7(15):3040–3048, 2009.

Hardy J. and Selkoe D. J. The amyloid hypothesis of alzheimer's disease: progress and problems on the road to therapeutics. *Science*, 297(5580):353–6, 2002.

Harold D., Abraham R., Hollingworth P., Sims R., Gerrish A., Hamshere M. L., Pahwa J. S., Moskvina V., Dowzell K., Williams A., Jones N., Thomas C., Stretton A., Morgan A. R., Lovestone S., Powell J., Proitsi P., Lupton M. K., Brayne C., Rubinsztein D. C., Gill M., Lawlor B., Lynch A., Morgan K., Brown K. S., Passmore P. A., Craig D., McGuinness B., Todd S., Holmes C., Mann D., Smith A. D., Love S., Kehoe P. G., Hardy J., Mead S., Fox N., Rossor M., Collinge J., Maier W., Jessen F., Schurmann B., van den Bussche H., Heuser I., Kornhuber J., Wiltfang J., Dichgans M., Frolich L., Hampel H., Hull M., Rujescu D., Goate A. M., Kauwe J. S., Cruchaga C., Nowotny P., Morris J. C., Mayo K., Sleegers K., Bettens K., Engelborghs S., De Deyn P. P., Van Broeckhoven C., Livingston G., Bass N. J., Gurling H., McQuillin A., Gwilliam R., Deloukas P., Al-Chalabi A., Shaw C. E., Tsolaki M., Singleton A. B., Guerreiro R., Muhleisen T. W., Nothen M. M., Moebus S., Jockel K. H., Klopp N., Wichmann H. E., Carrasquillo M. M., Pankratz V. S., Younkin S. G., Holmans P. A., O'Donovan M., Owen M. J., and Williams J. Genome-wide association study identifies variants at clu and picalm associated with alzheimer's disease. *Nat. Genet.*, 41(10):1088–93, 2009.

Hashimoto Y., Niikura T., Chiba T., Tsukamoto E., Kadowaki H., Nishitoh H., Yamagishi Y., Ishizaka M., Yamada M., Nawa M., Terashita K., Aiso S., Ichijo H., and

Nishimoto I. The cytoplasmic domain of alzheimer's amyloid-beta protein precursor causes sustained apoptosis signal-regulating kinase 1/c-jun nh2-terminal kinase-mediated neurotoxic signal via dimerization. *J Pharmacol Exp Ther*, 306(3):889–902, 2003.

He X., Schulz H., and Yang S. A human brain l-3-hydroxyacyl-coenzyme a dehydrogenase is identical to an amyloid -peptide-binding protein involved in alzheimer's disease. *J. Biol. Chem.*, 273(17):10741–10746, 1998.

He X., Merz G., Mehta P., Schulz H., and Yang S. Human brain short chain l-3-hydroxyacyl coenzyme a dehydrogenase is a single-domain multifunctional enzyme. characterization of a novel 17--hydroxysteroid dehydrogenase. *J. Biol. Chem.*, 274 (21):15014–15019, 1999.

Hebert L., Scherr P., Beckett L., Albert M., Pilgrim D., Chown M., Funkenstein H., and Evans D. Age-specific incidence of alzheimer's disease in a community population. *JAMA.*, 273(17):1354–1359, 1995.

Heffernan J. M., Eastwood S. L., Nagy Z., Sanders M. W., McDonald B., Harrison P. J., Reddy P. H., Mani G., Park B. S., Jacques J., Murdoch G., Whetsell J., W., Kaye J., and Manczak M. Temporal cortex synaptophysin mrna is reduced in alzheimer's disease and is negatively correlated with the severity of dementia differential loss of synaptic proteins in alzheimer's disease: implications for synaptic dysfunction. *Exp Neurol.*, 150(2):235–9., 1998.

Herholz K., Weisenbach S., and Kalbe E. Deficits of the cholinergic system in early ad. *Neuropsychologia*, 46(6):1642 – 1647, 2008.

Herrmann N. and Gauthier S. Diagnosis and treatment of dementia: 6. management of severe alzheimer disease. *CMAJ*, 179(12):1279–1287, 2008.

Hers I., Vincent E., and Tavar J. Akt signalling in health and disease. *Cell Signal*, 23 (10):1515–1527, Oct 2011.

Hoelscher C. Diabetes as a risk factor for alzheimer's disease: insulin signalling impairment in the brain as an alternative model of alzheimer's disease. *Biochem Soc Trans.*, 39(4):891–7., 2011.

Hoelscher C., Gengler S., Gault V. A., Harriott P., and Mallot H. A. Soluble beta-amyloid[25-35] reversibly impairs hippocampal synaptic plasticity and spatial learning. *Eur J Pharmacol*, 561(1-3):85–90, 2007.

Hogan D., Bailey P., Black S., Carswell A., Chertkow H., Clarke B., Cohen C., Fisk J., Forbes D., Man-Son-Hing M., Lanctot K., Morgan D., and Thorpe L. Diagnosis and treatment of dementia: 5. nonpharmacologic and pharmacologic therapy for mild to moderate dementia. *CMAJ*, 179(10):1019–1026, 2008.

Hornbruch-Freitag C., Griemert B., Buttgereit D., and Renkawitz-Pohl R. Drosophila swiprosin-1/efhd2 accumulates at the prefusion complex stage during drosophila myoblast fusion. *J Cell Sci*, 124(Pt 19):3266–3278, 2011.

Howard L., Nelson K., Maciewicz R., and Blobel C. Interaction of the metalloprotease disintegrins mdc9 and mdc15 with two sh3 domain-containing proteins, endophilin i and sh3px1. *J Biol Chem*, 274(44):31693–31699, 1999.

Hu D., Cao P., Thiels E., Chu C. T., Wu G. Y., Oury T. D., and Klann E. Hip-

pocampal long-term potentiation, memory, and longevity in mice that overexpress mitochondrial superoxide dismutase. *Neurobiol Learn Mem*, 87(3):372–84, 2007.

Hu X., Weng Z., Chu C., Zhang L., Cao G., Gao Y., Signore A., Zhu J., Hastings T., Greenamyre J., and Chen J. Peroxiredoxin-2 protects against 6-hydroxydopamine-induced dopaminergic neurodegeneration via attenuation of the apoptosis signal-regulating kinase (ask1) signaling cascade. *J. Neurosci.*, 31(1):247–261, 2011.

Hwang D. Y., Cho J. S., Lee S. H., Chae K. R., Lim H. J., Min S. H., Seo S. J., Song Y. S., Song C. W., Paik S. G., Sheen Y. Y., and Kim Y. K. Aberrant expressions of pathogenic phenotype in alzheimer's diseased transgenic mice carrying nse-controlled appsw. *Exp Neurol*, 186(1):20–32, 2004.

Imbimbo B. P. and Giardina G. A. gamma-secretase inhibitors and modulators for the treatment of alzheimer's disease: disappointments and hopes. *Curr Top Med Chem*, 11(12):1555–70, 2011.

Iqbal K., Liu F., Gong C. X., and Grundke-Iqbal I. Tau in alzheimer disease and related tauopathies. *Curr Alzheimer Res.*, 7(8):656–64., 2010.

Ittner L. M. and Gotz J. Amyloid-beta and tau–a toxic pas de deux in alzheimer's disease. *Nat Rev Neurosci*, 12(2):65–72, 2011.

Ittner L., Ke Y., Delerue F., Bi M., Gladbach A., van Eersel J., Wlfing H., Chieng B., Christie M., Napier I., Eckert A., Staufenbiel M., Hardeman E., and Gtz J. Dendritic function of tau mediates amyloid- toxicity in alzheimer's disease mouse models. *Cell*, 142(3):387–397, Aug 2010.

Iwata N., Tsubuki S., Takaki Y., Shirotani K., Lu B., Gerard N. P., Gerard C., Hama E., Lee H. J., and Saido T. C. Metabolic regulation of brain abeta by neprilysin. *Science*, 292(5521):1550–2, 2001.

Kaether C. and Haass C. A lipid boundary separates app and secretases and limits amyloid beta-peptide generation. *J Cell Biol*, 167(5):809–12, 2004.

Kaltschmidt B., Uherek M., Volk B., Baeuerle P. A., and Kaltschmidt C. Transcription factor nf-kappab is activated in primary neurons by amyloid beta peptides and in neurons surrounding early plaques from patients with alzheimer disease. *Proc Natl Acad Sci U S A*, 94(6):2642–7, 1997.

Kang J. and Mueller-Hill B. Differential splicing of alzheimer's disease amyloid a4 precursor rna in rat tissues: Prea4695 mrna is predominantly produced in rat and human brain. *Biochem Biophys Res Commun*, 166(3):1192 – 1200, 1990.

Kang J., Lemaire H., Unterbeck A., Salbaum C., JMand Masters, Grzeschik K., Multhaup G., Beyreuther K., and Muller-Hill B. The precursor of alzheimer's disease amyloid a4 protein resembles a cell-surface receptor. *Nature*, 325(6106):733–736, Feb 1987.

Kang S. W., Chae H. Z., Seo M. S., Kim K., Baines I. C., and Rhee S. G. Mammalian peroxiredoxin isoforms can reduce hydrogen peroxide generated in response to growth factors and tumor necrosis factor-alpha. *J Biol Chem*, 273(11):6297–302, 1998.

Kar A., Kuo D., He R., Zhou J., and Wu J. Y. Tau alternative splicing and frontotemporal dementia. *Alzheimer Dis Assoc Disord.*, 19(Suppl 1):S29–36., 2005.

Kashani A., Lepicard A., Poirel O., Videau C., David J., Fallet-Bianco C., Simon A.,

Delacourte A., Giros B., Epelbaum J., Betancur C., and El Mestikawy S. Loss of vglut1 and vglut2 in the prefrontal cortex is correlated with cognitive decline in alzheimer disease. *Neurobiol. Aging.*, 29(11):1619–1630, Nov 2008.

Keita T., Tetsuhiro N., Akinori A., Takeshi K., and Hachiro S. Amyloid precursor protein promotes endoplasmic reticulum stress-induced cell death via c/ebp homologous protein-mediated pathway. *J Neurochem*, 109(5):1324–1337, 2009.

Khvotchev M. and Sudhof T. C. Proteolytic processing of amyloid-beta precursor protein by secretases does not require cell surface transport. *J Biol Chem*, 279(45): 47101–8, 2004.

Kim M., Hersh L. B., Leissring M. A., Ingelsson M., Matsui T., Farris W., Lu A., Hyman B. T., Selkoe D. J., Bertram L., and Tanzi R. E. Decreased catalytic activity of the insulin-degrading enzyme in chromosome 10-linked alzheimer disease families. *J Biol Chem*, 282(11):7825–32, 2007.

Kirvell S. L., Elliott M. S., Kalaria R. N., Hortobagyi T., Ballard C. G., and Francis P. T. Vesicular glutamate transporter and cognition in stroke: a case-control autopsy study. *Neurology.*, 75(20):1803–9., 2010.

Kjaerulff O., Brodin L., and Jung A. The structure and function of endophilin proteins. *Cell Biochem Biophys*, Epub ahead of print, 2010.

Klein C., Kramer E. M., Cardine A. M., Schraven B., Brandt R., and Trotter J. Process outgrowth of oligodendrocytes is promoted by interaction of fyn kinase with the cytoskeletal protein tau. *J Neurosci*, 22(3):698–707, 2002.

Klein W. Addls & protofibrils–the missing links? *Neurobiol Aging*, 23(2):231–5, 2002.

Klein W. Synaptic targeting by a beta oligomers (addls) as a basis for memory loss in early alzheimer's disease. *Alzheimers Dement*, 2(1):43–55, Jan 2006.

Koh S. H., Noh M. Y., and Kim S. H. Amyloid-beta-induced neurotoxicity is reduced by inhibition of glycogen synthase kinase-3. *Brain Res*, 1188:254–62, 2008.

Kopan R. and Ilagan M. X. [gamma]-secretase: proteasome of the membrane? *Nat Rev Mol Cell Biol*, 5(6):499–504, Jun 2004.

Kopeikina K., Carlson G., Pitstick R., Ludvigson A., Peters A., Luebke J., Koffie R., Frosch M., Hyman B., and Spires-Jones T. Tau accumulation causes mitochondrial distribution deficits in neurons in a mouse model of tauopathy and in human alzheimer's disease brain. *Am J Pathol*, 179(4):2071–2082, October 2011.

Kosik K. S., Joachim C. L., and Selkoe D. J. Microtubule-associated protein tau (tau) is a major antigenic component of paired helical filaments in alzheimer disease. *Proc Natl Acad Sci U S A*, 83(11):4044–8, 1986.

Krapfenbauer K., Engidawork E., Cairns N., Fountoulakis M., and Lubec G. Aberrant expression of peroxiredoxin subtypes in neurodegenerative disorders. *Brain Res*, 967 (1-2):152–160, 2003.

Kroczek C., Lang C., Brachs S., Grohmann M., Dtting S., Schweizer A., Nitschke L., Jck S. F. H., and Mielenz D. Swiprosin-1/efhd2 controls b cell receptor signaling through the assembly of the b cell receptor, syk, and phospholipase c gamma2 in membrane rafts. *J Immunol*, 184(7):3665–3676, Apr 2010.

Kuhn P., Wang H., Dislich B., Colombo A., Zeitschel U., Ellwart J., Kremmer A.,

Roszner S., and Lichtenthaler S. Adam10 is the physiologically relevant, constitutive [alpha]-secretase of the amyloid precursor protein in primary neurons. *EMBO J*, 29 (17):3020–3032, Sep 2010.

Kuwako K., Nishimura I., Uetsuki T., Saido T., and Yoshikawa K. Activation of calpain in cultured neurons overexpressing alzheimer amyloid precursor protein. *Mol Brain Res*, 107(2):166–175, 2002.

LaFerla F. M. Pathways linking abeta and tau pathologies. *Biochem Soc Trans.*, 38 (4):993–5., 2010.

LaFerla F. and Oddo S. Alzheimer's disease: A[beta], tau and synaptic dysfunction. *Trends Mol Med*, 11(4):170–176, 2005.

LaFerla F., Green K., and Oddo S. Intracellular amyloid-[beta] in alzheimer's disease. *Nat Rev Neurosci*, 8(7):499–509, 2007.

Lagalwar S., Guillozet-Bongaarts A. L., Berry R. W., and Binder L. I. Formation of phospho-sapk/jnk granules in the hippocampus is an early event in alzheimer disease. *J Neuropathol Exp Neurol*, 65(5):455–64, 2006.

Lambert J. and Amouyel P. Genetics of alzheimer's disease: new evidences for an old hypothesis? *Curr Opin Genet Dev*, 21(3):295 – 301, 2011.

Lambert J., Heath S., Even G., Campion D., Sleegers K., Hiltunen M., Combarros O., Zelenika D., Bullido M., Tavernier B., Letenneur L., Bettens K., Berr C., Pasquier F., Fivet N., Barberger-Gateau P., Engelborghs S., De Deyn P., Mateo I., Franck A., Helisalmi S., Porcellini E., Hanon O., E. A. D. I. I., de Pancorbo M., Lendon C., Dufouil C., Jaillard C., Leveillard T., Alvarez V., Bosco P., Mancuso M., Panza F., Nacmias B., Boss P., Piccardi P., Annoni G., Seripa D., Galimberti D., Hannequin D., Licastro F., Soininen H., Ritchie K., Blanch H., Dartigues J., Tzourio C., Gut I., Van Broeckhoven C., Alprovitch A., Lathrop M., and Amouyel P. Genome-wide association study identifies variants at clu and cr1 associated with alzheimer's disease. *Nat Genet*, 41(10):1094–1099, Oct 2009.

Lane R. M. and Farlow M. R. Lipid homeostasis and apolipoprotein e in the development and progression of alzheimer's disease. *J Lipid Res*, 46(5):949–68, 2005.

Lee G., Newman S., Gard D., Band H., and Panchamoorthy G. Tau interacts with src-family non-receptor tyrosine kinases. *J Cell Sci*, 111(21):3167–3177, 1998.

Lee H., Kumar P., Fu Q., Rosen K., and Querfurth H. The insulin/akt signaling pathway is targeted by intracellular beta-amyloid. *Mol. Biol. Cell*, 20(5):1533–1544, 2009.

Lee K. W., Lee D. J., Lee J. Y., Kang D. H., Kwon J., and Kang S. W. Peroxiredoxin ii restrains dna damage-induced death in cancer cells by positively regulating jnk-dependent dna repair. *J Biol Chem.*, 286(10):8394–404. Epub 2010 Dec 9., 2011.

Lee M. S., Kao S. C., Lemere C. A., Xia W., Tseng H. C., Zhou Y., Neve R., Ahlijanian M. K., and Tsai L. H. App processing is regulated by cytoplasmic phosphorylation. *J Cell Biol*, 163(1):83–95, 2003.

Leibson C. L., Rocca W. A., Hanson V. A., Cha R., Kokmen E., O'Brien P. C., and Palumbo P. J. Risk of dementia among persons with diabetes mellitus: a population-based cohort study. *Am J Epidemiol.*, 145(4):301–8., 1997.

Leissring M. A., Farris W., Wu X., Christodoulou D. C., Haigis M. C., Guarente L., and Selkoe D. J. Alternative translation initiation generates a novel isoform of insulin-degrading enzyme targeted to mitochondria. *Biochem J*, 383(Pt. 3):439–46, 2004.

Leroy K., Ando K., Heraud C., Yilmaz Z., Authelet M., Boeynaems J. M., Buee L., De Decker R., and Brion J. P. Lithium treatment arrests the development of neurofibrillary tangles in mutant tau transgenic mice with advanced neurofibrillary pathology. *J Alzheimers Dis*, 19(2):705–19, 2010.

Leung A. W. and Halestrap A. P. Recent progress in elucidating the molecular mechanism of the mitochondrial permeability transition pore. *Biochim Biophys Acta*, 1777 (7-8):946–52, 2008.

Li Y., Johnson N., Capano M., Edwards M., and Crompton M. Cyclophilin-d promotes the mitochondrial permeability transition but has opposite effects on apoptosis and necrosis. *Biochem J*, 383(1):101–109, 2004.

Liang B., nd Duan, Zhou X., Gong J., and Luo Z. Calpain activation promotes bace1 expression, amyloid precursor protein processing, and amyloid plaque formation in a transgenic mouse model of alzheimer disease. *J Biol Chem*, 285(36):27737–27744, 2010.

Lin M. T. and Beal M. F. Mitochondrial dysfunction and oxidative stress in neurodegenerative diseases. *Nature*, 443(7113):787–95, 2006.

Liu F., Iqbal K., Grundke-Iqbal I., Hart G. W., and Gong C. X. O-glcnacylation regulates phosphorylation of tau: a mechanism involved in alzheimer's disease. *Proc Natl Acad Sci U S A*, 101(29):10804–9, 2004.

Liu J., Head E., Gharib A. M., Yuan W., Ingersoll R. T., Hagen T. M., Cotman C. W., and Ames B. N. Memory loss in old rats is associated with brain mitochondrial decay and rna/dna oxidation: partial reversal by feeding acetyl-l-carnitine and/or r-alpha -lipoic acid. *Proc Natl Acad Sci U S A*, 99(4):2356–61, 2002.

Llovera R. E., de Tullio M., Alonso L. G., Leissring M. A., Kaufman S. B., Roher A. E., de Prat Gay G., Morelli L., and Castano E. M. The catalytic domain of insulin-degrading enzyme forms a denaturant-resistant complex with amyloid beta peptide: implications for alzheimer disease pathogenesis. *J Biol Chem*, 283(25): 17039–48, 2008.

Lott I. and Head E. Alzheimer disease and down syndrome: factors in pathogenesis. *Neurobiol. Aging.*, 26(3):383 – 389, 2005.

Lu B. and Martinowich K. Cell biology of bdnf and its relevance to schizophrenia. *Novartis Found Symp.*, 289:119–29; discussion 129–35, 193–5., 2008.

Luengo-Fernandez J. G. A., R.; Leal. Dementia 2010. Technical report, Oxford University and the Alzheimer's Research Trust, 2010.

Lustbader J. W., Cirilli M., Lin C., Xu H. W., Takuma K., Wang N., Caspersen C., Chen X., Pollak S., Chaney M., Trinchese F., Liu S., Gunn-Moore F., Lue L. F., Walker D. G., Kuppusamy P., Zewier Z. L., Arancio O., Stern D., Yan S. S., and Wu H. Abad directly links abeta to mitochondrial toxicity in alzheimer's disease. *Science*, 304(5669):448–52, 2004.

MacGibbon G. A., Lawlor P. A., Walton M., Sirimanne E., Faull R. L., Synek B., Mee

E., Connor B., and Dragunow M. Expression of fos, jun, and krox family proteins in alzheimer's disease. *Exp Neurol*, 147(2):316–32, 1997.

Mandelkow E.-M., Biernat J., Drewes G., Gustke N., Trinczek B., and Mandelkow E. Tau domains, phosphorylation, and interactions with microtubules. *Neurobiol. Aging.*, 16(3):355–362, 1995.

Marques C. A., Keil U., Bonert A., Steiner B., Haass C., Muller W. E., and Eckert A. Neurotoxic mechanisms caused by the alzheimer's disease-linked swedish amyloid precursor protein mutation: oxidative stress, caspases, and the jnk pathway. *J Biol Chem*, 278(30):28294–302, 2003.

Martin B. L., Schrader-Fischer G., Busciglio J., Duke M., Paganetti P., and Yankner B. A. Intracellular accumulation of beta-amyloid in cells expressing the swedish mutant amyloid precursor protein. *J Biol Chem*, 270(45):26727–30, 1995.

Martin D., Salinas M., Lopez-Valdaliso R., Serrano E., Recuero M., and Cuadrado A. Effect of the alzheimer amyloid fragment abeta(25-35) on akt/pkb kinase and survival of pc12 cells. *J. Neurochem.*, 78(5):1000–8, 2001.

Martin L. J., Gertz B., Pan Y., Price A. C., Molkentin J. D., and Chang Q. The mitochondrial permeability transition pore in motor neurons: Involvement in the pathobiology of als mice. *Exp Neurol*, 218 (2):333–46, 2009.

Mathews P. M., Jiang Y., Schmidt S. D., Grbovic O. M., Mercken M., and Nixon R. A. Calpain activity regulates the cell surface distribution of amyloid precursor protein. inhibition of calpains enhances endosomal generation of beta-cleaved c-terminal app fragments. *J Biol Chem*, 277(39):36415–24, 2002.

Matsuda S., Yasukawa T., Homma Y., Ito Y., Niikura T., Hiraki T., Hirai S., Ohno S., Kita Y., Kawasumi M., Kouyama K., Yamamoto T., Kyriakis J., and Nishimoto I. c-jun n-terminal kinase (jnk)-interacting protein-1b/islet-brain-1 scaffolds alzheimer's amyloid precursor protein with jnk. *J Neurosci*, 21(17):6597–6607, 2001.

Matsui T., Ingelsson M., Fukumoto H., Ramasamy K., Kowa H., Frosch M., Irizarry M., and Hyman B. Expression of app pathway mrnas and proteins in alzheimers disease. *Brain Res*, 1161(0):116 – 123, 2007.

Mattson M. P., Cheng B., Davis D., Bryant K., Lieberburg I., and Rydel R. E. beta-amyloid peptides destabilize calcium homeostasis and render human cortical neurons vulnerable to excitotoxicity. *J Neurosci*, 12(2):376–89, 1992.

Mayeux R. Epidemiology of neurodegeneration. *Annu. Rev. Neurosci.*, 26(1):81–104, 2003.

McKhann G. M., Knopman D., HChertkow , Hyman B., Jack C., Kawas C., Klunk W., Koroshetz W., Manly J., Mayeux R., Mohs R., Morris J., Rossor M., Scheltens P., Carrillo M., Thies B., Weintraub S., and Phelps C. The diagnosis of dementia due to alzheimer's disease: recommendations from the national institute on aging-alzheimer's association workgroups on diagnostic guidelines for alzheimer's disease. *Alzheimers Dement*, 7(3):263–269, May 2011.

McLean C. A., Cherny R. A., Fraser F. W., Fuller S. J., Smith M. J., Beyreuther K., Bush A. I., and Masters C. L. Soluble pool of abeta amyloid as a determinant of severity of neurodegeneration in alzheimer's disease. *Ann Neurol*, 46(6):860–6, 1999.

Mehan S., Meena H., Sharma D., and Sankhla R. Jnk: a stress-activated protein kinase therapeutic strategies and involvement in alzheimer's and various neurodegenerative abnormalities. *J Mol Neurosci*, 43(3):376–90, 2011.

Melov S., Adlard P. A., Morten K., Johnson F., Golden T. R., Hinerfeld D., Schilling B., Mavros C., Masters C. L., Volitakis I., Li Q. X., Laughton K., Hubbard A., Cherny R. A., Gibson B., and Bush A. I. Mitochondrial oxidative stress causes hyperphosphorylation of tau. *PLoS One*, 2(6):e536, 2007.

Meng X. and Wilkins J. Compositional characterization of the cytoskeleton of nk-like cells. *J Proteome Res*, 4(6):2081–2087, 2005.

Micheva K., Kay B., and McPherson P. Synaptojanin forms two separate complexes in the nerve terminal. *J Biol Chem*, 272(43):27239–27245, 1997.

Mielenz D., Vettermann C., Hampel M., Lang C., Avramidou A., Karas M., and Jaeck H. Lipid rafts associate with intracellular b cell receptors and exhibit a b cell stage-specific protein composition. *J Immunol*, 174(6):3508–3517, 2005.

Milton N. G. Amyloid-beta binds catalase with high affinity and inhibits hydrogen peroxide breakdown. *Biochem J*, 344(2):293–296, 1999.

Milton N. G. and Harris J. R. Polymorphism of amyloid-beta fibrils and its effects on human erythrocyte catalase binding. *Micron*, 40(8):800–10, 2009.

Milton N. Inhibition of catalase activity with 3-amino-triazole enhances the cytotoxicity of the alzheimer's amyloid-[beta] peptide. *Neurotoxicology*, 22(6):767–774, 2001.

Miners J. S., Barua N., Kehoe P. G., Gill S., and Love S. Abeta-degrading enzymes: potential for treatment of alzheimer disease. *J Neuropathol Exp Neurol*, 70(11):944–59, 2011.

Minogue A., Schmid A., Fogarty M., Moore A., Campbell V., Herron C., and Lynch M. Activation of the c-jun n-terminal kinase signaling cascade mediates the effect of amyloid- on long term potentiation and cell death in hippocampus. *J Biol Chem*, 278(30):27971–27980, 2003.

Morishima Y., Gotoh Y., Zieg J., Barrett T., Takano H., Flavell R., Davis R., Shirasaki Y., and Greenberg M. beta-amyloid induces neuronal apoptosis via a mechanism that involves the c-jun n-terminal kinase pathway and the induction of fas ligand. *J. Neurosci.*, 21(19):7551–7560, 2001.

Morishima-Kawashima M., Hasegawa M., Takio K., Suzuki M., Yoshida H., Watanabe A., Titani K., and Ihara . Hyperphosphorylation of tau in phf. *Neurobiol. Aging.*, 16(3):365–371, 1995.

Morris M., Maeda K., Sand Vossel, and Mucke L. The many faces of tau. *Neuron*, 70 (3):410–426, May 2011.

Mueller T., Meyer H. E., Egensperger R., and Marcus K. The amyloid precursor protein intracellular domain (aicd) as modulator of gene expression, apoptosis, and cytoskeletal dynamics-relevance for alzheimer's disease. *Prog Neurobiol*, 85(4):393–406, 2008.

Mueller W. E., Kirsch C., and Eckert G. P. Membrane-disordering effects of beta-amyloid peptides. *Biochem Soc Trans*, 29(Pt 4):617–23, 2001.

Muirhead K., Borger E., Aitken L., Conway S., and Gunn-Moore F. The consequences

of mitochondrial amyloid -peptide in alzheimer's disease. *Biochem J*, 426(3):255–270, 2010.

Murakami Y., Ohsawa I., Kasahara T., and Ohta S. Cytoprotective role of mitochondrial amyloid [beta] peptide-binding alcohol dehydrogenase against a cytotoxic aldehyde. *Neurobiol. Aging*, 30(2):325–329, 2009.

Muynck L. and Damme P. Cellular effects of progranulin in health and disease. *J Mol Neurosci*, 45(3):549–560, Nov 2011.

Nagele R. G., D'Andrea M. R., Anderson W. J., and Wang H. Y. Intracellular accumulation of [beta]-amyloid1-42 in neurons is facilitated by the [alpha]7 nicotinic acetylcholine receptor in alzheimer's disease. *Neuroscience*, 110(2):199–211, 2002.

NCCMH N. C. C. f. M. H. *Dementia: Supporting people with dementia and their carers in health and social care.*, volume Number 42 of *National Clinical Practice Guideline*. The British Psychological Society and Gaskell, 2006-2011.

Nikolaev A., McLaughlin T., O'Leary D. D., and Tessier-Lavigne M. App binds dr6 to trigger axon pruning and neuron death via distinct caspases. *Nature*, 457(7232): 981–9, 2009.

Nonis D., Schmidt M. H., van de Loo S., Eich F., Dikic I., Nowock J., and Auburger G. Ataxin-2 associates with the endocytosis complex and affects egf receptor trafficking. *Cell Signal*, 20(10):1725–39, 2008.

Nordberg A. Pet imaging of amyloid in alzheimer's disease. *Lancet Neurol*, 3(9):519–527, Sep 2004.

Oddo S., Caccamo A., Smith I. F., Green K. N., and LaFerla F. M. A dynamic relationship between intracellular and extracellular pools of abeta. *Am J Pathol*, 168 (1):184–94, 2006.

Oldreive C. E., Gaynor S., and Doherty G. H. Developmental changes in the response of murine cerebellar granule cells to nitric oxide. *Neurochem Int*, 52(8):1394–401, 2008.

Olgiati A. P. G. D. R. D. S. A., P.; Politis. Genetics of late-onset alzheimer's disease: Update from the alzgene database and analysis of shared pathways. *Int J Alzheimers Dis*, 2011, 2011.

Omalu B., Bailes J., Hamilton R. L., Kamboh M. I., Hammers J., Case M., and Fitzsimmons R. Emerging histomorphologic phenotypes of chronic traumatic encephalopathy in american athletes. *Neurosurgery*, 69(1):173–83; discussion 183, 2011.

Oppermann U. C., Salim S., Tjernberg L. O., Terenius L., and Jornvall H. Binding of amyloid beta-peptide to mitochondrial hydroxyacyl-coa dehydrogenase (erab): regulation of an sdr enzyme activity with implications for apoptosis in alzheimer's disease. *FEBS Lett*, 451(3):238–42, 1999.

Palmer A. Neuroprotective therapeutics for alzheimer's disease: progress and prospects. *Trens Pharmacol Sci*, 32(3):141 – 147, 2011.

Park H. J., Kim S. S., Kang S., and Rhim H. Intracellular abeta and c99 aggregates induce mitochondria-dependent cell death in human neuroglioma h4 cells through recruitment of the 20s proteasome subunits. *Brain Res*, 1273:1–8, 2009.

Parker J., W. D., Mahr N. J., Filley C. M., Parks J. K., Hughes D., Young D. A., and

Cullum C. M. Reduced platelet cytochrome c oxidase activity in alzheimer's disease. *Neurology*, 44(6):1086–90, 1994a.

Parker J., W. D., Parks J., Filley C. M., and Kleinschmidt-DeMasters B. K. Electron transport chain defects in alzheimer's disease brain. *Neurology*, 44(6):1090–6, 1994b.

Pearson A. G., Byrne U. T., MacGibbon G. A., Faull R. L., and Dragunow M. Activated c-jun is present in neurofibrillary tangles in alzheimer's disease brains. *Neurosci Lett*, 398(3):246–50, 2006.

Pei J., Grundke-Iqbal I., Iqbal K., Bogdanovic N., Winblad B., and rF. Cowburn . Accumulation of cyclin-dependent kinase 5 (cdk5) in neurons with early stages of alzheimer's disease neurofibrillary degeneration. *Brain Res*, 797(2):267 – 277, 1998.

Pellistri f., Bucciantini m., Relini a., Nosi d., Gliozzi A., Robello M., and Stefani M. Nonspecific interaction of prefibrillar amyloid aggregates with glutamatergic receptors results in ca2+ increase in primary neuronal cells. *J. Biol. Chem.*, 283(44): 29950–29960, 2008.

Perry E., Court J., Johnson M., Piggott M., and Perry R. Autoradiographic distribution of [3h]nicotine binding in human cortex: Relative abundance in subicular complex. *J Chem Neuroanat*, 5(5):399 – 405, 1992.

Puzzo D., Privitera L., Leznik E., Fa M., Staniszewski A., Palmeri A., and Arancio O. Picomolar amyloid-beta positively modulates synaptic plasticity and memory in hippocampus. *J. Neurosci.*, 28(53):14537–14545, 2008.

Qiu W. Q., Walsh D. M., Ye Z., Vekrellis K., Zhang J., Podlisny M. B., Rosner M. R., Safavi A., Hersh L. B., and Selkoe D. J. Insulin-degrading enzyme regulates extracellular levels of amyloid beta-protein by degradation. *J Biol Chem*, 273(49):32730–8, 1998.

Qu D., Rashidian J., Mount M., Aleyasin H., Parsanejad M., Lira A., Haque E., Zhang Y., Callaghan S., Daigle M., Rousseaux M., Slack R., Albert P., Vincent I., Woulfe J., and Park D. Role of cdk5-mediated phosphorylation of prx2 in mptp toxicity and parkinson's disease. *Neuron*, 55(1):37–52, 2007.

Ralser M., Nonhoff U., Albrecht M., Lengauer T., Wanker E., Lehrach H., and Krobitsch S. Ataxin-2 and huntingtin interact with endophilin-a complexes to function in plastin-associated pathways. *Hum Mol Genet*, 14(19):2893–2909, October 2005.

Ramesh T. P., Kim Y.-D., Kwon M.-S., Jun C.-D., and Kim S.-W. Swiprosin-1 regulates cytokine expression of human mast cell line hmc-1 through actin remodeling. *Immune Netw*, 9(6):274–284, Dec 2009.

Ramjaun A., Angers A., Legendre-Guillemin V., Tong X., and McPherson P. Endophilin regulates jnk activation through its interaction with the germinal center kinase-like kinase. *J. Biol. Chem.*, 276(31):28913–28919, 2001.

Rankin C. A., Sun Q., and Gamblin T. Pre-assembled tau filaments phosphorylated by gsk-3b form large tangle-like structures. *Neurobiol Dis*, 31(3):368–377, Sep 2008.

Reaume A., Howland D., Trusko S., Savage M. M., Lang M., Greenberg B., Siman R., and Scott R. Enhanced amyloidogenic processing of the -amyloid precursor protein in gene-targeted mice bearing the swedish familial alzheimer's disease mutations and a humanized a sequence. *J Biol Chem*, 271(38):23380–23388, 1996.

Reddy P. H., Mani G., Park B. S., Jacques J., Murdoch G., Whetsell J., W., Kaye J., and Manczak M. Differential loss of synaptic proteins in alzheimer's disease: implications for synaptic dysfunction. *J Alzheimers Dis.*, 7(2):103–17; discussion 173–80., 2005.

Ren Y., Xu H. W., Davey F., Taylor M., Aiton J., Coote P., Fang F., Yao J., Chen D., Chen J. X., Yan S. D., and Gunn-Moore F. J. Endophilin i expression is increased in the brains of alzheimer disease patients. *J Biol Chem*, 283(9):5685–91, 2008.

Reutens A. and Begley G. Endophilin-1: a multifunctional protein. *Int J Biochem Cell Biol*, 34(10):1173–1177, 2002.

Reynolds C. H., Betts J. C., Blackstock W. P., Nebreda A. R., and Anderton B. H. Phosphorylation sites on tau identified by nanoelectrospray mass spectrometry: differences in vitro between the mitogen-activated protein kinases erk2, c-jun n-terminal kinase and p38, and glycogen synthase kinase-3beta. *J Neurochem*, 74(4):1587–95, 2000.

Rhee S. G., Chae H. Z., and Kim K. Peroxiredoxins: a historical overview and speculative preview of novel mechanisms and emerging concepts in cell signaling. *Free Radic Biol Med*, 38(12):1543–52, 2005.

Richter C., Park J. W., and Ames B. N. Normal oxidative damage to mitochondrial and nuclear dna is extensive. *Proc Natl Acad Sci U S A*, 85(17):6465–6467, 1988.

Ringstad N., Nemoto Y., and De Camilli P. The sh3p4/sh3p8/sh3p13 protein family: binding partners for synaptojanin and dynamin via a grb2-like src homology 3 domain. *Proc Natl Acad Sci U S A*, 94(16):8569–8574, Aug 1997.

Ringstad N., Gad H., Loew P., Di Paolo G., Brodin L., Shupliakov O., and De Camilli P. Endophilin/sh3p4 is required for the transition from early to late stages in clathrin-mediated synaptic vesicle endocytosis. *Neuron*, 24(1):143–154, 1999.

Ringstad N., Nemoto Y., and De Camilli P. Differential expression of endophilin 1 and 2 dimers at central nervous system synapses. *J Biol Chem*, 276(44):40424–40430, 2001.

Rogaev E. I., Sherrington R., Rogaeva E. A., Levesque G., Ikeda M., Liang Y., Chi H., Lin C., Holman K., Tsuda T., Mar L., Sorbi S., Nacmias B., Piacentini S., Amaducci L., Chumakov I., Cohen D., Lannfelt L., Fraser P. E., Rommens J. M., and George-Hyslop P. H. S. Familial alzheimer's disease in kindreds with missense mutations in a gene on chromosome 1 related to the alzheimer's disease type 3 gene. *Nature*, 376 (6543):775–778, 1995.

Rogaeva E., Meng Y., Lee J. H., Gu Y., Kawarai T., Zou F., Katayama T., Baldwin C. T., Cheng R., Hasegawa H., Chen F., Shibata N., Lunetta K. L., Pardossi-Piquard R., Bohm C., Wakutani Y., Cupples L. A., Cuenco K. T., Green R. C., Pinessi L., Rainero I., Sorbi S., Bruni A., Duara R., Friedland R. P., Inzelberg R., Hampe W., Bujo H., Song Y. Q., Andersen O. M., Willnow T. E., Graff-Radford N., Petersen R. C., Dickson D., Der S. D., Fraser P. E., Schmitt-Ulms G., Younkin S., Mayeux R., Farrer L. A., and St George-Hyslop P. The neuronal sortilin-related receptor sorl1 is genetically associated with alzheimer disease. *Nat Genet*, 39(2):168–77, 2007.

Rusinol A. E., Cui Z., Chen M. H., and Vance J. E. A unique mitochondria-associated

membrane fraction from rat liver has a high capacity for lipid synthesis and contains pre-golgi secretory proteins including nascent lipoproteins. *J Biol Chem*, 269(44): 27494–27502, 1994.

Ryder J., Su Y., and Ni B. Akt/gsk3beta serine/threonine kinases: evidence for a signalling pathway mediated by familial alzheimer's disease mutations. *Cell Signal*, 16(2):187–200, 2004.

Saito K., Elce J. S., Hamos J. E., and Nixon R. A. Widespread activation of calcium-activated neutral proteinase (calpain) in the brain in alzheimer disease: a potential molecular basis for neuronal degeneration. *Proc Natl Acad Sci U S A*, 90(7):2628–2632, 1993.

Saunders A. M., Strittmatter W. J., Schmechel D., George-Hyslop P. H., Pericak-Vance M. A., Joo S. H., Rosi B. L., Gusella J. F., Crapper-MacLachlan D. R., Alberts M. J., and et al. . Association of apolipoprotein e allele epsilon 4 with late-onset familial and sporadic alzheimer's disease. *Neurology*, 43(8):1467–72, 1993.

Scheinfeld M. H., Roncarati R., Vito P., Lopez P. A., Abdallah M., and D'Adamio L. Jun nh2-terminal kinase (jnk) interacting protein 1 (jip1) binds the cytoplasmic domain of the alzheimer's beta-amyloid precursor protein (app). *J Biol Chem*, 277 (5):3767–75, 2002.

Schiene-Fischer C. and Yu C. Receptor accessory folding helper enzymes: the functional role of peptidyl prolyl cis/trans isomerases. *FEBS Lett*, 495(1-2):1–6, 2001.

Schindowski K., Belarbi K., and Buee L. Neurotrophic factors in alzheimer's disease: role of axonal transport. *Genes Brain Behav*, 7 Suppl 1:43–56, 2008.

Schinzel A. C., Takeuchi O., Huang Z., Fisher J. K., Zhou Z., Rubens J., Hetz C., Danial N. N., Moskowitz M. A., and Korsmeyer S. J. Cyclophilin d is a component of mitochondrial permeability transition and mediates neuronal cell death after focal cerebral ischemia. *Proc Natl Acad Sci U S A*, 102(34):12005–10, 2005.

Selkoe D. and Wolfe M. Presenilin: Running with scissors in the membrane. *Cell*, 131 (2):215–221, Oct 2007.

Selkoe D., Yamazaki T., Citron M., Podlisny M. B., Koo E. H., Teplow D. B., and Haass C. The role of app processing and trafficking pathways in the formation of amyloid -protein. *Ann. N. Y. Acad. Sci.*, 777(Bioartificial Organs: Science, Medicine, and Technology):57–64, 1996.

Sharma V. M., Litersky J. M., Bhaskar K., and Lee G. Tau impacts on growth-factor-stimulated actin remodeling. *J Cell Sci*, 120(Pt 5):748–57, 2007.

Shaulian E. Ap-1–the jun proteins: Oncogenes or tumor suppressors in disguise? *Cell Signal*, 22(6):894–9, 2010.

Shepardson N., Shankar G., and Selkoe D. Cholesterol level and statin use in alzheimer disease: Ii. review of human trials and recommendations. *Arch Neurol*, 68(11):1385–1392, 2011.

Sherrington R., Rogaev E. I., Liang Y., Rogaeva E. A., Levesque G., Ikeda M., Chi H., Lin C., Li G., Holman K., Tsuda T., Mar L., Foncin J. F., Bruni A. C., Montesi M. P., Sorbi S., Rainero I., Pinessi L., Nee L., Chumakov I., Pollen D., Brookes A., Sanseau P., Polinsky R. J., Wasco W., Da Silva H. A., Haines J. L., Perkicak-Vance

M. A., Tanzi R. E., Roses A. D., Fraser P. E., Rommens J. M., and St George-Hyslop P. H. Cloning of a gene bearing missense mutations in early-onset familial alzheimer's disease. *Nature*, 375(6534):754–760, Jun 1995.

Shi Y., Kirwan P., Smith J., MacLean G., Orkin S., and Livesey F. A human stem cell model of early alzheimers disease pathology in down syndrome. *Sci Transl Med*, 4 (124):124ra29, 2012a.

Shi Y., Kirwan P., Smith J., Robinson H., and Livesey F. Human cerebral cortex development from pluripotent stem cells to functional excitatory synapses. *Nat Neurosci*, 15(3):477–486, 2012b.

Shipton O., Leitz J., Dworzak J., Acton C. E. J., Tunbridge E. M., Denk F., Dawson H., Vitek M., Wade-Martins R., Paulsen O., and Vargas-Caballero M. Tau protein is required for amyloid -induced impairment of hippocampal long-term potentiation. *J Neurosci*, 31(5):1688–1692, 2011.

Shirotani K., Tsubuki S., Iwata N., Takaki Y., Harigaya W., Maruyama K., Kiryu-Seo S., Kiyama H., Iwata H., Tomita T., Iwatsubo T., and Saido T. C. Neprilysin degrades both amyloid beta peptides 1-40 and 1-42 most rapidly and efficiently among thiorphan- and phosphoramidon-sensitive endopeptidases. *J Biol Chem*, 276(24): 21895–901, 2001.

Shoji M., Iwakami N., Takeuchi S., Waragai M., Suzuki M., Kanazawa I., Lippa C. F., Ono S., and Okazawa H. Jnk activation is associated with intracellular beta-amyloid accumulation. *Brain Res Mol Brain Res*, 85(1-2):221–33, 2000.

Singh P., Suman S., Chandna S., and Das T. K. Possible role of amyloid-beta, adenine nucleotide translocase and cyclophilin-d interaction in mitochondrial dysfunction of alzheimer's disease. *Bioinformation*, 3(10):440–5, 2009.

Smith P. D., Crocker S. J., Jackson-Lewis V., Jordan-Sciutto K. L., Hayley S., Mount M. P., O'Hare M. J., Callaghan S., Slack R. S., Przedborski S., Anisman H., and Park D. S. Cyclin-dependent kinase 5 is a mediator of dopaminergic neuron loss in a mouse model of parkinson's disease. *Proc Natl Acad Sci U S A*, 100(23):13650–5, 2003.

Smith W. W., Norton D. D., Gorospe M., Jiang H., Nemoto S., Holbrook N. J., Finkel T., and Kusiak J. W. Phosphorylation of p66shc and forkhead proteins mediates abeta toxicity. *J Cell Biol*, 169(2):331–9, 2005.

Soubeyran P., Kowanetz K., Szymkiewicz I., Langdon W., and Dikic I. Cbl-cin85-endophilin complex mediates ligand-induced downregulation of egf receptors. *Nature*, 416(6877):183–187, Mar 2002.

Sparks A. B., Hoffman N. G., McConnell S. J., Fowlkes D. M., and Kay B. K. Cloning of ligand targets: systematic isolation of sh3 domain-containing proteins. *Nat Biotechnol*, 14(6):741–744, Jun 1996.

Stagi M., Gorlovoy P., Larionov S., Takahashi K., and Neumann H. Unloading kinesin transported cargoes from the tubulin track via the inflammatory c-jun n-terminal kinase pathway. *FASEB J*, 20(14):2573–2575, 2006.

Stine J., W. B., Dahlgren K. N., Krafft G. A., and LaDu M. J. In vitro characterization of conditions for amyloid-beta peptide oligomerization and fibrillogenesis. *J Biol*

Chem, 278(13):11612–22, 2003.

Stone S., Levin M., Zhou P., Han J., Walther T., and Farese R. The endoplasmic reticulum enzyme dgat2 is found in mitochondria-associated membranes and has a mitochondrial targeting signal that promotes its association with mitochondria. *J Biol Chem*, 284(8):5352–5361, 2009.

Suzuki N., Cheung T., Cai X., Odaka A., Otvos J., L, Eckman C., Golde T., and Younkin S. An increased percentage of long amyloid beta protein secreted by familial amyloid beta protein precursor (beta app717) mutants. *Science*, 264(5163):1336–1340, 1994.

Swatton J., Sellers L., Faull R., Holland A., Iritani S., and Bahn S. Increased map kinase activity in alzheimer's and down syndrome but not in schizophrenia human brain. *Eur J Neurosci*, 19(10):2711–2719, 2004.

Tackenberg C. and Brandt R. Divergent pathways mediate spine alterations and cell death induced by amyloid-beta, wild-type tau, and r406w tau. *J Neurosci*, 29(46): 14439–50, 2009.

Takahashi R. H., Milner T. A., Li F., Nam E. E., Edgar M. A., Yamaguchi H., Beal M. F., Xu H., Greengard P., and Gouras G. K. Intraneuronal alzheimer abeta42 accumulates in multivesicular bodies and is associated with synaptic pathology. *Am J Pathol*, 161(5):1869–79, 2002.

Takuma K., Yao J., Huang J., Xu H., Chen X., Luddy J., Trillat A. C., Stern D. M., Arancio O., and Yan S. S. Abad enhances abeta-induced cell stress via mitochondrial dysfunction. *FASEB J.*, 19(6):597–8, 2005.

Tamagno E., Parola M., Bardini P., Piccini A., Borghi R., Guglielmotto M., Santoro G., Davit A., Danni O., Smith M. A., Perry G., and Tabaton M. Beta-site app cleaving enzyme up-regulation induced by 4-hydroxynonenal is mediated by stress-activated protein kinases pathways. *J Neurochem*, 92(3):628–36, 2005.

Tamagno E., Guglielmotto M., Aragno M., Borghi R., Autelli R., Giliberto L., Muraca G., Danni O., Zhu X., Smith M. A., Perry G., Jo D. G., Mattson M. P., and Tabaton M. Oxidative stress activates a positive feedback between the gamma- and beta-secretase cleavages of the beta-amyloid precursor protein. *J Neurochem*, 104(3): 683–95, 2008.

Tang Y., Hu L., Miller W., Ringstad N., Hall R., Pitcher J., DeCamilli P., and Lefkowitz R. Identification of the endophilins (sh3p4/p8/p13) as novel binding partners for the [alpha]-adrenergic receptor. *Proc Natl Acad Sci U S A*, 96(22):12559–12564, 1999.

Tanzi R., Haines J., Watkins P., Stewart G., Wallace M., Hallewell R., Wong C., Wexler N., Conneally P., and Gusella J. Genetic linkage map of human chromosome 21. *Genomics*, 3(2):129 – 136, 1988a.

Tanzi R., McClatchey A., Lamperti E., Villa-Komaroff L., Gusella J., and Neve R. Protease inhibitor domain encoded by an amyloid protein precursor mrna associated with alzheimer's disease. *Nature*, 331(6156):528–530, Feb 1988b.

Taru H., Iijima K., Hase M., Kirino Y., Yagi Y., and Suzuki T. Interaction of alzheimer's beta -amyloid precursor family proteins with scaffold proteins of the jnk signaling cascade. *J Biol Chem.*, 277(22):20070–8. Epub 2002 Mar 22., 2002.

Thakur A., Wang X., Siedlak S., Perry G., Smith M., and Zhu X. c-jun phosphorylation in alzheimer disease. *J. Neurosci. Res.*, 85(8):1668–1673, 2007.

Thinakaran G. and Koo E. Amyloid precursor protein trafficking, processing, and function. *J Biol Chem*, 283(44):29615–29619, 2008.

Thylur R., Kim Y., Kwon M., Oh H., Kwon H., Kim S., Im S., Chun J., Park Z., and Jun C. Swiprosin-1 is expressed in mast cells and up-regulated through the protein kinase c beta i/eta pathway. *J Cell Biochem*, 108(3):705–715, Oct 2009.

Tolboom N., Koedam E. L., Schott J. M., Yaqub M., Blankenstein M. A., Barkhof F., Pijnenburg Y. A., Lammertsma A. A., Scheltens P., and van Berckel B. N. Dementia mimicking alzheimer's disease owing to a tau mutation: Csf and pet findings. *Alzheimer Dis Assoc Disord.*, 24(3):303–7., 2010.

Trempe J. F., Chen C. X., Grenier K., Camacho E. M., Kozlov G., McPherson P. S., Gehring K., and Fon E. A. Sh3 domains from a subset of bar proteins define a ubl-binding domain and implicate parkin in synaptic ubiquitination. *Mol Cell*, 36 (6):1034–47, 2009.

Troy C. M., Rabacchi S. A., Xu Z., Maroney A. C., Connors T. J., Shelanski M. L., and Greene L. A. beta-amyloid-induced neuronal apoptosis requires c-jun n-terminal kinase activation. *J Neurochem*, 77(1):157–64, 2001.

Uehara T., Nakamura T., Yao D., Shi Z. Q., Gu Z., Ma Y., Masliah E., Nomura Y., and Lipton S. A. S-nitrosylated protein-disulphide isomerase links protein misfolding to neurodegeneration. *Nature*, 441(7092):513–7, 2006.

Umeda T., Tomiyama T., Sakama N., Tanaka S., Lambert M., Klein W., and Mori H. Intraneuronal amyloid oligomers cause cell death via endoplasmic reticulum stress, endosomal/lysosomal leakage, and mitochondrial dysfunction in vivo. *J Neurosci Res*, 89(7):1031–1042, 2011.

Vaishnav M., MacFarlane M., and Dickens M. Disassembly of the jip1/jnk molecular scaffold by caspase-3-mediated cleavage of jip1 during apoptosis. *Exp Cell Res*, 317 (7):1028 – 1039, 2011.

Van Broeck B., Van Broeckhoven C., and Kumar-Singh S. Current insights into molecular mechanisms of alzheimer disease and their implications for therapeutic approaches. *Neurodegener Dis*, 4(5):349–65, 2007.

van Eersel J., Bi M., Ke Y., Hodges J., Xuereb J., Gregory G., Halliday G., Gotz J., Kril J., and Ittner L. Phosphorylation of soluble tau differs in picks disease and alzheimers disease brains. *J Neural Transm*, 116:1243–1251, 2009.

Veal E. A., Findlay V. J., Day A. M., Bozonet S. M., Evans J. M., Quinn J., and Morgan B. A. A 2-cys peroxiredoxin regulates peroxide-induced oxidation and activation of a stress-activated map kinase. *Mol Cell.*, 15(1):129–39., 2004.

Vega I. E., Traverso E. E., Ferrer-Acosta Y., Matos E., Colon M., Gonzalez J., Dickson D., Hutton M., Lewis J., and Yen S. H. A novel calcium-binding protein is associated with tau proteins in tauopathy. *J Neurochem*, 106(1):96–106, 2008.

Velliquette R., O'Connor T., and Vassar R. Energy inhibition elevates beta-secretase levels and activity and is potentially amyloidogenic in app transgenic mice: Possible early events in alzheimer's disease pathogenesis. *J. Neurosci.*, 25(47):10874–10883,

2005.

Vepsalainen S., Parkinson M., Helisalmi S., Mannermaa A., Soininen H., Tanzi R. E., Bertram L., and Hiltunen M. Insulin-degrading enzyme is genetically associated with alzheimer's disease in the finnish population. *J Med Genet*, 44(9):606–8, 2007.

Vepsalainen S., Hiltunen M., Helisalmi S., Wang J., van Groen T., Tanila H., and Soininen H. Increased expression of abeta degrading enzyme ide in the cortex of transgenic mice with alzheimer's disease-like neuropathology. *Neurosci Lett*, 438(2): 216–20, 2008.

Verdier Y., Zarandi M., and Penke B. Amyloid beta-peptide interactions with neuronal and glial cell plasma membrane: binding sites and implications for alzheimer's disease. *J Pept Sci*, 10(5):229–48, 2004.

Vetrivel K. and Thinakaran G. Amyloidogenic processing of beta-amyloid precursor protein in intracellular compartments. *Neurology*, $66(1_s uppl_1) : S69 - -73, 2006$.

Viesselmann C., Ballweg J., Lumbard D., and Dent E. W. Nucleofection and primary culture of embryonic mouse hippocampal and cortical neurons. *J Vis Exp.*, (47).(pii): 2373. doi: 10.3791/2373., 2011.

Vinatier J., Herzog E., Plamont M., Wojcik S., Schmidt A., Brose N., Daviet L., El Mestikawy S., and Giros B. Interaction between the vesicular glutamate transporter type1 and endophilina1, a protein essential for endocytosis. *J Neurochem*, 97 (4):1111–1125, 2006.

Vuadens F., Rufer N., Kress A., Corthesy P., Schneider P., and Tissot J. D. Identification of swiprosin 1 in human lymphocytes. *Proteomics*, 4(8):2216–20, 2004.

Walsh D. M. and Selkoe D. J. A beta oligomers - a decade of discovery. *J Neurochem*, 101(5):1172–84, 2007.

Walsh D. M., Klyubin I., Fadeeva J. V., Cullen W. K., Anwyl R., Wolfe M. S., Rowan M. J., and Selkoe D. J. Naturally secreted oligomers of amyloid beta protein potently inhibit hippocampal long-term potentiation in vivo. *Nature*, 416(6880):535–9, 2002a.

Walsh D. M., Klyubin I., Fadeeva J. V., Rowan M. J., and Selkoe D. J. Amyloid-beta oligomers: their production, toxicity and therapeutic inhibition. *Biochem Soc Trans*, 30(4):552–7, 2002b.

Wang H. Y., Lee D. H., D'Andrea M. R., Peterson P. A., Shank R. P., and Reitz A. B. beta-amyloid(1-42) binds to alpha7 nicotinic acetylcholine receptor with high affinity. implications for alzheimer's disease pathology. *J Biol Chem*, 275(8):5626–32, 2000.

Wang W., Fang H., Groom L., Cheng A., Zhang W., Liu J., Wang X., Li K., Han P., Zheng M., Yin J., Wang W., Mattson M. P., Kao J. P., Lakatta E. G., Sheu S. S., Ouyang K., Chen J., Dirksen R. T., and Cheng H. Superoxide flashes in single mitochondria. *Cell*, 134(2):279–90, 2008.

Wang X., Su B., Lee H., Li X., Perry G., Smith M., and Zhu X. Impaired balance of mitochondrial fission and fusion in alzheimer's disease. *J. Neurosci.*, 29(28):9090–9103, 2009.

Wegiel J., Kuchna I., Nowicki K., Frackowiak J., Mazur-Kolecka B., Imaki H., Wegiel J., Mehta P. D., Silverman W. P., Reisberg B., Deleon M., Wisniewski T., Pirttilla T., Frey H., Lehtimaki T., Kivimaki T., Visser F. E., Kamphorst W., Potempska A.,

Bolton D., Currie J. R., and Miller D. L. Intraneuronal abeta immunoreactivity is not a predictor of brain amyloidosis-beta or neurofibrillary degeneration. *Acta Neuropathol*, 113(4):389–402, 2007.

Wei W., Wang X., and Kusiak J. W. Signaling events in amyloid beta-peptide-induced neuronal death and insulin-like growth factor i protection. *J Biol Chem*, 277(20): 17649–56, 2002.

Weston R., MC andNehring, Wojcik S., and Rosenmund C. Interplay between vglut isoforms and endophilin a1 regulates neurotransmitter release and short-term plasticity. *Neuron*, 69(6):1147 – 1159, 2011.

Winkler K., Scharnagl H., Tisljar U., Hoschutzky H., Friedrich I., Hoffmann M. M., Huttinger M., Wieland H., and Marz W. Competition of abeta amyloid peptide and apolipoprotein e for receptor-mediated endocytosis. *J Lipid Res*, 40(3):447–55, 1999.

Wolfe M. S., Xia W., Ostaszewski B. L., Diehl T. S., Kimberly W. T., and Selkoe D. J. Two transmembrane aspartates in presenilin-1 required for presenilin endoproteolysis and gamma-secretase activity. *Nature*, 398(6727):513–7, 1999.

Wood Z., Schroder E., Robin Harris J., and Poole L. Structure, mechanism and regulation of peroxiredoxins. *Trends Biochem Sci*, 28(1):32–40, 2003.

Wu Z. L., Ciallella J. R., Flood D. G., O'Kane T. M., Bozyczko-Coyne D., and Savage M. J. Comparative analysis of cortical gene expression in mouse models of alzheimer's disease. *Neurobiol Aging.*, 27(3):377–86. Epub 2005 May 31., 2006.

Yan S. D., Fu J., Soto C., Chen X., Zhu H., Al-Mohanna F., Collison K., Zhu A., Stern E., Saido T., Tohyama M., Ogawa S., Roher A., and Stern D. An intracellular protein that binds amyloid-beta peptide and mediates neurotoxicity in alzheimer's disease. *Nature*, 389(6652):689–95, 1997.

Yan S., Shi Y., Zhu A., Fu J., Zhu H., Zhu Y., Gibson L., Stern E., Collison K., Al-Mohanna F., Ogawa S., Roher A., Clarke S., and Stern D. Role of erab/l-3-hydroxyacyl-coenzyme a dehydrogenase type ii activity in a-induced cytotoxicity. *J. Biol. Chem.*, 274(4):2145–2156, 1999.

Yan S., Zhu Y., Stern E., Hwang Y., Hori O., Ogawa S., Frosch M., Connolly E., McTaggert R., Pinsky D., Clarke S., Stern D., and Ramasamy R. Amyloid beta -peptide-binding alcohol dehydrogenase is a component of the cellular response to nutritional stress. *J. Biol. Chem.*, 275(35):27100–27109, 2000.

Yang A. J., Chandswangbhuvana D., Margol L., and Glabe C. G. Loss of endosomal/lysosomal membrane impermeability is an early event in amyloid abeta1-42 pathogenesis. *J Neurosci Res*, 52(6):691–8, 1998.

Yankner B., Duffy L., and Kirschner D. Neurotrophic and neurotoxic effects of amyloid beta protein: reversal by tachykinin neuropeptides. *Science*, 250(4978):279–282, 1990.

Yao J., Taylor M., Davey F., Ren Y., Aiton J., Coote P., Fang F., Chen J. X., Yan S. D., and Gunn-Moore F. J. Interaction of amyloid binding alcohol dehydrogenase/abeta mediates up-regulation of peroxiredoxin ii in the brains of alzheimer's disease patients and a transgenic alzheimer's disease mouse model. *Mol Cell Neurosci*, 35(2):377–82, 2007.

Yao J., Irwin R., Zhao L., Nilsen J., Hamilton R., and Brinton R. Mitochondrial bioen-

ergetic deficit precedes alzheimer's pathology in female mouse model of alzheimer's disease. *Proc. Natl. Acad. Sci. U.S.A.*, 106(34):14670–14675, 2009.

Yao J., Du H., Yan S., F F., Wang C., Lue L.-F., Guo L., Chen D., Stern D., Gunn-Moore F., Chen J., Arancio O., and Yan S. Inhibition of abad-abeta interaction reduces abeta accumulation and improves mitochondrial function in a mouse model of alzheimer's disease. *J Neurosci*, 31:2313–20, 2011.

Yoon E. J., Park H. J., Kim G. Y., Cho H. M., Choi J. H., Park H. Y., Jang J. Y., Rhim H. S., and Kang S. M. Intracellular amyloid beta interacts with sod1 and impairs the enzymatic activity of sod1: implications for the pathogenesis of amyotrophic lateral sclerosis. *Exp Mol Med*, 41(9):611–7, 2009.

Yu C. E., Seltman H., Peskind E. R., Galloway N., Zhou P. X., Rosenthal E., Wijsman E. M., Tsuang D. W., Devlin B., and Schellenberg G. D. Comprehensive analysis of apoe and selected proximate markers for late-onset alzheimer's disease: patterns of linkage disequilibrium and disease/marker association. *Genomics*, 89(6):655–65, 2007.

Yu M., JZand Rasenick. Tau associates with actin in differentiating pc12 cells. *FASEB J*, 20(9):1452–1461, 2006.

Zakzanis K., Graham S., and Campbell Z. A meta-analysis of structural and functional brain imaging in dementia of the alzheimer's type: a neuroimaging profile. *Neuropsychol Rev*, 13(1):1–18, Mar 2003.

Zeitelhofer M., Vessey J., Xie Y., Tubing F., Thomas S., Kiebler M., and Dahm R. High-efficiency transfection of mammalian neurons via nucleofection. *Nat. Protocols*, 2(7): 1692–1704, jul 2007.

Zempel H., Thies E., Mandelkow E., and Mandelkow E. M. Abeta oligomers cause localized ca(2+) elevation, missorting of endogenous tau into dendrites, tau phosphorylation, and destruction of microtubules and spines. *J Neurosci*, 30(36):11938–50, 2010.

Zhai J., Strm A., Kilty R., Venkatakrishnan P., White K., Everson W., Smart E., and Zhu H. Proteomic characterization of lipid raft proteins in amyotrophic lateral sclerosis mouse spinal cord. *FEBS J*, 276(12):3308–3323, Jun 2009.

Zhang Y., McLaughlin R., Goodyer C., and LeBlanc A. Selective cytotoxicity of intracellular amyloid beta peptide1-42 through p53 and bax in cultured primary human neurons. *J Cell Biol*, 156(3):519–29, 2002.

Zhang Y. W., Wang R., Liu Q., Zhang H., Liao F. F., and Xu H. Presenilin/gamma-secretase-dependent processing of beta-amyloid precursor protein regulates egf receptor expression. *Proc Natl Acad Sci U S A*, 104(25):10613–8, 2007.

Zhang Y., Thompson R., Zhang H., and Xu H. App processing in alzheimer's disease. *Mol Brain*, 4(1):3, 2011.

Zhao L., Teter B., Morihara T., Lim G. P., Ambegaokar S. S., Ubeda O. J., Frautschy S. A., and Cole G. M. Insulin-degrading enzyme as a downstream target of insulin receptor signaling cascade: implications for alzheimer's disease intervention. *J. Neurosci.*, 24(49):11120–6, 2004.

Zhao Y., Cui J. G., and Lukiw W. J. Reduction of sortilin-1 in alzheimer hippocampus and in cytokine-stressed human brain cells. *Neuroreport*, 18(11):1187–91, 2007.

Zhu X., Raina A., Rottkamp C., Aliev G., Perry G., Boux H., and Smith M. Activa-

tion and redistribution of c-jun n-terminal kinase/stress activated protein kinase in degenerating neurons in alzheimer's disease. *J Neurochem*, 76(2):435–441, 2001.